Mestrado Integrado em Engenharia Mecânica

Low Power Loss Gears:Design and Experimental Testing

Ivo Miguel Gomes Oliveira

Final Project Report
MIEM Thesis

Thesis supervised in Feup by
Prof. Jorge H. Oliveira Seabra
Feup's Associated Professor

Thesis supervised in Cetrib by
Dr. Ramiro C. Martins
Feup's External Researcher

Departamento de Engenharia Mecânica
DEMec - Cetrib - INEGI

Porto, February of 2011

Acknowledgements

This work could not have been done without the help of a wide group of people from all kinds of personal relationship levels.

First of all I would like to begin by expressing my enormous gratitude to my Parents for their love, effort, and encouragement during, not only, this present work, but also in all these years of college education. Their kind and unconditional support in my most difficult moments, helped me to prevail despite all difficulties.

I would also like to thank my brothers, and all the remaining family for their support and contribution for my education.

Secondly, I would like to express my sincere appreciation to my Feup supervisor Prof. Jorge Seabra for his time, guidance and permanent support throughout all of my thesis.

I would also like to express my gratitude to Dr. Ramiro C. Martins, which was always available to help me during this thesis.

I wish to thank my colleagues at CETRIB, for their remarkable help and companionship in all the work and moments passed in Cetrib: Carlos Fernandes, Rui Silva, Beatriz Graça, José Brandão, Luís Magalhães, Tiago Cousseau, Armando Campos and Jorge Castro.

I wish to thank my closest friends for their support, particularly, my girlfriend Mariana Silva, for her's comprehension and help during my last years in Feup and during the execution of this thesis.

Finally I would like to thank INEGI (Instituto Nacional de Engenharia e Gestão Industial), FEUP (Faculdade de Engenharia da Universidade do Porto), for the conditions provided to the realization of this dissertation.

to my family

Abstract

High energy consumption, leads companies and their engineers, to search new ways to save energy. This can be accomplished by developing new and more efficient gear geometries ("Low Loss"), better suited oils with low-toxicity, as well as, new combination between lubricants, geometry's and lubricant level's.

Nowadays gear transmissions are widely used in industrial machines, so there is a constant need to improve the efficiency of these kind of gears. With that idea in mind the "Low Loss Gear" where created. Since the costs are an important part, present in todays manufacturing processes, these gears have the particularity that they may be produced with ordinary day-by-day tools, available in any tool-shop, and it does not need any particularly or expensive procedure.

In the present work three different "Low Loss" geometries were tested, manufactured in two different materials (Carburized steel and Austempered Ductile Iron) and tested with two lubricant oils, an ester base oil (E1) and an fully synthetic polyalphaolefine base oil (P1). All gears and lubricants were tested in the FZG test rig, using two different oil levels in order to observe the influence of the oil level in the power losses.

In the end of each power loss test the data was analyzed and the results discussed, several trends were observed:

1. The module reduction has an advantage, since it has been proved that the 610 gear geometry has best results.

2. Both 611 or 612 gears have a similar performance working with E1 or P1 lubricating oils.

3. The steel gears have always lower mass losses and lower CPUC and ISUC values when compared with the ADI gears, using both high and low oil levels, as well as, E1 and P1 lubricants.

4. It was proved that working with low oil level presents better results, whatever the lubricant used.

5. Generally, low oil level and P1 lubricant has better results with ADI gears and E1 lubricant with steel gears.

Sumário

O alto consumo de energia, leva as empresas e seus engenheiros a pesquisar novas formas de economizar energia. Isto pode ser conseguido através do desenvolvimento de geometrias novas e mais eficientes ("Low Loss"), óleos mais eficazes e de baixa toxicidade, bem como, novas combinações entre lubrificantes, geometria e nível de lubrificante.

Transmissões por engrenagens são muito utilizadas hoje em dia em máquinas industriais, de modo que, existe constantemente a necessidade de melhorar a eficiência deste tipo de engrenagens. Com essa ideia em mente foi criado o conceito das engrenagens de baixa perda de potência ("'Low Loss Gears"'). Dado que os custos são uma parte importante e presente nos processos de produção de hoje, estas engrenagens têm a particularidade de poderem ser produzidas com ferramentas comuns do dia-a-dia, e que podem ser compradas em qualquer loja de ferramentas, não precisando portanto de nenhum processo caro nem especial para serem produzidas.

No presente trabalho foram testadas três diferentes geometrias "Low Loss", fabricadas em dois materiais diferentes (Aço de cementação e ferro nodular austemperado) e foram também testados dois tipos de óleos lubrificantes, um óleo de base éster (E1) e um de base polialfaolefinica sintético (P1). Todas as engrenagens e lubrificantes foram testados na máquina de teste FZG.

Os testes de perda de potência foram realizados com dois níveis de óleo distintos, a fim de observar a influência do nível de óleo nas perdas de energia.

No final dos testes de perda de potência, os dados foram analisados e os resultados discutidos, concluindo que:

1. A redução do módulo tem vantagens, pois foi mostrado que a geometria 610 tem os melhores resultados.
2. As engrenagens da serie 610 têm um desempenho semelhante quando lubrificadas com os óleos E1 ou P1.
3. As engrenagens de aço têm sempre menores perdas de massa e menores valores de CPUC e ISUC, quando comparadas com as engrenagens em ADI, usando os dois níveis de óleo e os lubrificantes E1 e P1.
4. Observa-se que operar com baixo nível de óleo apresenta melhores resultados, qualquer que seja o lubrificante utilizado.
5. Globalmente o lubrificante P1 e um baixo nível de óleo conduz a menor perda de potência com ADI mas o aço apresenta melhores resultados quando combinado com E1.

Contents

Acknowledgements . . . iii
Abstract . . . vii
Sumário . . . viii
Table of contents . . . ix
Figures Index . . . xiii
Tables Index . . . xvii
Nomenclature . . . xix
Introduction . . . xxiii

1. Gear Tribology **1**
1.1. Gear Design . . . 1
1.1.1. Contact length in helical gears . . . 2
1.1.2. Load between contacting flanks . . . 5
1.1.3. Radius of Curvature . . . 7
1.1.4. Contact pressure and shear stress variation along the contact path . . . 9
1.1.5. Surface velocities . . . 15
1.1.6. Lubricant film thickness . . . 20
1.1.7. Inlet shear heating in an EHD contact . . . 23
1.1.8. Specific lubricant film thickness . . . 25
1.1.9. Lubricant regimes . . . 27
1.1.10. Coefficient of friction in gear teeth . . . 28
1.1.11. Teeth flank and Lubricant temperature . . . 32
1.2. Lubricant oils . . . 35
1.2.1. Vegetable and animal lubricant oils . . . 35
1.2.2. Mineral based lubricant oils . . . 36
1.2.3. Synthetic base lubricant oils . . . 36
1.2.4. Additives . . . 37
1.2.5. Lubricant classification-Viscosity Grades . . . 38
1.3. Gear lubrication Methods and Level . . . 42
1.4. Gear failure modes . . . 44
1.4.1. Abrasion or slow wear . . . 45
1.4.2. Scoring and scuffing . . . 46
1.4.3. Pitting and Micro-Pitting . . . 46
1.5. Gear Power loss . . . 49
1.5.1. Load dependent power losses . . . 50
1.5.2. No-Load dependent power losses . . . 52

1.5.3. Reference friction torque loss . . . 53
1.5.4. Heat Removal . . . 54

2. Gears, Materials and Oils 57
2.1. Low Loss Gear . . . 57
2.2. Gears Geometry . . . 59
2.2.1. Low Loss Gears Geometry: 310, 410 and 610 . . . 60
2.3. Gears Material . . . 61
2.3.1. Carburized Steel (DIN 20MnCr5) . . . 61
2.3.2. Austempered Ductile Iron (ADI) . . . 63
2.3.3. Safety coefficients and working parameter comparison . . . 65
2.4. Tested Oils . . . 67

3. Test Machines and Procedures 69
3.1. FZG Test Rig . . . 69
3.2. Pressure Pads . . . 70
3.3. Power Loss Test Procedure . . . 71
3.4. Churning Loss Test Procedure . . . 73
3.5. Surface Roughness and Topography Measurement . . . 74
3.6. Mass Loss Procedure . . . 78
3.7. Oil Analysis . . . 79
3.7.1. Direct Reading Ferrometry: Equipment and procedure . . . 79
3.7.2. Analytic Ferrometry: Equipment and procedure . . . 81

4. Experimental Results 85
4.1. Ester base lubricant oil (E1) gear test and low oil level . . . 85
4.1.1. Stabilization temperatures . . . 85
4.1.2. Ferrometry . . . 92
4.1.3. Surface Roughness . . . 98
4.1.4. Mass Loss . . . 101
4.2. Ester base lubricant oil (E1) gear test and high oil level . . . 102
4.2.1. Stabilization temperatures . . . 102
4.2.2. Ferrometry . . . 108
4.2.3. Surface Roughness . . . 114
4.2.4. Mass Loss . . . 117
4.3. Ester base lubricant oil gear (E1) test and high vs low oil Level. 118
4.3.1. Stabilization temperatures . . . 118
4.3.2. Ferrometry . . . 120
4.3.3. Mass Loss . . . 123
4.4. Polyalolephine base lubricant oil (P1) gear test and low oil Level 125
4.4.1. Stabilization temperatures . . . 125
4.4.2. Ferrometry . . . 132
4.4.3. Surface Roughness . . . 138
4.4.4. Mass Loss . . . 141

4.5. Polyalolephine base lubricant oil (P1) gear test and high oil Level 142
4.5.1. Stabilization temperatures 142
4.5.2. Ferrometry 148
4.5.3. Surface Roughness 154
4.5.4. Mass Loss 157
4.6. Polyalolephine base lubricant oil gear (P1) test and high vs low oil Level 158
4.6.1. Stabilization temperatures 158
4.6.2. Ferrometry 160
4.6.3. Mass Loss 163
4.7. Polyalolephine base (P1) vs Ester base (E1) lubricant oil gear test and low oil Level 165
4.7.1. Stabilization temperatures 165
4.7.2. Mass Loss 170
4.8. Polyalolephine base (P1) vs Ester base (E1) lubricant oil gear test and high oil Level 172
4.8.1. Stabilization temperatures 172
4.8.2. Mass Loss 176
4.9. No load test - Churning loss 178

5. Conclusions and Future work **181**
5.1. Conclusion 181
5.2. Future work 181

Bibliography **183**

A. Appendix **187**
A.1. Power Loss Data Sheets 189
A.2. Power Loss oil Reports 227

List of Figures

1.1. Contact path representation. 3
1.2. Length distribution in the contact path for helical gear. 4
1.3. Contact loads in helical gears [1]. 6
1.4. Teeth normal contact load. 6
1.5. Generic points in the contact path for helical gears [2]. 7
1.6. Equivalent radius of curvature for gears: a) 310, b) 410 and c) 610. 8
1.7. Hertzian contact pressure for gears: a) 310, b) 410 and c) 610. . 10
1.8. Hertzian half-width for gears: a) 310, b) 410 and c) 610. 11
1.9. Shear stresses for gears: a) 310, b) 410 and c) 610. 13
1.10. Shear stress depth (Z_s and Z_0)variation for gears: a) 310, b) 410 and c) 610. 14
1.11. Velocities V_1 and V_2 of generic point M of the contact path [2]. 15
1.12. Tangential velocities U_1 and U_2 of generic point M of the contact path [2]. 16
1.13. Variation of tangential velocities along the contact path [2]. . . . 17
1.14. Variation of sliding and tangential velocities the contact path for gears: a) 310, b) 410 and c) 610. 18
1.15. Specific sliding the contact path for gears: a) 310, b) 410 and c) 610. 19
1.16. Center and minimum film thickness [2]. 20
1.17. Center and minimum film thickness along the contact path for gears: a) 310, b) 410 and c) 610. 22
1.18. Corrected center film thickness along the contact path for gears: a) 310, b) 410 and c) 610. 24
1.19. Thermal corrected film thickness variation along the contact path for gears: a) 310, b) 410 and c) 610. 26
1.20. Lubrication regimes [2]. 27
1.21. Relation between 5% probability of failure and specific lubricant film thickness Λ. 28
1.22. Stribeck curve. 29
1.23. Friction coefficient for gears: a) 310, b) 410 and c) 610. 31
1.24. Oil surface tooth flank temperatures along the contact path for gears: a) 310, b) 410 and c) 610. 34
1.25. SAE J300 Classification [3]. 39
1.26. SAE J306 Classification [3]. 39
1.27. ISO Classification [3]. 40

1.28. Comparison of Classification Rates [4]. 41
1.29. Oil bath lubrication [4]. 42
1.30. Jet oil lubrication [5]. 43
1.31. Abacus for selection of lubrication type 43
1.32. Most important gear failure modes [5]. 44
1.33. Several types of Wear. 45
1.34. Several types of Scuffing. 47
1.35. Several types of Pitting. 48
1.36. Micro-Pitting [6]. 48
1.37. Power losses diagram [7]. 50

2.1. Power loss comparison between Type C and Hohn Low Loss gears [8]. 58
2.2. Visual Representation Comparison of the two gear types. 59
2.3. Pinion teeth of gears 310, 410 and 610 (from left to right) [9]. . 60
2.4. Procedure of ADI austempering heat treatment. 64
2.5. ADI Microstructure. 65

3.1. Representation of FZG test rig. 70
3.2. Pressure pads. 71
3.3. "Dead weight" load combinations. 72
3.4. Oil samples and oil pump. 73
3.5. Hommewerke T8000 controller. 75
3.6. Tk300 Probe. 75
3.7. Roughness measurement software (Turbowave). 76
3.8. Roughness measurement datasheet. 77
3.9. Example of the roughness measuring in a gear tooth. 77
3.10. Electronic *Metler-Toledo PR1203* weighing-machine. 78
3.11. Reference pinion (left) and Tested Pinion (right). 79
3.12. Direct Reading Ferrographer scheme [10]. 80
3.13. Direct Reading Ferrographer. 81
3.14. Analytic Ferrographer scheme [10]. 82
3.15. Analytic Ferrographer. 82
3.16. Bi-Chromatic microscope (ferroscope). 83
3.17. Ferrogram taken after k9 load stage of a power loss test (Appendix A.2: Power Loss Data Sheets of a 411 with E1 oil) 1000x. 83

4.1. Stabilization temperatures in gear power loss tests: steel gears (311, 411, 611), E1 lubricant, low oil level. 87
4.2. Stabilization temperatures in gear power loss tests: ADI gear (612), E1 lubricant, low oil level. 89
4.3. Stabilization temperatures in gear power loss tests with lubricant E1 and low oil level: a) gear 311; b) gear 411; c) gear 611 vs 612. 91

4.4. Ferrography in gear power loss tests: steel gears (311, 411, 611), E1 lubricant, low oil level. 93
4.5. Ferrography in gear power loss tests: ADI gear (612), E1 lubricant, low oil level. 95
4.6. Ferrography in gear power loss tests: Steel vs ADI, with lubricant E1 and low oil level. 97
4.7. Mass loss in gear power loss tests: steel vs ADI, with lubricant E1 and low oil level. 101
4.8. Stabilization temperatures in gear power loss tests: steel gears (311, 411, 611), E1 lubricant, high oil level. 103
4.9. Stabilization temperatures in gear power loss tests: ADI gears (312, 412, 612), E1 lubricant, high oil level. 105
4.10. Stabilization temperatures in gear power loss tests with lubricant E1 and low oil level: a) gear 311 vs 312; b) gear 411 vs 412; c) gear 611 vs 612. 107
4.11. Ferrography in gear power loss tests: steel gears (311, 411, 611), E1 lubricant, high oil level. 109
4.12. Ferrography in gear power loss tests: ADI gears (312, 412, 612), E1 lubricant, high oil level. 111
4.13. Ferrography in gear power loss tests: steel vs ADI gears, E1 lubricant, high oil level. 113
4.14. Mass loss in gear power loss tests: steel vs ADI gears, E1 lubricant, high oil level 117
4.15. Stabilization temperatures in gear power loss tests: high vs low oil level, E1 lubricant, steel and ADI gears. 119
4.16. Ferrography in gear power loss tests: high vs low oil level, E1 lubricant, steel gears. 121
4.17. Ferrography in gear power loss tests: high vs low oil level, E1 lubricant, ADI gears. 122
4.18. Mass loss in gear power loss tests: high vs low oil level, E1 lubricant, steel and ADI gears. 123
4.19. Stabilization temperatures in gear power loss tests: steel gears (311, 411, 611), P1 lubricant, low oil level. 127
4.20. Stabilization temperatures in gear power loss tests: ADI gear (612), P1 lubricant, low oil level. 129
4.21. Stabilization temperatures in gear power loss tests with lubricant P1 and low oil level: a) gear 311; b) gear 411; c) gear 611 vs 612. 131
4.22. Ferrography in gear power loss tests: steel gears (311, 411, 611), P1 lubricant, low oil level. 133
4.23. Ferrography in gear power loss tests: ADI gear (612), P1 lubricant, low oil level. 135
4.24. Ferrography in gear power loss tests: steel vs ADI, with lubricant P1 and low oil level. 137

4.25. Mass loss in gear power loss tests: steel vs ADI, with lubricant P1 and low oil level. 141
4.26. Stabilization temperatures in gear power loss tests: steel gears (311, 411, 611), P1 lubricant, high oil level. 143
4.27. Stabilization temperatures in gear power loss tests: ADI gears (312, 412, 612), P1 lubricant, high oil level. 145
4.28. Stabilization temperatures in gear power loss tests with lubricant P1 and low oil level: a) gear 311 vs 312; b) gear 411 vs 412; c) gear 611 vs 612. 147
4.29. Ferrography in gear power loss tests: steel gears (311, 411, 611), P1 lubricant, high oil level. 149
4.30. Ferrography in gear power loss tests: ADI gears (312, 412, 612), P1 lubricant, high oil level. 151
4.31. Ferrography in gear power loss tests: steel vs ADI gears, P1 lubricant, high oil level. 153
4.32. Mass loss in gear power loss tests: steel vs ADI gears, P1 lubricant, high oil level. 157
4.33. Stabilization temperatures in gear power loss tests: high vs low oil level, P1 lubricant, steel and ADI gears. 159
4.34. Ferrography in gear power loss tests: high vs low oil level, P1 lubricant, steel gears. 161
4.35. Ferrography in gear power loss tests: high vs low oil level, P1 lubricant, ADI gears. 162
4.36. Mass loss in gear power loss tests: high vs low oil level, P1 lubricant, steel and ADI gears. 163
4.37. Stabilization temperatures in gear power loss tests: steel gears (311, 411, 611), P1 and E1 lubricants, low oil level. 167
4.38. Stabilization temperatures in gear power loss tests: ADI gear (612), P1 and E1 lubricants, low oil level. 169
4.39. Mass loss in gear power loss tests: a) steel and b) ADI gears, E1 vs P1 gear oils, and low oil level. 171
4.40. Stabilization temperatures in gear power loss tests: steel gears (311, 411, 611), P1 and E1 lubricants, high oil level. 173
4.41. Stabilization temperatures in gear power loss tests: ADI gears (312, 412, 612), P1 and E1 lubricants, high oil level. 175
4.42. Mass loss in gear power loss tests: a) steel and b) ADI gears, E1 vs P1 gear oils, and high oil level. 177
4.43. Stabilization temperatures in gear churning loss tests: steel and ADI gears (311, 411, 611 and 612), P1 and E1 lubricant oils, high and low oil levels. 179

List of Tables

1.1. Geometric characteristics and working conditions of 310/410/610 gears. 2
1.2. Values of contact length for 310/410/610 gears. 4
1.3. Value of b1 exponent for each lubricant test 30

2.1. FZG Type C and "Low Loss" gears [8]. 58
2.2. Geometric characteristics of 310/410/610 gears. 61
2.3. Heat treatment steps for the Carburized Steel (DIN 20MnCr5). 62
2.4. Chemical composition (weight %) of Carburized Steel (DIN 20MnCr5). 62
2.5. Properties of Carburized Steel [11]. 62
2.6. Chemical composition (weight %) of Austempered Ductile Iron (DIN 1.0Cu-0.5Mn). 63
2.7. Properties of Austempered Ductile Iron [12]. 64
2.8. Safety Coefficient for all gears with the correct widths. 66
2.9. Safety Coefficient and Working Parameters [11]. 66
2.10. Lubricant Properties. 67

3.1. Power loss test operating conditions. 72
3.2. Churning loss test operating conditions. 74

4.1. Tooth flank surface roughness of 20MnCr5 steel gear 311 with E1 gear oil and low oil level. 98
4.2. Tooth flank surface roughness of 20MnCr5 steel gear 411 with E1 gear oil and low oil level. 99
4.3. Tooth flank surface roughness of 20MnCr5 steel gear 611 with E1 gear oil and low oil level. 99
4.4. Tooth flank surface roughness of ADI gear 612 with E1 gear oil and low oil level. 99
4.5. Tooth flank surface roughness of 20MnCr5 steel gear 311 with E1 gear oil and high oil level. 114
4.6. Tooth flank surface roughness of 20MnCr5 steel gear 411 with E1 gear oil and high oil level. 115
4.7. Tooth flank surface roughness of ADI gear 312 with E1 gear oil and high oil level. 115
4.8. Tooth flank surface roughness of ADI gear 412 with E1 gear oil and high oil level. 115

4.9. Tooth flank surface roughness of 20MnCr5 steel gear 311 with P1 gear oil and low oil level. 138
4.10. Tooth flank surface roughness of 20MnCr5 steel gear 411 with P1 gear oil and low oil level. 139
4.11. Tooth flank surface roughness of 20MnCr5 steel gear 611 with P1 gear oil and low oil level. 139
4.12. Tooth flank surface roughness of ADI gear 612 with P1 gear oil and low oil level. 139
4.13. Tooth flank surface roughness of 20MnCr5 steel gear 311 with P1 gear oil and high oil level. 154
4.14. Tooth flank surface roughness of 20MnCr5 steel gear 411 with P1 gear oil and high oil level. 155
4.15. Tooth flank surface roughness of ADI gear 312 with P1 gear oil and high oil level. 155
4.16. Tooth flank surface roughness of ADI gear 412 with P1 gear oil and high oil level. 155

Nomenclature

Symbol	Designation	Units
A_{base}	Base support area	[m^2]
A_h	Horizontal surface area of case	[m^2]
A_i	Immersed area	[m^2]
A_{Rad}	Radiation surface area of case	[m^2]
A_v	Vertical surface area of case	[m^2]
a	Center distance	[mm]
a_w	Working center distance	[mm]
b	Teeth width	[mm]
c	Specific weight	[J/Kg °C]
CPUC	Ferrometric index for the concentration of wear particles	[/]
d	Pitch diameter	[mm]
D	Bearing mean diameter	[m]
d	Dilution factor	[/]
d	Pitch diameter	[mm]
d_a	Addendum diameter	[mm]
d_a	Tip diameter	[mm]
d_{aw}	Working tip diameter	[mm]
d_b	Base diameter	[mm]
d_i	Shaft diameter	[m]
DL	Ferrometric index for the amount of large particles	[/]
d_p	Pitch diameter	[m]
DS	Ferrometric index for the amount of small particles	[/]
d_w	Working pitch diameter	[mm]
E*	Equivalent young modulus	[Pa]
f_l	Coeficient for bearing losses	[/]
f_T	Thermal correction factor	[/]
$f_{0,1}$	Coefficient for bearing losses	[/]
F_a	Axial load	[N]
F_{bt}	Tooth normal load, transverse section	[N]
f_{cn}	Conduction factor	[/]
F_r	Radial load	[N]
FR	Froud number	[/]
g	Path of contact (length)	[mm]
h	Dinamic viscosity	[Pa.s]
h_0	Lubricant film thickness	[μm]
h_{0T}	Corrected lubricant film thickness	[μm]
h_{aw}	Working addendum	[mm]

Symbol	Designation	Units
h_{ca}	Height of case	[m]
h_h	Natural convection coefficient, horizontal surface	[W/(m^2°K)]
h_v	Natural convection coefficient, vertical surface	[W/(m^2°K)]
H_{vl}	Torque losse factor	[/]
ISUC	Ferrometric index for the severity of wear large particles	[/]
k*m	Tip diam. Mod. Coef.	[mm]
K_f	Lubricant thermal conductivity	[W/(m^2°K)]
K_{FZG}	FZG load stage	[/]
L	Thermal parameter	[/]
L_{ca}	Characteristic horizontal length	[m]
L_t	Total roughness measurement length	[mm]
m	Module	[mm]
m_w	Working modulus	[mm]
n	Rotational speed	[rpm]
ν	Kinematic viscosity	[mm^2/s]
ν_{100}	Kinematic viscosity @ 100°C	[cSt]
ν_{40}	Kinematic viscosity @ 40°C	[cSt]
nE1	Resonance speed	[/]
P	Power	[w]
p_0	Contact pressure	[Pa]
p_b	Base pitch	[mm]
P_{fr}	Gear friction loss	[W]
P_{in}	Input power	[W]
P_{M0}	Bearing load Dependant losses	[W]
P_{M1}	Bearing no load Dependant losses	[W]
P_{sl}	Seal losses	[W]
P_{spl}	Gear churning losses	[W]
Q_{cn}	Heat removal by conduction	[W]
Q_{ncn}	Heat removal by natural convection	[W]
Q_{rad}	Heat removal by radiation	[W]
R_a	Roughness average (according to DIN 4768, ISO 4287)	[μm]
Re	Reynolds number	[/]
R_k	Core roughness depth (DIN 4776)	[μm]
R_{max}	Maximum peak-to-valley height(DIN 4768)	[μm]
R_{pk}	Reduced peak height(DIN 4776)	[μm]
R_q	RMS roughness average(DIN 4768, ISO 4287)	[μm]
R_{vk}	Reduced valley depth (DIN 4776)	[μm]
R_M	Equivalent radius	[m]
R_z	Mean peak-to-valley height	[mm]
s	Piezoviscosity parameter	[/]
SF	Tooth root stress	[/]
SH	Surface pressure	[/]
Sp Gr	Density @ 15°C	[g/cm^3]

Symbol	Designation	Units
t	Piezoviscosity parameter	[/]
T	Lubricant Absolute temperature	[°K]
T_f	Oil working temperature	[°C]
T_0	Oil bath temperature	[°C]
T_a	Ambient temperature	[°C]
T_{CR}	Critical lubricant temperature	[°C]
T_{vz}	Reference friction torque loss	[N.m]
T_w	Wall temperature	[°K]
T_{wheel}	Wheel torque	[N.m]
u	Gear ratio	[/]
U_1	Pinion surface speed	[m/s]
U_2	Wheel surface speed	[m/s]
VI	Lubricant viscosity index	[/]
V_{oil}	Oil volume	[m^3]
V_S	Sliding rate	[m/s]
x	Addendum modification coefficient	[/]
X_L	Lubricant factor	[/]
Z_1	Pinion teeth number	[/]
Z_2	Wheel teeth number	[/]
α	Pressure angle	[°]
α_{wt}	Working pressure angle	[°]
α_{100}	Piezoviscosity @ 100°C	[$GPa^{-}1$]
α_{40}	Piezoviscosity @ 40°C	[GPa^{-1}]
α_{rad}	Radiation heat transfer coefficient	[/]
α_v	Thermal expansion	[g/(cm^3°C)]
β	Helical angle	[°]
β_b	Base helical angle	[°]
β_{100}	Thermoviscosity @ 100°C	[cSt/°C]
β_{40}	Thermoviscosity @ 40 °C	[cSt/°C]
ϵ	Case surface emissivity	[/]
ϵ_α	Transverse contact ratio	[/]
ϵ_β	Overlap contact ratio	[/]
ϵ_γ	Total contact ratio	[/]
η	Dynamic viscosity	[mPa.s]
Λ	Specific lubricant film thickness	[/]
λ_c	Cut-off filter	[mm]
μ	Friction coefficient	[/]
μ_m	Average friction coefficient	[/]
ν	Kinematic viscosity	[mm^2/s]
$v_{\sum c}$	Sum velocity at pitch point	[m/s]
ω_{in}	Rotational speed	[rad/s]
ρ	Specific weight	[Kg/m^3]
ρ_c	Equivalent curvature radius at pitch point	[mm]
σ	Equivalent roughness	[μm]

Introduction

During the last decades, the need to reduce energy consumption, lead companies and their engineers, to search new ways of reducing power losses in mechanical gear power transmissions. This can be accomplished by developing new and more efficient gear geometries, better suited oils, as well as, new combination between lubricants, geometry's and lubricant volume.

The environmental awareness is leading to a growing interest in biodegradable low-toxicity lubricants. Biodegradability is considered to be accomplished when industries start to use biodegradable base fluid in their machines, but low-toxicity requires the use of an environmental beneficial additivation [13].
However, the main goal in industrial application is not only to improve performance, but also, to find out technical and economical advantages.

Lubricant performance (friction, wear, lifetime, load bearing, efficiency, etc.) has an important contribution to the global environmental blame, since premature wear or high energy needs are harmful to the environment. The technical performance of gear oils must be demonstrated in power loss, scuffing and micropitting gear tests [13].

An important factor that contributes to oil aging, wear, scuffing, pitting and micro-pitting, load capacity of the gears is the high oil operating temperatures, so besides load carrying capacity rating also thermal rating of a gear drive is important [14].
Thus, the major concerns in the modern gearboxes, are achieving low operating temperatures, low power losses and high efficiencies, in which gear materials and oils can have significant influence.

Inside the gearbox, there are: churning losses, bearings and seals losses, and also friction losses generated in gears and bearings.
Churning losses are related to moving parts immersed in the oil sump and friction losses are generated in the contacts between gear teeth, between rolling elements and raceways in rolling bearings [13].

The most influent parameters that dictate friction power loss are load, geometry and friction coefficient, and there are lots of options available to control these parameters [8, 14].

Years of investigations, concluded that, some precious steeps could be followed in order to accomplished an improvement in low-loss gears.

Some steep can be assumed as unconventional, but already proven to work in the increase of gear efficiency and power saving. This is not a unidirectional process, but an progressive and iterative process.

Some of the parameters that can be modified are: [8].

i. Corrections for load reduction in areas of contact with high sliding speed;

ii. Reduction of module down to tooth root fracture limit;

iii. Reduction of transverse contact ratio down to pitting capacity limit;

iv. Tooth root fillet radius as large as possible;

v. Increase of pressure angle;

vi. Increase of face width;

vii. Helix angle for adequate overlap contact ratios;

The idea of creating and developing the "Low Loss Gear", came from the concept that it is possible to reduce the coefficient of friction in the teeth contact during the meshing cycle.

To do so, there are different approaches [9]:

a) Reduce the specific sliding by changing the tooth geometry;

b) Chose a lubricant that promotes a lower friction;

c) Or a combination of both approaches, if possible.

When submitted to the same torque the normal gear generate more heat than the new low loss gears [11].

The low loss gears can be produced with ordinary day-by-day tools, present in any tool-shop, and they do not need any particularly or expensive procedure.

The main objective of this work, is to study the various influences of:

a) Gear Geometry (310, 410, 610);

b) Gear Materials (Carburized steel and Austempered Ductil Iron (ADI));

c) Gear base lubricant oils (E1 (ester) and P1 (PAO));

d) Oil level (Standard (1500cm^3) and reduced (1000cm^3));

The gear geometries used in this experimental work were previously calculated using an computer software. Three gears with different low-loss geometries were defined, aiming progressive degrees of friction reduction. Several gear pairs were built accordingly, both in carburized steel and ADI [11].

1. Gear Tribology

The term tribology descends from the addition of the Greek words: “Tribos” and “logos”, the first one means friction and the second science. It means: the science and technology of friction, lubrication and wear, and it is a very important element of engineering [15, 16].

The term tribology first appears in the late sixties, when the engineers concluded that it was needed to study the problems in the interacting surfaces, they found out that the problem was not only pour maintenance or lubrication, but also a problem of machine design [15, 16].

Some industries responsible for designing and producing mechanical equipments, submitted to hard environments, huge workloads and high temperatures, have to implement tribological practices in order to prevent excessive wear and breakdowns. This type of science leads to a minimization of the cost caused by failures in the industrial equipments. The application of tribological knowledge becomes even more important since there is a reduction of natural resources and energy in today’s planet [15, 16].

1.1. Gear Design

This section presents and applies the concepts of contact mechanics and the elastohydrodynamic lubrication, and studies, the contact between the teeth of an helical gear along the contact path. The concept of EHD Contact and Lubrication Mechanics will be applied in order to determine the contact pressure and stresses, the film thickness and the oil and surface temperatures.

In this work, three different gear geometries were adopted, 310, 410 and 610, respectively.

Their main characteristics are presented in Table 1.1.

Gear Parameters	**Symbol**	**[units]**	**310**		**410**		**610**	
			pinion	**wheel**	**pinion**	**wheel**	**pinion**	**wheel**
Module	m	[mm]	2.5		2.25		1.75	
Working pressure angle	α_{wt}	[°]	22.12		26.7		28.34	
Number of teeth	Z	[-]	28	42	30	45	38	57
Gear ratio	u	[/]	1.5					
Teeth width	b	[mm]	20					
Helical angle	β	[°]	15					
Pitch diameter	d	[mm]	72.47	108.7	69.88	104.82	68.85	103.27
Base diameter	d_b	[mm]	67.81	101.72	65.39	98.09	64.42	96.64
Addendum mod. Coef.	x	[-]	0.13	0.25	0.96	1.15	1.74	1.95
Tip diameter	d_a	[mm]	78.05	114.89	77.5	113.29	76.41	111.56
Tip diam. Mod. Coef.	k*m	[mm]	-0.03		-0.61		-1.02	
Working pitch diameter	d_w	[mm]	73.2	109.8	73.2	109.8	73.2	109.8
Transverse contact ratio	ϵ_α	[-]	1.52		1.17		0.93	
Overlap contact ratio	ϵ_β	[-]	0.66		0.73		0.94	
Total contact ratio	ϵ_γ	[-]	2.18		1.9		1.87	
Path of contact (length)	g	[mm]	11.58		8.02		4.97	
Tooth flank roughness	R_a	[mm]	0.5 ± 0.1					
Power	P	[W]	50776					
Torque	T	[N.m]	215.6	323.4	215.6	323.4	215.6	323.4
Rotational velocity	n	[rpm]	2250	1500	2250	1500	2250	1500
**Considering an ester-based fully saturated gear oil, ISO VG 100.								

Table 1.1.: Geometric characteristics and working conditions of 310/410/610 gears.

1.1.1. Contact length in helical gears

The dimension of the meshing line and the average contact length were obtained using the deduction made by P. Velex and M. Maatar [17] and is presented in this sub-chapter (Equation 1.1 and Equation 1.4).

This deduction shows that in a determined period a particular line enter the contact and it will pass for each point (ABCDE) and then it will leave the contact zone (see Figure 1.1), reentering some period P after. The period P its based on the velocity of the gear, but since the function is periodical, there is not needed to know the exact value of the period P, it must only be higher than the time needed to accomplish one complete turn of the gear set.

Multiplying the line distribution to the average length of the gear width, (see Equation 1.5), total distribution of the contact length in the contact zone is obtained, as it is shown in Figure 1.2.

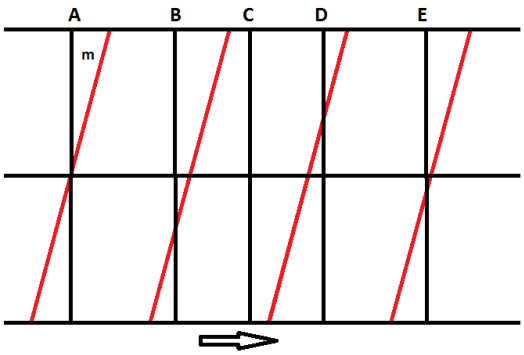

Figure 1.1.: Contact path representation.

The determination of the contact length $L(\tau)$, (Equations 1.1 to 1.7), was implemented in Matlab®.

As shown in Figure 1.1, tooth flank (m) enters the meshing zone, passes through points A, B, C, D and E of the contact path and exits the meshing zone. It will reenter the meshing zone after some period P.

$$\overline{L}(\tau) = 1 + \sum_{K=1}^{\infty} \left[A_k \cos(2\pi k\tau) + B_k \sin(2\pi k\tau)\right] \tag{1.1}$$

with,

$$A_k = \frac{1}{2\epsilon_\beta \epsilon_\alpha \pi^2 k^2} \left[\cos(2\pi k\epsilon_\beta) + \cos(2\pi k\epsilon_\alpha) - \cos(2\pi k(\epsilon_\alpha + \epsilon_\beta)) - 1\right] \tag{1.2}$$

$$B_k = \frac{1}{2\epsilon_\beta \epsilon_\alpha \pi^2 k^2} \left[\sin(2\pi k\epsilon_\beta) + \sin(2\pi k\epsilon_\alpha) - \sin(2\pi k(\epsilon_\alpha + \epsilon_\beta))\right] \tag{1.3}$$

$$L_m = \frac{b\epsilon_\alpha}{\cos(\beta_b)} \tag{1.4}$$

$$L(\tau) = \overline{L}(\tau) \cdot L_m \tag{1.5}$$

$$L_{min} = min\,[L(\tau)] \tag{1.6}$$

$$L_{max} = max\,[L(\tau)] \tag{1.7}$$

$\tau = \frac{t}{T_m}$ is an normalized time, and being T_m the mesh period

k - is the number of polynomials used in the Fourier series approximation

ϵ_α the transverse contact ratio

ϵ_β the overlap contact ratio

The values obtained for L_{min} and L_{max} are shown in the Table 1.2, for the gears 310, 410 and 610.

		Gears		
	Units	310	410	610
L_{min}	mm	26.297	20.6192	19.1159
L_{max}	mm	36.9655	25.3934	20.3976

Table 1.2.: Values of contact length for 310/410/610 gears.

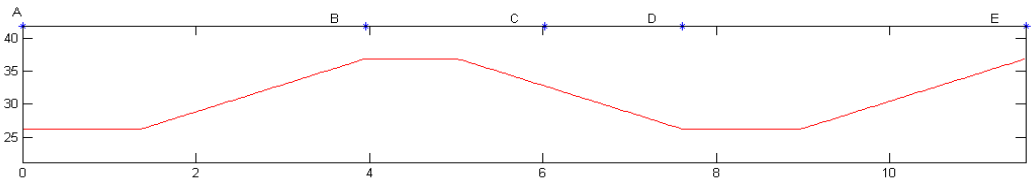

Figure 1.2.: Length distribution in the contact path for helical gear.

1.1.2. Load between contacting flanks

The load applied to the tooth flanks is applied at the middle of the width, at the point of tangency of the pitch circles, in the pinion. This load designated as Normal Load (Equation 1.11) and in the case of the helical gears it generates three components, because of the influence of two angles: β and α [1].

The three components of F_n are:

1. Tangential load (F_t)

$$F_t = \frac{2000 \times n_1}{d_1} = \frac{2000 \times n_2}{d_2} \tag{1.8}$$

2. Radial load(F_r)

$$F_r = \frac{F_t \times \tan(\alpha_n)}{\cos(\beta)} \tag{1.9}$$

3. Axial load (F_x)

$$F_x = F_t \times \tan(\beta) \tag{1.10}$$

The normal load is given by:

$$F_n = \frac{F_t}{\cos(\beta) \times \cos(\alpha_n)} \tag{1.11}$$

The normal load (Equation 1.11) and all is components are transported to the wheel.

In spur gears the load is distributed along the meshing line, and there is at least one tooth engaged in the process, so the length of the meshing line is equal to the face width.

This happens when the contact takes place between the points “B” and “D”, before and after, there are two tooth engaged. The distribution of the load between the points “B” and “D” its equal to the load it self, and before and after it is divided by two as is shown in Figure 1.4b.

In helical gears it is different, because at any time there are more than one teeth engaged, as it was shown in subsection 1.1.1, so the load follows a different distribution on the path of contact as is shown in Figure 1.4c.

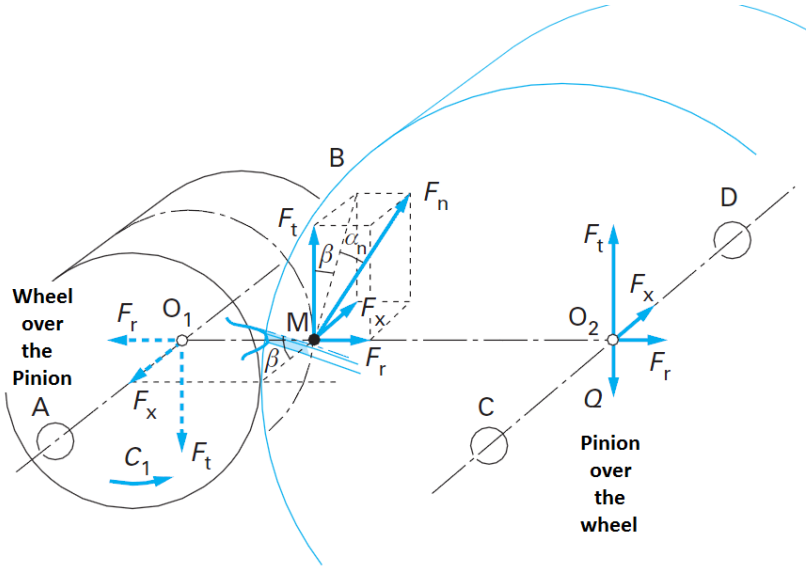

Figure 1.3.: Contact loads in helical gears [1].

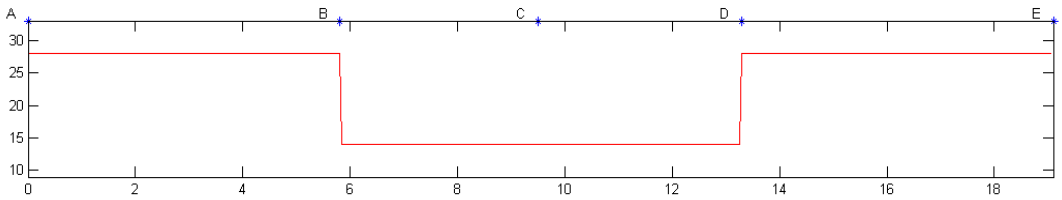

(a) Contact length in the path of contact for a spur gear.

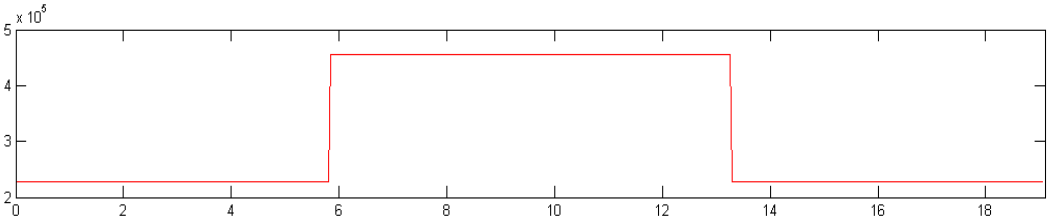

(b) Load distribution in a spur gear.

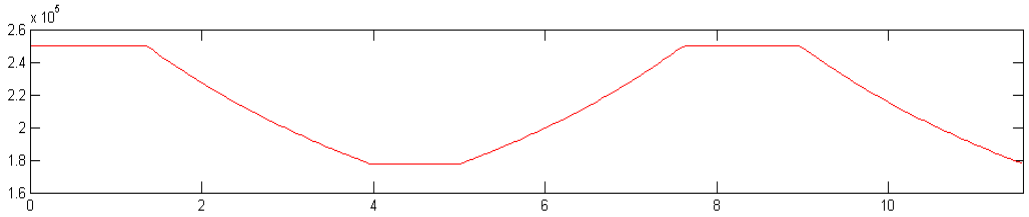

(c) Load distribution in a helical gear.

Figure 1.4.: Teeth normal contact load.

1.1.3. Radius of Curvature

The radius of curvature is an important gear parameter, because it influences the contact between gear tooth in a point. At any point M of the contact path, the contact between tooth flanks can be simulated by "Osculating discs" and the corresponding radius of curvature.

The equivalent radius of curvature can be defined for the path of contact, using Equation 1.12 [2].

$$R_M = \left[\frac{1}{2} \times \left(\frac{1}{R_{x1}} + \frac{1}{R_{x2}}\right)\right]^{-1} \tag{1.12}$$

Where,

- R_{x1} is the radius of the pinion surface and is equal to $\overline{T_1 M}$ (see Figure 1.5).
- R_{x2} is the radius of the wheel surface and is equal to $\overline{T_2 M}$ (see Figure 1.5).

A representation of the equivalent curvature radius, for the three chosen geometries (310 410 610), can be seen in the Figure 1.6.

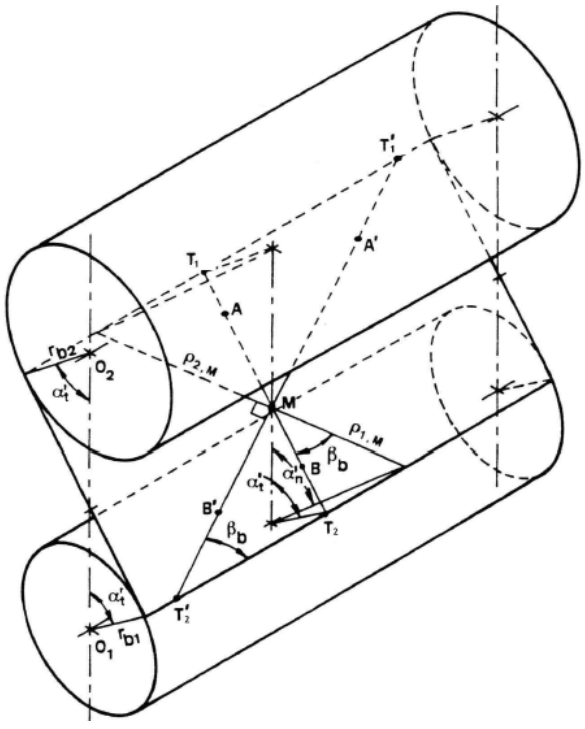

Figure 1.5.: Generic points in the contact path for helical gears [2].

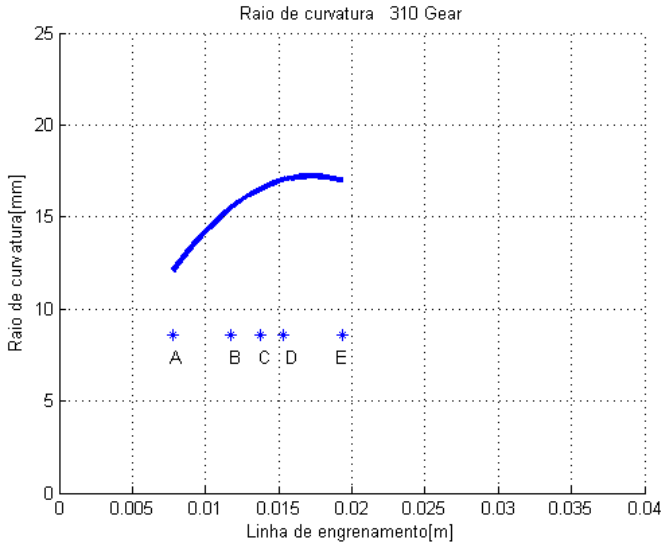

(a)

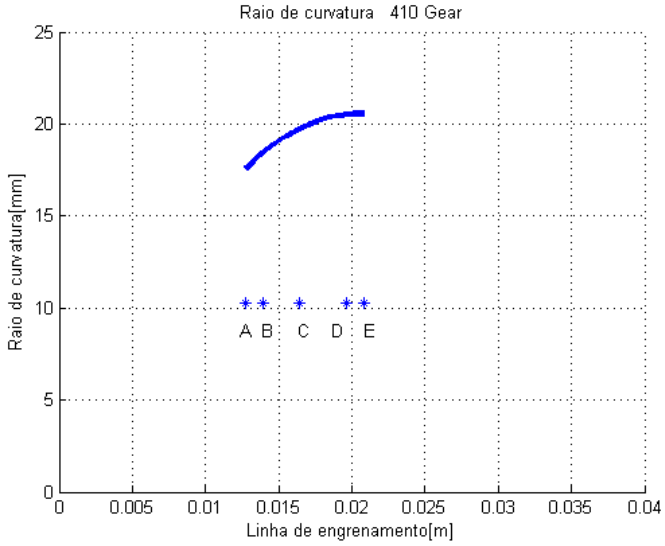

(b)

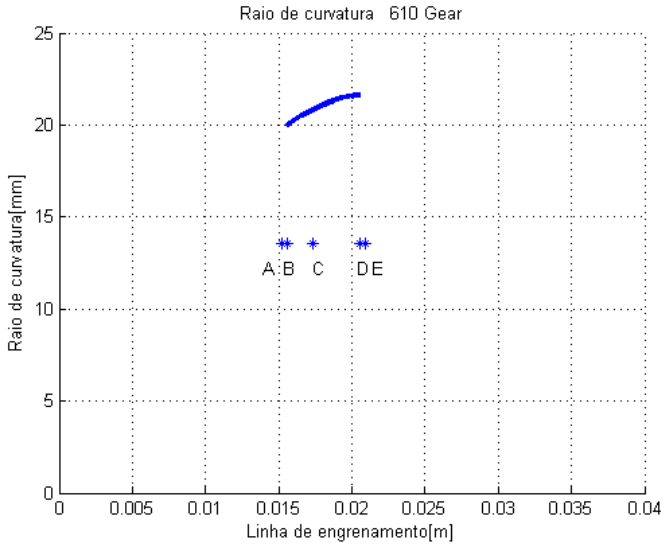

(c)

Figure 1.6.: Equivalent radius of curvature for gears: a) 310, b) 410 and c) 610.

1.1.4. Contact pressure and shear stress variation along the contact path

The Hertz pressure or contact pressure, p_0 or p_h, can be calculated along the contact path, using Hertz theory. This theory considers that the contact between two solid elastic discs happens in a linear path (Equation 1.12). It is calculated using the Equation 1.13, where L_{min} is the minimum value that the length of the path of contact takes during the gearing (shown in subsection 1.1.1) [2].

$$p0 = ph = \sqrt{\frac{2 \cdot F_N \cdot E^*}{\pi \cdot L_{min} \cdot R_M}} \tag{1.13}$$

F_N is the normal contact load, b is the gear face width, R_M is the equivalent radius of curvature and E^* is the equivalent Young's modulus for two contacting solids (Equation 1.14).

$$E^* = \left[\frac{1-\nu_1^2}{E_1} + \frac{1-\nu_2^2}{E_2}\right]^{-1} \tag{1.14}$$

Materials Young's modulus (E) and the Poisson coefficients (ν) are, E_1, ν_1 and E_2, ν_2, respectively for the pinion and wheel.

A rectangular contact area generated by teeth contact, is defined by $2 \cdot a$ and L_{min}, being "a" the Hertzian contact half-width (Equation 1.15).

$$a = \sqrt{\frac{2 \cdot F_N \cdot R_M}{\pi \cdot L_{min} \cdot E^*}} \tag{1.15}$$

The variation of the Hertzian contact pressure, and the variation of the Hertzian half-width along the meshing line can be seen in the Figure 1.7 and Figure 1.8 respectively, for all 3 geometries.

Through Hertz theory for two contacting solids and Boussinesq theory for the elastic half-space, it is possible to evaluate the stress state in the sub-surface of contacting tooth [2].

σ_{xx} and σ_{zz} stresses along OZ have their maximum compression near the surface, being equal to maximum Hertz pressure p_0, and the maximum shear stress

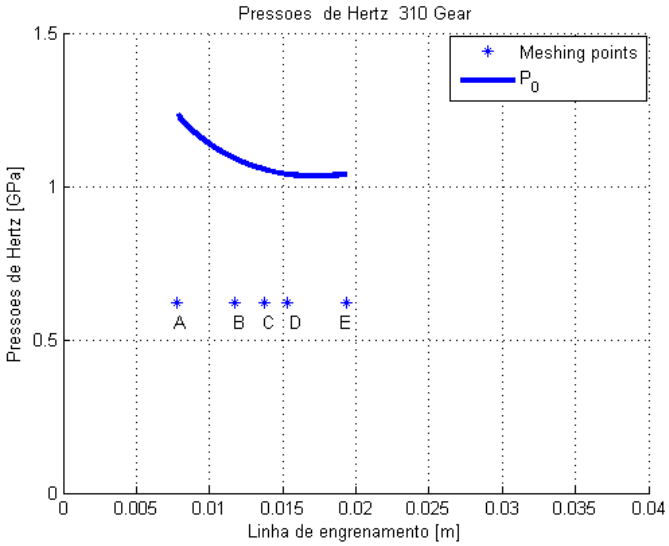

(a)

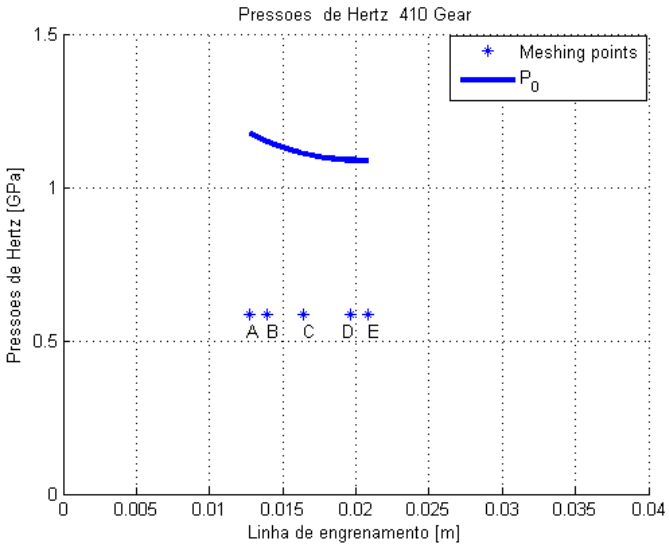

(b)

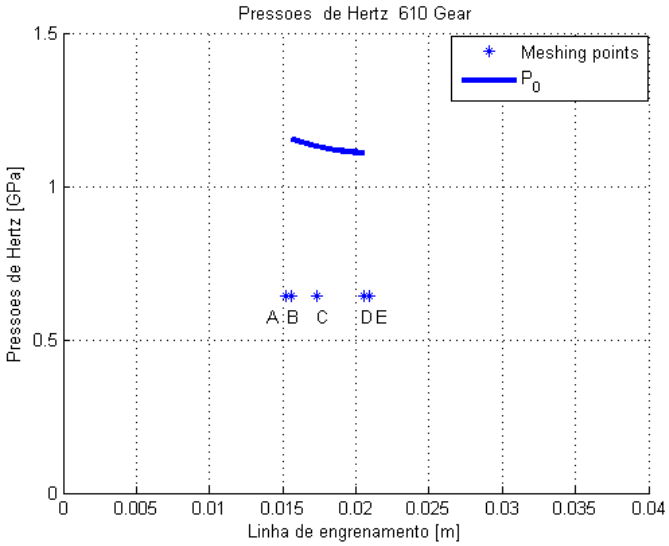

(c)

Figure 1.7.: Hertzian contact pressure for gears: a) 310, b) 410 and c) 610.

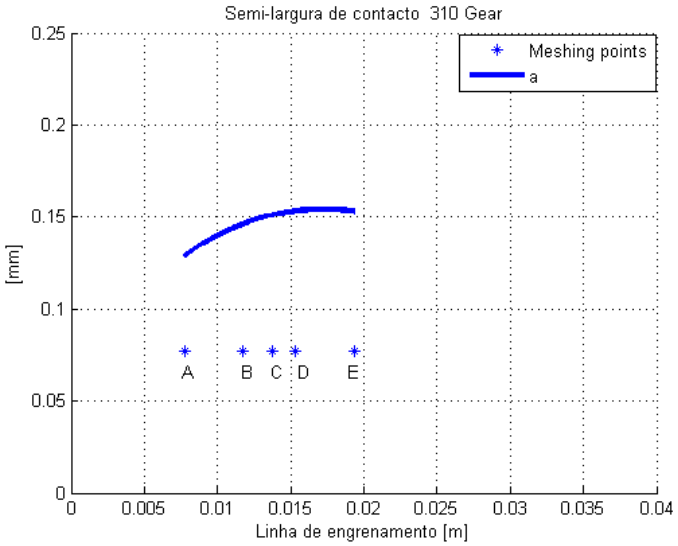

(a)

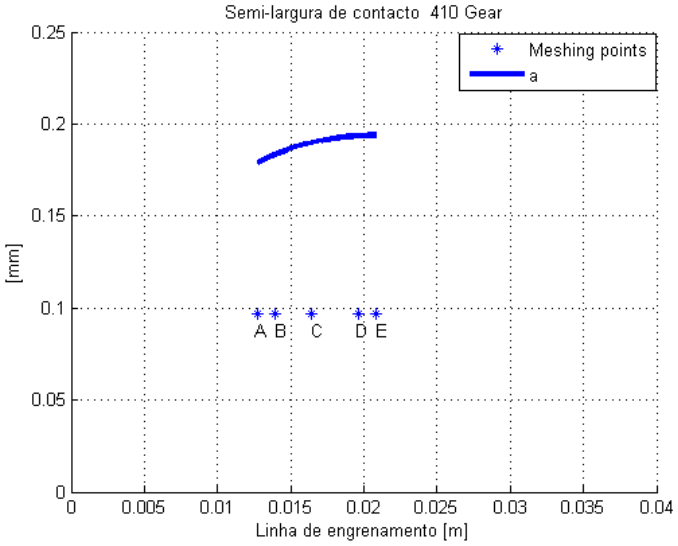

(b)

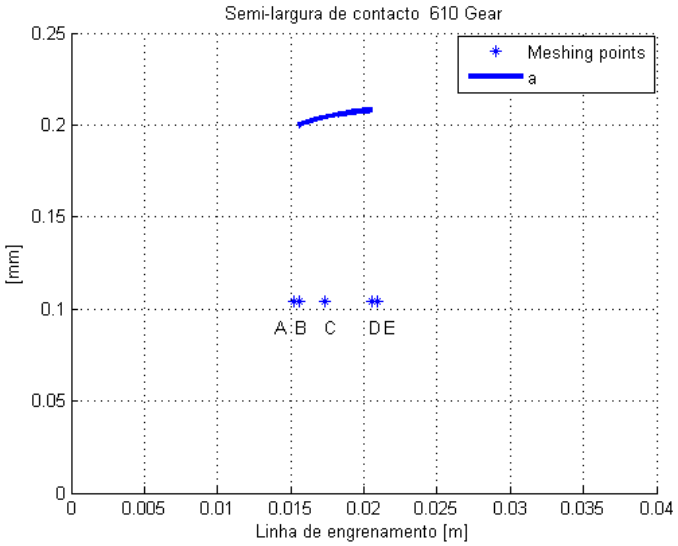

(c)

Figure 1.8.: Hertzian half-width for gears: a) 310, b) 410 and c) 610.

τ_{max} reaches its higher value over OZ [2].

The Maximum shear stress can be calculated using the Equation 1.16.

$$\tau_{max} = 0.3 \cdot p_0 \tag{1.16}$$

The depth Z_s where the maximum shear stress reaches its maximum value, is calculated by Equation 1.17.

$$Z_s = 0.786 \cdot a \tag{1.17}$$

The maximum value that the orthogonal shear stress is defined by Equation 1.18.

$$\tau_{xz}^{max} = \tau_0 = 0.25 \cdot p_0 \tag{1.18}$$

The depth Z_0 where τ_0 reaches its maximum value is given by Equation 1.19.

$$Z_0 = 0.42 \cdot a \tag{1.19}$$

Both the maximum shear stress and the orthogonal shear stress are presented in the Figure 1.9, and the corresponding depths are given in Figure 1.10, for the three gears used.

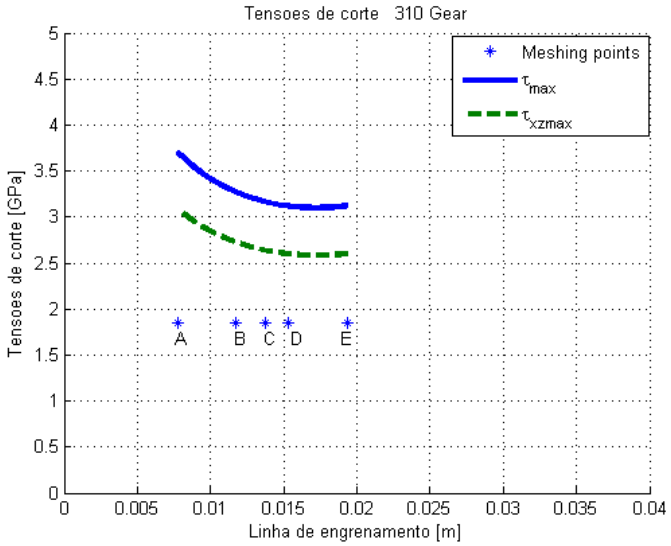

(a)

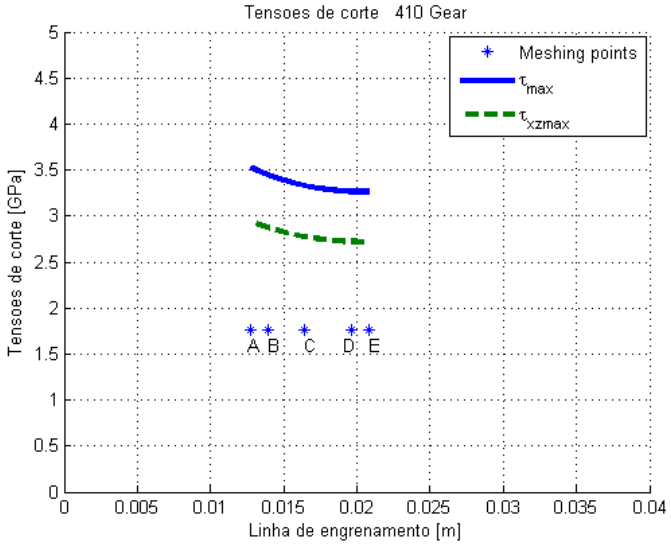

(b)

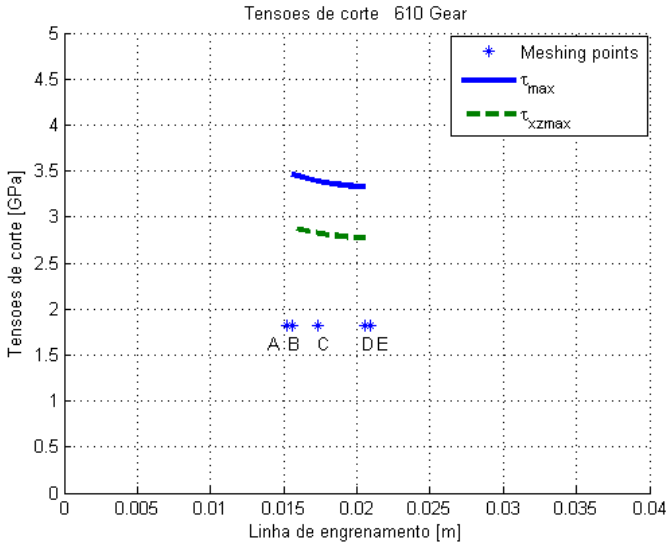

(c)

Figure 1.9.: Shear stresses for gears: a) 310, b) 410 and c) 610.

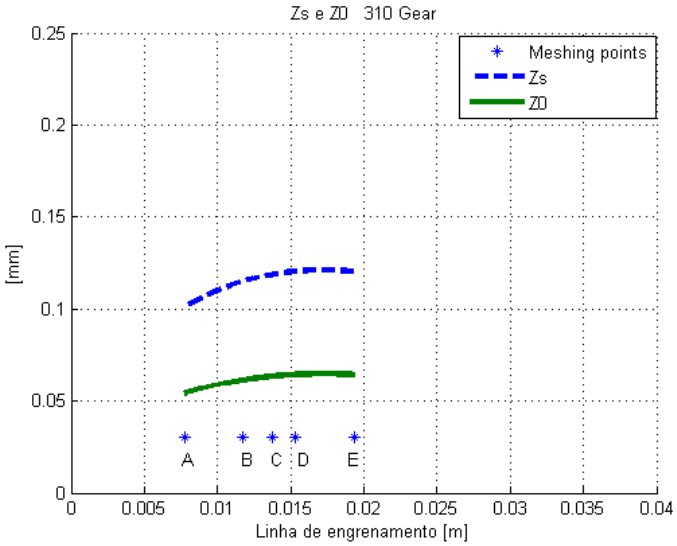

(a)

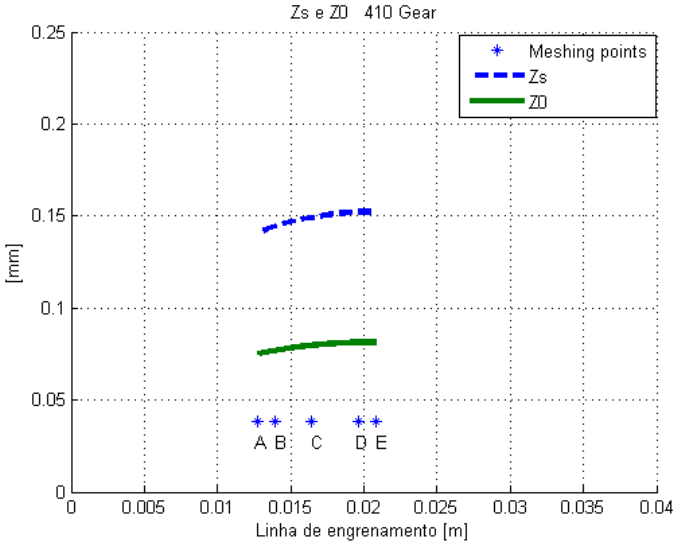

(b)

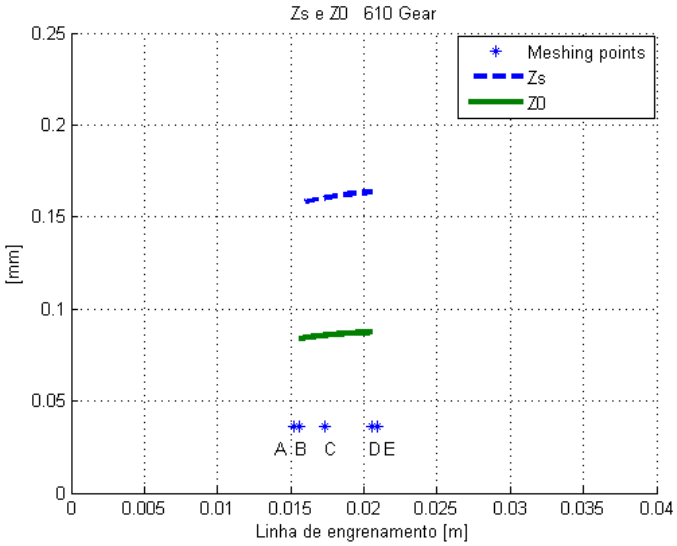

(c)

Figure 1.10.: Shear stress depth (Z_s and Z_0)variation for gears: a) 310, b) 410 and c) 610.

1.1.5. Surface velocities

Considering a generic point M from the contact path placed between points A and B, the absolute velocities of point M, belonging to the two surfaces in contact, are designated by V_1 and V_2, Figure 1.11, and their projections in a perpendicular direction to the contact path respectively U_1 and U_2.

The contact point, M, velocity along the contact path is translated by the projection of V_1 and V_2 velocities in the direction of the contact path, and it is defined by V.

The tangential velocity U_1 and U_2 of an generic point M in the contact path, located between points A and B at the length AI, or a different point N located at the distance IB, as is shown in the Figure 1.12. U_1 and U_2 can be determined with the Equation 1.20 and 1.21 respectively.

$$U_1 = \overline{T_1 M} \cdot \omega_1 = \rho_1 \cdot \omega_1 \tag{1.20}$$

$$U_2 = \overline{T_2 M} \cdot \omega_2 = \rho_2 \cdot \omega_2 \tag{1.21}$$

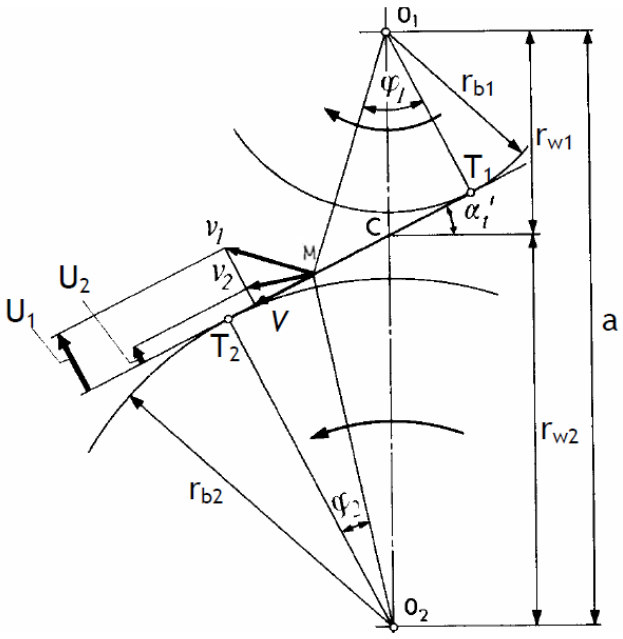

Figure 1.11.: Velocities V_1 and V_2 of generic point M of the contact path [2].

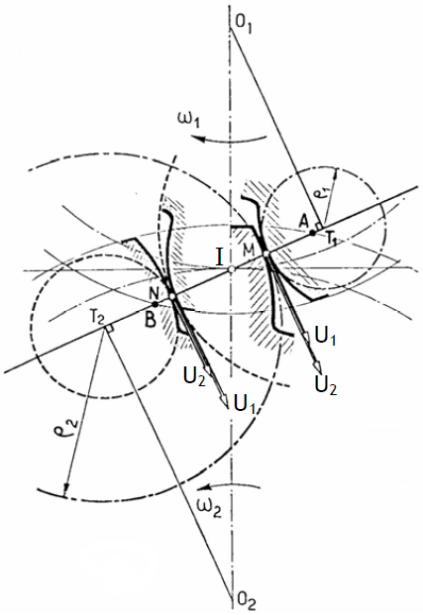

Figure 1.12.: Tangential velocities U_1 and U_2 of generic point M of the contact path [2].

The sliding velocity can be calculated using the Equation 1.22.

$$V_s = U_2 - U_1 = (\rho_2 \cdot \omega_2) - (\rho_1 \cdot \omega_1) \tag{1.22}$$

The discs with radius ρ_1 and ρ_2, present in the Figure 1.12, are the osculating discs and can be used to simulate contact between gears teeth.

In Figure 1.13 the rolling and sliding velocities at each point of the contact path are presented. Observing this figure it is clear that the sliding speed is negative in the approximation to the point I, and then, when it reaches the point I there is no sliding. When it passes the pitch point it changes to positive and as further it move to the end of contact the sliding velocity becomes higher reaching its maximum in the end of meshing line (point B) [2].

Figure 1.13 also shows the specific sliding, that can be defined by the Equations 1.23 and 1.24.

$$\gamma_1 = \frac{U_1 - U_2}{U_1} \tag{1.23}$$

$$\gamma_2 = \frac{U_2 - U_1}{U_2} \tag{1.24}$$

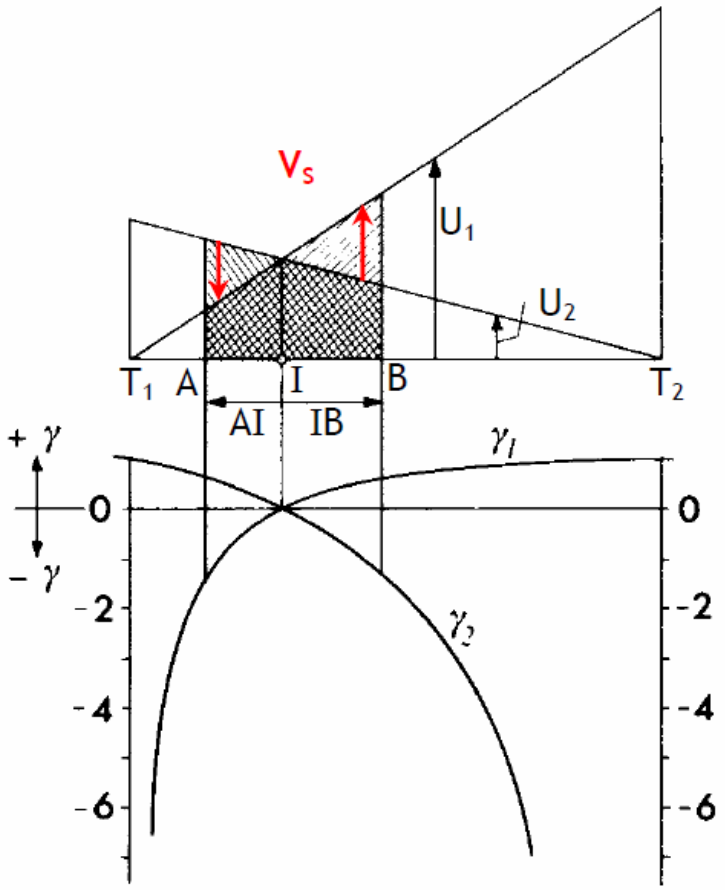

Figure 1.13.: Variation of tangential velocities along the contact path [2].

Both the tangential and the sliding velocities variation along the contact path can be observed in the Figure 1.14 and the specific sliding is shown in Figure 1.15, for the three gear geometries.

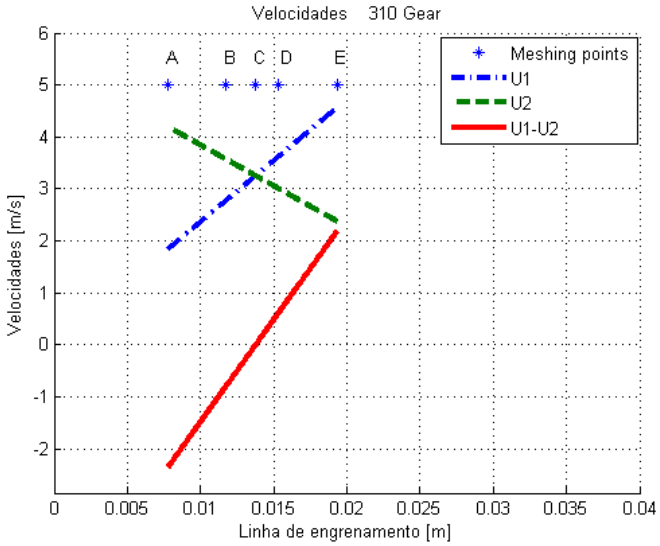

(a)

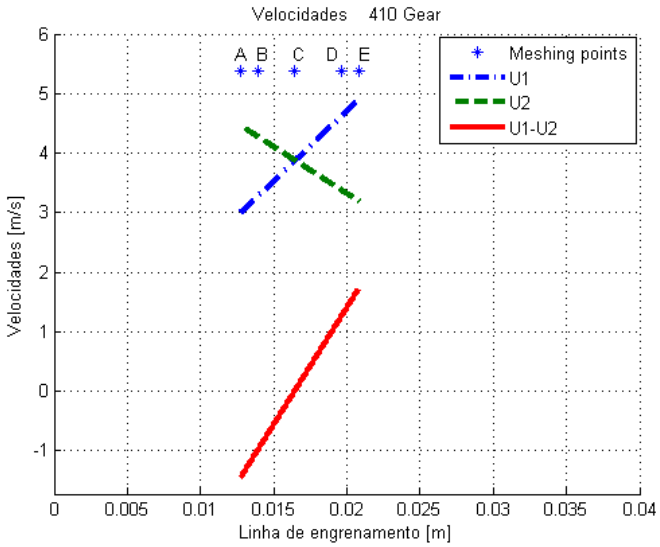

(b)

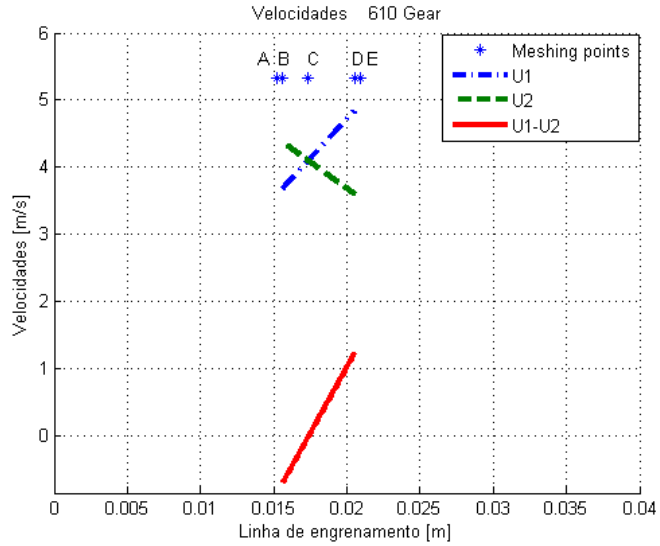

(c)

Figure 1.14.: Variation of sliding and tangential velocities the contact path for gears: a) 310, b) 410 and c) 610.

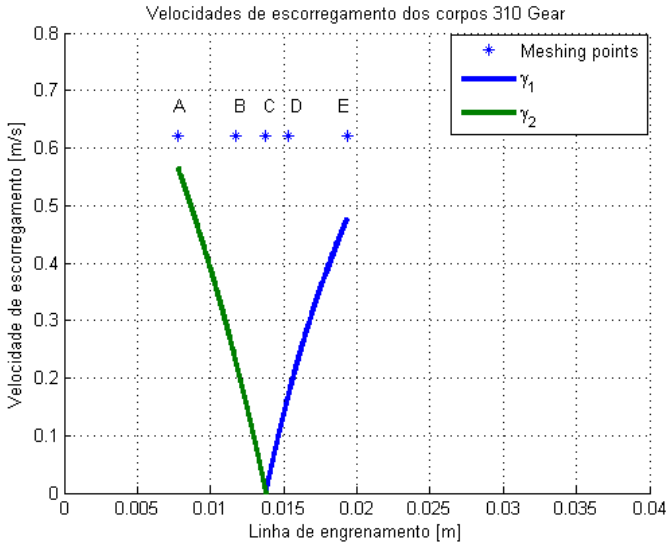

(a)

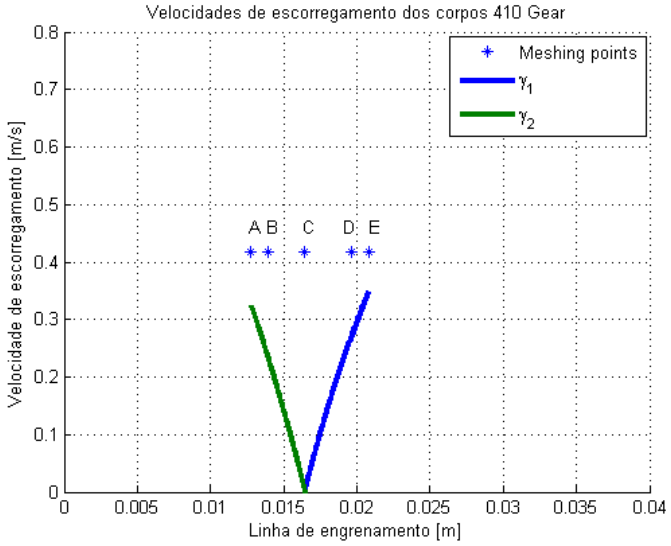

(b)

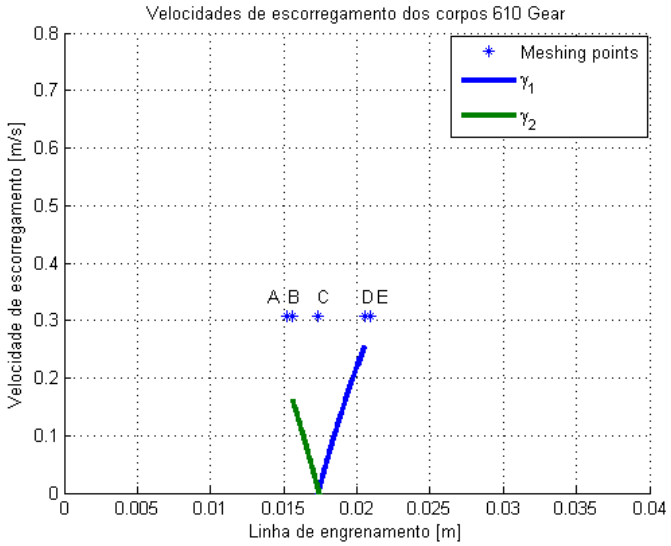

(c)

Figure 1.15.: Specific sliding the contact path for gears: a) 310, b) 410 and c) 610.

1.1.6. Lubricant film thickness

In lubricated contacts where high external loads per unit area are applied, the elastohydrodynamic lubrication (EHL) in the dominant lubrication mechanism.

If the surfaces roll, slide or spin relative to each other, the lubricant will be dragged into the converging gap of the contact due to the shear stresses exerted on the lubricant from the surfaces, and this can be observed in Figure 1.16 [18].

The lubricant film thickness between gear tooth can be estimated using the D. Dowson and G.R. Higginson equation [19], under isothermal conditions, smooth surfaces and fully flooded [2].

According to Dowson and Higginson [19,20] the lubricant film thickness inside a elastohydrodynamic linear contact is presented in Figure 1.16.

The film thickness in the center of contact h_0 and the minimum lubricant film thickness h_m are expressed in Equation 1.25 and Equation 1.26 respectively. They can be seen in Figure 1.17 for all gear geometries.

$$h_0 = 0.975 \cdot R_M \cdot U^{0.727} \cdot G^{0.727} \cdot W^{-0.091} \tag{1.25}$$

$$h_m = 1.325 \cdot R_M \cdot U^{0.7} \cdot G^{0.54} \cdot W^{-0.13} \tag{1.26}$$

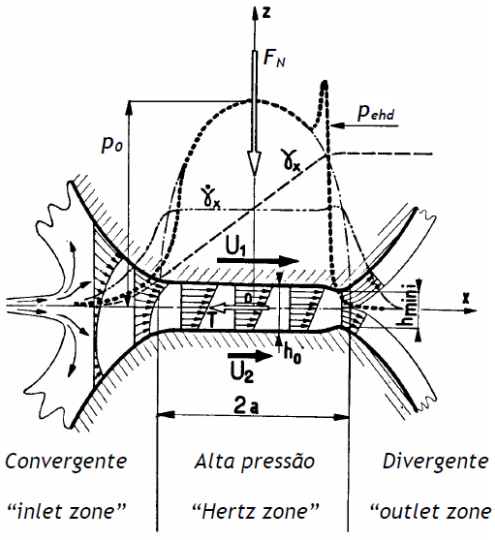

Figure 1.16.: Center and minimum film thickness [2].

Where,

U is the velocity parameter:

$$U = \frac{\eta_0 \cdot (U_1 + U_2)}{2 \cdot R_M \cdot E^*} \tag{1.27}$$

G is the material parameter:

$$G = 2 \cdot \alpha \cdot E^* \tag{1.28}$$

W is the load parameter:

$$W = \frac{F_N}{R_M \cdot L_m in \cdot E^*} \tag{1.29}$$

η_0 - Lubricant dinamic viscosity at lubricant feeding temperature;

α - Lubricant Piezoviscosity coefficient at lubricant feeding temperature;

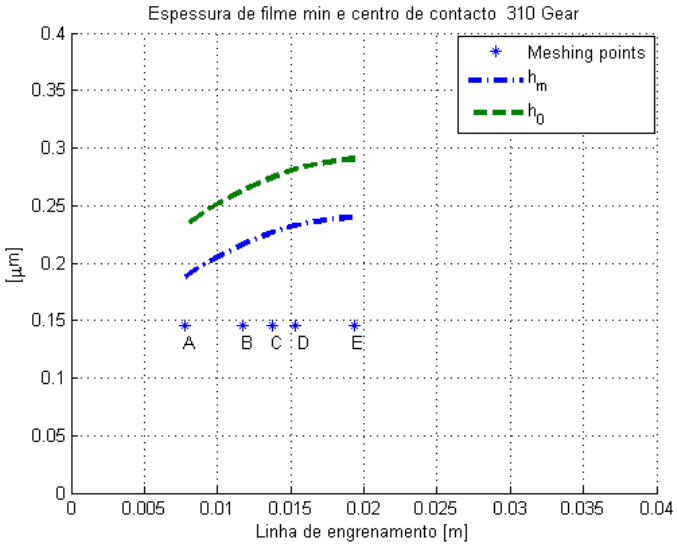

(a)

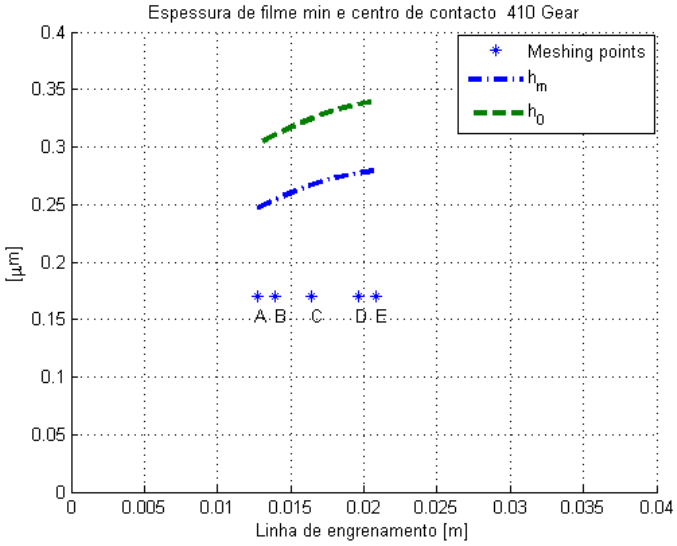

(b)

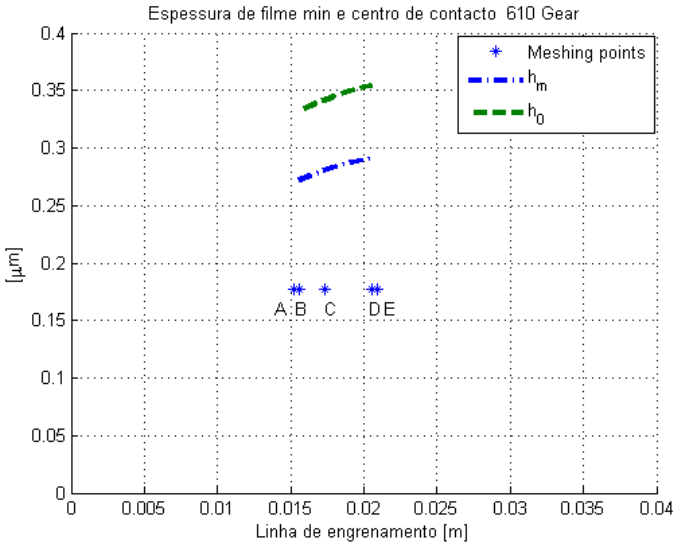

(c)

Figure 1.17.: Center and minimum film thickness along the contact path for gears: a) 310, b) 410 and c) 610.

1.1.7. Inlet shear heating in an EHD contact

EHD classic theories, considering that the flow inside an EHD contact is isothermal, are not valid for gears, due to the intense sliding between the contacting surfaces along the contact path.

In the convergent part of the gearing, a significant power dissipation and temperature rise occurs, designated as"inlet shear heating". In this zone the lubricant is submitted to a high shear deformation caused by the pressure gradient, the rolling and sliding velocities. This shear deformation originates energy dissipation leading to a increase of the lubricant temperature (Δ_{Tf}), viscosity (η_{0T}) decrease and consequently, lubricant film thickness (h_{0T}) decrease. The decrease of lubricant film thickness is expressed by the factor ϕ_T, and the correct film thickness is obtained using Equation 1.30 [2].

$$h_{0T} = \phi_T \cdot h_0 \tag{1.30}$$

where,

$$\phi_T = 1 + 0.1[(1 + 14.8 \cdot V_e^{0.83}) \cdot L^{0.64}]^{-1} \tag{1.31}$$

$$V_e = \frac{|U_1 - U_2|}{|U_1 + U_2|} \tag{1.32}$$

$$L = \frac{\beta \cdot \eta_0 \cdot (U_1 + U_2)^2}{K_f} \tag{1.33}$$

β - Lubricant thermoviscosity coefficient at lubricant feeding temperature;

K_f - Lubricant thermal conductivity;

The new film thickness for the three chosen geometries can be seen in the Figure 1.18.

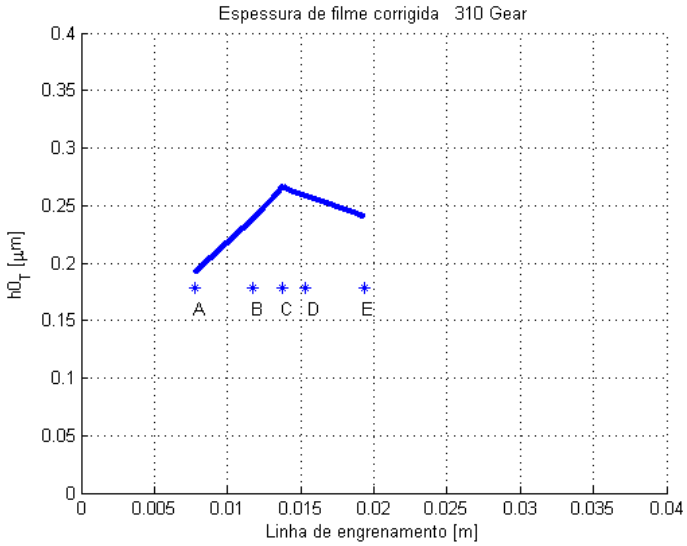

(a)

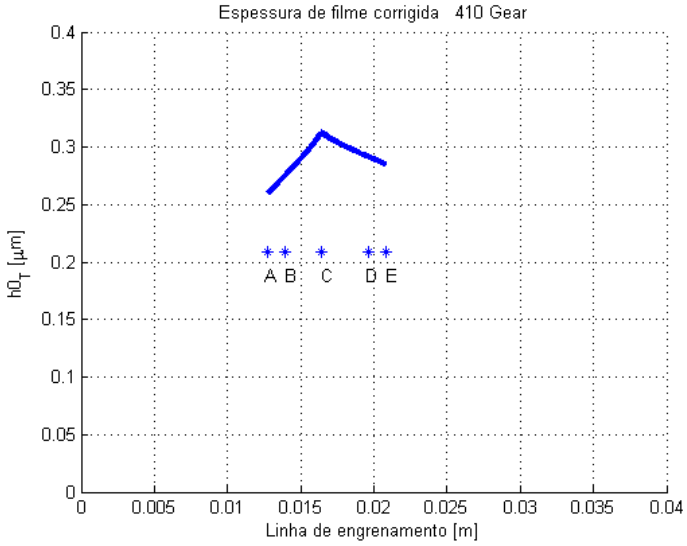

(b)

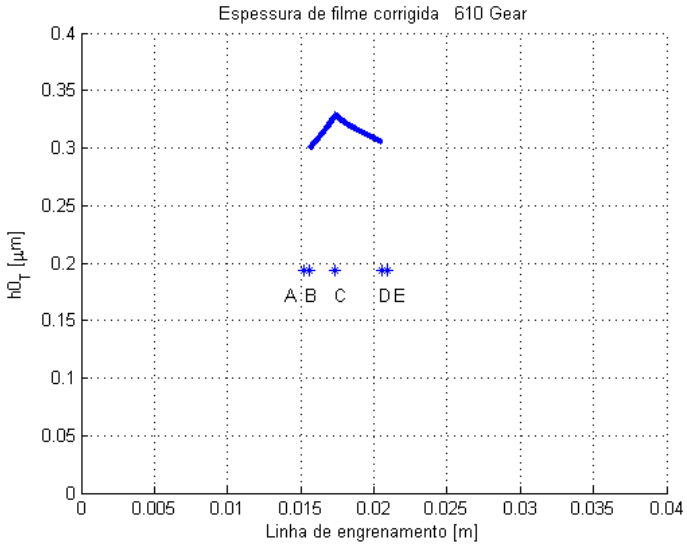

(c)

Figure 1.18.: Corrected center film thickness along the contact path for gears: a) 310, b) 410 and c) 610.

1.1.8. Specific lubricant film thickness

EHD analysis should take in account the surface roughness of the gear tooth flanks. This roughness is oriented in perpendicular direction to the rolling speed of osculating circles, and might have the same order of magnitude of the lubricant film thickness (Λ), typically less than 1μm. The elastic deformation of the tooth in contact must be also considered, instead of only considering the overall elastic deformation of the surface it must also considered the local deformations at the level of surface roughness.

The influence of roughness on the film thickness is analysed using the concept of specific lubricant film thickness. This parameter is defined using the Equation 1.34 [2].

$$\Lambda = \frac{h_{0T}}{\sigma} = \frac{h_{0T}}{\sqrt{(R_{q1})^2 + (R_{q2})^2}} \tag{1.34}$$

Where,

h_{0T} is the lubricant center film thickness with thermal correction;

$\sigma = \sqrt{(R_q1)^2 + (R_q2)^2}$ is the composed roughness of both contacting flanks;

The variation of specific film thickness along contact path is represented in Figure 1.19, for the gear geometries considered.

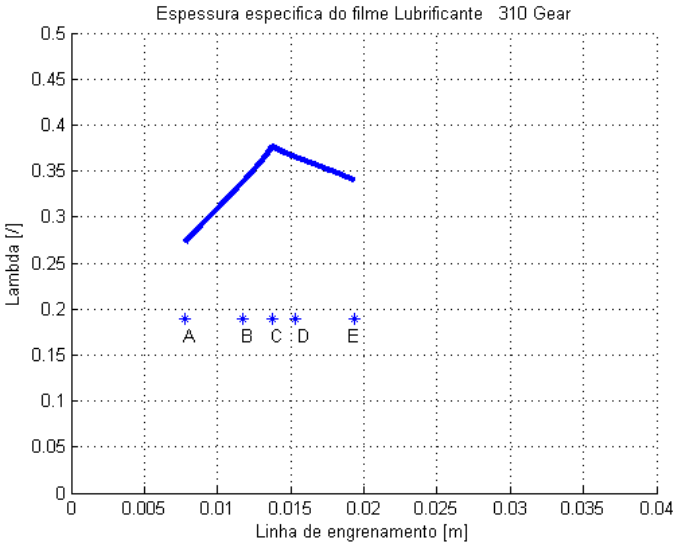

(a)

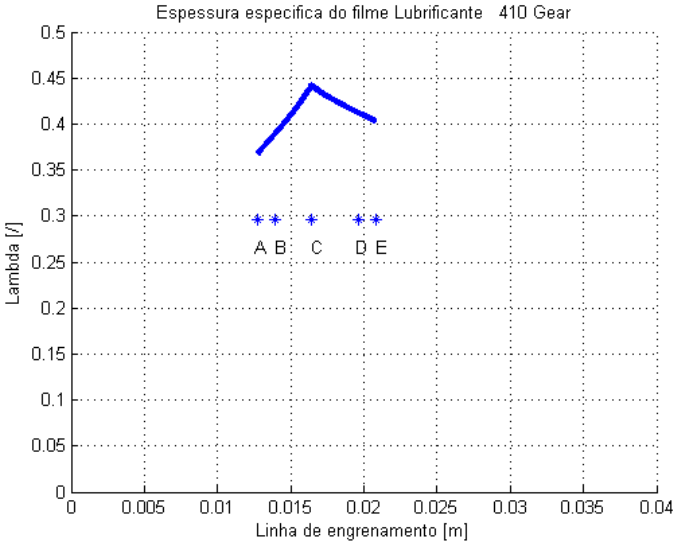

(b)

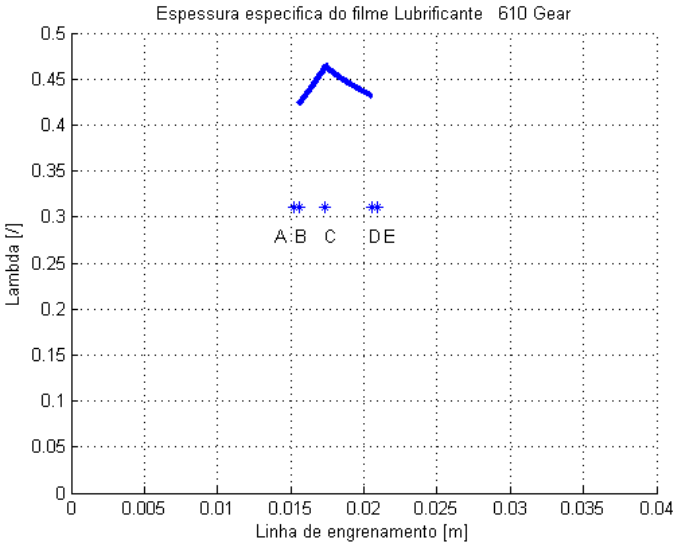

(c)

Figure 1.19.: Thermal corrected film thickness variation along the contact path for gears: a) 310, b) 410 and c) 610.

1.1.9. Lubricant regimes

If two surfaces get into contact, the transmitted load is supported by the roughness of each surface. During sliding, the force needed to shear these roughness is very high, and this causes an unbearable amount of friction, wear and surface damage. To reduce this problem a lubricant is deliberately introduced to separate the surfaces either totally or partially. If the lubricant used is an liquid or gas, it is called fluid film lubrication [21].

There are three possible lubrication regimes:

1. Full film lubrication
2. Mixed film lubrication
3. Boundary film lubrication

The first one refers to the total separation of the surfaces by a lubricant film thickness, ($\Lambda > 2$) (Figure 1.20a).
The second one refers to a partial first lubrication regime. In this case if part of the load is carried by the fluid pressure and the rest is supported by the surface roughness, ($0.7 < \Lambda < 2$) (Figure 1.20b).
The third means that there is no lubricant film present between the surfaces, so the normal load is supported by the roughness and so there is a metal-metal contact, ($\Lambda < 0.7$) (Figure 1.20c).

The specific lubricant film thickness changes along the contact path, so multiple lubrication regimes may occur.

It can be established a direct relation between the probability of failure, by contact fatigue or severe adhesive wear, and the specific lubricant film thickness Λ, in function of the sliding velocity and lubricant type (see Figure 1.21) [2].

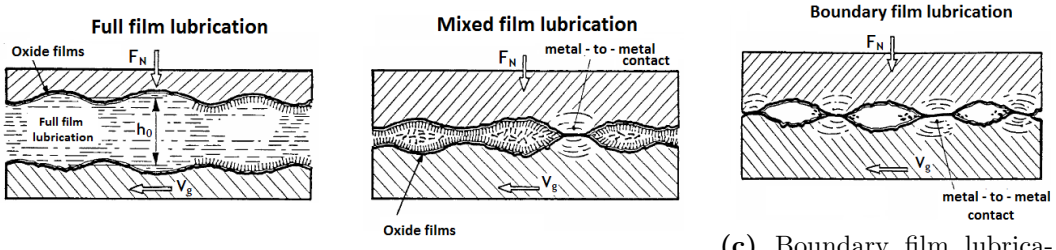

(a) Full film lubrication **(b)** Mixed film lubrication **(c)** Boundary film lubrication

Figure 1.20.: Lubrication regimes [2].

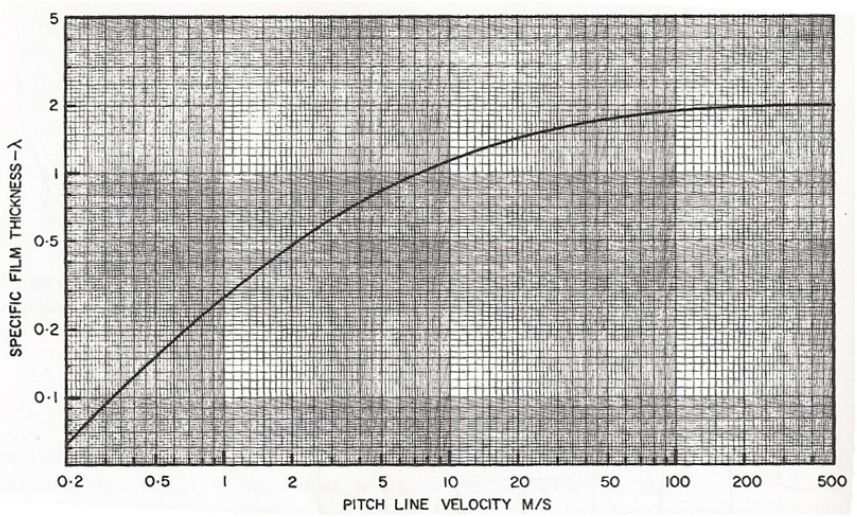

Figure 1.21.: Relation between 5% probability of failure and specific lubricant film thickness Λ.

1.1.10. Coefficient of friction in gear teeth

Friction between gear teeth is very important in the study of gears, because it controls every aspect in the contact between the teeth, e.g. heat generation, wear, film thickness, among others [22].

The friction load is quantified as a sum between the rolling resistance load (F_{TR}) and sliding friction load (F_{TS}). And the coefficient of friction (μ) is an relation between the Normal load (F_N) and the Tangential load (F_T), as it is shown in Equation 1.35.

$$\mu = \frac{F_T}{F_N} \tag{1.35}$$

The coefficient of friction is related to the specific lubricant film thickness, this same relation is usually represented by a group of curves that define the Stribeck curve Figure 1.22.

The definition of the coefficient of friction, applied to gears, is very complex, because in some cases several lubrication regimes can coexist along the contact path. The amplitude or orientation of the gear roughness have high influence on the coefficient of friction, which is higher if the surface roughness is oriented in the transverse direction [2].

It is common in the empirical formulation of this parameter to have into account experimental results gathered in discs machine tests or power dissipation

gear tests being this empirical results valid for all lubrication regimes.

There are four fundamental formulations that are commonly used in the calculation of the coefficient of friction:

1. Formulation according to DIN 3990
2. Formulation according to ISO 6336 standard
3. Kelly expression
4. Michaelis expression

In this work the coefficient of friction proposed by Michaelis will be used, being expressed by the Equation 1.36.

$$\mu_{Mich} = 0.048 \cdot \left[\frac{F_N}{L_{min} \cdot R_m \cdot (U_1 + U_2)}\right]^{0.20} \cdot \eta_0^{-0.05} \cdot R_a^{0.25} \cdot X_L \tag{1.36}$$

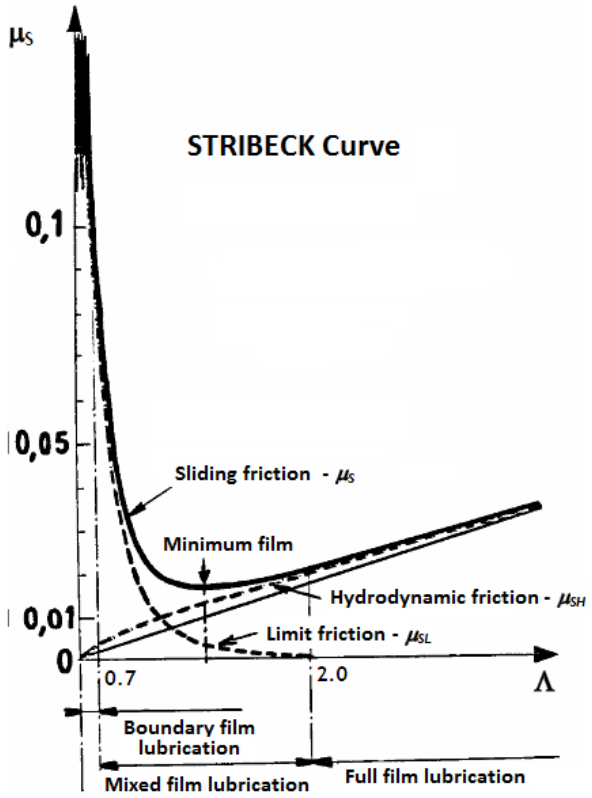

Figure 1.22.: Stribeck curve.

Where,

η_0 - Oil dynamic viscosity at oil bath temperature (m.Pa.s)

R_a - Equivalent average roughness - $R_a = \frac{1}{2} \cdot [R_{a1} + R_{a2}]\,(\mu m)$

R_{eq} - Equivalent curvature radius at each point (mm)

X_L - The lubricant factor and equal to:

i) 1 for mineral oils with no additives

ii) $\frac{1}{\left(\frac{F_{bt}}{L_{min}}\right)^{b_1}}$ for oils with additives and based on experimental tests results [23]

The value of b_1 for the ester base oil tested in this work present in the Table 1.3. The PAO value is not yet available [23].

Test Ref.	Lubricant	*b1*
E1	Ester	0.0738
P1	PAO	-

Table 1.3.: Value of b1 exponent for each lubricant test

The variation of the coefficient of friction along the contact path is present in the Figure 1.23, for all three gear geometries.

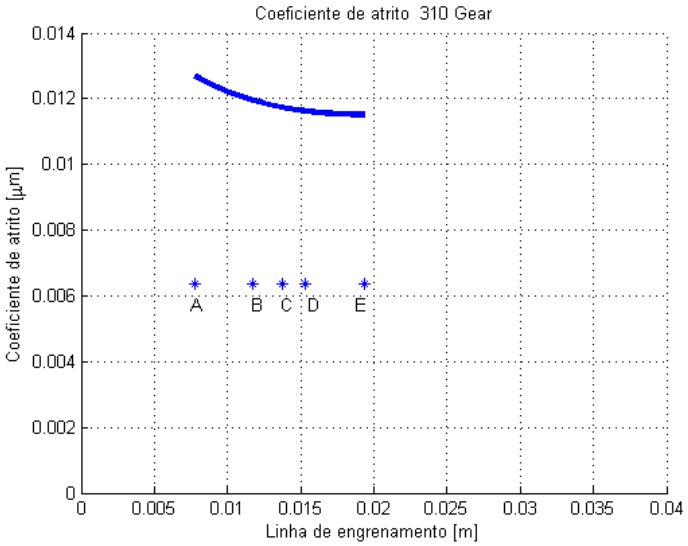

(a)

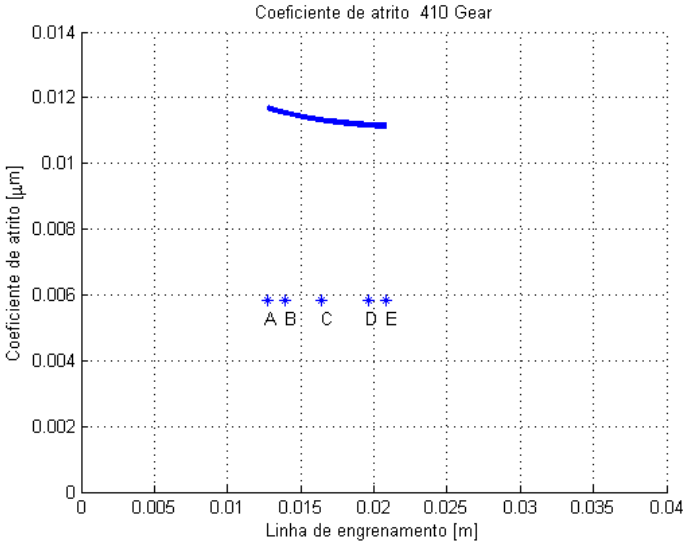

(b)

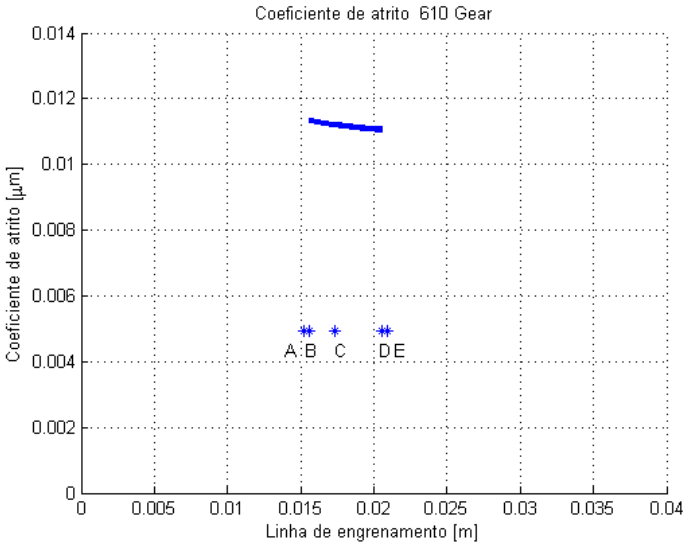

(c)

Figure 1.23.: Friction coefficient for gears: a) 310, b) 410 and c) 610.

1.1.11. Teeth flank and Lubricant temperature

Normal loads transmitted through the contact of gear tooth and the high sliding rates between flanks, produce a significant amount of power dissipation in the contact which causes the teeth surfaces temperature and lubricants temperature to increase [2].

The first analysis performed to determine the maximum temperature achieved in contacting tooth flanks are directly related with gear failure studies [2].

Failures are often results of a brutal rupture of the lubricant film, causing severe wear or tooth scuffing, being directly related to the concept of the lubricant specific film thickness mentioned above, and the critical temperature concept which is also in the base of different failure criteria. The Critical Temperature concept was first formulated by the professor H. Blok [2].

Teeth surface contact temperature is defined by the Expression 1.39.

$$T_{flash} = 0.910 \cdot \left(\frac{F_N}{L_{min}}\right)^{0.75} \cdot \left(\frac{E^*}{R_M}\right)^{0.25} \cdot \left(\frac{\mu \cdot |U_1 - U_2|}{t_1 \cdot \sqrt{U_1} + t_2 \cdot \sqrt{U_2}}\right) \tag{1.37}$$

$$T_M = T_0 + 0.49 \cdot T_{flash} \tag{1.38}$$

$$T_S = T_M + T_{flash} \tag{1.39}$$

Being,

T_M - the gear mass temperature

T_{flash} - the localized increase of temperature in each meshing line point

T_0 - oil bath temperature

t_1 - surface 1 thermal parameter and it is equal to $(C_1 \cdot k_1 \cdot \rho_1)^{0.5}$

t_2 - surface 2 thermal parameter and it is equal to $(C_1 \cdot k_2 \cdot \rho_2)^{0.5}$

with,

k_i - Thermal conductivity parameter of solid (i)

C_i - Specific heat of the solid surface (i)

ρ_i - Specific mass of the solid (i)

The maximum temperature of the contacting surfaces is defined according with Equation 1.40.

$$T_S^{max} = T_M + T_{flash}^{max} = T_0 + 1.49 \cdot T_{flash}^{max} \tag{1.40}$$

The lubricant temperature T_F inside the contact between gear teeth is define by the expression 1.41.

$$T_F = T_S + \Delta T_F \tag{1.41}$$

Where, ΔT_F (Equation 1.42) represents the the lubricant increase temperature above the surface temperature.

$$\Delta T_F = 0.157 \cdot \left[\left(\frac{F_N}{L_{min}} \cdot \frac{E^*}{R_M} \right)^{\frac{1}{2}} \cdot \left(\frac{\mu \cdot |U_1 - U_2| \cdot h_0}{k_F} \right) \right] \tag{1.42}$$

Being,

K_F - thermal conductivity of the lubricant film

h_0 - specific film thickness in contact center

Equation 1.43 represent the maximum lubricant temperature along the meshing line.

$$T_F^{max} = (T_S + \Delta T_F)^{max} \tag{1.43}$$

The surface increased temperature (T_f), oil bath increased temperature (T_c), surface maximum temperature (T_m) and oil maximum temperature (T_l) are present in the Figure 1.24 for the three gear geometries.

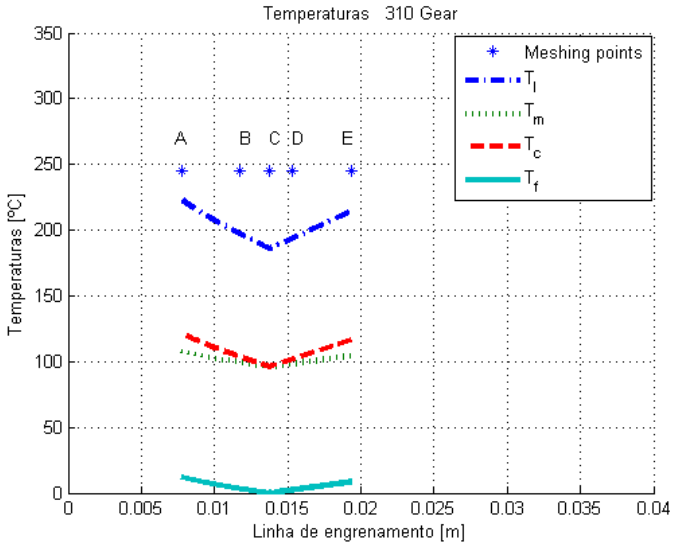

(a)

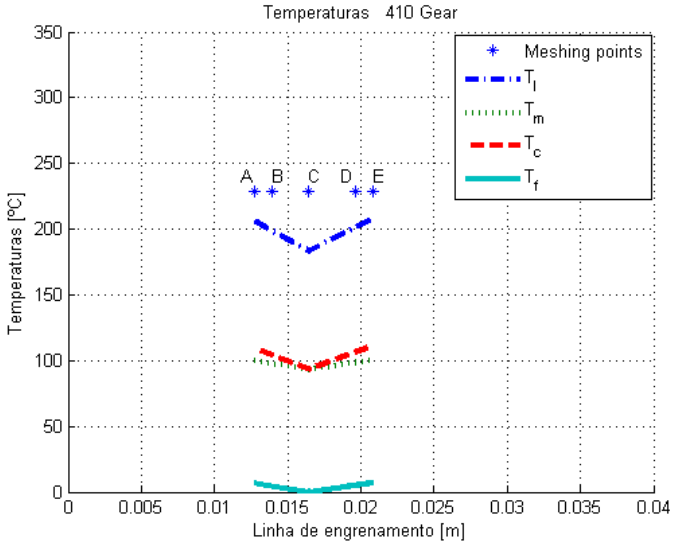

(b)

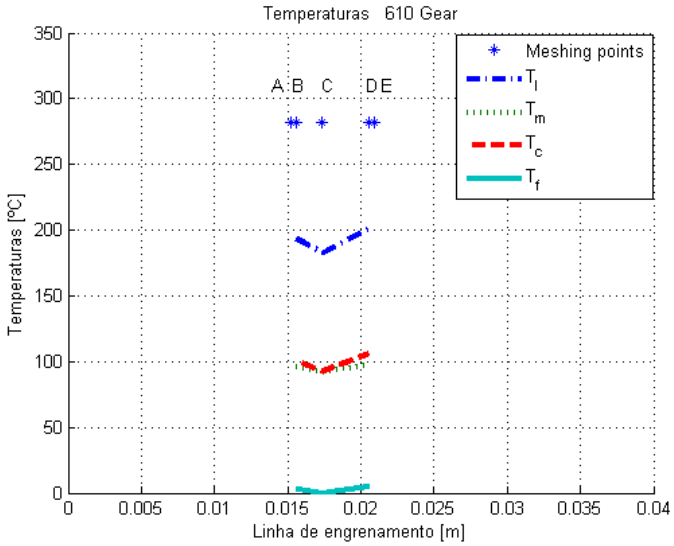

(c)

Figure 1.24.: Oil surface tooth flank temperatures along the contact path for gears: a) 310, b) 410 and c) 610.

1.2. Lubricant oils

Lubricant oils is the name given to the group of lubricating materials that are applied in the form of fluids. The lubricating oils are composed of the main product, called the base, and additives to enhance some needed special characteristics [4].

The primary goal while choosing a lubricant is to minimize friction and wear present in the contact of the moving surfaces. Then the lubricant must be able to evacuate the heat, remove the wear particles caused by the contact, be resistant to thermal decomposition and oxidation, and finally should not attack other mechanical components. To accomplish this, there is a need to choose a compatible lubricant to the application [24].

The most important properties of the lubricant oils are: oxidation stability, acidity, demulsification, emulsification, pour point, specific gravity and density, specific heat, thermal conductivity and viscosity [22].
One of the concerns when choosing an lubricant must be its viscosity, and the ability that it has to keep this viscosity to a minimum value during the oscillations in the working temperature. This is obtained by choosing one with an high viscosity index [24].

Lubricant oils can have four different origins, such as vegetable, animal, mineral and synthetic, and all of these will be presented in this section. Furthermore it will be discussed the additive packages available nowadays and their advantage to each situation, as well as, the comparison between high and low oil level in a gearbox [4].

1.2.1. Vegetable and animal lubricant oils

Animal and vegetable oils, had considerably less importance than the mineral oils, but they are still used nowadays. They were the first lubricants used by men, but due to new and more demanding needs they have been put aside by the petroleum and synthetic based lubricants. These kind of lubricants cannot be distilled without decomposition. Animal and vegetable oils contain fatty acids so they must be used with caution in order to avoid corrosion to other surfaces [24].
The reasons for the prevail of these kind of lubricants nowadays are, not only an environmental concern, but also because of their high viscosity index (VI), low evaporation rate, and finally their quick biodegradability. These kind of oils also have desadvantages: they oxidize very rapidly and have low resistance to high temperatures. In some cases these kind of oils are used as additives due to their special lubricant properties like greasiness [2].

1.2.2. Mineral based lubricant oils

Mineral oils are complex mixtures of organic and inorganic compounds.

Mineral oils have been made for long time, and they will continue to be manufactured in the future, since they come from mineral sources, their base oils are basically hydrocarbons and they are obtained from petroleum [2, 22, 24].

The mineral oils can be divided in three types :

a) Paraffinic - Mineral oil characterized by its high-level fluidity point, high viscosity index (VI), good oxidation resistance, good oiliness and high amount of carbon residue.

b) Naphthenic - Mineral oil with the opposite characteristics of paraffinic mineral oil, that is, low level fluidity point, low viscosity index (VI), low oxidation resistance, large oiliness and low amount of carbon residue.

c) Mixed - are mixtures of oils, manufactured using paraffinic and naphthenic base oils, widely used as lubricants because they are available in several viscosity grades, have low volatility, are resistant to deterioration, are corrosion protectors and above all they have a low cost.

1.2.3. Synthetic base lubricant oils

The synthetic-based lubricants have been used in aviation and in industrial applications for many years now. In the past, the synthetic lubricants were preferred to the mineral ones, because they have good resistance to burning and a better protective capability to extreme operating conditions, very low and very high working temperatures, and they can also be environmental friendly [4].

A synthetic material is a combination of several materials. This combination starts with a synthetic base, and then other compounds are added in order to obtain the adequate viscosity and other required properties, this being a technical advantage comparing with mineral base oils [4].

Synthetic-based lubricants are more expensive because the properties are unique to the application in hand, but they “pay-out”, since synthetic oil have better performance than the mineral oils [4].

Synthetic lubricants can be grouped in three categories [2, 25]:

a) Polyalphaolephines (PAO) - are the most common synthetic base lubricant, and they have a low fluidity point, good thermal stability, a high viscosity index, but on the other hand they are bad to dissolve additives.

b) Polyglycols - are characterized by their low friction coefficient, making them ideal for high sliding applications. Their compatibility with seals, paints and oil screens should be carefully analyzed.

c) Esters - are a wide class of lubricants, and they can be divided in dibasic acids esters, Polyol esters. Each one of these esters has different characteristics, such as, high thermal resistance, good behavior at low temperatures, and biodegradability, being this last one a vital and important property in many current applications that need to be environmental friendly.

1.2.4. Additives

Additive are agents that are added to base lubricant fluids in order to improve the lubricant properties and performance and to suit the requirements of the applications.

Some times, there is the need to create a lubricant that combines certain properties from a base oil and other properties from another base oil. The solution for this problem is to use additives, creating a lubricant with the intended properties [2, 24].

In addition to the properties of each additive, all of them must have some general properties. These properties are: solubility in the base petroleum product, insolubility in aqueous solutions, color, volatility, stability, compatibility, flexibility, odor and controlled activity [4, 24].

The additives can be classified in two groups [25]:

1. Those that modify the physical characteristics, such as, fluidity, foam formation and viscosity index;

2. Those that have an effect on chemical nature, such as oxidation inhibitors, detergents, extreme pressure agents.

The variety of lubricant additives is very large and their characterization is not the scope of this work. Nevertheless, the most common additives are: Pour point depressants, viscosity index improvers, defoamants, oxidation inhibitors, rust and corrosion inhibitors, detergents and dispersants, antiwear, extreme pressure, alkaline agent [25].

The main influences of such additives are [24, 25]:

I) Oxidation-inhibitor - Increase oil and machine life and decreases the varnish and the sludge on metal parts;

II) Corrosion inhibitors - Protect against chemical attack on metal surfaces;

III) Pour point depressants - Increase oil flow at low temperatures;

IV) Detergent - Clean the lubricated surfaces;

V) Viscosity index improvers - are polymers that increase the relative viscosity of the oil at high temperature and at low temperatures;

VI) Antiwear improvers - Protects rubbing surfaces operating with thin films;

VII) Antifoam agent - Prevents the foam formation;

VIII) Extreme pressure -are used when lubricants are submitted to high temperatures and/or heavy loads where more severe sliding conditions occur, to reduce friction, control wear and prevent severe surface damage.

1.2.5. Lubricant classification-Viscosity Grades

When choosing a lubricant the main concern is its viscosity, since there is the need to have a high viscosity lubricant, so it can have a sufficient lubricating film, but it can not be very high because it will cause excessive friction losses. Another parameter that must be taken into account is the working temperature, since the viscosity decreases significantly when the temperature increases.

In order to choose a proper lubricant have been developed several classification methods, and at the moment are available three viscosity numbering systems. Three methods for automotive lubricants and one for industrial lubricants [4].

The two classifications for automotive lubricants, SAE J300 and SAE J306, are from the Society of Automotive Engineers and the classification for industrial lubricants has been developed by the American Society for Testing Materials (ASTM) and the Society of Tribologists and Lubrication Engineers (STLE).

SAE J300 classifies oils according to their viscosity, evaluated at low shear rates and high temperatures (100°C), at high shear rates and high temperature (150°C) and also in a combination of both (high and low) shear rates and low temperatures(-5°C to -40°C). The grades described are presented in the Figure 1.25.

SAE viscosity grade	Low temperature viscosity		High temperature viscosity		
	Low temperature cranking viscosity cP ,°C [1]	Low temperature pumping viscosity cP, °C [2]	Kinematic viscosity cSt at 100°C (low speed deformation)[3]		Minimun viscosity cP at 150°C (high speed deformation)[4]
			min	max	
0W	6200 a -35	60,000 a -40	3.8	—	—
5W	6600 a -30	60,000 a -35	3.8	—	—
10W	7000 a -25	60,000 a -30	4.1	—	—
15W	7000 a -20	60,000 a -25	5.6	-	—
20W	9500 a -15	60,000 a -20	5.6	—	—
25W	13,000 a -10	60,000 a -15	9.3	—	—
20	—	—	5.6	<9.3	2.6
30	—	—	9.3	<12.5	2.9
40	—	—	12.5	<16.3	2.9 (0W-40, 5W-40, 10W-40)
40	—	—	12.5	<16.3	3.7 (15W-40, 20W-40, 25W-40, 40)
50	—	—	16.3	<21.9	3.7
60	—	—	21.9	<26.1	3.7

[1] ASTM D 5293, [2] ASTM D 4684, [3] ASTM D 445, [4] ASTM D 4683, ASTM D 4741

1cP = 1mPa s; 1 cSt = 1mm^2/S

Figure 1.25.: SAE J300 Classification [3].

In the present classification the suffix letter W, designates the use of the lubricant at low ambient temperatures, and the grades without suffix letter, are developed for more warmer temperatures [2, 4].

SAE J306 viscosity classification is measured at 100°C , and by the maximum temperature achieved when the viscosity reaches of 150 Pa.s, then when cooled and measured in accordance with ASM Standard D2983 (Method that Testing the apparent viscosity at low temperature using the Brookfiel viscometer) [4].

The grades for the SAE J306 are presented in the Figure 1.26.

SAE viscosity grade	Maximum temperature for a dynamic viscosity of 150,000 cP, °C	Kinematic viscosity cSt @ 100°C	
		Min	Max
70W	-55	4.1	-
75W	-40	4.1	-
80W	-26	7.0	-
85W	-22	11.0	-
80	-	7.0	<11.0
85	-	11.0	<13.5
90	-	13.5	<24.0
140	-	24.0	<41.0
250	-	41.0	-

Figure 1.26.: SAE J306 Classification [3].

In automotive industry multigrade oils are very common. Multigrade oils can be formulated for example to reach the low temperature of -26°C , specified in the Figure 1.26 as 80W grade, and at the same time the 100°C limits for the 90 grade, resulting in the following designation of SAE 80W-90 grade. The SAE J300 does not contemplate multigrade oils [2, 4].

Finally, the third possible system was developed by ASTM and the Society of Tribologists and Lubrication Engineers (STLE). This classification establishes viscosity grades that could be often used to specify the viscosity of industrial fluid lubricants, and eliminate the unjustified intermediate grades.

The viscosity's are measured at the temperature of 40°C and nowadays are present on ASTM Standard D2422, American Nation standard Z11.232, Din N° 51519 and International Standards Organization (ISO) Standard 3448. The ISO viscosity grades are shown in the Figure 1.27 [2, 4].

ISO Standard 3448 ASTM D-2422	Midpoint viscosity [cSt (mm^2/s)] at 40.0°C	Kinematic viscosity limits [cSt (mm^2/s)] at 40.0°C	
		Minimum	Maximum
ISO VG 2	2,2	1,98	2,42
ISO VG 3	3,3	2,88	3,52
ISO VG 5	4,6	4,14	5,06
ISO VG 7	6,8	6,12	7,48
ISO VG 10	10	9,00	11,0
ISO VG 15	15	13,5	16,5
ISO VG 22	22	19,8	24,2
ISO VG 32	32	28,8	35,2
ISO VG 46	46	41,4	50,6
ISO VG 68	68	61,2	74,8
ISO VG 100	100	90,0	110
ISO VG 150	150	135	165
ISO VG 220	220	198	242
ISO VG 320	320	288	352
ISO VG 460	460	414	506
ISO VG 680	680	612	748
ISO VG 1000	1000	900	1100
ISO VG 1500	1500	1350	1650

Figure 1.27.: ISO Classification [3].

Using the charts of Figure 1.28, the comparison between different grades can be easily done.

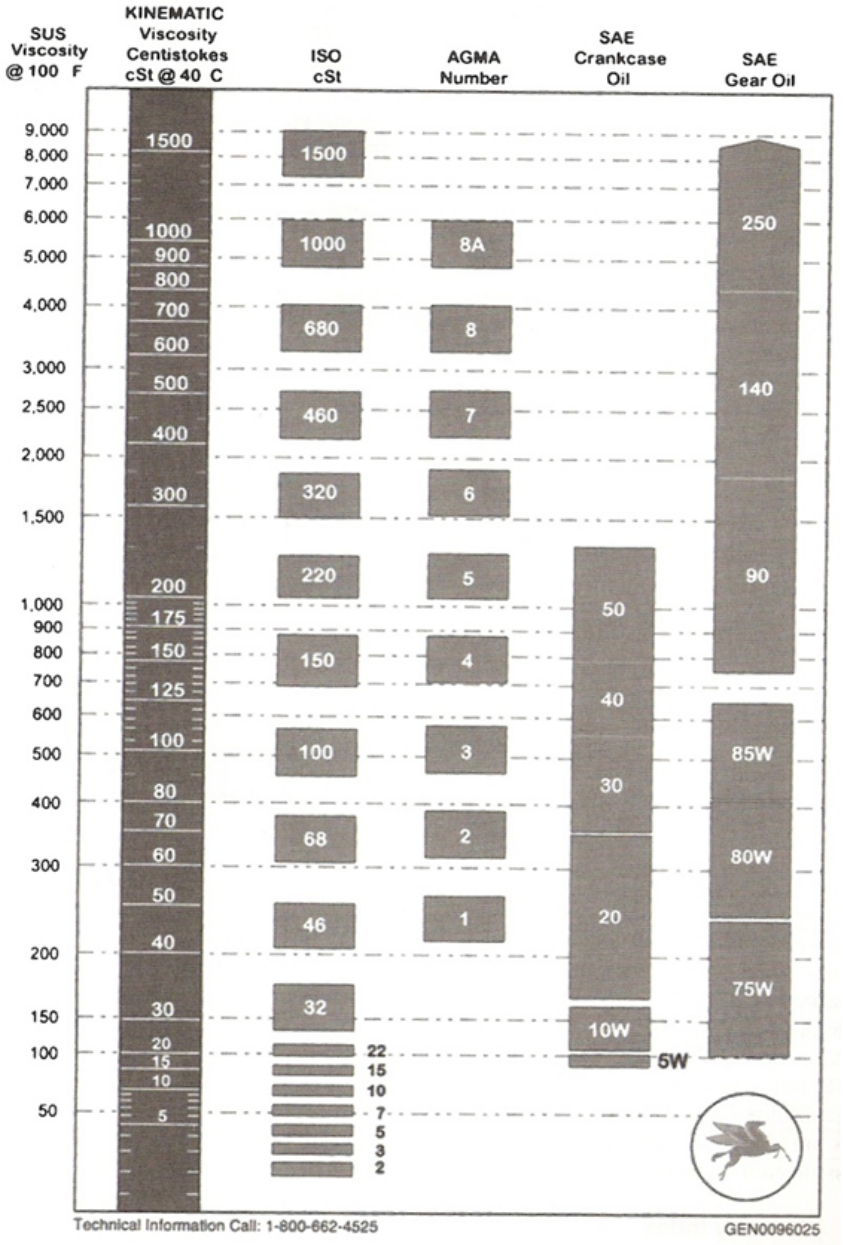

Figure 1.28.: Comparison of Classification Rates [4].

1.3. Gear lubrication Methods and Level

In gear lubrication, two methods can be used: dip or oil bath lubrication (Figure 1.29) and jet oil lubrication (Figure 1.30). Both methods have their pros and cons, depending of the conditions that they are going to be used in.

In the first method (oil bath lubrication) the most important parameter is the oil level. In this case there is the possibility to have high or low oil level.

If the level is to high and pitch-line speeds are high, it will cause an excessive churning and agitation, inducing high operating temperatures and higher power losses. The high operating temperatures for long time will also cause the deterioration of the oil through oxidation. On the other hand too low oil level will cause inadequate lubrication, and that will bring other problems associated [5, 26].

Two cases should be considered:

a) Slow running gears;

b) Fast running gears;

In case (a), there is little or no splash at all, comparatively with deep immersion, so there is the need to control the amount of oil that reaches the contact zone, in order to have the necessary oil volume there, for lubrication and heat evacuation. Also high oil level with slow running gears may cause an appreciable power loss due to the viscous drag of the oil. At low or medium speed gears, an immersion dept of two or three times the height of the teeth, might be required.

In case (b), a small depth of immersion, not more than half of the tooth height, may be enough to have the spray at the required rate [5, 26].

The second lubrication method is jet oil or circulation lubrication, consisting in pumping the oil into the gear tooth near the gearing point, being the

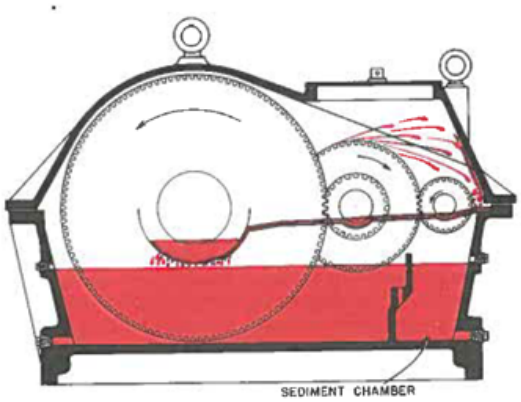

Figure 1.29.: Oil bath lubrication [4].

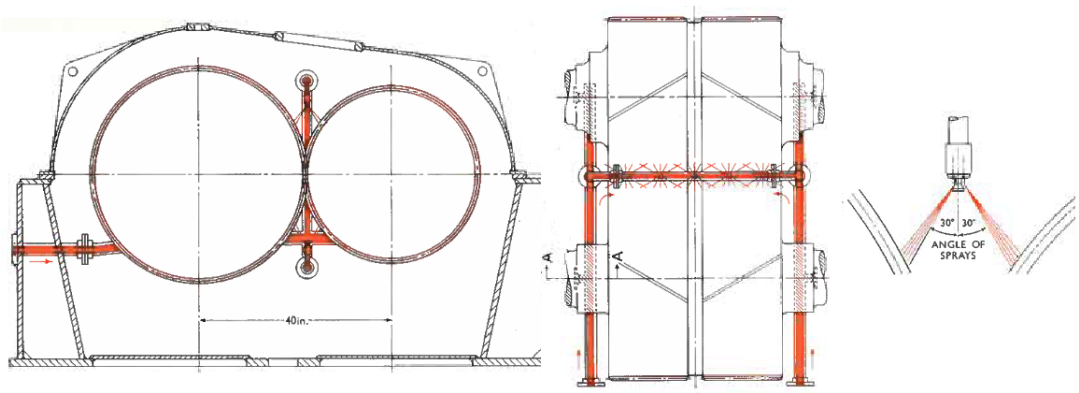

Figure 1.30.: Jet oil lubrication [5].

oil collected in the gearbox bottom, them the oil is filtered and return to the oil reservoir, where it is cooled to the operating temperature selected and re-circulated [4].

The two described methods are dependent of the pitch line velocity, i.e, the gear size (diameter), and rotational speed, and as was shown above, there is the need to choose the right method to obtain effective lubrication. Figure 1.31 gives an indication to achieve a good choice quickly and efficiently.

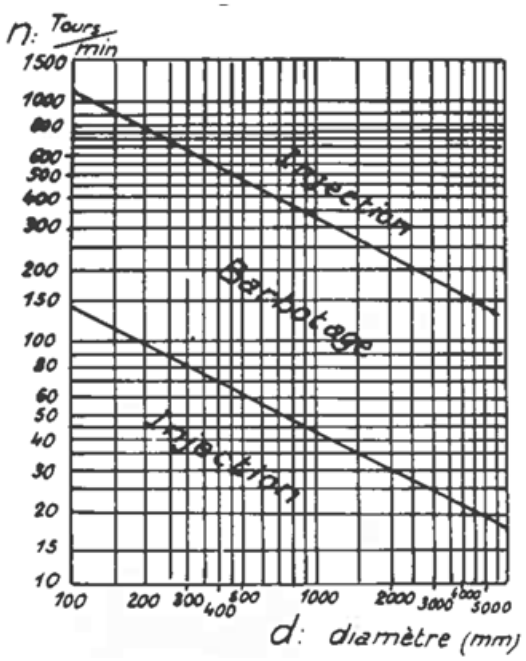

Figure 1.31.: Abacus for selection of lubrication type

1.4. Gear failure modes

Gear have multiple failure mechanisms, but the main factor that lead to failure is the application of load. The major failure modes associated to the lubricants are:

i) Abrasion or slow wear;

ii) Scuffing or disruption of the working surface through collapse of lubrication;

iii) Surface fatigue (pitting and micro-pitting) or bending fatigue;

iv) Plastic yielding: impact fracture;

These kind of failures depend mainly of load and speed combination, and they might be schematize as shown in the Figure 1.32.

They should be taken into account during gear design and optimization, because it can cause major damage not only to the gear set, to the machine, but also to everyone in the vicinity of the machine. The failure mode detected can indicate that some changes need to be made, both at the level of lubricant type or at level of gear design [5].

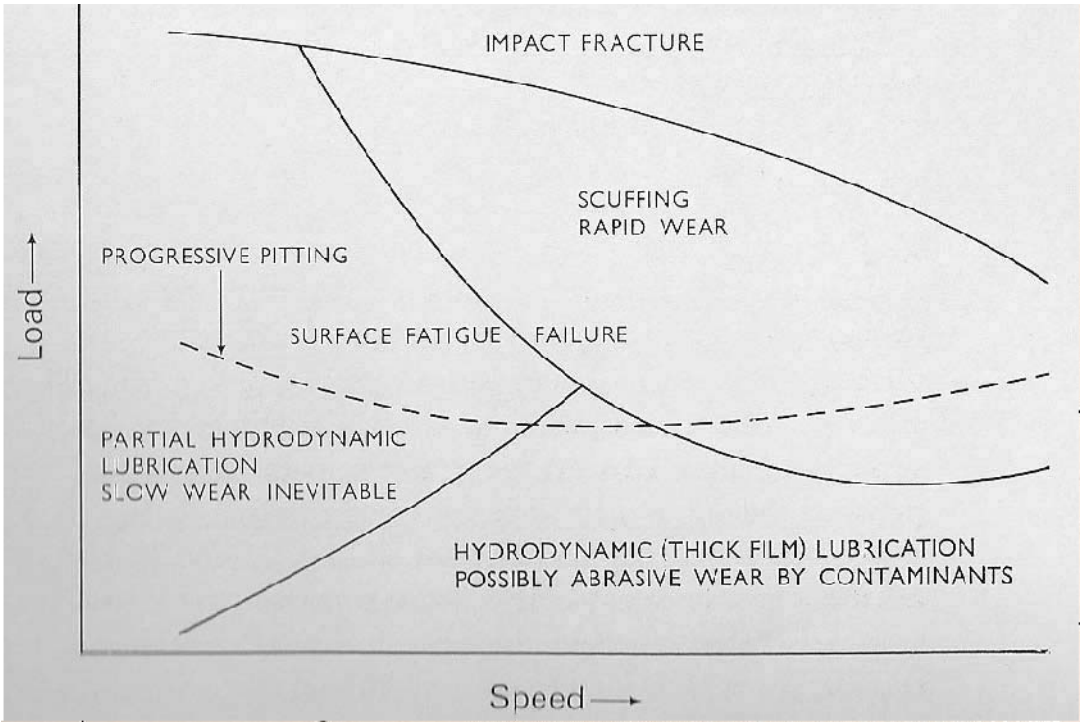

Figure 1.32.: Most important gear failure modes [5].

1.4.1. Abrasion or slow wear

Abrasion is caused by a general and continuous wearing of the tooth surface. The surfaces that present abrasion normally remain fairly smooth not far from polished, they have a matt appearance due to hedging with scratches marks in the direction of the surfaces sliding. Some surfaces that present some wear, light and severe abrasion are shown in the Figures 1.33a to c, respectively.

The abrasion can be caused by contamination of the oil by metallic particles capable of bridging the oil film between the working surfaces during the meshing cycles of the teeth. The solution for this kind of problem is to clean the oil bath or system, and filter properly the oil.

In some cases, abrasion can be caused by overloading or by inadequate lubrication, this can cause the surface to become with some degree of asperity contact, in other cases that different material types are used in the same gear set, abrasion can occur. The solution to this two cases can pass by increasing the oil thickness at the load area, the oil viscosity or by relieving the excessive load [5, 27].

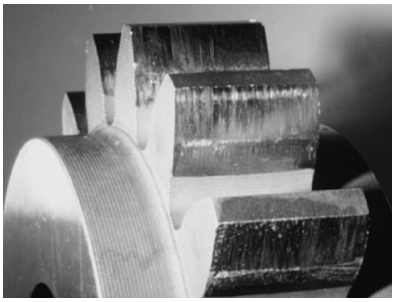

(a) Wear caused by a pitting test [28]

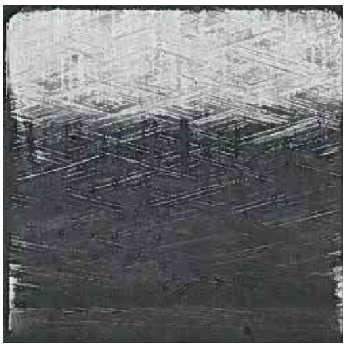

(b) Light Abrasion [5]

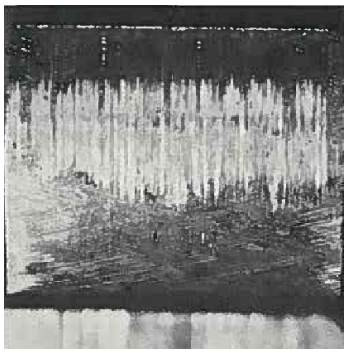

(c) Severe Abrasion [5]

Figure 1.33.: Several types of Wear.

1.4.2. Scoring and scuffing

Scoring or scratching is another kind of abrasion, in which the scratch marks are more deep and more extensive than those found on the abrasion wear type. The cause for this wear type, are some particles that circulate with the oil on to the meshing line, particles that are separated from teeth as result of the surface deterioration, or may be caused by a local breakdown of the film and causing only scratch marks in some limited parts of the tooth [5, 29].

Scuffing is caused by subjecting the gears to an high load and then having an oil film breakdown, this is characterized by welding, tearing and consequently roughening of the tooth surface. In the more severe cases of scuffing it can be visible some metallic tearing in the tooth surface. The problem can be identifiable by an increase of noise and vibration, a sudden increase of friction and occasionally smoke release.

Scuffing results from the generation of high heat and high sliding speeds at the points of contact, or even so, a combination of high sliding speeds and high loads, conducing to an rupture of oil film. So it can be said that, slow running gears have little tendency to present scuffing, since the sliding speeds are very low and in the presence of metal-to-metal contact between teeth it will cause slow abrasive wear rather then scuffing. In fast gear sets it must be maintained an high oil film in order to decrease the tendency to have metal-to-metal contact [5, 29].

The solution to this kind of problems passes by choosing an appropriated material, micro-structure and hardness to the each application, and also of course, a lubricant compatible to these kind of surfaces, in order to have a good surface/lubricant combination [5].

Examples of scuffing can be seen in the Figures 1.34a to c.

1.4.3. Pitting and Micro-Pitting

Pitting is a problem that involves the progression of a small shallow craters in the working surfaces, that resulted from local fragmentation of the metal surface. This kind of problem can appear anywhere along the tooth surface, but usually it starts in the vicinity of the pitch line (Figure 1.35b), and then it increases and spread until it cracks permanently. The pits can have the same dimension of the Hertzian contact size.

The term Spalling is applied when pitting progresses and leads to weaken the surface and then eventually it breaks off (see Figure 1.35a) [5, 30].

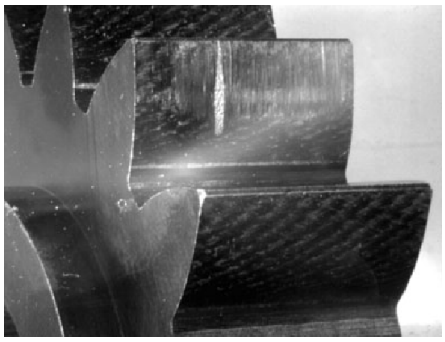

(a) Scuffing [28]

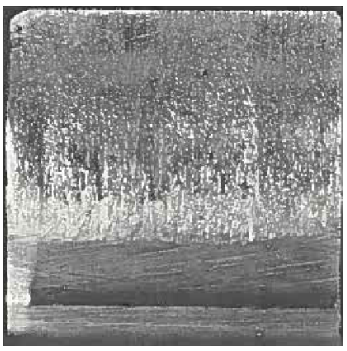

(b) Slight Scuffing [5]

(c) Severe Scuffing [5]

Figure 1.34.: Several types of Scuffing.

The conditions that favor crack propagation are:

a) The increasing pressure - caused by the negative sliding;

b) Surface shear stress - this is caused by general increase of the load on the gears or from variation in stress from point to point or between limited areas of the tooth surface.

c) Misalignment of the gears, thermal distortion and also contamination of the oil by hard particles.

After pitting starts, nothing can be done to stop it, but there are some measures that can be taken in order to retard its effects, such as [5]:

i) An increase in the viscosity grade of the lubricant oil;

ii) Alleviation of the effect of the surface roughness, by using an oil additive.

Micro-pitting is caused by the high stress on the surface due to the load transfer, this is done essentially through roughness contact and can be seen in Figure 1.36. This problem normally is non destructive, but can in some cases lead to pitting.

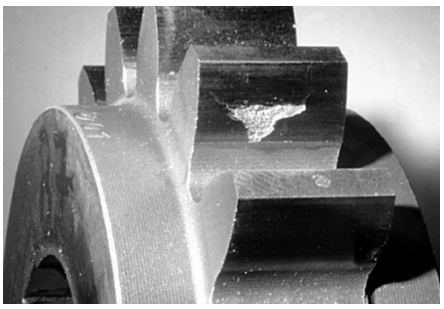

(a) Pitting [6]

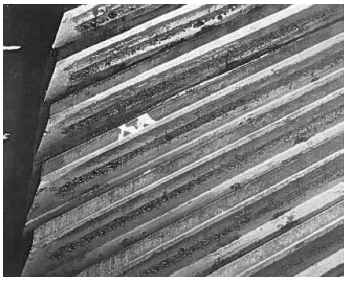

(b) Pitting at picth point [5]

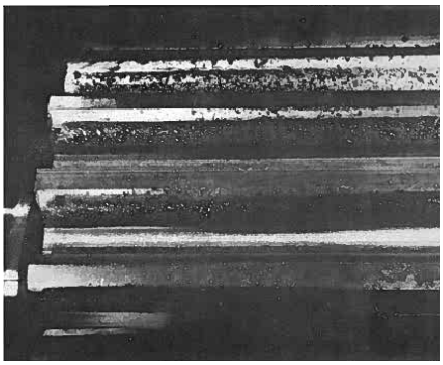

(c) Severe Pitting [5]

Figure 1.35.: Several types of Pitting.

It is a fatigue failure characterized by appearing mostly in micro cracking in the negative sliding areas below pitch line, leading the surface material to break, happening more frequently in good quality or nearly inclusion-free materials. In a more qualitative view it can be characterized by being shallow small pits measured in the micron range, spread by a large area of the tooth, normally resulting in a gray like patches, being for that reason commonly called gray staining [6, 30].

Figure 1.36.: Micro-Pitting [6].

1.5. Gear Power loss

Nowadays, it is very important to predict and control power losses in geared systems, and also anticipate the consequences of designed modifications before the actual drives are tested. To do so, there is the need to know the origin and the type of these power losses [31].

It is recognized that the main sources of power loss in geared transmissions are sliding friction between gear teeth and churning losses, for low to medium speed geared transmissions [14, 32].

Power losses in geared transmissions are divided in two main contribution factors [14, 31, 33]:

a) Load

Tooth Friction Losses - are due to the sliding of the gear tooth and to the friction coefficient between the contacting surfaces;

Bearing Losses - are due to sliding friction of the bearing parts;

b) No-Load

Bearing Losses - include the viscous friction losses, and are due to all kinematic friction phenomena;

Churning Losses - are independent of the torque applied and have three main causes:

- The churning of the rotating gear set immerse in the oil bath, at higher rotational speeds, power losses are found to be largely independent of oil viscosity and it can be concluded that the inertia forces are much more important than the viscous ones;
- The churning of the rotating rolling bearings immerse in the oil bath;
- Friction between other moving components and the oil bath.

All the power loss mechanisms mentioned above generate heat and the temperature of the oil bath rises. At the same time, the heat generated is evacuated (by conduction, radiation and convection) to the surrounding environment. After a long operating period both the temperature of the oil and of the test rig tend to a certain thermal equilibrium state.

When the gearbox reaches an energetic equilibrium, the power loss inside the gear box equals the heat evacuated (Equation 1.44), as shown in Figure 1.37 [14, 31, 33].

$$P_{fr} + P_{M1} + P_{spl} + P_{M0} + P_{sl} = Q_{rad} + Q_{cnv} + Q_{cn} \tag{1.44}$$

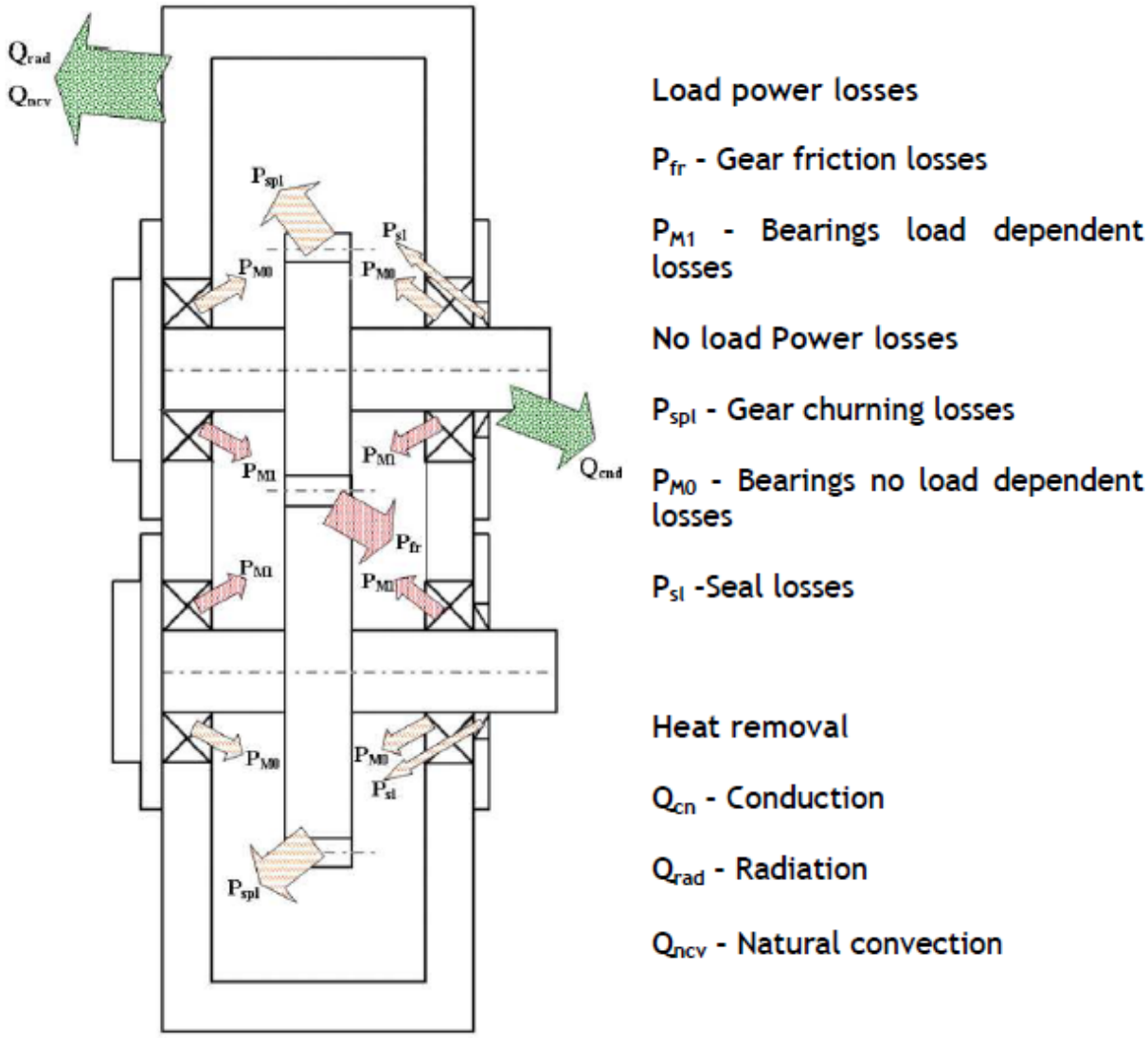

Figure 1.37.: Power losses diagram [7].

1.5.1. Load dependent power losses

Gear friction losses (P_{fr}), defined in Equation 1.45, depend on the geometric conditions of the gearing, input power, coefficient of friction and most importantly the number of teeth [14, 33].

$$P_{fr} = \mu_{Mich} \cdot P_{in} \cdot H_{Vl} \tag{1.45}$$

The coefficient of friction is of major importance factor in this study, since it depends on the operating conditions. It is given by the Equation 1.36, previously defined in sub-chapter 1.1.10 [14].

The loss factor (H_{vl}) given by Equation 1.46, defined by A. J. Wimmer [34], has a major influence on the gear friction power losses.

$$H_{vl} = \frac{\pi(u+1)}{u}\frac{1}{Z_1 \cdot \cos(\beta_b)} \cdot \cdot \frac{1}{[a_0 + a_1 \cdot |\epsilon_1| + a_2 \cdot |\epsilon_2| + a_3 \cdot |\epsilon_1| \cdot \epsilon_1 + a_4 \cdot |\epsilon_2| \cdot \epsilon_2]} \tag{1.46}$$

The a_0, a_1, a_2, a_3 and a_4 are presented below with the following conditions:

If $\epsilon_\alpha < 1$

$$\begin{cases} a_0 = 0 \\ a_1 = 0 \\ a_2 = 0 \\ a_3 = \frac{1}{\epsilon_\alpha} \\ a_4 = \frac{1}{\epsilon_\alpha} \end{cases}$$

If $\epsilon_\alpha > 1$ and $(\epsilon_1 < 0$ or $\epsilon_2 < 0)$

$$\begin{cases} a_0 = 0 \\ a_1 = 1 \\ a_2 = 1 \\ a_3 = 0 \\ a_4 = 0 \end{cases}$$

If $\epsilon_\alpha > 1$ and $l + m = n$

$$\begin{cases} a_0 = \frac{2 \cdot l \cdot m}{n} \\ a_1 = \frac{l \cdot (l-1) - m \cdot (m-1) - 2 \cdot l \cdot m}{n \cdot (n-1)} \\ a_2 = \frac{-l \cdot (l-1) + m \cdot (m-1) - 2 \cdot l \cdot m}{n \cdot (n-1} \\ a_3 = \frac{2 \cdot m}{n \cdot (n-1)} \\ a_4 = \frac{2 \cdot l}{n \cdot (n-1)} \end{cases}$$

If $\epsilon_\alpha > 1$ and $l + m = n + 1$

$$\begin{cases} a_0 = \frac{2\cdot(l\cdot m-n)}{n-1} \\ a_1 = \frac{l\cdot(l-1)+m\cdot(m-1)-2\cdot(m-1)\cdot n}{n\cdot(n-1)} \\ a_2 = \frac{l\cdot(l-1)+m\cdot(m-1)-2\cdot(l-1)\cdot n}{n\cdot(n-1)} \\ a_3 = \frac{2\cdot(m-1)}{n\cdot(n-1)} \\ a_4 = \frac{2\cdot(l-1)}{n\cdot(n-1)} \end{cases}$$

where,

$$l = Roundup(\epsilon_1)$$
$$m = Roundup(\epsilon_2)$$
$$n = Roundup(\epsilon_\alpha)$$

Rolling bearing friction power losses depend on several factors like the type of rolling bearing, the combined applied load, the bearing diameter and the coefficient of friction, being this last one constant for the FZG test box rolling bearings [35].

$$P_{M1} = \frac{\pi}{30} \cdot N \cdot \sqrt{F_r^2 + F_a^2} \cdot f_l \cdot D \tag{1.47}$$

Where F_r and F_a are the radial and the axial loads respectively, N is the input speed, f_l is the coefficient for bearing losses and D the diameter.

1.5.2. No-Load dependent power losses

The gear churning losses are independent of the load. The most influent parameters are:

1. Gear pitch diameter d_1;
2. Rotational speed - N;
3. Gears immersion area;
4. Gear width - b;
5. Oil viscosity - η;
6. Oil density - ρ.

The gear churning losses depend on the Froude (F_R) and Reynolds (Re) numbers, being defined by Equation 1.48 [33].

$$P_{spl} = \frac{\pi}{30} N \left(\frac{1}{2} \rho \left(\frac{\pi N}{30} \right)^2 A_1 \left(\frac{D_1}{2} \right)^3 \right) \left[\left(\frac{2h}{D_1} \right)^{0.45} \left(\frac{V_{oil}}{D_1} \right)^{0.1} F_R^{-0.6} Re^{-0.21} \right] \quad (1.48)$$

The no load power loss in the rolling bearings depend mainly on the rotational speed, bearing diameter, type of bearing and lubricant viscosity and operating temperature, as shown in Equation 1.49 [35].

$$P_{M0} = \frac{\pi}{30} \cdot N \cdot (f_0 \cdot 10^{-7} \cdot (N \eta_{oil})^{\frac{2}{3}} \cdot D^3) \cdot 10^{-3} \quad (1.49)$$

Seals power losses represent the friction losses in the contact between seal leaps and shafts, depending mostly on the rotational speed and shaft diameter, defined by Equation 1.50 [14].

$$P_{sl} = 7,69 \cdot 10^{-6} \cdot d_1^2 \cdot N \quad (1.50)$$

1.5.3. Reference friction torque loss

A reference friction torque loss was used to compare all the experimental results obtained.

The torque loss value present in some experimental results graphics, was calculated using the combination of [14, 34] papers.
The reference friction torque loss is defined as: (see Equation 1.51).

$$T_{vz} = \frac{P_{fr}}{\omega_{in}} \quad (1.51)$$

Where,

T_{vz} reference friction torque loss (N.m)

P_{fr} Gear friction losses (W)

ω_{in} Rotational speed (rad/s)

1.5.4. Heat Removal

The heat evacuation mechanisms from the FZG test gearbox are conduction, convection and radiation. In the case of the FZG test gearbox, the heat removal depends on the wall temperature, which in this case, is the oil temperature.

The FZG test rig room is equipped with ventilation, generating a continuous air flow, allowing the room temperature to be kept constant. The air velocity is considered low, so only natural convection is considered. The natural convection was separated into two parts, one for the vertical walls and other for the horizontal ones [36].

Vertical wall convection coefficient is given by the Equation 1.52.

$$h_v = 11,06 \cdot h_{ca}^{-0.1} \cdot \left(\frac{T_w - T_a}{T_a} \right)^{0.3} \tag{1.52}$$

Being, h_{ca} the height of gearbox.

Horizontal wall convection coefficient is presented in the Equation 1.53.

$$h_h = 12.87 \cdot L_{ca}^{-0.04} \cdot \left(\frac{T_w - T_a}{T_a} \right)^{0.32} \tag{1.53}$$

where L_{ca} is the characteristic dimension of the horizontal wall (mean value of width and length).

Total heat removed by convection, combining both vertical and horizontal walls is shown in the Equation 1.54.

$$Q_{cnv} = h_v \cdot A_v \cdot (T_w - T_a) + h_h \cdot A_h \cdot (T_w - T_a) \tag{1.54}$$

The amount of power removed by radiation is determined from the Stefan-Boltzman law, and the heat radiation coefficient (α_{rad}) is defined in Equation 1.55 [14].

$$\alpha_{rad} = 0.23 \cdot 10^{-6} \cdot \epsilon \cdot \left(\frac{T_w + T_a}{2} \right)^3 \tag{1.55}$$

The removed heat by radiation is calculated using the Equation 1.56.

$$Q_{rad} = \alpha_{rad} \cdot A_{rad} \cdot (T_w - T_a) \tag{1.56}$$

In FZG test gearbox the heat removal by conduction is complex and difficult to calculate, since it is bi-dimensional and the gearbox has a complex shape. So an accurate solution for this requires a elaborated numerical solution.

In order to solve this problem Winter et al. proposed the substitution of the conduction heat by an increase of convection and radiation area by a factor (f_{cn}) of 1.5 to 2.5 times the gearbox base contact area (conduction area, A_b) [37].

So the increase in the radiation heat due to conduction is present in the Equation 1.57.

$$Q_{cn}^{rad} = \alpha_{rad} \cdot (T_w - T_a) \cdot f_{cn} \cdot A_b \tag{1.57}$$

The increase in the convection heat due to conduction is present in the Equation 1.58.

$$Q_{cn}^{cnv} = A_b \left[h_v (T_w - T_a) \left(\frac{A_v}{A_v + A_h} \right) + h_h (T_w - T_a) A_h \left(\frac{A_h}{A_v + A_h} \right) \right] f_{cn} \tag{1.58}$$

Finally the total evacuated heat from the FZG gear box is given by the Equation 1.59.

$$Q_{cn} = Q_{cn}^{cnv} + Q_{cn}^{rad} \tag{1.59}$$

The f_{cn} factor used in our test rig was determined from the result of no load tests resulting in a value of f_{cn} =2.5.

2. Gears, Materials and Oils

2.1. Low Loss Gear

"Low loss" gears are an engineered type of gears. They have a special design that aims the reduction of the sliding speed and, consequently, a reduction in friction between contacting teeth during operating, in comparison with standard FZG Type C gear.

These types of gears produce less heat and have less power consumption. They can be manufactured through simple geometric modifications, using standard 20° pressure angle gear cutting tools, available in most tool-shops, without demanding any particularly or expensive procedure [9, 11].

Years of investigations, concluded that, some precious steps could be followed in order to accomplished an improvement in low-loss gears.

Some step can be assumed as unconventional, but already proven to work in the increase of gear efficiency and power saving. This is not a unidirectional process, but an progressive and iterative process.

Some of the things that can change on the gears set are [8]:

I. Corrections for load reduction in areas of contacts with high sliding speed;

II. Reduction of module down to tooth root fracture limit;

III. Reduction of transverse contact ratio down to pitting capacity limit;

IV. Tooth root fillet radius as large as possible;

V. Increase of pressure angle;

VI. Increase of face width;

VII. Helix angle for adequate overlap contact ratios;

The idea of creating and developing the "Low Loss Gear", came from the concept that it is possible to reduce the coefficient of friction in the teeth contact during the meshing cycle.

So Low Loss gears appear due to the existing need to minimize losses in the existing gearboxes. The starting point was the standard FZG type C gear (with

the geometric properties presented in the Table 2.1), and then there were applied the enumerated steps above in order to improve the gear efficiency and power loss. One geometry proposed by Hohn et al [8] for the power loss gear is present in the Table 2.1 as well.

The comparison between them is present in the Figure 2.1, and a visual comparison of the design can be seen in the Figure 2.2 [9].

	Symbol	Units	Type C	Low Loss
Module	m	[mm]	4.5	1.75
Number of teeth	Z1/Z2	[/]	16/24	40/60
Pressure angle	α	[°]	20	40
Helix angle	β	[°]	0	15
Teeth width	b	[mm]	14	20
Normal Contact ratio	ϵ_α	[/]	1.43	0.55
Complementary contact ratio	ϵ_β	[/]	0	0.94
Overall contact ratio	ϵ_γ	[/]	1.43	1.49

Table 2.1.: FZG Type C and "Low Loss" gears [8].

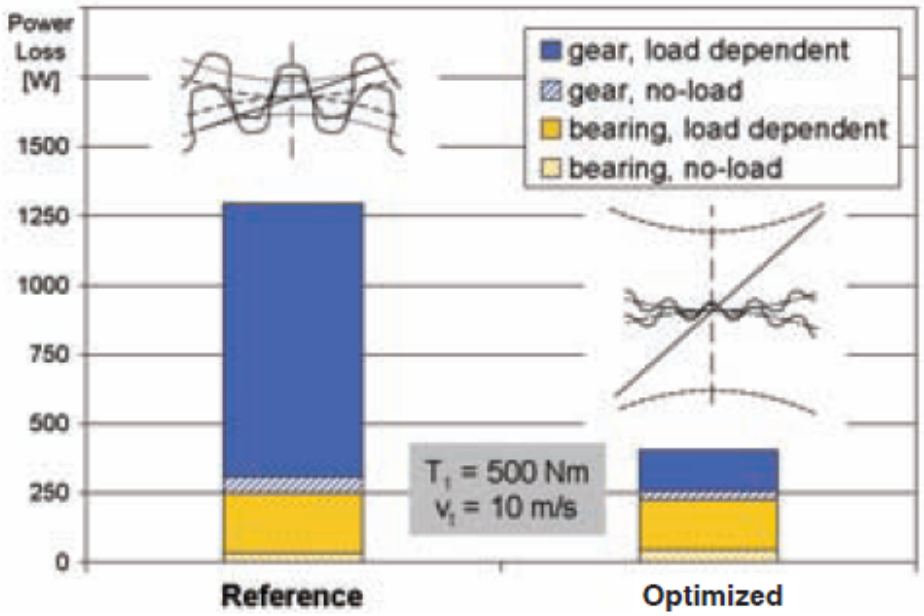

Figure 2.1.: Power loss comparison between Type C and Hohn Low Loss gears [8].

Figure 2.2.: Visual Representation Comparison of the two gear types.

2.2. Gears Geometry

Unlike the low loss gear proposed by Hohn et al [8] for the low loss gear, present in the Table 2.1, in this study there were developed three new gear sets, with a 20° pressure angle.

Gear module and transverse contact ratio are fundamental to reach the main objective of this work, as well as, the pressure angle. However the optimization of this parameters can lead to a weak gear in terms of mechanical resistance. The reduction of the module and the consequent increase in the number of gear teeth causes an important reduction of the transverse contact ratio. In order to solve this problem it was necessary to convert from a spur gear to an helical one, thus introducing the helix angle, and therefore assuring an aceptable total contact ratio [38].

The reduction of the gear module has the following effects [39, 40]:

a) Teeth become smaller and more numerous;

b) Contact occurs in shorter periods along a shorter contact path;

c) The transverse contact ratio decreases. If it reaches a value lower than 1, it must be compensated with the creation of the helix angle (assuring a global contact ratio of 2 or more);

d) The tooth root bending resistance diminishes, and this may be compensated by wider teeth or higher pressure angles;

e) Wear, scuffing probability and friction coefficient tend to diminish, favoring the operation conditions;

f) Reduction of the power dissipation by gear friction;

Three gear geometries (Figure 2.3) were made resorting to computational resources, in order to simulate possible profiles. Then the contact pressure, teeth bending and root resistance were calculated to ensure the mechanical resistance of the new developed gears. As it was mentioned before and in order to comply with the FZG test bench requirements, the Type C gear was chosen to be the start point in the development [41].

The process was long, and it involved sixteen different profiles. These included pressure angles from 20 to 40°, helix angles from 15 to 20°, teeth with from 20 to 30[mm], and some other different modifications.

Another parameter that has a very significant influence is the addendum modification coefficient, since this allows the gear working pressure angle of 30°. It should be mentioned that these gears were manufactured using standard 20° pressure angles cutting tools [38].

2.2.1. Low Loss Gears Geometry: 310, 410 and 610

The three geometries developed, hereafter will be designated as 310, 410 and 610 series (varying the last number according with the material that they were manufactured in).

The 310 is the geometry that most seems with the standard Type C gear, the two other are increasingly modified aiming to the less teeth friction. All the gears have 20° pressure angle, 15° helix angle and they all are 20mm wide and still be able to present the improvements observed in the "Low Loss" gear model presented by Hohn et al [38].

A summary of the main geometric properties, safety coefficients, contact parameters and friction power loss were calculated.

These parameters are present in Table 2.2 and a representation of the geometries is shown in Figure 2.3.

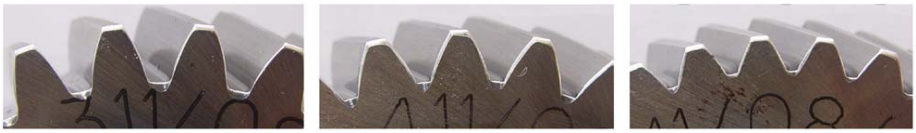

Figure 2.3.: Pinion teeth of gears 310, 410 and 610 (from left to right) [9].

Gear Parameters	**Symbol**	**[units]**	**310**		**410**		**610**	
			pinion	**wheel**	**pinion**	**wheel**	**pinion**	**wheel**
Module	m	[mm]	2.5		2.25		1.75	
Working pressure angle	α_{wt}	[°]	22.12		26.7		28.34	
Number of teeth	Z	[-]	28	42	30	45	38	57
Gear ratio	u	[/]	1.5					
Teeth width	b	[mm]	20					
Helical angle	β	[°]	15					
Pitch diameter	d	[mm]	72.47	108.7	69.88	104.82	68.85	103.27
Base diameter	d_b	[mm]	67.81	101.72	65.39	98.09	64.42	96.64
Addendum mod. Coef.	x	[-]	0.13	0.25	0.96	1.15	1.74	1.95
Tip diameter	d_a	[mm]	78.05	114.89	77.5	113.29	76.41	111.56
Tip diam. Mod. Coef.	k*m	[mm]	-0.03		-0.61		-1.02	
Working pitch diameter	d_w	[mm]	73.2	109.8	73.2	109.8	73.2	109.8
Transverse contact ratio	ϵ_α	[-]	1.52		1.17		0.93	
Overlap contact ratio	ϵ_β	[-]	0.66		0.73		0.94	
Total contact ratio	ϵ_γ	[-]	2.18		1.9		1.87	
Path of contact (length)	g	[mm]	11.58		8.02		4.97	
Contact Parameters*								
Max. Sliding speed (tip)	vg_a	[m/s]	2.18	2.37	1.71	1.44	1.24	0.71
Calculated Gear Friction Power Loss**								
Gear Friction Power Loss	P_{fr}	[W]	413		299		240	

*Torque applied to wheel -323 Nm. wheel rotation - 1500rpm
**Considering an ester-based fully saturated gear oil, ISO VG 100

Table 2.2.: Geometric characteristics of 310/410/610 gears.

2.3. Gears Material

The three gear geometries were manufactures with two diferent materials: Carburized Steel and Austempered Ductile Iron (ADI).

2.3.1. Carburized Steel (DIN 20MnCr5)

Carburized Steel is manufactured in steel, according to the norm DIN 20MnCr5. This material is often used to produce gears and other highly stressed mechanical components.

The high mechanical properties present in this kind of material are obtained with an heat treatment described in Table 2.3.

The tooth flancks have high hardness, normally around 60 HRC, while the core keeps a high strength and a high elongation [42].

Heat treatment step	Temperature	Time period
Pre-heating	100°C	
Austenitization	900°C	
Carburizing temperature	900-950°C	5h
Diffusion during cooling	Cooling to 860°C	2h30
Stabilization before quenching	860°C	00h30
Quenching in oil	60°C	
Tempering temperature	220°C	1h00

Table 2.3.: Heat treatment steps for the Carburized Steel (DIN 20MnCr5).

Chemical composition of the Carburized Steel is presented in Table 2.4.

C	Si	Mn	Cr
0.2	0.2	1.25	1.15

Table 2.4.: Chemical composition (weight %) of Carburized Steel (DIN 20MnCr5).

The main mechanical characteristics are present in the Table 2.5.

Parameter	Units	Value
Elastic module	GPa	210
Density	g/cm^3	7.85
Poisson ration	[/]	0.3
Hardness	HRC	60
Tensile strength	N/mm^2	1300
Yield strength 0.2%	N/mm^2	850
Elongation*	%	8
Tensile strength measured from test specimens (average values)		

Table 2.5.: Properties of Carburized Steel [11].

From now on the carburized steel gears used in this work will be designated 311, 411 and 611, thereby using the last digit as 1 for carburized steel gears.

2.3.2. Austempered Ductile Iron (ADI)

The Austempered Ductile Iron (ADI) is an iron alloy manufactured accordingly with the norm DIN 1.0Cu-0.5Mn, that have been used since late 1970s. These materials have been remarkably improved since then, being one of the most interesting Fe-C alloys, having a very interesting combination of mechanical properties [42, 43].

ADI iron alloy has lower Young's modulus than steel therefore different elastic properties that influence the contact parameters.

Ductil iron has several advantages when compared with steel, namely lower weight, better vibration absorption, high resistance to wear and scuffing, being very useful in cases of temporary breakdowns, like a lubrication system failure, and lower production costs. This lower production costs derives from the manufacturing process since they are cast materials and so they don't have lower costs associated to the machining operations [11, 42, 43].

The ADI is obtained through an austenitisation during 40 min at temperatures around 900 °C followed by an isothermal transformation during 4h at temperatures around 300 °C , are then cooled for 2 min in water at room temperature. A scheme representing the process used is present in the Figure 2.4 [11, 44].

The ADI surface, microstructure and the graphite nodules formed during the process are shown in the Figures 2.5a to c.

Chemical composition of ADI is presented in Table 2.6 [11, 12, 42].

C	Si	Mn	Cu	P	S
3.38	2.43	0.55	1.11	0.01	0.02

Table 2.6.: Chemical composition (weight %) of Austempered Ductile Iron (DIN 1.0Cu-0.5Mn).

The main mechanical characteristics are present in the Table 2.7.

From now on the Austempered Ductile Iron gears used in this work will be called 312, 412 and 612, thereby designating the last digit as 2 for Austempered Ductile Iron gears.

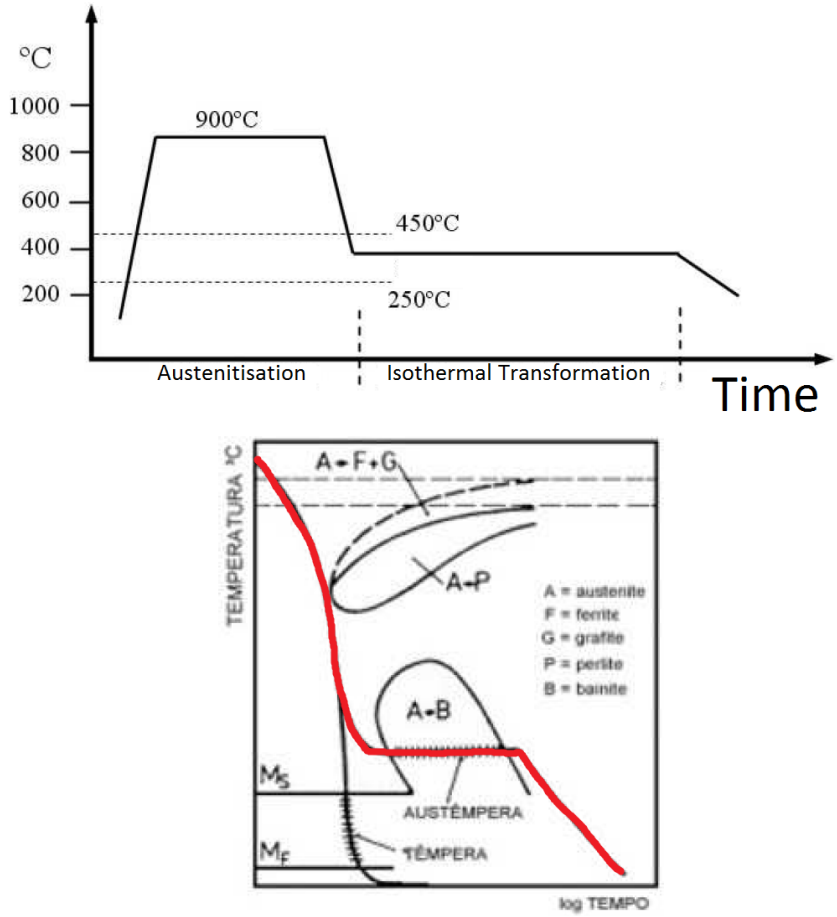

Figure 2.4.: Procedure of ADI austempering heat treatment.

Parameter	Units	Value
Elastic module	GPa	170
Density	g/cm^3	7.06
Poisson ration	[/]	0.25
Hardness	HRC	42
Tensile strength	N/mm^2	1433
Yield strength 0.2%	N/mm^2	1178
Elongation*	%	6
Tensile strength measured from test specimens (average values)		

Table 2.7.: Properties of Austempered Ductile Iron [12].

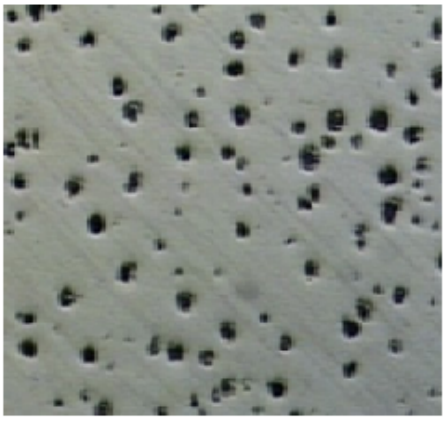

(a) ADI Surface (x50) [11]

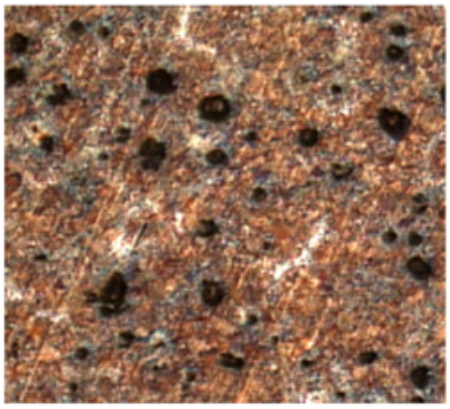

(b) ADI Microstructure (x100) [12]

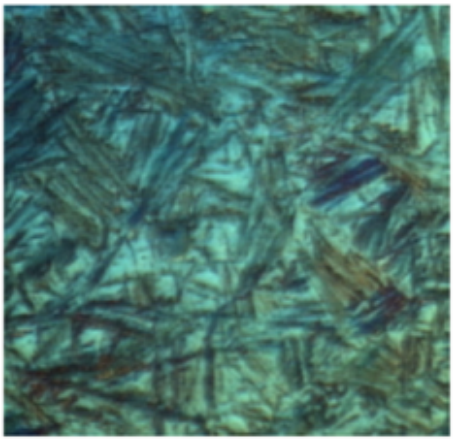

(c) ADI Microstructure (x1000) [12]

Figure 2.5.: ADI Microstructure.

2.3.3. Safety coefficients and working parameter comparison

Initially the gears were designe to have similar safety factors (as presented in the Table 2.8), being the width of the the gears different as its presented in the Table 2.8, but due to an assembly problem (that will be mentioned ahead in the Section 3.2) the width of the gears was balanced to 20mm for all gears, and the safety factors had a small decrease, specially gear 610.

In Table 2.9, for a width of 20mm, are displayed that the scuffing, bending and pitting safety coefficient and some working parameters like the resonance speed, Hertzian pressure and gear friction power loss, so that they can be compared.

In general, the safety factors for the steel gears are better than the ADI ones for the three chosen geometries except for the scuffing coefficient, this might

be explained by the fact of all ADI gears have lower Hertz pressure compared to the steel ones. In ADI the surface texture is worse than the steel one, this explains the increase of gear friction power loss in ADI gears relatively to their steel equivalent.

Gear Parameters	**Symbol**	**Units**	**310**		**410**		**610**	
			pinion	**wheel**	**pinion**	**wheel**	**pinion**	**wheel**
Tooth width	b	mm	20		22		26	
Safety coefficients*								
Tooth root stress	SF	-	1.79	1.79	1.6	1.6	1.92	1.91
Surface pressure	SH	-	1.18	1.19	1.19	1.21	1.21	1.21
Contact Parameters*								
Max. Hertz pressure	P0	GPa	0.96		1.08		0.96	

Table 2.8.: Safety Coefficient for all gears with the correct widths.

			310		410		610	
Safety Coefficient	**Symbol**	**Units**	Steel	ADI	Steel	ADI	Steel	ADI
Bending	SF	-	1.8	1	1.5	1	1.5	1.4
Pitting	SH	-	1.2	1	1.2	1	1.1	0.9
Scuffing	SB	-	3.5	2.58	4.21	2.96	-	-
Working Parameters								
Hertz pressure*	P_0	GPa	1.17	0.97	1.19	1.01	1.29	1.11
Resonance speed	nE1	rpm	13139	11753	11407	10209	7778	6969
Friction Power Loss*	P_{fr}	kW	0.417	0.624	0.303	0.453	0.243	0.363
*speed=1500rpm, torque=323Nm (applied to wheel), transmitted power=50.8kW								

Table 2.9.: Safety Coefficient and Working Parameters [11].

2.4. Tested Oils

For this work two gear oil types, E1 and P1, were selected, with different base oil formulations. Both gear oil types are fully formulated and classified as CLP gear oils according to DIN 51517, and the main properties of these two oils type are presented in Table 2.10.

P1 and E1 are both commercial products with viscosity grades ISO VG 150 and ISO VG 100 respectively. P1 has a polyalolephine (PAO) base oil and E1 has a highly saturated biodegradable ester base oil.

Oil Reference **Base Oil**		**E1** **Ester**	**P1** **PAO**	
Oil properties	**Symbol**	**Value**	**Value**	**Units**
Kinematic viscosity @ 40°C	ν_{40}	99.4	151	cSt
Kinematic viscosity @ 100°C	ν_{100}	14.6	19.4	cSt
Density @ 15°C	ρ	0.925	0.848	g/cm^3
Viscosity Index	VI	152.0	147.0	[/]
Thermoviscosity @ 40°C	β_{40}	0.0443	0.0471	cSt/°C
Thermoviscosity @ 100°C	β_{100}	0.0229	0.0244	cSt/°C
Piezoviscosity at 0,2 GPa ($\alpha = s.\nu^t$)				
Piezoviscosity parameter	s	6.605	7.382	[/]
Piezoviscosity parameter	t	0.136	0.1335	[/]
Piezoviscosity @ 40°C	α_{40}	12.35	14.41	GPa^{-1}
Piezoviscosity @ 100°C	α_{40}	9.51	10.97	GPa^{-1}
Oil working temperature	T_f	90.00	90.00	°C
Viscosity by ASTM D341	a	0.700	0.700	[/]
log log (ν+a) = n - m log T	m	2.987	2.936	[/]
	n	7.756	7.666	[/]
Andrade expression: v = v_0 exp [b (1/T - 1/T_0)]	b	3732.33	3992.83	K
Lubricant type - ALFAP mineral = 1.216; synthetic = 0.914	ALFAP	0.914	0.914	E^{-8}/Pa
Lubricant Absolute temperature	T	363	363	K
Kinematic viscosity	**n**	18.57	25.09	mm^2/s
Dynamic viscosity	**h**	0.017	0.022	Pa s
Piezoviscosity coefficient	**a**	1.34E^{-8}	1.48E^{-8}	Pa^{-1}
Thermoviscosity coefficient	**b**	0.025	0.027	K^{-1}
Thermal conductivity	**k**	0.128	0.134	w/m °C
Specific weight	**c**	2012.96	2062.61	J/Kg °C

Table 2.10.: Lubricant Properties.

The two gear oils have different physical properties, for example, their kinematic viscosities at 100 °C are 19.4 cSt and 14.6 cSt, for P1 and E1 oils respectively. At the same temperature their piezoviscosities are 10.97 GPa^{-1} and 9.51 GPa^{-1}, for P1 and E1 oils respectively.

E1 has the lowest viscosity and piezoviscosity coefficient. These two physical properties have similar contributions to the lubricant film buildup, being the film thickness higher if the piezoviscosity coefficient and the viscosity are also higher, so P1 is better in these two items.

Because these two lubricating oils have different physical properties, they will generate different friction coefficients between gear teeth and therefore different gear friction power loss, being the operative conditions entirely dependent on gear oil type.

3. Test Machines and Procedures

Several test rigs and measurements devices were used in this work, such as, the FZG test rig, the Hommelwerk roughness measuring system and the Direct Reading Ferrometer (DRIII). So in this chapter an overview of these equipments, tests procedures and analysis techniques used during this work will be presented.

3.1. FZG Test Rig

The FZG test rig is a well known back-to-back spur gear test rig with "power circulation", shown in Figure 3.1. The test pinion (1) and the test wheel (2) are connected by two shafts to the driving gears (3). The front shaft is divided in two parts with the load clutch in-between (4). One half of the load clutch can be fixed to the foundation by a locking pin (5) while the other part can be twisted using a load lever and weights (6). After bolting the clutch together the load can be removed and the shaft unlocked. Now a static torque is applied to the system that can be measured by the torque measuring clutch (7). The maximum speed of the AC-motor (9) is 3000 rpm. The test gears can be dip lubricated or jet lubricated. When dip lubrication is used, the oil may be heated using the electrical heaters mounted in the test gearbox. The heater and cooling coil allows the settling of a constant oil temperature measured by the temperature sensor (8) [41].

Several types of standard gear tests [41] may be performed on the FZG gear test rig:

i) Gear scuffing tests;

ii) Gear pitting tests;

iii) Gear micropitting tests;

iv) Gear power loss tests,

v) Gear oil scoring tests;

vi) Gear grease scoring and wear tests;

vii) Shear stability test.

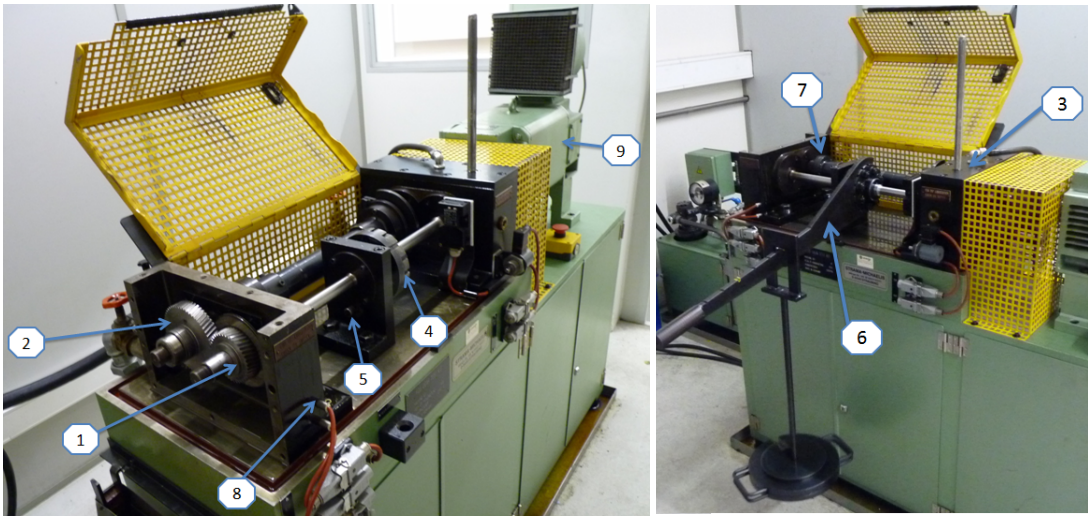

Figure 3.1.: Representation of FZG test rig.

3.2. Pressure Pads

The pressure pads are a pair of metallic hydrodynamic discs designed to absorb the axial forces produced during the meshing cycle of helical gears sets, Figure 3.2a. Each side of the pinion has a pad mounted in, and a picture of this assembly can be seen in the Figure 3.2b.

Pressure pads were the solution to the fact that the standard FZG test gearbox was only prepared to test spur gears, and this kind of gears do not generate axial forces. Since the helical gear produce axial forces, there was the need to find a solution to absorb those efforts.

With this solution only a residual amount of axial forces are transmitted to the roller bearings that can only sustain small amounts of axial loads and leaving them free to support the radial loads generated during the meshing cycle of the helical gears. With this solution there is no damage to the test gearbox that could compromise the data gathered during the tests, affecting this way the result and the conclusions of the studies made on the subject.

The use of pressure pads imposes two constraints. The first one, is that pressure pads are designed for a particular gear width, 20mm in the present case. Thus all the gears had the same width, and consequently gears 410 and 610 have lower safety factors (S_F and S_H) than gear 310 [9].

The second constraint is that the pressure pads increase the "No Load Power Losses" because of the Couette flow between the pads and the FZG gear wheel, and also increase the churning losses.

(a) Pressure pads **(b)** Pressure pads assembly

Figure 3.2.: Pressure pads.

3.3. Power Loss Test Procedure

Power loss tests were performed in the FZG machine using a spur gear test gearbox with pressure pads (see Section 3.2) for axial load absorption. The gear set geometries tested in this experimental work, were the ones described in the Table 2.2 (Chapter 2, Section 2.2, Sub-section 2.2.1). For each geometry they were manufactured with the two materials already presented, carburized steel and ADI (see Chapter 2, Section 2.3).

The different torques applied correspond to the Standard FZG Load stages, using a 0.35m load arm, and the four load stages were accomplished using the combination of weights that give the intended torques.
The different load (torque) combinations can be seen in Figure 3.3, for K1, K5, K7 and K9 load stages, respectively. The obtained torques are referred in Table 3.1 and for every load stage the test was performed at three different speeds: 500 rpm, 1000 rpm and 2000 rpm.

For each load stage and speed combination, the FZG machine operates during 4 hours in order to achieve a state of energetic equilibrium between the power loss inside the FZG gear box and the heat evacuated to the surrounding environment, reaching in this way a constant oil operating temperature.

Every load stage had three periods of 4 hours each, performed at constant speed, performing a total of 120 000 cycles at 500rpm, 240 000 cycles at 1000rpm and 480 000 cycles at 2000rpm, making a total of 840 000 cycles per load stage.

At the end of each load stage cycle, an oil sample was collected (Figure 3.4a) with an appropriate equipment (Figure 3.4b), containing approximately 40ml

of used oil, in order to be analyzed by Direct Reading Ferrography (DRIII) and Analytical Ferrography (FMII). (see Section 3.7 below).

Two versions of each test were performed, one using an oil volume of 1000 cm^3 (low oil level) and another using 1500 cm^3 (high oil level) (see Chapter 4).

Test Type	**Wheel Torque [Nm]**	**Wheel Speed [rpm]**	**Input Power [kW]**	**Initial Temperature [°C]**	**Operating Time [Hours]**	**Number of Cycles [$\times 10^6$]**	**Lubricant Monitoring Samples**
No	4.95	500	0.52	Room	4		
Load	(k_{FZG}=1)	1000	1.04	Temperature	4		
Tests		2000	1.56		4	0.84	40 ml
	105	500	11	≤ 40	4		
	(k_{FZG}=5)	1000	21.99		4		
		2000	32.99		4	0.84	40 ml
Load	198.8	500	20.81	≤ 40	4		
Tests	(k_{FZG}=7)	1000	41.63		4		
		2000	62.44		4	0.84	40 ml
	323.4	500	33.87	≤ 40	4		
	(k_{FZG}=9)	1000	67.73		4		
		2000	101.6		4	0.84	40 ml
Total	/	/	/	/	48	3.36	/

Table 3.1.: Power loss test operating conditions.

(a) K1 **(b)** K5 **(c)** K7 **(d)** K9

Figure 3.3.: "Dead weight" load combinations.

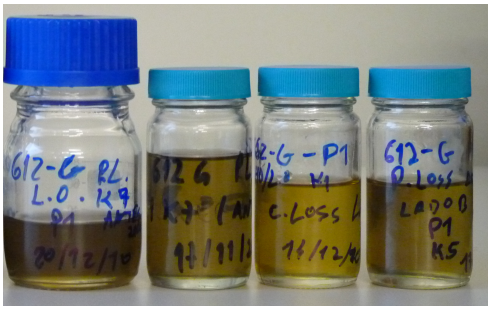

(a) Oil Samples

(b) Vacuum oil pump

Figure 3.4.: Oil samples and oil pump.

3.4. Churning Loss Test Procedure

The need to known how the oil level influences the performance of the gears and gear power loss, an more extended version of the churning loss test was developed.

The churning loss test consists in the application of minimum torque (load stage K1, $T_2 = 4.95$ N.m), and then perform the test at several different speeds, from 500 to 2500 rpm, as shown in Table 3.2. In resemblance to the power loss test, the churning loss test has the duration of 4 hours for each designated speed, in order to achieve a state of energetic equilibrium inside the FZG gear box and the evacuation heat to the surrounding environment, reaching in this way a constant oil operating temperature.

All gear geometries were submitted to the Churning loss gear test, described in Table 3.2, for high and low oil levels. All the other post test analysis procedures like the roughness measurement, oil analysis and mass loss remain the same done in the power loss test where also done in this case.

At the end of test (36 hours), an oil sample was collected, analyzed by the Reading Ferrometry and Analytical Ferrography (see section 3.7 below).

Test Type	Wheel Torque [Nm]	Wheel Speed [rpm]	Initial Temperature [°C]	Operating Time [Hours]	Number of Cycles [$\times 10^6$]	Lubricant Monitoring Samples
		500		4		
		750		4		
		1000		4	0.54	
Churning	4.95	1250	Room	4		
Tests	(k_{FZG}=1)	1500	Temperature	4		
		1750		4	1.08	
		2000		4		
		2250		4		
		2500		4	1.62	40 ml
Total	/	/	/	36	3.24	

Table 3.2.: Churning loss test operating conditions.

3.5. Surface Roughness and Topography Measurement

Tooth flank roughness is an important parameter in gear power loss. Therefore an accurate measurement is essential to do a complete study of surfaces submitted to a power loss test.

The roughness measurements were performed on a *Hommewerke* T8000 controller with a linear unit Lv50/50E (Figure 3.5), using a $\pm 300 \mu m$ probe, designated by TK300 (Figure 3.6), having a tip radius of 5 μm and a cone angle of 90°.

A total measuring length of L_t = 4.8mm and a cut-off filter λ_c=0.8mm with a velocity V_t=0.5mm/s, were selected, being the roughness profile digitally filtered with the help of the TurboWave software provided by the machine manufacturer (Figure 3.7) [45].

The determination of the roughness parameters was performed according to the standards DIN4762, DIN4768 and DIN4776 [45].

The roughness measurement equipment also performs surface topography, although this is a very time consuming operation. The topographies performed are basically parallel roughness measurements at a well defined distance.

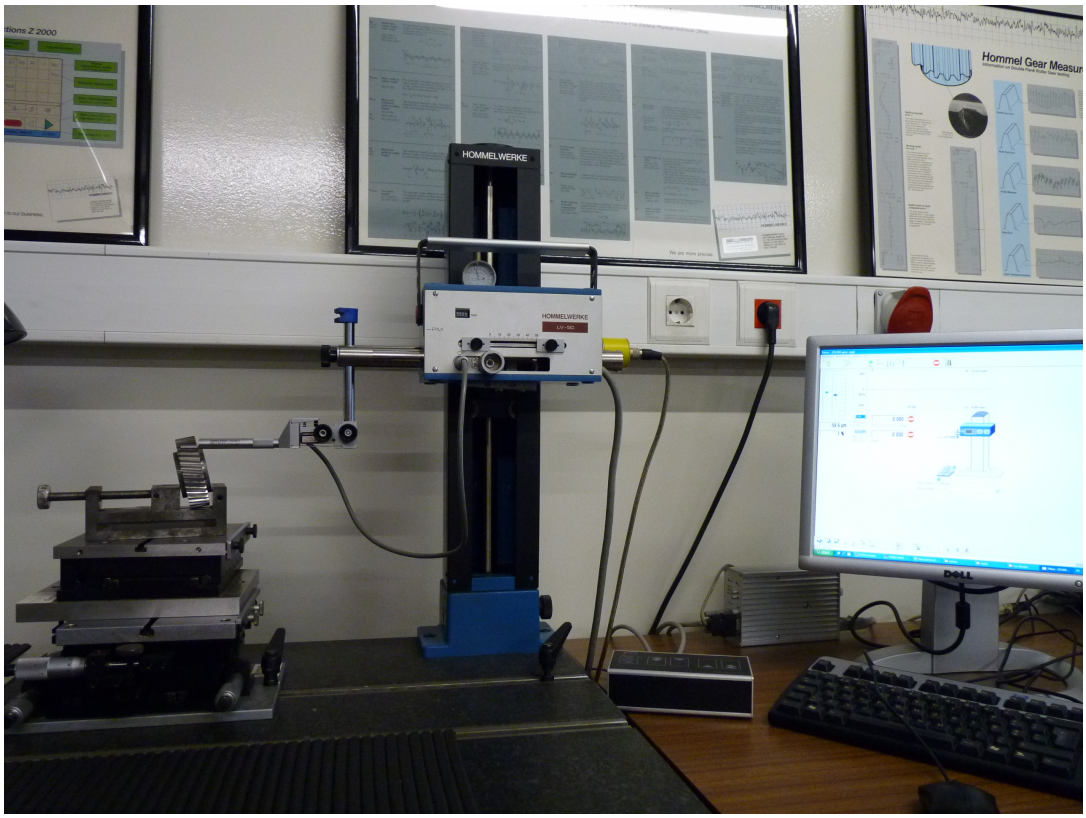

Figure 3.5.: Hommewerke T8000 controller.

Figure 3.6.: Tk300 Probe.

The manufactures program calculates several of the most important roughness parameters and they are [45]:

i) The average roughness value (R_a) - The average deviation of the absolute values of the distances from the mean line to roughness profile within the sampling length, and it is used control the production process quality of the surfaces.

ii) The root mean-square profile (R_q) - The square root of the average of the square of th deviation of the profile form the mid line. This parameter is more sensitive than R_a to peaks and valleys, it can basically be considered as the standard deviation from statistics.

iii) The mean peak-to-valley height, ($R_{Z_{(DIN)}}$) - The average of the 5 peak-to-valley heights measured from the filtered profile, and is more sensitive to surface finish than R_a.

iv) The reduced peak height (R_{pk}) and the reduced valley depth (R_{vk}) - The first is the average height of the highest peaks above the core roughness, and can be caused by the grinding process. The second is the average depth of the lowest valleys below the core roughness and result from the raw material composition and cannot be significantly altered by the grinding process.

The roughness measurement, integrates the power loss test procedures. Thus, was made at the beginning and at the end of each power loss test a roughness measurement.

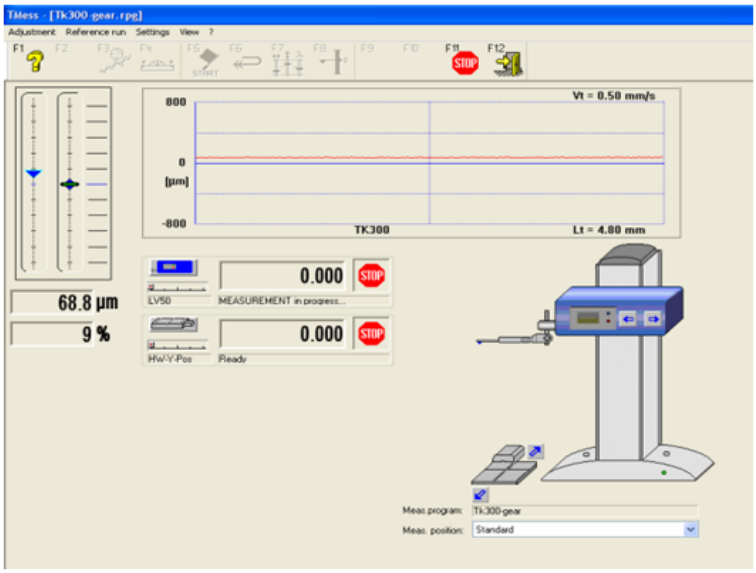

Figure 3.7.: Roughness measurement software (Turbowave).

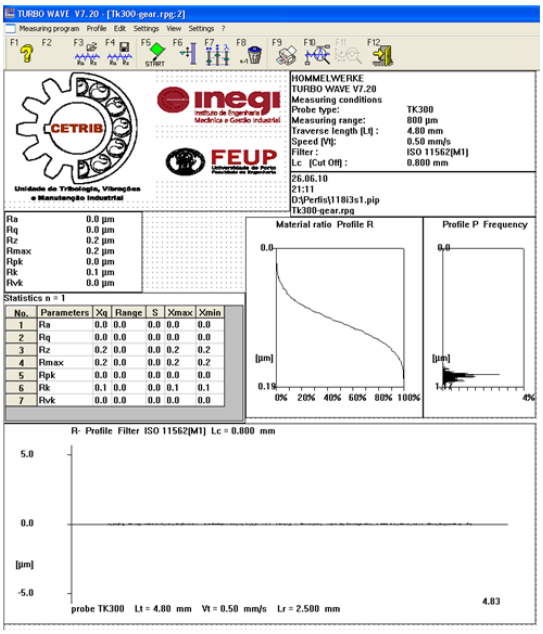

Figure 3.8.: Roughness measurement datasheet.

The first and fifth tooth of each pinion and wheel tested were measured, being both measurements made in the axial direction of the gear teeth. In order to get an accurate representation of each tooth roughness three measurements were made, one below the pitch line, another above the pitch line and the third the closest possible to the pitch line, in a total of six roughness measurements for each gear.

An example of the roughness measuring in a gear tooth can be seen in the Figure 3.9 , being the image representative of the three measurements made in a helical gear tooth.

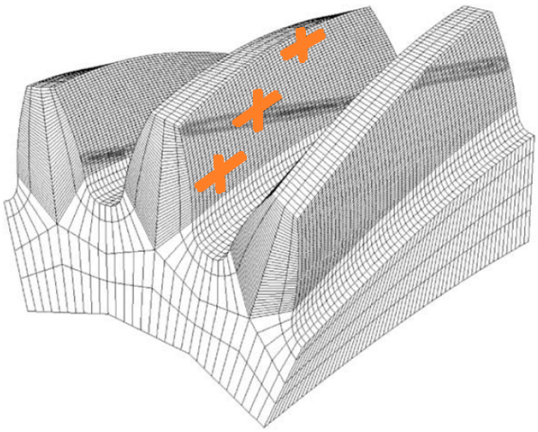

Figure 3.9.: Example of the roughness measuring in a gear tooth.

3.6. Mass Loss Procedure

In this work the mass loss measurements were made with an electronic *Metler-Toledo PR1203* weighing-machine with a max capacity of 1210 g and precision of ±1 mg, present in the Figure 3.10.

The mass loss evaluation concerns the amount of material that was lost during the churning loss or power loss test. A reference pinion was used in order to prevent any weighting measurement deviation (see Figure 3.11). After the power loss tests the pinions were weighed (average of three weighings).

Before any weighing, the component was washed in an ultrasonic bath of solvent and cleaned in order to remove all the oil and any other type of particles that might be glued to the surface. The weighing-machine was turned on 30min before the measurements take place, avoiding electronic oscillations.

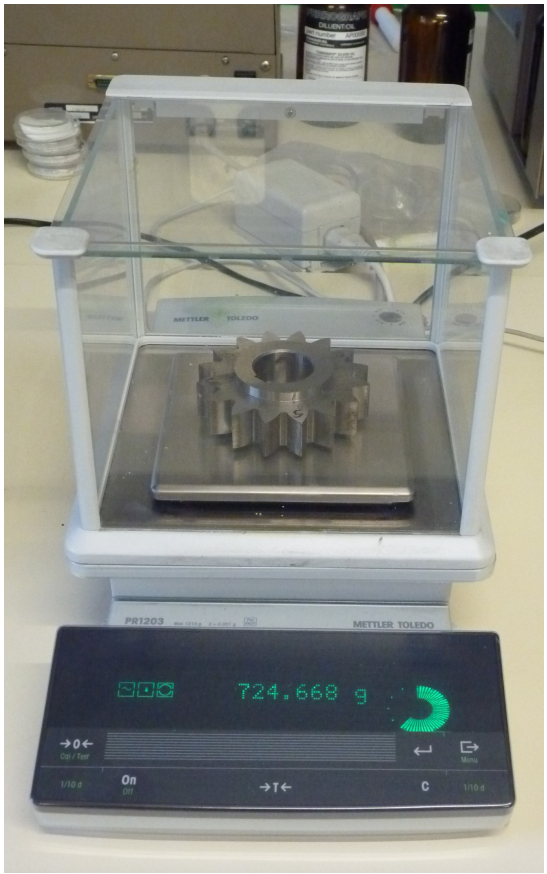

Figure 3.10.: Electronic *Metler-Toledo PR1203* weighing-machine.

Figure 3.11.: Reference pinion (left) and Tested Pinion (right).

3.7. Oil Analysis

The analysis of particles contained in lubricant samples gives a quite good indication about the wear of lubricated parts, since those particles in a closed box are generated in the contacting surfaces. All the tests performed during this work were followed by regular oil analysis as it was mentioned above (Section 3.3).

If the wear particles concentration is high, the sample is diluted with a solvent, being the dilution a function of the contamination level.

Two main techniques were always used, Direct Reading Ferrometry (DR III) and Analytical Ferrography (FM III) [46, 47].

These analysis allow the identification and characterization of the wear particles present in the oil samples generated during the tests performed. This allows the comparison of lubricants and materials. Based on the size of wear particles and the amount of wear particles the wear degree is measured.

3.7.1. Direct Reading Ferrometry: Equipment and procedure

Direct Reading Ferrographer (see Figure 3.13) measures quantitatively the ferrous particles concentration contained in the lubricant. A 1ml sample is forced to pass through a capillary tube submitted to a strong magnetic field and two light beams (see Figure 3.12), and then a optical system in which opacity measurements are performed, and quantifies the intensity of light that passes through the tube, being directly proportional to the density of the deposited particles.

This measure the ferrometric parameters D_L (large wear particles index - particles with size greater than $5\mu m$) and D_S (small wear particles index - particles with size smaller than 5μm).

From the knowledge of these two indexes is possible to calculate the wear particle concentration index (CPUC) and the wear severity index (ISUC), using the Equation 3.1 and Equation 3.2, respectively.

$$CPUC = \frac{D_L + D_S}{d} \tag{3.1}$$

$$ISUC = \frac{D_L^2 - D_S^2}{d^2} \tag{3.2}$$

Where d represents the dilution factor of the sample in cases of excessive contamination, as it was discussed above in the introductory section.

The CPUC index grows when the sum of large and small particles increase, while the ISUC index grows when the number of large particles is greater than the number of small particles.

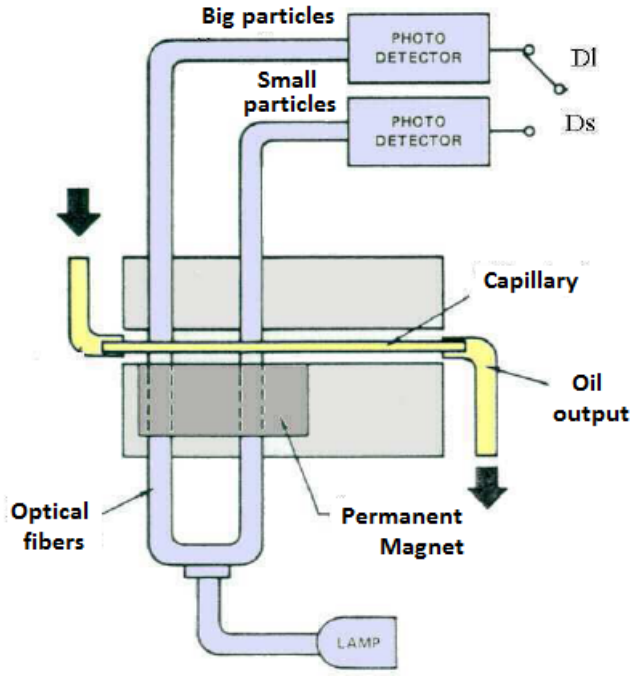

Figure 3.12.: Direct Reading Ferrographer scheme [10].

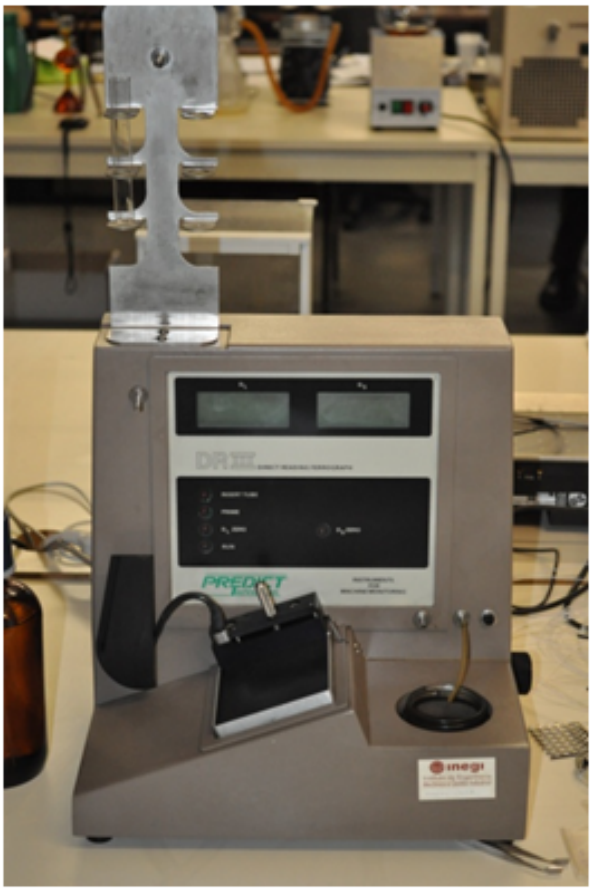

Figure 3.13.: Direct Reading Ferrographer.

3.7.2. Analytic Ferrometry: Equipment and procedure

Analytical ferrography (Figure 3.15), is used to obtain more detailed information of the lubricant contaminant particles and is performed on a diluted oil sample that is passed through a slide (the ferrogram) and submitted to a magnetic field, being the wear particles positioned along the slide as function of their magnetic sensibility and size, being the larger particles deposit in the beginning of the ferrogram and progressively decrease in size along the length of the ferrogram.

A schematic view of the process is shown in Figure 3.14.

The ferrogram, is then observed on a microscope (Figure 3.16), with bichromatic light (also known as ferroscope), and analyzed.

The analytical ferrography provides information concerning the size of the wear particles, their morphologies, the particles concentration, the type of wear that originates the particle, allowing a more complete knowledge of the wear mechanism.

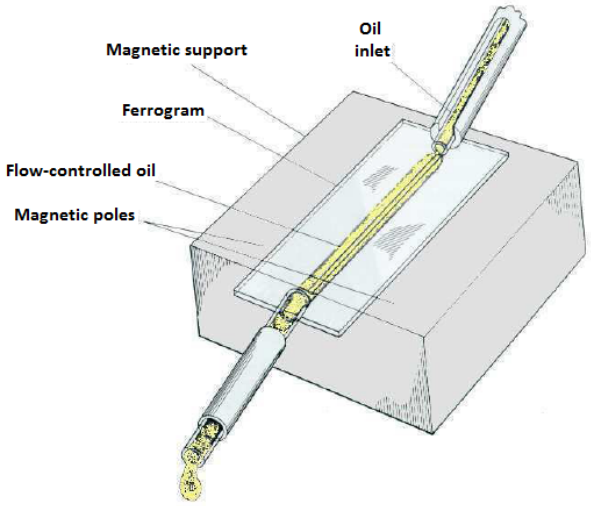

Figure 3.14.: Analytic Ferrographer scheme [10].

Two images from a ferrogram analysis, observed in the microscope and amplified 1000 times, can be seen in Figure 3.17. In the Figure 3.17a a ferrous laminar particle is shown, that resulted from a combined wear (fatigue + slip), and in the Figure 3.17b several wear particles typical of laminar fatigue wear, are presented.

Figure 3.15.: Analytic Ferrographer.

Figure 3.16.: Bi-Chromatic microscope (ferroscope).

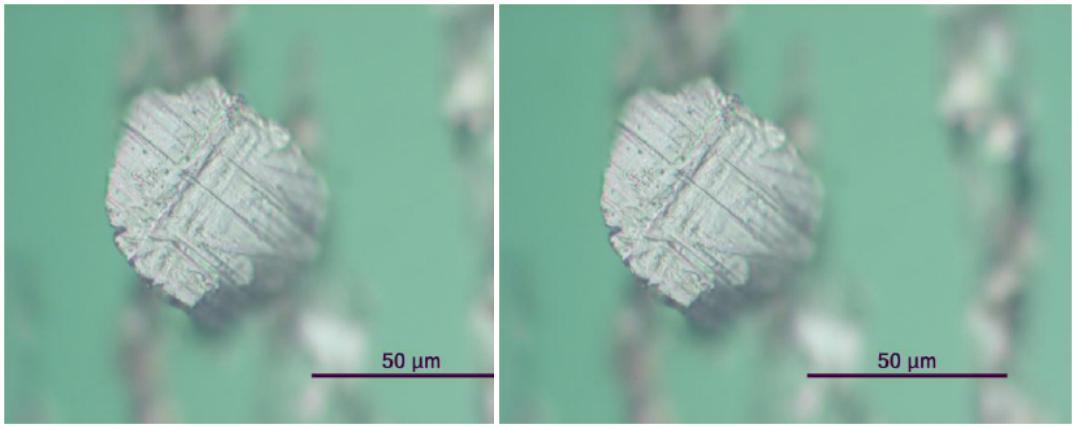

(a) **(b)**

Figure 3.17.: Ferrogram taken after k9 load stage of a power loss test (Appendix A.2: Power Loss Data Sheets of a 411 with E1 oil) 1000x.

4. Experimental Results

The results of the stabilization temperatures measured during the gear power loss tests are present in this chapter, for all gear geometries, gear oils, gear materials and for the two oil levels (high and low).

The results from oil analysis, surface roughness analysis and gear mass loss are also presented.

4.1. Ester base lubricant oil (E1) gear test and low oil level

4.1.1. Stabilization temperatures

The stabilization temperature is the parameter that will be observed in the following analysis. It represents the difference between the oil bath temperature and the room temperature, that is, $\Delta T = T_{oil} - T_{room}$, after stabilization, when the power loss inside the FZG gearbox is in equilibrium with the heat flow from the FZG gearbox to the surrounding environment.

The stabilization temperatures were taken after 4 hours of operation at specified operating conditions (torque and speed).

4.1.1.1. Steel gear 311, 411 and 611 - lubricant E1 and low oil level

Figure 4.1 presents the stabilization temperatures of the steel gears (311, 411 and 611), lubricated with gear oil E1, and a low oil level (LO), for all applied torques (K1, K5, K7 and K9) and all operating speeds (500, 1000 and 2000 rpm), in relation to the corresponding reference gear friction torque loss.

Whatever the operating conditions, applied torque and speed, steel gear 611 generates lower stabilization temperatures than gear 411, and the latter lower temperatures than gear 311. This trends is very clear for an operating speed of 500 rpm. At 1000 rpm and 2000 rpm and low torques (K5), gear 411 and 611 showed similar stabilization temperatures.

Figure 4.1, shows that, for almost all load stages and speeds, gear 611 showed the best performance.
In load stage K5, the stabilization temperatures of the gears are close to each other.

On the other hand gear 311 had the worst performance whatever the operating conditions. The stabilization temperatures are higher then for other steel gears.

Gear 411 had an average performance in all load stages and velocities. To enhance that the stabilization temperatures in the k5 and k7 load stages are near the 611 gear.

310 gear geometry had the highest friction torque loss of all the 3 geometries used.

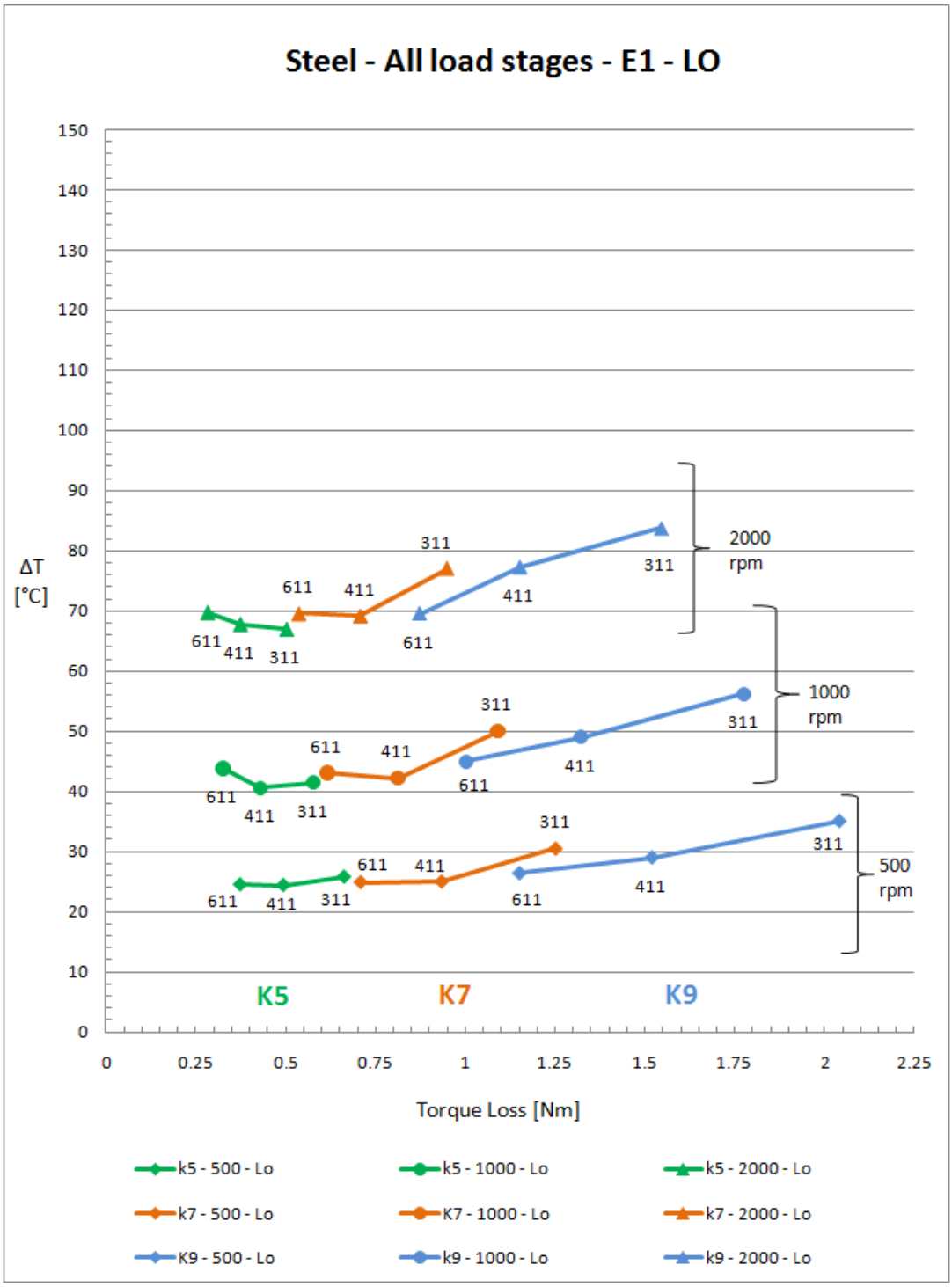

Figure 4.1.: Stabilization temperatures in gear power loss tests: steel gears (311, 411, 611), E1 lubricant, low oil level.

4.1.1.2. ADI gear 612 - lubricant E1 and low oil level

Figure 4.2 shows the stabilization temperatures as a function of the theoretical friction torque loss, for the ADI gears geometries, operating with a low oil level, for all velocities and load stages.

Unfortunately, in the case of ADI gears, there is not much data to compare, since the power loss tests with E1 oil and low oil level for ADI gears 312 and 412 were not performed due to some technical problems in the manufacturing process of the gears sets. So Figure 4.2 only shows the results related with the 612 geometry.

The stabilization temperatures are similar at 500 or 1000 rpm, regardless the load stage. At 2000 rpm there is a slight increment in the stabilization temperature with the increase of the load.

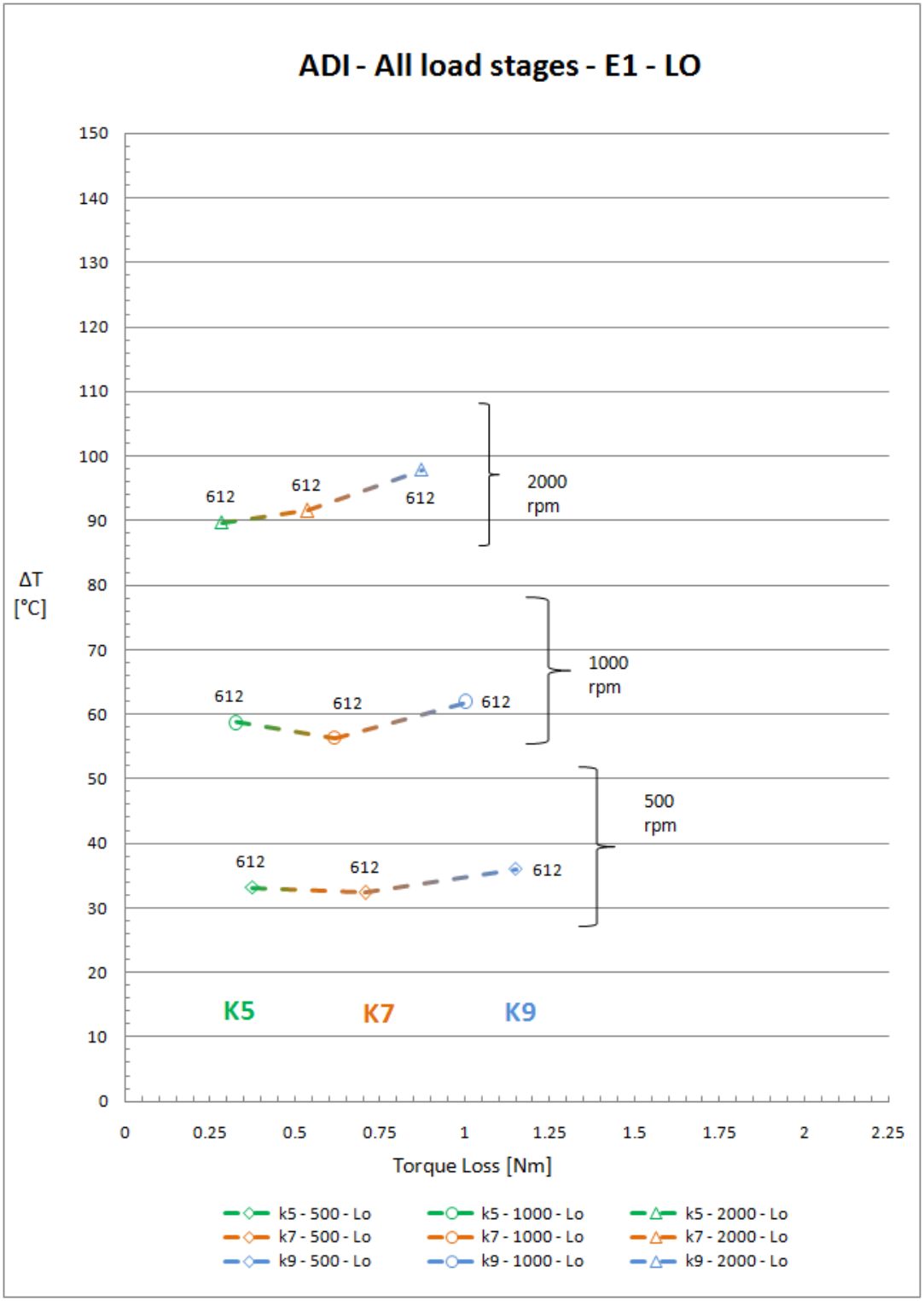

Figure 4.2.: Stabilization temperatures in gear power loss tests: ADI gear (612), E1 lubricant, low oil level.

4.1.1.3. Steel vs ADI gears - lubricant E1 and low oil level

The three graphics present in the Figure 4.3 should show, the comparison of the stabilization temperatures between Steel and Adi gear materials. Unfortunately there is only possible to compare the 610 geometries, since as it was stated in the subsection 4.1.1.2 there was a problem with gear manufacturing.

Nevertheless, there is one graphic for each geometry in the Figure 4.3. The stabilization temperatures are a function of the reference friction torque loss using a low oil level, for all velocities and load stages.

Figure 4.3c showed that the stabilization temperatures of the ADI gear (612) are always higher than those of steel gear (611). At 2000 rpm the difference is around 10 to 20 °C , being this difference shortened with the lowering of the gear velocity.

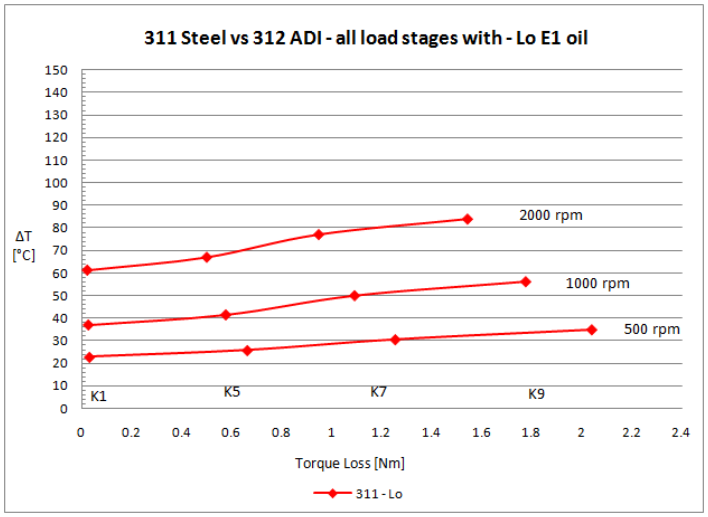

(a)

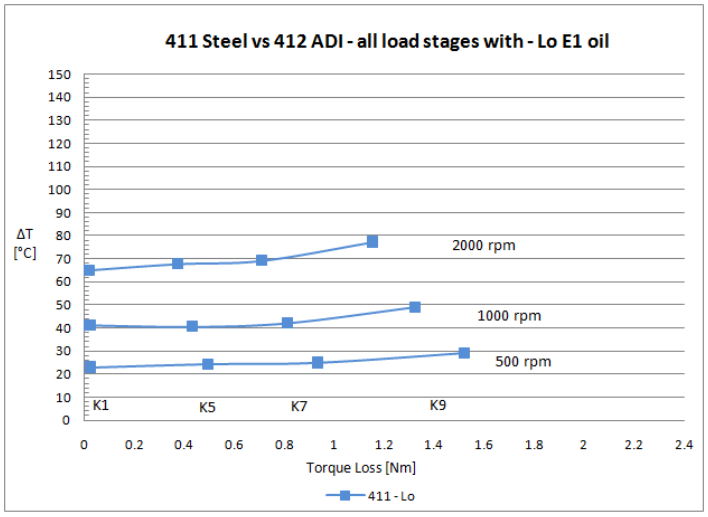

(b)

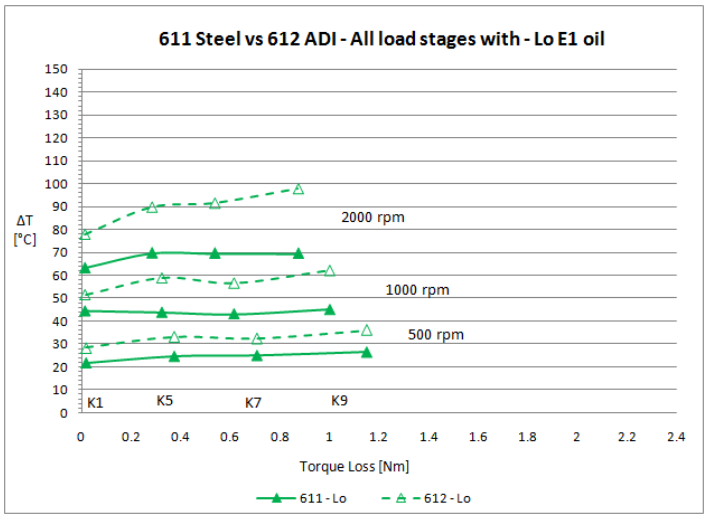

(c)

Figure 4.3.: Stabilization temperatures in gear power loss tests with lubricant E1 and low oil level: a) gear 311; b) gear 411; c) gear 611 vs 612.

4.1.2. Ferrometry

A summary of the Direct Reading Ferrography results are presented in this section.

4.1.2.1. Steel gears - lubricant E1 and low oil level

Figure 4.4 displays and compares the wear particles concentration index (CPUC) and the wear severity index (ISUC), for the steel gears lubricated with oil E1 and low oil level.

At the end of the power loss test, after load stage K9, its clear that gears 311 and 411 generated similar CPUC and ISUC wear particles indexes, while gear 611 generated significantly lower wear particles.

Figure 4.4a, shows that, the wear particle concentration index is higher for the gear 311 in all load stages, followed by the gear 411.

Gear 611 presented the lowest CPUC indexes in all load stages, so, its the gear that presented lower wear from the three geometries used with E1 and low oil level.

Figure 4.4b shows the corresponding ISUC indexes.

Gear 311, shows the highest wear severity indexes, proving not only that its the gear that generates more particles, but also the one with the more severe wear, the only exception occurs in load stage K9, where gear 411 has a slightly higher ISUC index.

Gear 611 ISUC indexes is also the lowest from the 3 gear geometries, concluding that gear 611 has the best performance in the low oil tests with E1 oil.

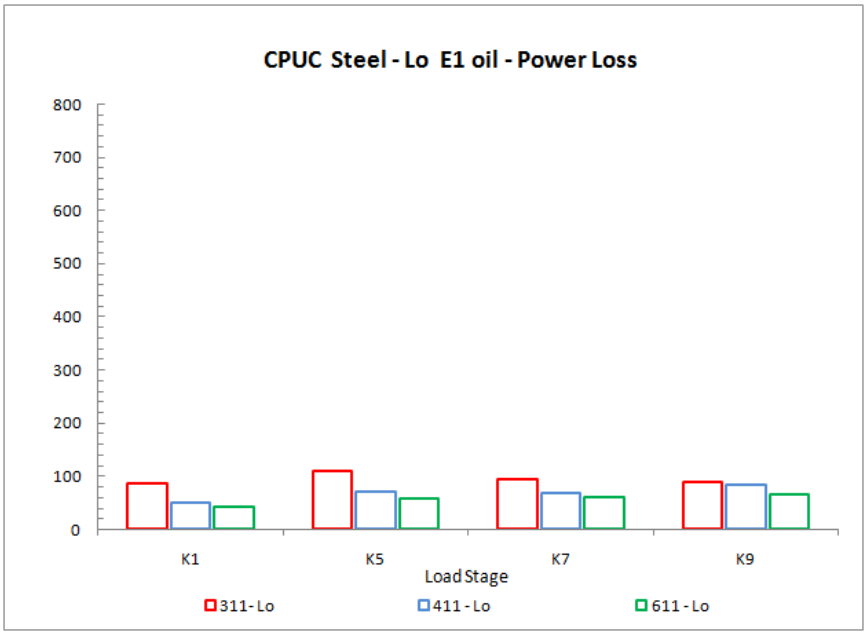

(a)

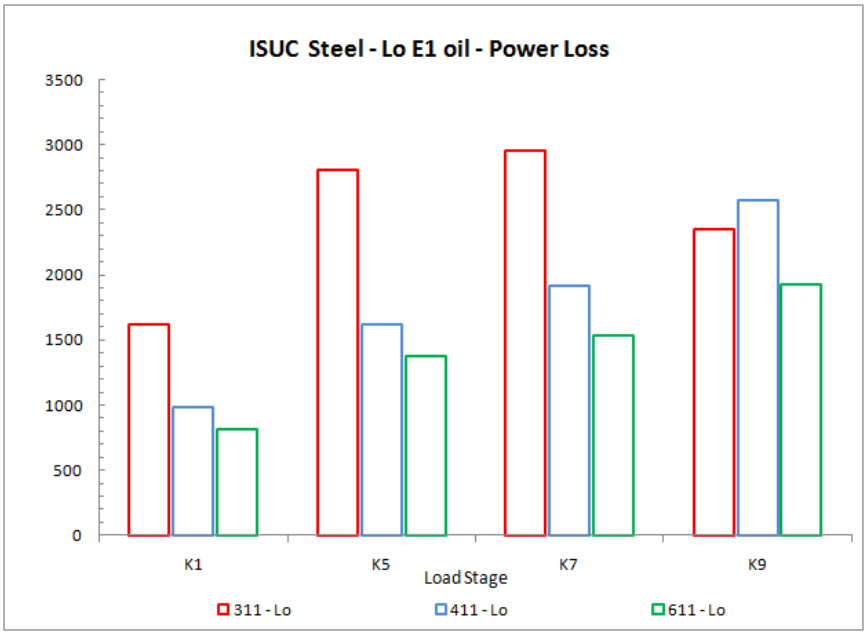

(b)

Figure 4.4.: Ferrography in gear power loss tests: steel gears (311, 411, 611), E1 lubricant, low oil level.

4.1.2.2. ADI gear 612 - lubricant E1 and low oil level

Figure 4.5, displays the wear particles concentration index (CPUC) and the wear severity index (ISUC), for the ADI gears with the use of a low oil level and in each load stage. As it was stated above (see subsection 4.1.1.2) it is not possible to show all ADI gears, so there will only be show the indexes for the 612 gear geometry.

Figure 4.5a shows that the wear particles concentration index is much higher in K9 load stage that in any other load stage.

The same can be said in the ISUC case, being the severity index low in the K1, K5 and K7 load stages but elevated in the K9 load stage. This can be observed in the Figure 4.5b.

These results indicate that ADI material, is not able to withstand the high contact pressures generated in load stage K9, generating in such conditions a very high wear volume.

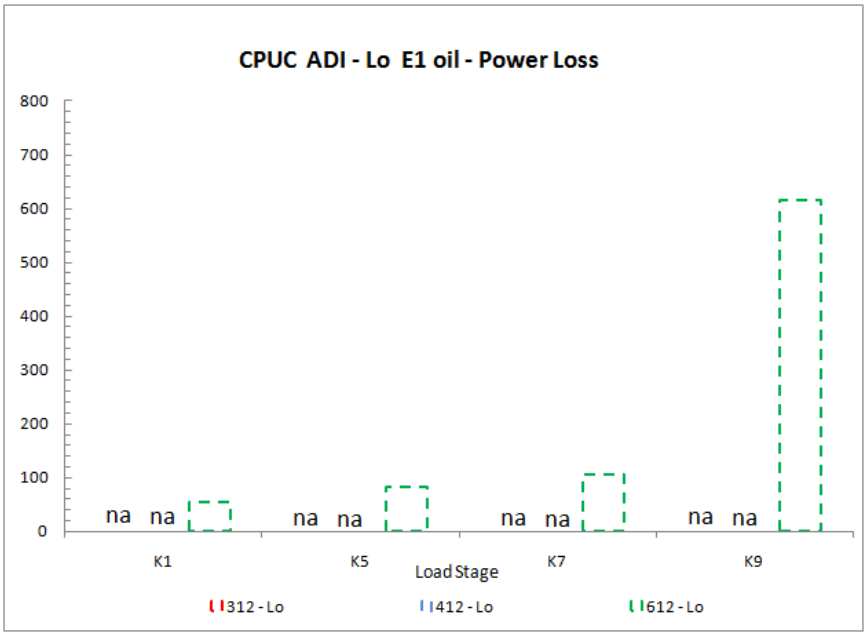

(a)

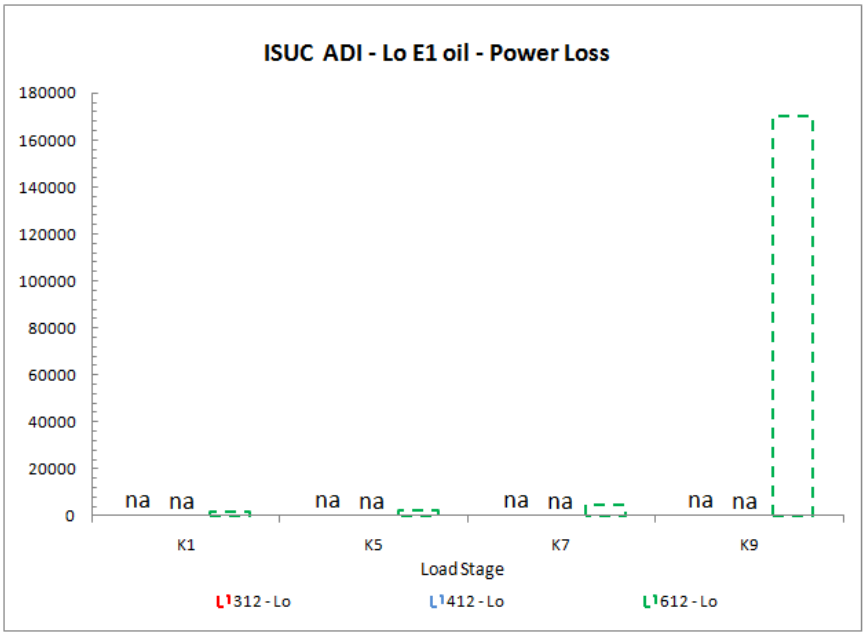

(b)

Figure 4.5.: Ferrography in gear power loss tests: ADI gear (612), E1 lubricant, low oil level.

4.1.2.3. Steel (611) vs ADI (612) gears - lubricant E1 and low oil level

Figure 4.6, displays and compares the wear particles concentration index (CPUC) and the wear severity index (ISUC), for the steel (611) and ADI (612) gears, with the use a low oil level.

Figure 4.6a, shows that the ADI gear (612) had a higher level of wear particle concentration than the steel gear (611), in the K9 load stage.

The results for the ISUC show that gear 612 had also an higher index than the 611 gear. This is shown in Figure 4.6b.

In the other load stages (K1, K5 and K7) the index results (CPUC and ISUC) were very similar, being the index for the 612 slightly superior to the 611.

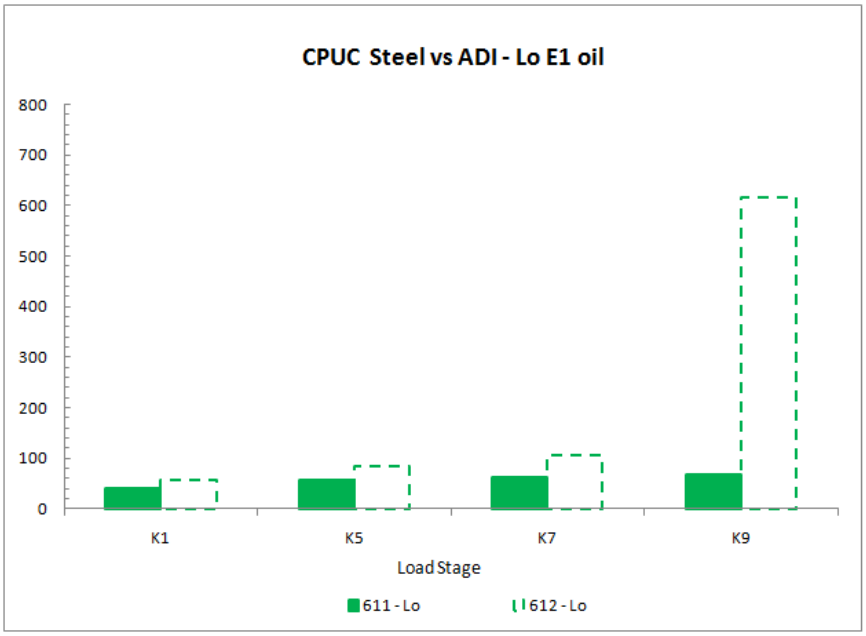

(a)

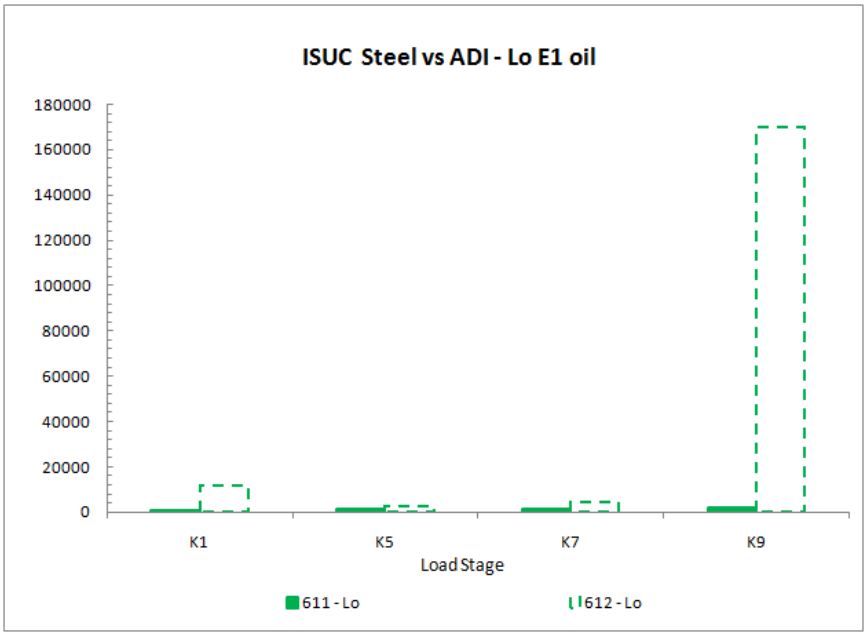

(b)

Figure 4.6.: Ferrography in gear power loss tests: Steel vs ADI, with lubricant E1 and low oil level.

4.1.3. Surface Roughness

Flank surface roughness measurements were made along the radial direction and on two different teeth for each pinion and wheel, before and after the power loss tests.

Table 4.1, Table 4.2 and Table 4.3 show the values of the flank roughness measurements for steel gears 311, 411 and 611, respectively, and Table 4.4 values of the flank roughness measurements for ADI gear 612, all lubricated with E1 ester based oil and low oil level.

And the values measured for the 610 series (using both materials) are not very reliable since it was very difficult to measure, because of the very small height of the teeth.

The steel pinion of the gears 311 and 411 show a very significant evolution of the tooth flank roughness, since all the pinion related parameters decreased, some between 11% and 50%. The 311 wheel showed a very significant increase in all of the parameters, with values starting from 57% up to 178%, being this last one the R_k value. The 411 wheel presented at the end of the tests a decrease in the R_q, R_z and R_{vk} parameter, but a increase in the R_a and R_{pk} parameters.

The 611 showed an increase in all the values of roughness, going from 51% up to 150% being the R_z the one that least increased and the R_{pk} the one that most increased, both for the pinion and the wheel.

In the case of the ADI gear 612 showed an decrease in almost all the values of roughness, going from 3% up to 36%, both for the pinion and the wheel. The only value that increase was the R_{pk} of the wheel, and the increase was only of 12%. Concluding a poor evolution of the tooth flank roughness in the ADI case.

Surface roughness [μm]									
	Probe	Direction	R_a	R_q	R_z	R_{max}	R_{pk}	R_k	R_{vk}
Initial	Pinion	Radial	0.20	0.20	0.90	1.10	0.15	0.50	0.35
Initial	Wheel	Radial	0.12	0.17	0.78	1.35	0.12	0.32	0.28
Final	Pinion	Radial	0.12	0.15	0.72	1.05	0.13	0.33	0.27
Final	Wheel	Radial	0.30	0.35	1.43	1.90	0.18	0.88	0.57
Pinion roughness evolution (%)			-41.67	-25.0	-20.37	-4.55	-11.11	-33.33	-23.81
Wheel roughness evolution (%)			157.14	110.0	82.98	40.74	57.14	178.95	100.0

Table 4.1.: Tooth flank surface roughness of 20MnCr5 steel gear 311 with E1 gear oil and low oil level.

Surface roughness [μm]									
	Probe	Direction	R_a	R_q	R_z	R_{max}	R_{pk}	R_k	R_{vk}
Initial	Pinion	Radial	0.25	0.32	1.53	2.02	0.27	0.73	0.50
Initial	Wheel	Radial	0.15	0.22	1.08	1.43	0.10	0.47	0.33
Final	Pinion	Radial	0.18	0.22	0.93	1.20	0.13	0.55	0.30
Final	Wheel	Radial	0.17	0.20	0.95	1.23	0.17	0.50	0.30
Pinion roughness evolution (%)			-26.67	-31.58	-39.13	-40.50	-50.00	-25.00	-40.0
wheel roughness evolution (%)			11.11	-7.69	-12.31	-13.95	66.67	7.14	-10.0

Table 4.2.: Tooth flank surface roughness of 20MnCr5 steel gear 411 with E1 gear oil and low oil level.

Surface roughness [μm]									
	Probe	Direction	R_a	R_q	R_z	R_{max}	R_{pk}	R_k	R_{vk}
Initial	Pinion	Radial	0.12	0.17	0.75	1.22	0.10	0.28	0.40
Initial	Wheel	Radial	0.13	0.20	0.98	1.33	0.12	0.42	0.32
Final	Pinion	Radial	0.22	0.33	1.13	1.98	0.25	0.50	0.68
Final	Wheel	Radial	0.28	0.35	1.50	2.03	0.28	0.82	0.53
Pinion roughness evolution (%)			85.71	100.0	51.11	63.01	150.0	76.47	70.83
wheel roughness evolution (%)			112.50	75.00	52.54	52.50	142.86	96.0	68.42

Table 4.3.: Tooth flank surface roughness of 20MnCr5 steel gear 611 with E1 gear oil and low oil level.

Surface roughness [μm]									
	Probe	Direction	R_a	R_q	R_z	R_{max}	R_{pk}	R_k	R_{vk}
Initial	Pinion	Radial	0.47	0.60	2.87	3.72	0.52	1.38	0.87
Initial	Wheel	Radial	0.40	0.55	2.87	4.30	0.57	1.18	0.82
Final	Pinion	Radial	0.317	0.383	1.95	2.467	0.5	1	0.383
Final	Wheel	Radial	0.4	0.533	2.65	3.55	0.633	1.217	0.683
Pinion roughness evolution (%)			-32.1	-36.1	-32	-33.6	-3.23	-27.7	-55.8
wheel roughness evolution (%)			0	-3.03	-7.56	-17.4	11.76	2.817	-16.3

Table 4.4.: Tooth flank surface roughness of ADI gear 612 with E1 gear oil and low oil level.

4.1.4. Mass Loss

The following graphic (Figure 4.7), displays and compares the pinion mass loss during the power loss tests, for Steel versus ADI gears, for lubricant E1 and low oil level.

The results presented in Figure 4.7, show a lower mass loss for all steel gears.

Gear 411 showed the best result, followed by gear 611 with values of 3mg and 3.67 mg respectively.

ADI gear 612 had the highest mass loss. Gear 612 had a higher mass loss due to the microstructure of the ADI material, since the material has graphite spheres that become lose with wear and leave some craters in the material, causing more material to become lose.

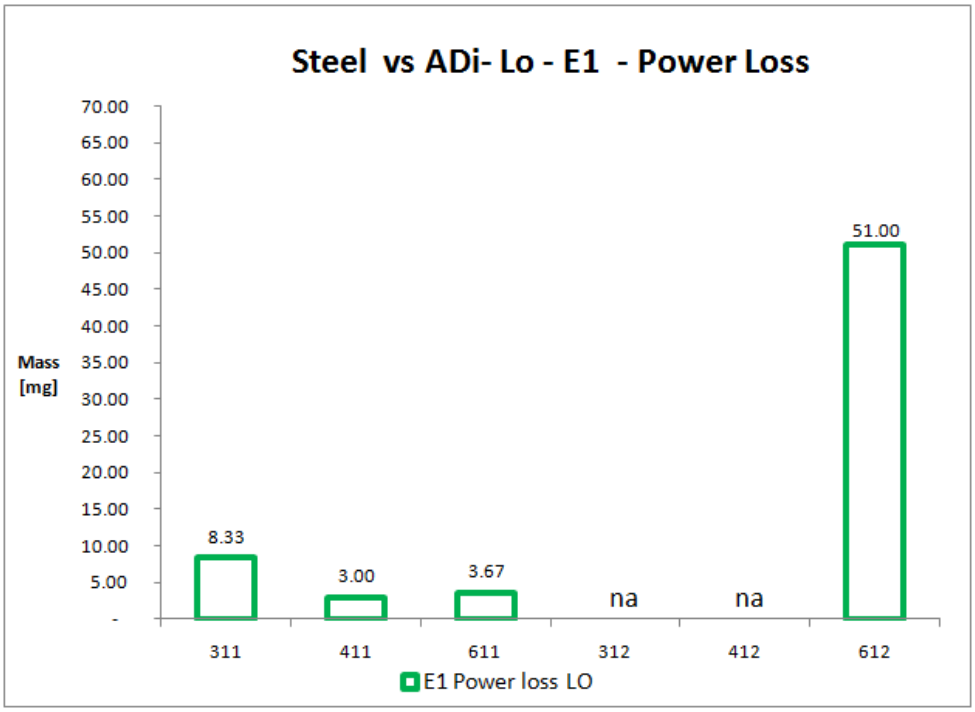

Figure 4.7.: Mass loss in gear power loss tests: steel vs ADI, with lubricant E1 and low oil level.

4.2. Ester base lubricant oil (E1) gear test and high oil level

The power loss tests presented in this section were performed by Rui Silva [48] and Cristiano Locateli [9, 49]

4.2.1. Stabilization temperatures

The stabilization temperature is the parameter that will be observed in the following analysis for gear oil E1 and high oil volume. The stabilization temperature is the difference between the maximum oil bath temperature and the room temperature, that is, $\Delta T = T_{oil} - T_{room}$.

4.2.1.1. Steel gear 311, 411 and 611 - lubricant E1 and high oil level

Figure 4.8 presents and compares the stabilization temperatures in function of the reference torque loss, for the steel gear geometries, operating with a high oil level. These tests were performed for all velocities and load stages used during the power loss tests.

In the results presented in the Figure 4.8, it can be observed that, for almost all load stages and velocities, gear 611 had the best performance. The only exception occurred at 2000 rpm, since it shows a higher stabilization temperature than the other 2 steel gear geometries (311 and 411).

The 411 has an average performance, being the one that presents the second best performance. Only in two cases, at 2000 rpm, in load stages K5 and K9, gear 411 can be respectively better and worst than the other steel gear geometries (311 and 611).

Finally the worst gear performance was obtained by gear 311. The stabilization temperatures are, whatever operating conditions, 10°C higher than gear 611 geometry.

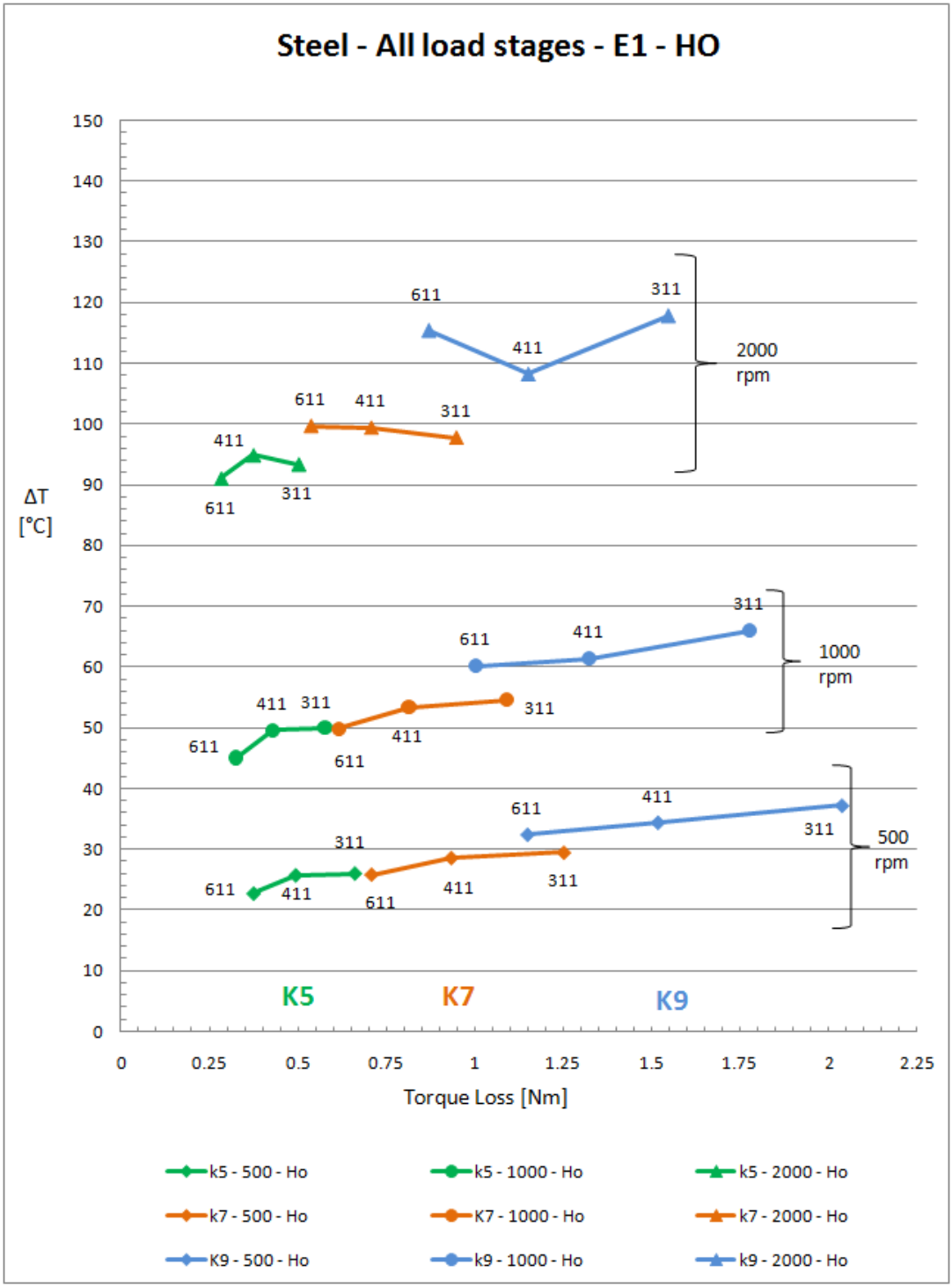

Figure 4.8.: Stabilization temperatures in gear power loss tests: steel gears (311, 411, 611), E1 lubricant, high oil level.

4.2.1.2. ADI gear 312, 412 and 612- lubricant E1 and high oil level

Figure 4.9 compares the stabilization temperatures in function of the reference torque loss, for ADI gears geometries (312, 412 and 612), operating with a high oil level, for all velocities and load stages used during the power loss tests.

Figure 4.9, shows that, for all load stages and velocities, ADI gear 612 had the best performance.

At 2000 rpm and in load stage K9, the stabilization temperatures of gear 612 are 50°C lower than those of gear 312.

The 412 has an average performance, being the one that presented the second best performances.

The worst performance was obtained by gear 312. The corresponding stabilization temperatures are significantly higher than those of the two gear geometries in all cases (load stages and velocities).

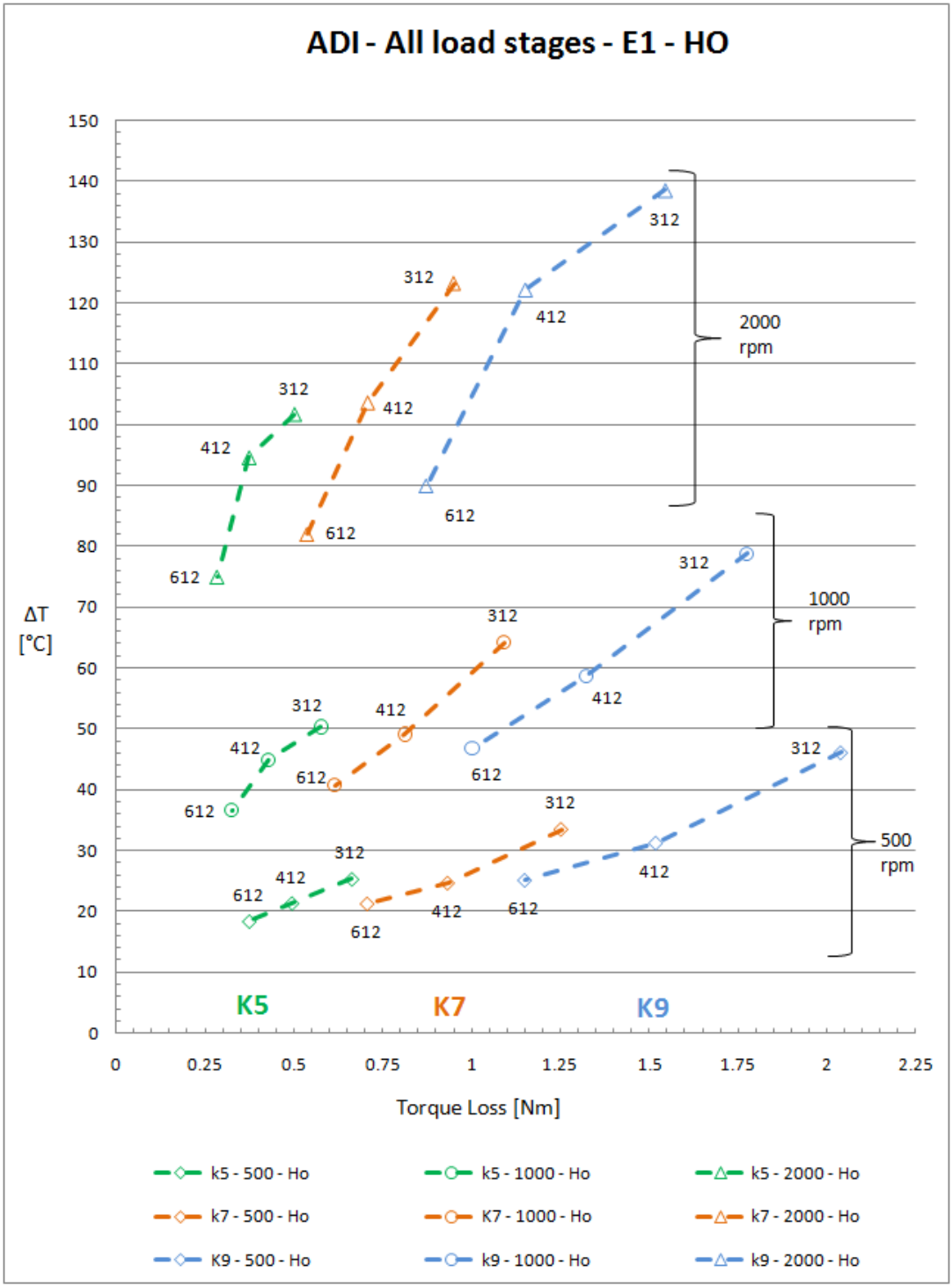

Figure 4.9.: Stabilization temperatures in gear power loss tests: ADI gears (312, 412, 612), E1 lubricant, high oil level.

4.2.1.3. Steel vs ADI gears - lubricant E1 and high oil level

Figure 4.10 shows the comparison of the stabilization temperatures between steel and ADI gear materials. The stabilization temperatures are presented in function of the reference torque loss, using a high oil level, for all velocities and load stages used during the power loss test.

The comparison presented in the Figure 4.10a, shows that gear 312 (ADI) has a higher stabilization temperature, in all the load stages and speeds, when compared with gear 311 (Steel).
In the first two load stages (K1 and K5) the stabilization temperatures are similar, and they start to diverge in the K7 load stage.

Working at 2000 rpm, steel gear 411 had a lower stabilization temperature than ADI gear 412 for all load stages. But as Figure 4.10b shows, for lower rotational speeds, gear 412 had a better performances achieving lower stabilization temperatures than the 411.

The 610 gear geometries (see Figure 4.10c) show a complete opposite case when compared with the 310 gear geometries, since ADI gear 612 always had a superior performance.
The difference between steel and ADI stabilization temperatures, increased with the increase of rotational speed, reaching 20°C in load stage K9 at 2000rpm.

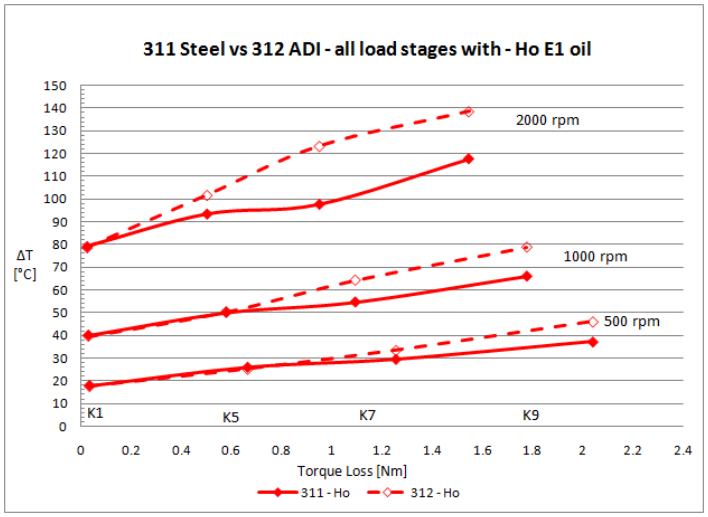

(a)

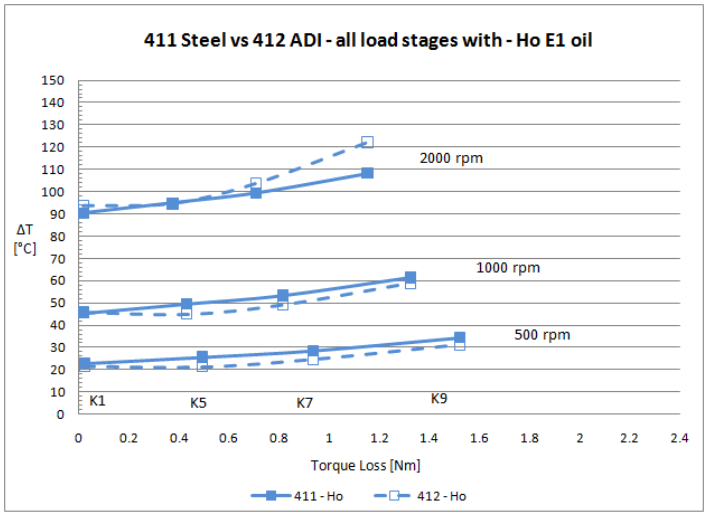

(b)

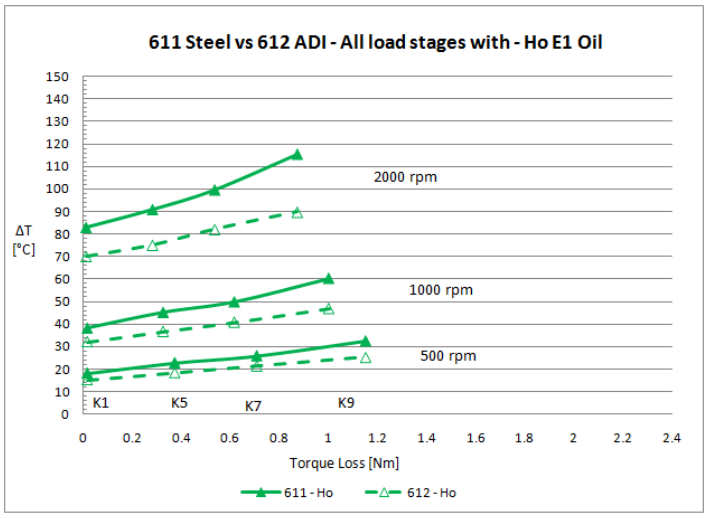

(c)

Figure 4.10.: Stabilization temperatures in gear power loss tests with lubricant E1 and low oil level: a) gear 311 vs 312; b) gear 411 vs 412; c) gear 611 vs 612.

4.2.2. Ferrometry

A summary of the Direct Reading Ferrography results are presented in this section.

4.2.2.1. Steel gears - lubricant E1 and high oil level

The results presented in the Figure 4.11, display and compare the wear particles concentration index (CPUC) and the wear severity index (ISUC), for the steel gears with the use of an high oil level, for each load stage of the power loss tests.

The results presented, show that, the wear particle concentration index is higher for 311 steel gear in all load stages.

It can also be seen that 311 steel gear had a higher wear severity index, showing that this gear generates more particles and more severe wear than steel gears 411 and 611.

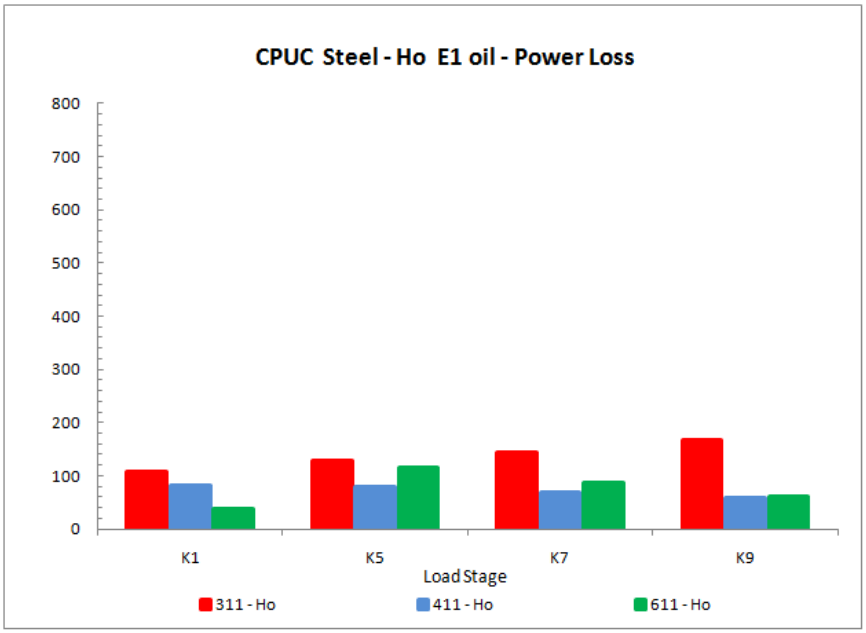

(a)

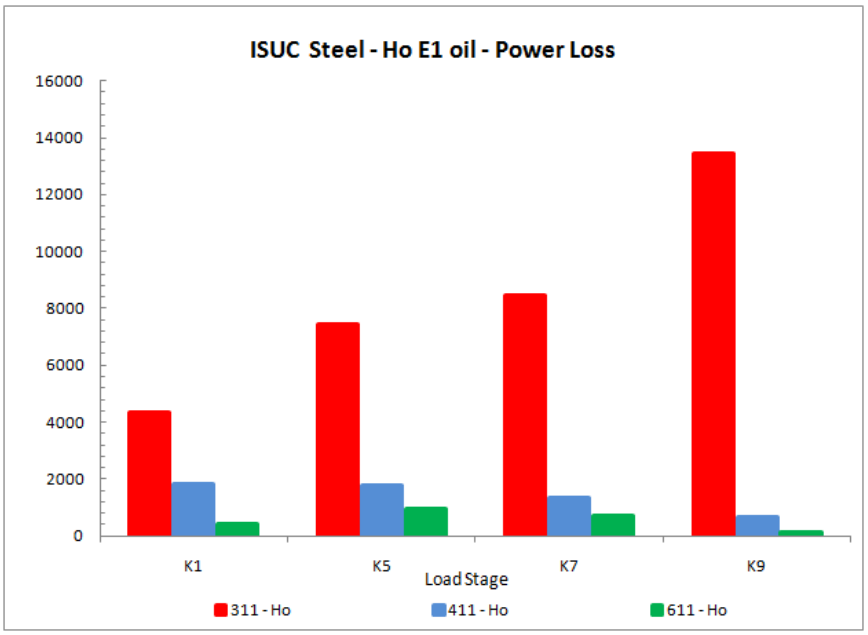

(b)

Figure 4.11.: Ferrography in gear power loss tests: steel gears (311, 411, 611), E1 lubricant, high oil level.

4.2.2.2. ADI gears - lubricant E1 and high oil level

Figure 4.12, displays and compares the wear particles concentration index (CPUC) and the wear severity index (ISUC), for ADI gears operating with high oil level, and for each load stage.

In load stage K1, 412 ADI gear presented the highest concentration of wear particles index (CPUC) and also the highest wear severity index (see Figure 4.12).

For the intermediate load stages (K5 and K7), gear 312 had the highest concentration particles indexes and also the highest wear severity indexes.
In load stage K5, 412 and 612 ADI gears had similar values of CPUC and ISUC.

In load stage K9, 312 and 612 ADI gears, had the highest CPUC values (Figure 4.12a), but 312 gear had the most sever wear, since the values of the ISUC are higher for this gear (see Figure 4.12b).

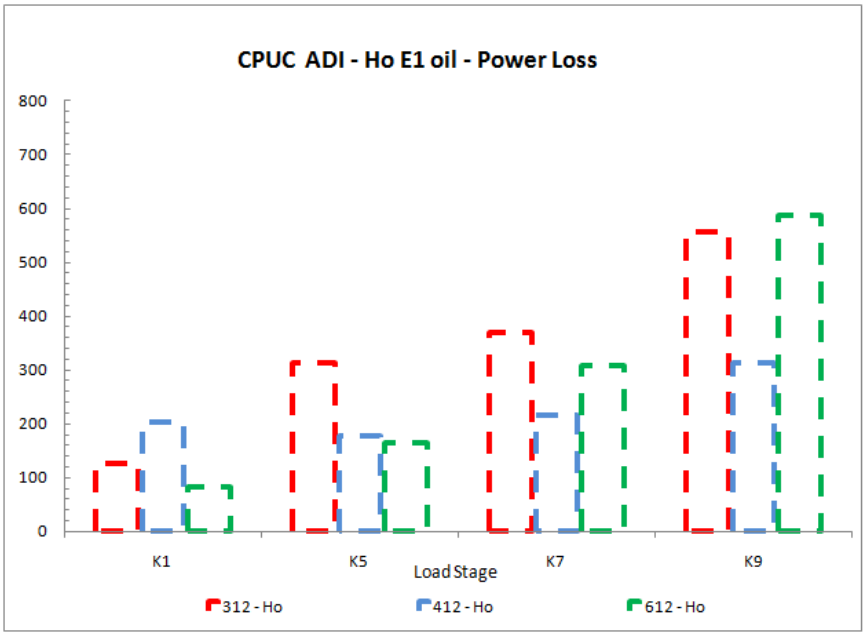

(a)

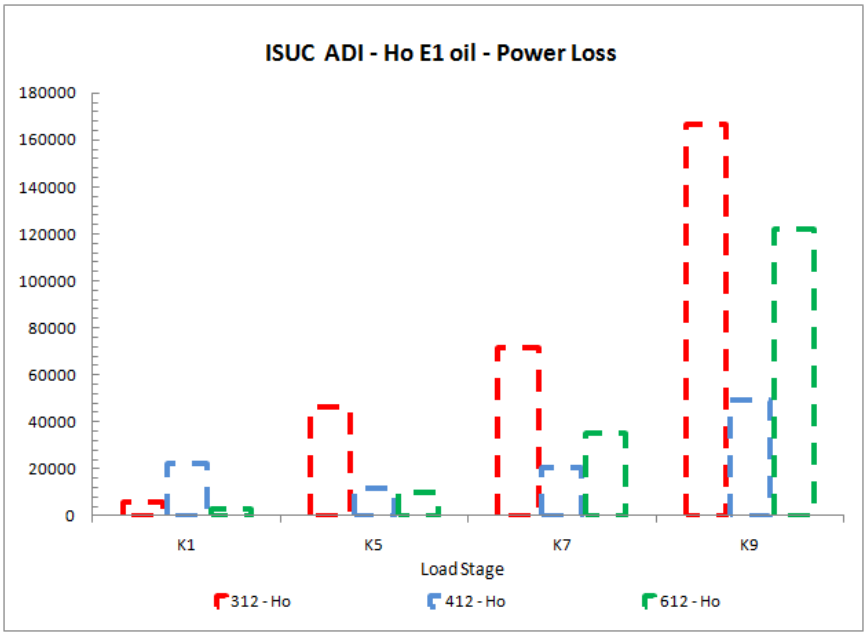

(b)

Figure 4.12.: Ferrography in gear power loss tests: ADI gears (312, 412, 612), E1 lubricant, high oil level.

4.2.2.3. Steel vs ADI gears - lubricant E1 and high oil level

Figure 4.13, shows and compares the wear particles concentration index (CPUC) and the wear severity index (ISUC), for steel and ADI gears, when lubricated with a high oil level.

The results shown are from all load stage of the power loss tests, containing data from all gear geometry used.

In load stage K1, the gears manufactured in ADI generate more wear particles (see Figure 4.13a) and more severe (see Figure 4.13b), than the similar gears manufactured in steel.

In load stages K5, K7 and K9, ADI gears always generate more wear than the steel ones.

After load stage K9, ADI gear 312 presented the highest values of CPUC and ISUC, although similar to those of gear 612, and significantly higher to those corresponding to gear 412.

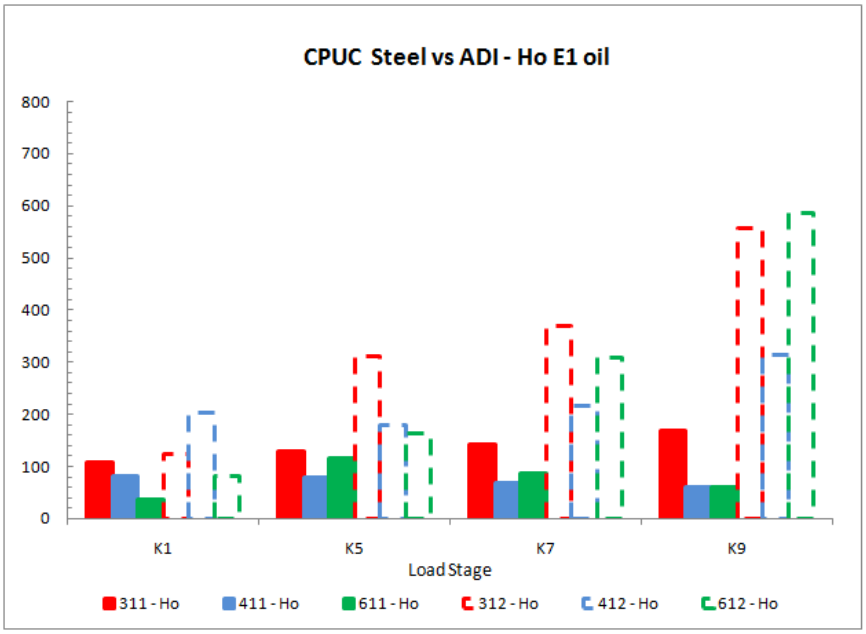

(a)

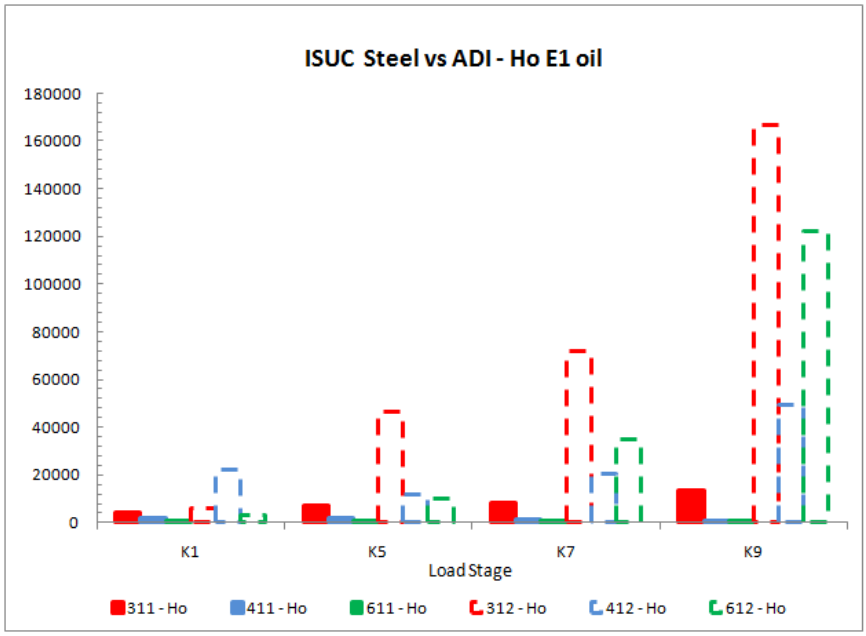

(b)

Figure 4.13.: Ferrography in gear power loss tests: steel vs ADI gears, E1 lubricant, high oil level.

4.2.3. Surface Roughness

Table 4.5 and Table 4.6 show the tooth flank roughness values measured for steel gears 311 and 411, respectively. Table 4.7 and Table 4.8 show values measured for ADI gears 312 and 412, all lubricated with E1 ester based oil and high oil level.

In the case of 610 gears series, the mesurements were not performed.

Steel gears 311 and 411 show a very significant evolution of the tooth flank roughness, since all the parameters decreased, between 40% and 50%, both for pinions and wheels.

In the case of ADI gears 312 and 412 the initial roughness values were significantly higher than those of the steel gears.

Gear 312 also showed a very significant evolution of the tooth flank roughness, since almost all parameters decreased between 20% and 50%, both for pinions and wheels. Only R_{max} and R_{vk} increased in the case of gear wheel 312.

Gear 412 had a completely different evolution, showing a very significant increase of the tooth flank roughness since almost all parameters increased between 20% and 200% both for the pinions and wheels. Both 412 pinion and wheel presented a very high increase of the R_{vk} parameter, respectively 200% and 475%, meaning that a significant number of graphite nodules were emptied during the power loss test.

During operation ADI graphite nodules become empty, losing the graphite, and generating surface holes that contribute to the increase of roughness valleys.

			Surface roughness [μm]						
	Probe	Direction	R_a	R_q	R_z	R_{max}	R_{pk}	R_k	R_{vk}
Initial	Pinion	Radial	0.28	0.34	1.62	1.96	0.2	0.88	0.47
Initial	Wheel	Radial	0.29	0.38	1.77	2.76	0.4	0.83	0.6
Final	Pinion	Radial	0.16	0.21	0.86	1.16	0.1	0.47	0.3
Final	Wheel	Radial	0.14	0.18	0.78	0.97	0.1	0.38	0.34
Pinion roughness evolution (%)			-40.96	-39.81	-46.6	-40.92	-33.85	-46.42	-36.17
wheel roughness evolution (%)			-50.57	-53.04	-55.66	-64.86	-81.42	-54	-43.33

Table 4.5.: Tooth flank surface roughness of 20MnCr5 steel gear 311 with E1 gear oil and high oil level.

Surface roughness [μm]									
	Probe	Direction	R_a	R_q	R_z	R_{max}	R_{pk}	R_k	R_{vk}
Initial	Pinion	Radial	0.3	0.38	1.81	2.16	0.2	0.89	0.59
Initial	Wheel	Radial	0.24	0.3	1.45	1.93	0.2	0.75	0.44
Final	Pinion	Radial	0.15	0.19	0.87	1.06	0.1	0.42	0.33
Final	Wheel	Radial	0.12	0.15	0.71	0.94	0.1	0.37	0.24
Pinion roughness evolution (%)			-50.56	-50.88	-52.02	-50.93	-55.56	-52.63	-43.75
wheel roughness evolution (%)			-50.7	-50	-51.38	-51.21	-51.79	-50.88	-45.45

Table 4.6.: Tooth flank surface roughness of 20MnCr5 steel gear 411 with E1 gear oil and high oil level.

Surface roughness [μm]									
	Probe	Direction	R_a	R_q	R_z	R_{max}	R_{pk}	R_k	R_{vk}
Initial	Pinion	Radial	0.81	1.01	4.59	5.6	0.7	2.57	1.31
Initial	Wheel	Radial	0.76	0.96	4.29	5.07	0.7	2.47	1.06
Final	Pinion	Radial	0.43	0.59	2.97	4.03	0.4	1.21	1.17
Final	Wheel	Radial	0.54	0.79	3.19	5.85	0.5	1.37	1.46
Pinion roughness evolution (%)			-47.11	-41.29	-35.4	-27.99	-45.85	-52.92	-10.09
wheel roughness evolution (%)			-29.26	-17.1	-25.56	15.53	-24.94	-44.53	37.74

Table 4.7.: Tooth flank surface roughness of ADI gear 312 with E1 gear oil and high oil level.

Surface roughness [μm]									
	Probe	Direction	R_a	R_q	R_z	R_{max}	R_{pk}	R_k	R_{vk}
Initial	Pinion	Radial	0.52	0.62	3.07	4.08	0.6	1.63	0.78
Initial	Wheel	Radial	0.33	0.43	2.42	3.98	0.5	1.08	0.53
Final	Pinion	Radial	0.6	1.05	5.17	10.65	0.5	1.28	2.33
Final	Wheel	Radial	0.73	1.28	6.57	11.08	0.6	1.5	3.07
Pinion roughness evolution (%)			16.13	70.27	68.48	160.8	-24.32	-21.43	197.9
wheel roughness evolution (%)			120	196.2	171.72	178.2	6.45	38.46	475

Table 4.8.: Tooth flank surface roughness of ADI gear 412 with E1 gear oil and high oil level.

4.2.4. Mass Loss

Figure 4.14, displays and compares the pinion mass loss during the power loss tests, for steel and ADI gears, lubricated with gear oil E1 using a high oil level.

The Figure 4.14, shows that the ADI gears have significantly higher mass losses (3 to 6 times higher) than the steel ones.

Among the gears manufactured in steel material, gear 411 had the highest mass loss, followed by gear 611 and 311, although all mass losses are small and similar.

Among the gears manufactured in ADI material, gear 312 had the highest mass loss, followed by gear 612 and 412.

Gear 312 lost 57mg more than the 311, gear 412 lost more 19mg than gear 411, and gear 612 lost more 38 mg than gear 611, concluding that the largest difference is in the case of the 310 tooth geometry.

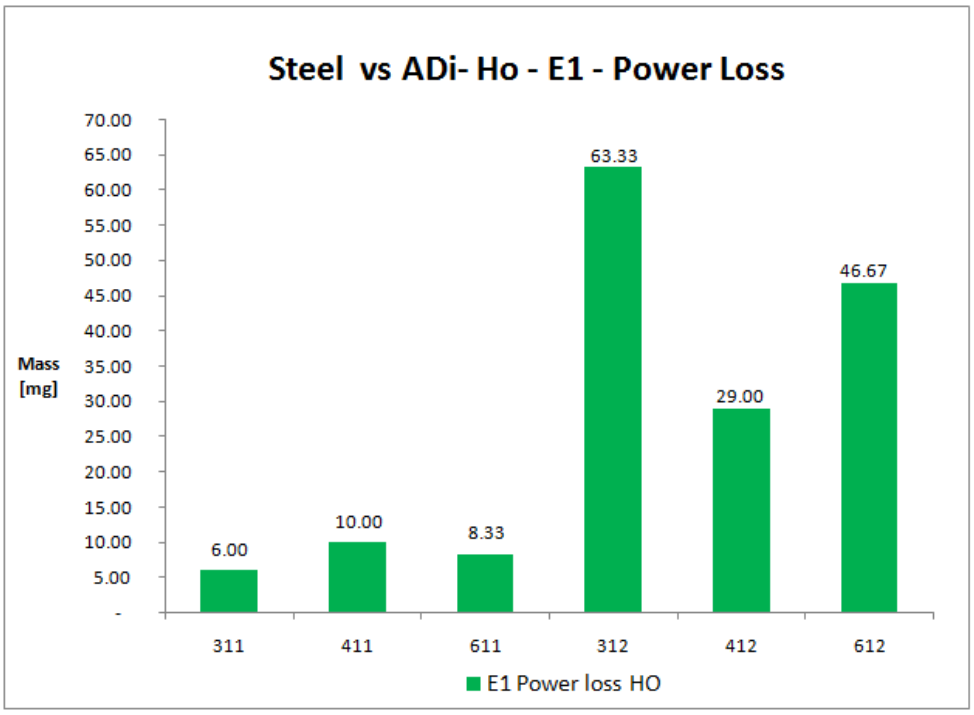

Figure 4.14.: Mass loss in gear power loss tests: steel vs ADI gears, E1 lubricant, high oil level

4.3. Ester base lubricant oil gear (E1) test and high vs low oil Level.

4.3.1. Stabilization temperatures

Figure 4.15 compares stabilization temperatures generated by the gears, using high and low oil levels. The objective is to understand the influence of oil level on the stabilization temperature.

In the case of the steel gears (see Figure: 4.15a, b and c), whatever the velocity, load stage and gear geometries, a low oil level always generate a lower stabilization temperature.

The difference is mainly dependent on the operating speed: at 500 rpm the differences are very small (-1 to -3°C , in the case of the low oil level), at 1000 rpm, the difference reaches -10°C (in favor of a low oil level) and at 2000 rpm the difference can reach -40°C ate high torque (K9), again in favor of a low oil level. The influence of gear geometry is not significant, except in the case of the geometry 611 at high speed and torque.

In the case of ADI gears (see Figures: 4.15d, e and f) there is not much to compare, since there is no data available as it was already explain (see subsection 4.1.1.2).

With the available data there can be said that, the performance of the 612 gear with high oil level is better than with low oil (see Figure 4.15f). The difference is higher in low speed and low load stages, decreasing as the speeds and load increase.

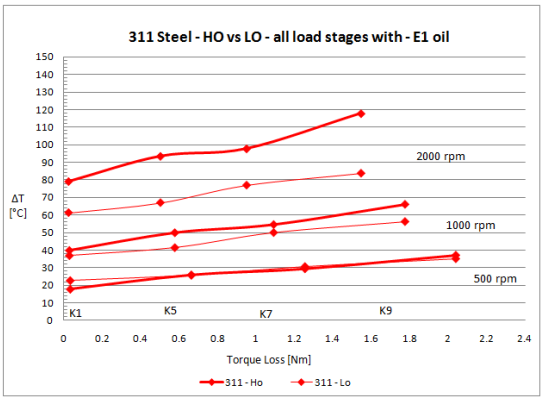

(a)

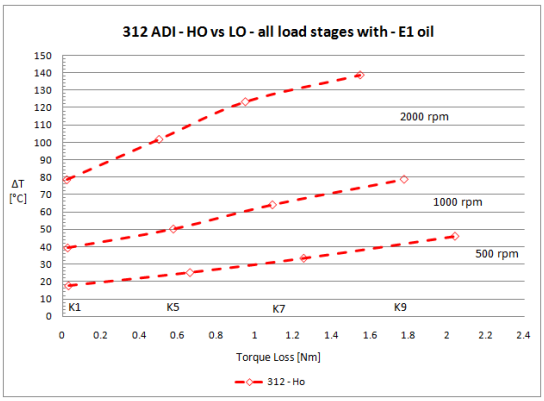

(d)

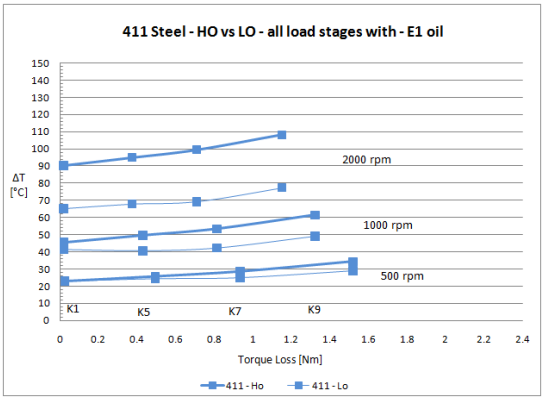

(b)

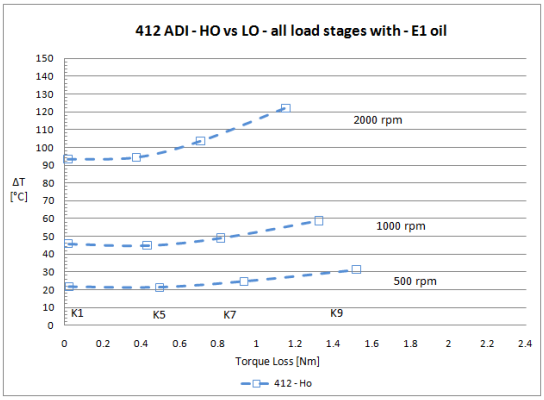

(e)

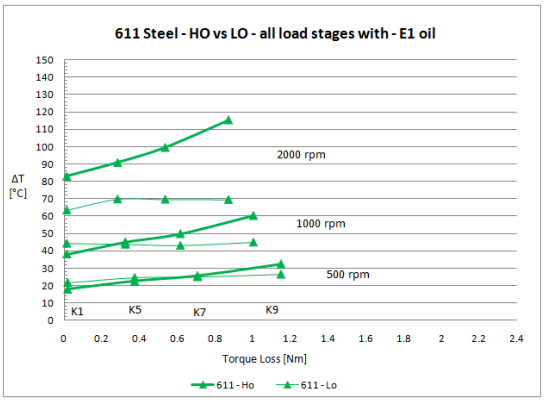

(c)

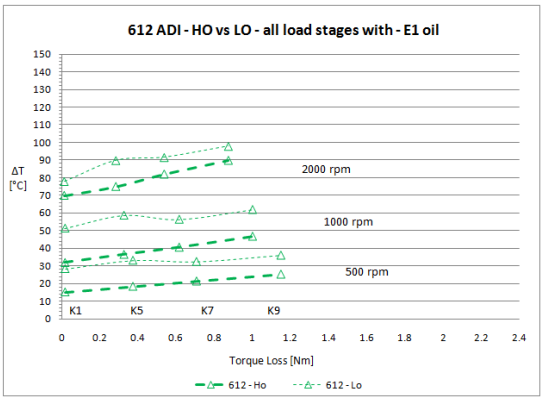

(f)

Figure 4.15.: Stabilization temperatures in gear power loss tests: high vs low oil level, E1 lubricant, steel and ADI gears.

4.3.2. Ferrometry

In the Figures 4.16 and 4.17 are compared the CPUC and ISUC indexes generated by steel and ADI gears lubricated with high and low oil level. The objective is to understand the influence of the oil level on the gears wear.

In load stage K9, gear 311 gear operating with an high or low oil level, had highest level of CPUC (Figure 4.16a) and the highest severe wear (high ISUC) (Figure 4.16b).
Gear 411 working in the load stage K9 and lubricated with a low oil level had values for both CPUC and ISUC similar to those of gear 311.

Gear 611, working in load stage K9, had similar values of CPUC both operating in high and low oil, having higher values of ISUC indexes when operating with a low oil level.

For the ADI values there is only possible to establish a direct comparison between gear 612 operating with high and low oil levels. In this case the high oil level, had a lower level of CPUC (Figure 4.17a) and ISUC (Figure 4.17b) in load stage K9.

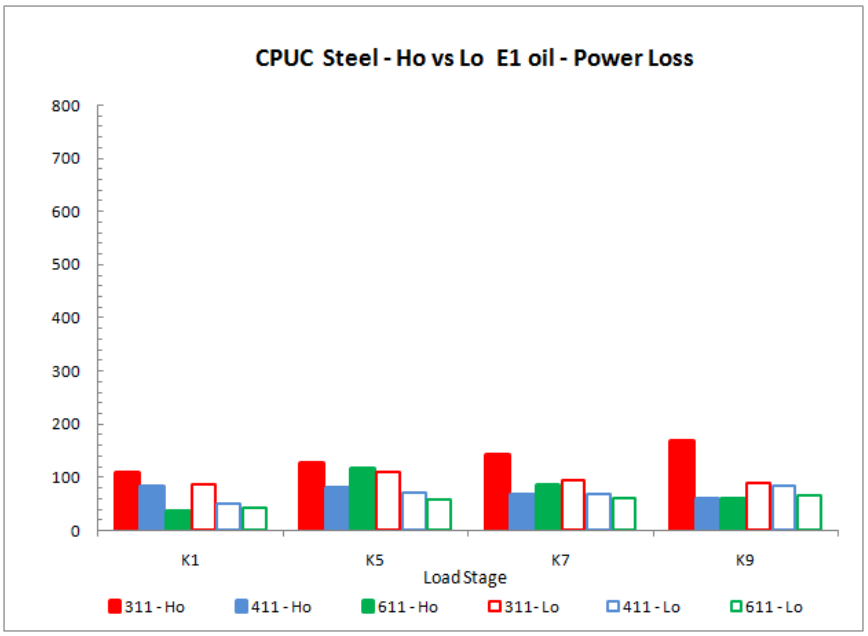

(a)

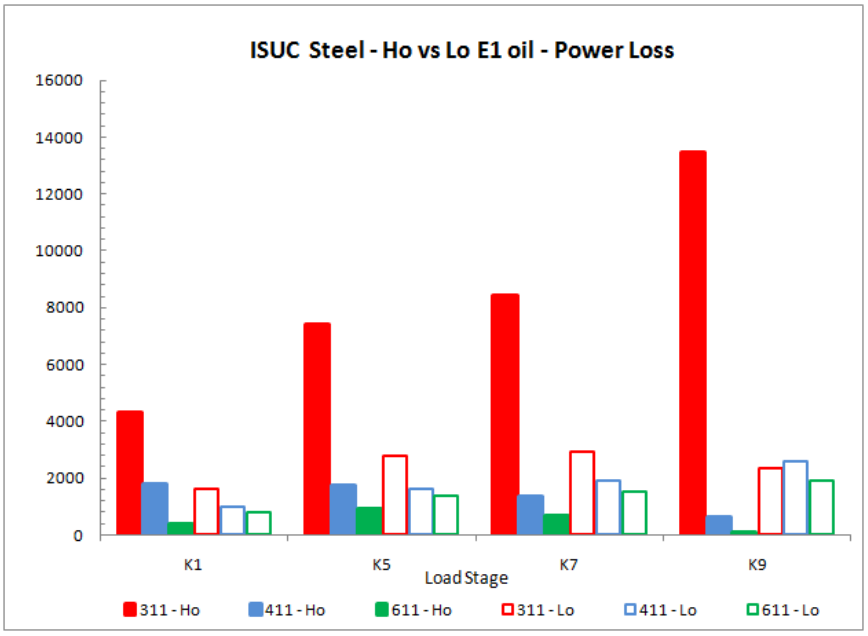

(b)

Figure 4.16.: Ferrography in gear power loss tests: high vs low oil level, E1 lubricant, steel gears.

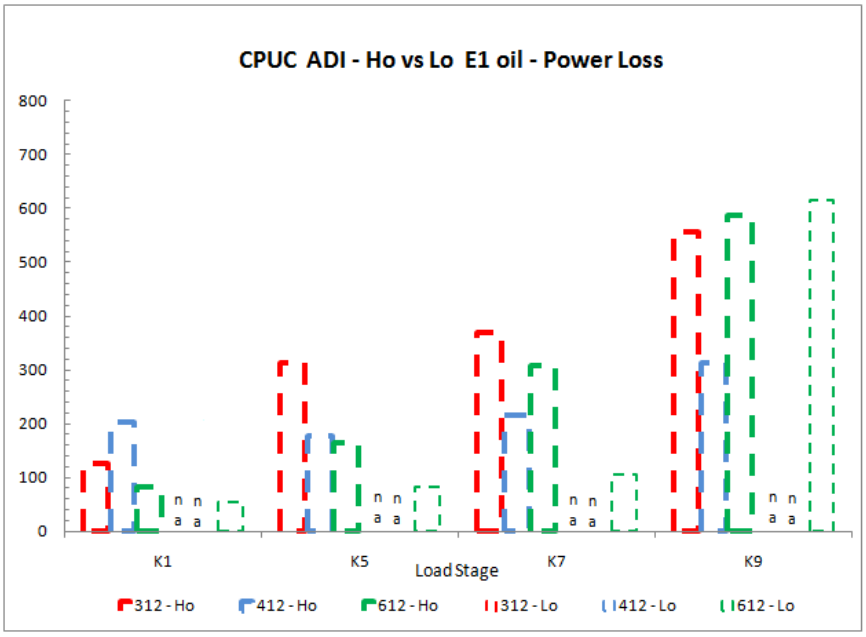

(a)

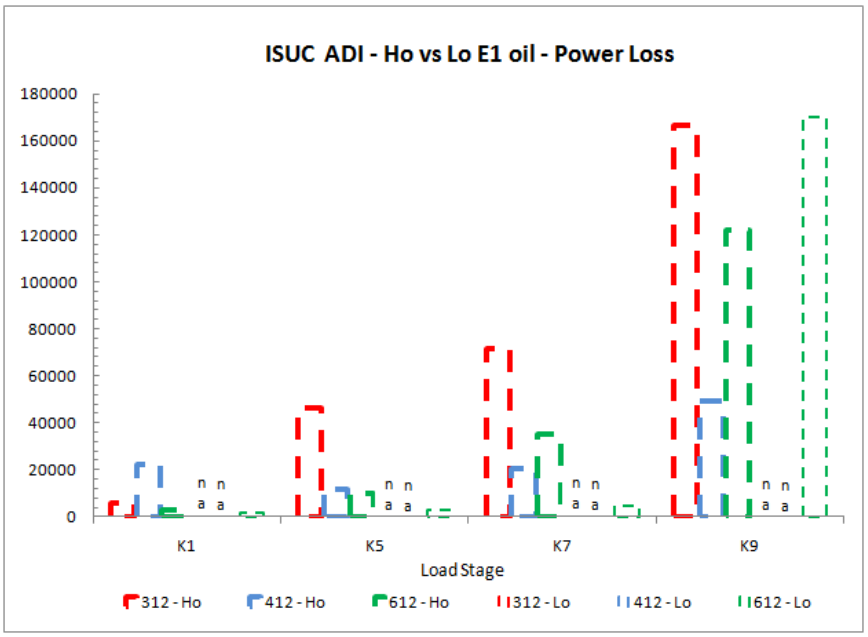

(b)

Figure 4.17.: Ferrography in gear power loss tests: high vs low oil level, E1 lubricant, ADI gears.

4.3.3. Mass Loss

Figure 4.18, displays and compares the pinion mass loss during the power loss tests, for steel and ADI gears, lubricated with E1, high and low oil levels. The results for gear geometry 412 and 312 in ADI material and operating with low oil level were not realized, so there were no values available to be compared.

Figure 4.18, shows that the ADI gears had higher mass losses than the steel ones.

Gears 311 and 612 operating with low oil level had a lower value of mass loss than the same gears operating with an high oil level. On the other hand gears 411 and 611 had a lower values of mass loss operating with a low oil level than the same gears operating with a high oil level.

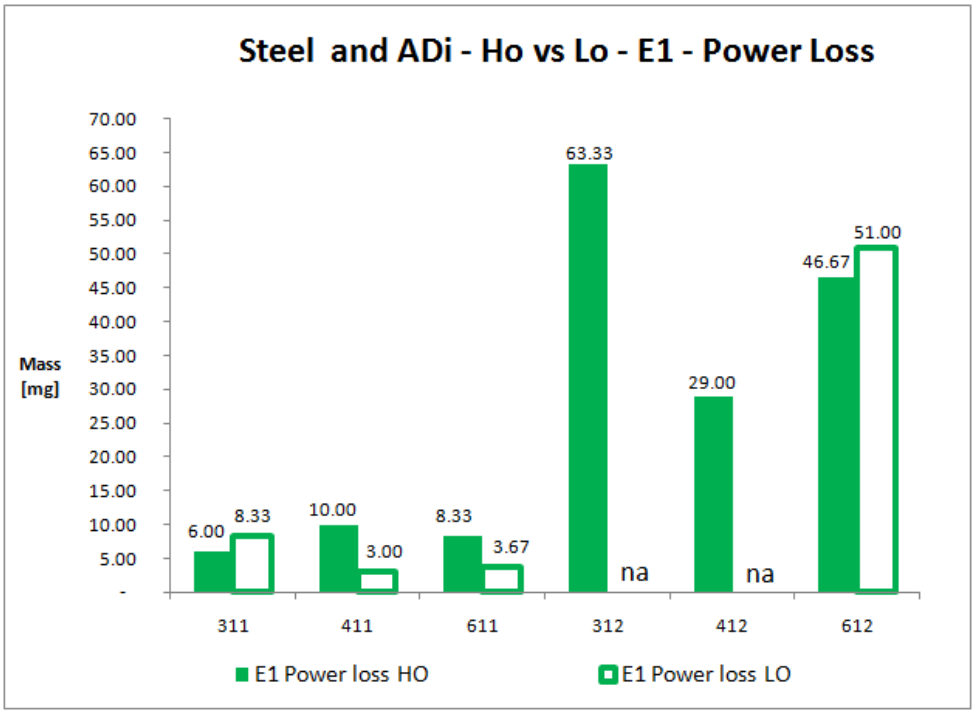

Figure 4.18.: Mass loss in gear power loss tests: high vs low oil level, E1 lubricant, steel and ADI gears.

4.4. Polyalolephine base lubricant oil (P1) gear test and low oil Level

4.4.1. Stabilization temperatures

The stabilization temperature is the parameter that will be observed in the following analysis . It represents difference between the oil bath temperature and the room temperature, that is, $\Delta T = T_{oil} - T_{room}$, after stabilization, when the power loss inside the FZG gearbox is in equilibrium with the heat flow from the FZG gearbox to the surrounding environment.

The stabilization temperatures were taken after 4 hours of operation at specified operating conditions (torque and speed).

4.4.1.1. Steel gear 311, 411 and 611 - lubricant P1 and low oil level

The power loss tests presented in this subsection were performed by Rui Silva [48] and Cristiano Locateli [9, 49].

Figure 4.19 presents the stabilization temperatures of the steel gears (311, 411 and 611), lubricated with gear oil P1, and a low oil level (LO), for all applied torques (K1, K5, K7 and K9) and all operating speeds (500, 1000 and 2000 rpm), in relation to the corresponding reference gear friction torque loss.

Whatever the operating conditions, applied torque and speed, steel gear 611 generates lower stabilization temperatures than gear 411, and the latter lower temperatures than gear 311. This trends is very clear for an operating speed of 2000 rpm. At 500 rpm and 1000 rpm and medium torques (K7), gear 411 and 611 showed similar stabilization temperatures.

Figure 4.19, shows that, for all load stages and velocities, gear 611 had the best performance.

In load stage K7, gear 411 stabilization temperatures are similar to those of gear 611.

On the other hand, the worst gear performance was obtained by gear 311. The stabilization temperatures are, whatever the operating conditions, higher than those of the other steel gears. The stabilization temperatures are in almost all the cases 10°C superior to those of gear 611.

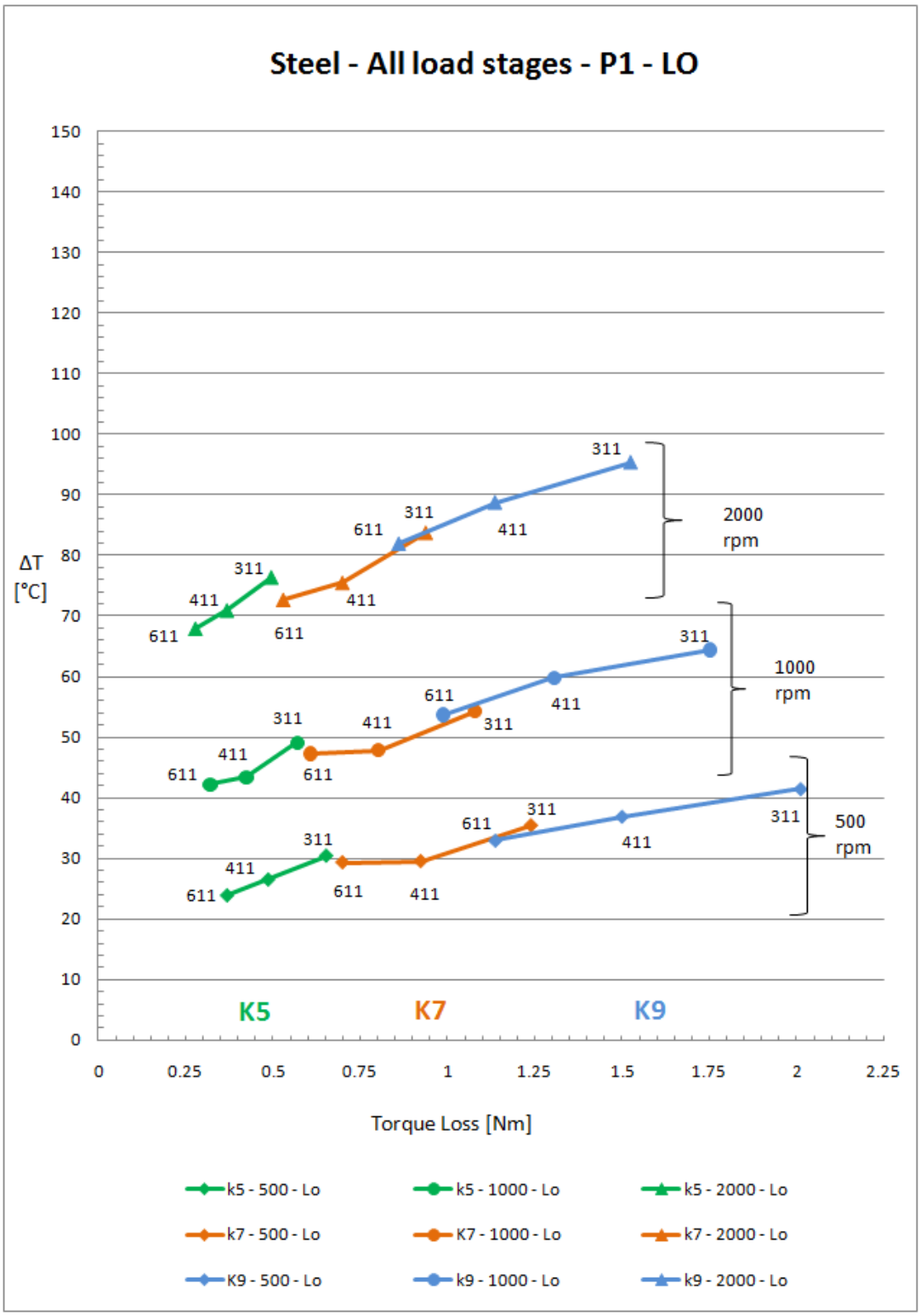

Figure 4.19.: Stabilization temperatures in gear power loss tests: steel gears (311, 411, 611), P1 lubricant, low oil level.

4.4.1.2. ADI gear 612 - lubricant P1 and low oil level

Figure 4.20, shows and compares the stabilization temperatures in function of the reference friction torque loss, for the ADI gears geometries, operating with a low oil level, for all velocities and load stages.

Unfortunately, in the case of the ADI gears there is not much data to compare, since the power loss tests with P1 oil and low oil level for ADI gears (312 and 412) were not performed due to some technical problems in the manufacturing process of the gears sets. So Figure 4.20 shows the results related with ADI gear 612.

The maximum stabilization temperature was 90°C , and occurred for the speed of 2000 rpm, at 1000 rpm the maximum stabilization temperature was 50°C , and at 500 rpm was 30°C , being all of this for the load stage K9.

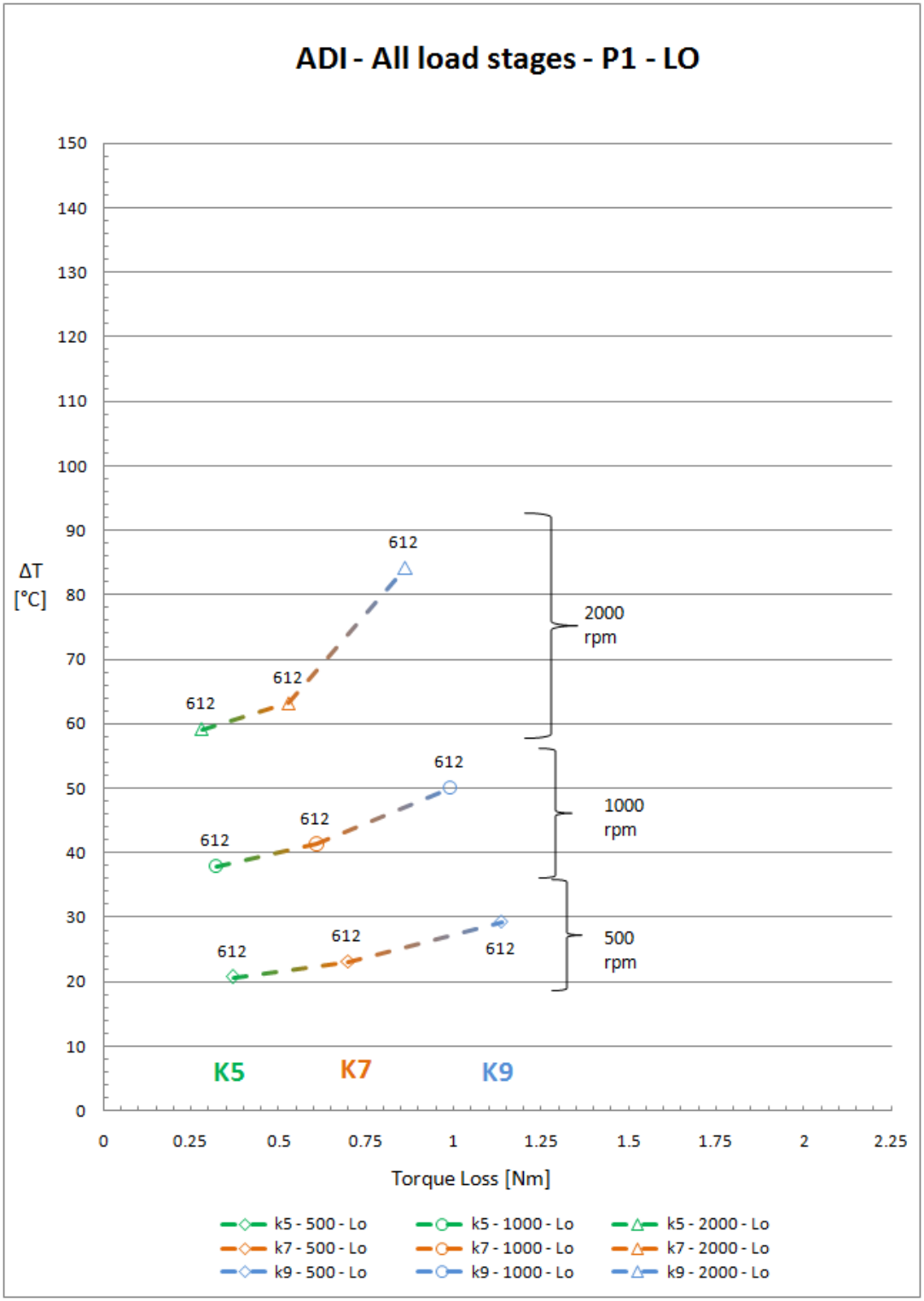

Figure 4.20.: Stabilization temperatures in gear power loss tests: ADI gear (612), P1 lubricant, low oil level.

4.4.1.3. Steel vs ADI gears - lubricant P1 and low oil level

The three graphics present in the Figure 4.21 should show, the comparison of the stabilization temperatures between Steel and Adi gear materials. Unfortunately there is only possible to compare the 610 geometries, since as it was stated in the subsection 4.4.1.2 there was a problem with gear manufacturing.

Nevertheless there is present in the Figure 4.21 one graphic for each geometry. The stabilization temperatures are in function of the reference friction torque loss, using low oil level, for all velocities and load stages.

Figure 4.21c,showed that, the stabilization temperatures of the ADI gear (612) are always lower than those of steel gear (611).

In load stage K9, and for any considered speed, gear 612 has a very similar performance to gear 611.

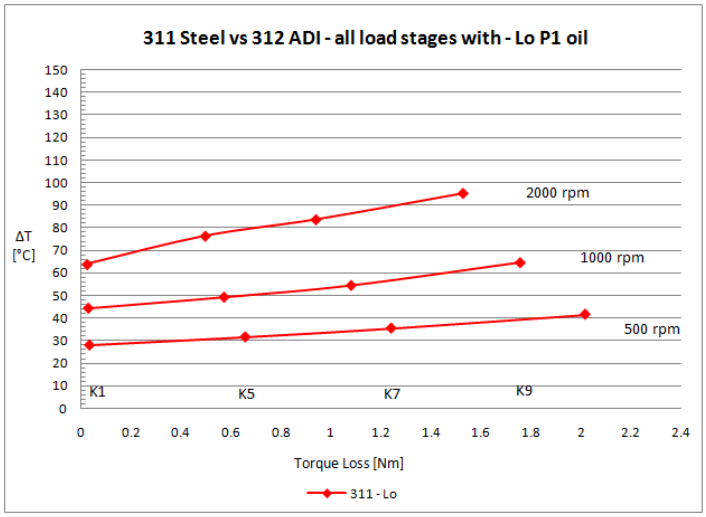

(a)

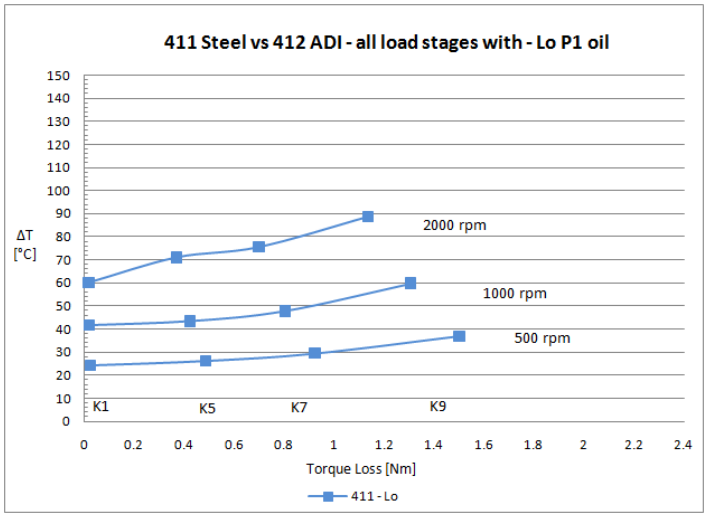

(b)

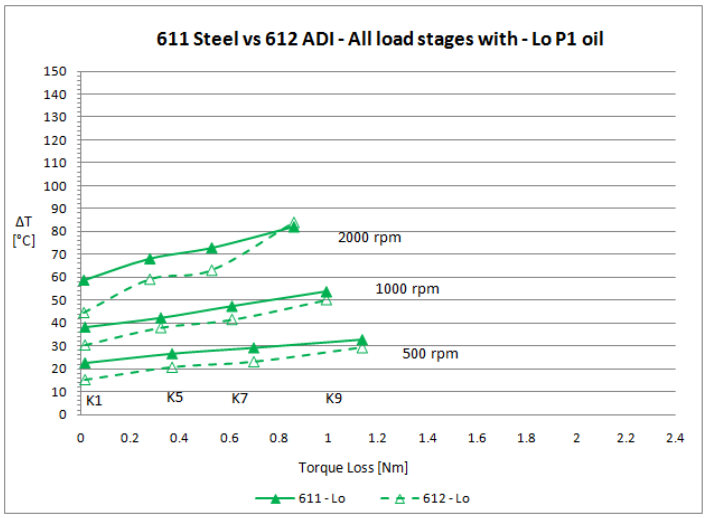

(c)

Figure 4.21.: Stabilization temperatures in gear power loss tests with lubricant P1 and low oil level: a) gear 311; b) gear 411; c) gear 611 vs 612.

4.4.2. Ferrometry

A summary of the Direct Reading Ferrography results are presented in this section.

4.4.2.1. Steel gears - lubricant P1 and low oil level

Figure 4.22, displays and compares the wear particles concentration index (CPUC) and the wear severity index (ISUC), for the steel gears lubricated with oil P1 and low oil level.

At the end of the power loss test, after load stage K9, its clear that gears 311 and 411 generated similar CPUC and ISUC wear particles indexes, while gear 611 generated an higher value of wear particles.

Figure 4.22a, shows that, the wear particle concentration index is higher for gear 611 in all load stages.

Gears 311 and 411 gears presented similar values for the CPUC index in almost all load stages. In load stage K1, there was a slight advantage to the gear 311, with the lowest CPUC index, and for the remaining load stages this advantage belongs to gear 411.

Figure 4.22b, shows that gear 611, was the gear that presented the highest wear severity indexes, proving not only that its the gear that has more wear particles, but also the one with the more severe wear.

Gear 411 ISUC indexes in load stages K1 and K7, were higher than those of gear 311. In load stages K5 and K9, gear 311 values were higher than those of the gear 411.

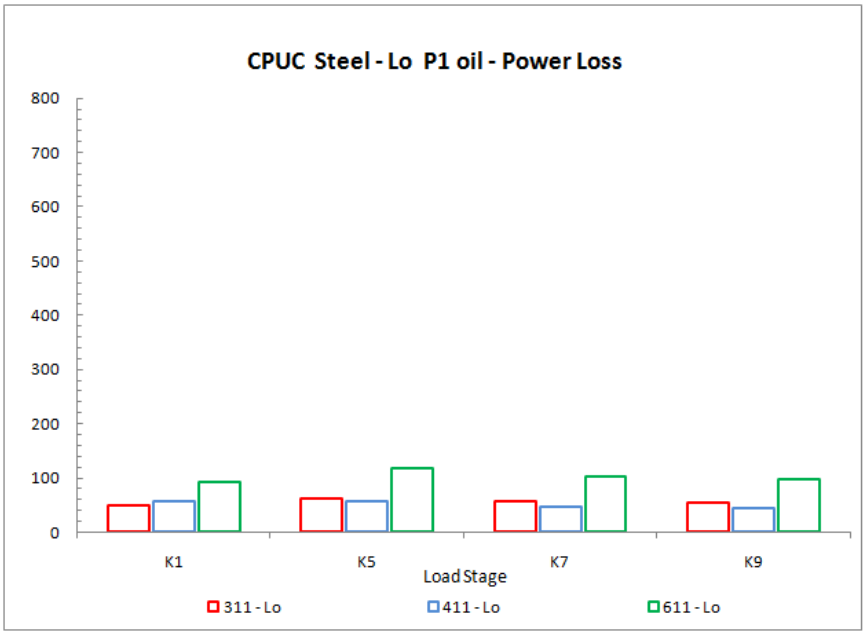

(a)

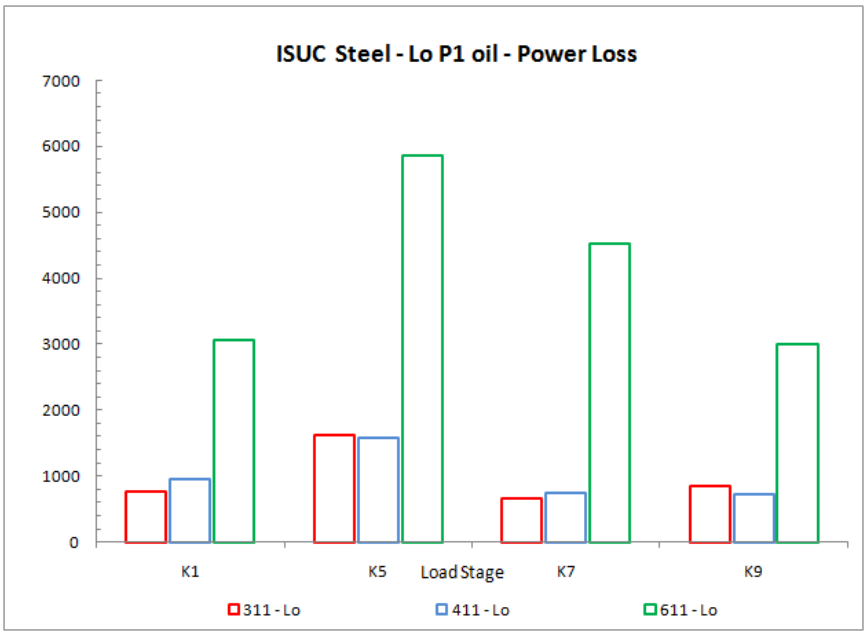

(b)

Figure 4.22.: Ferrography in gear power loss tests: steel gears (311, 411, 611), P1 lubricant, low oil level.

4.4.2.2. ADI gear 612 - lubricant P1 and low oil level

Figure 4.23, displays the wear particles concentration index (CPUC) and the wear severity index (ISUC), for the ADI gears with the use of an low oil level and in each load stage.

Figure 4.23a, shows that the wear particles concentration index was significantly higher in load stage K9 that in any other load stage.

In the ISUC case, the indexes were lower for the load stages K1, K7 and K9, but higher in the load stage K5. This is shown in Figure 4.23b.

These results indicate that ADI material, is not able to withstand the high contact pressures generated in higher load stages, generating in such conditions a very high wear volume.

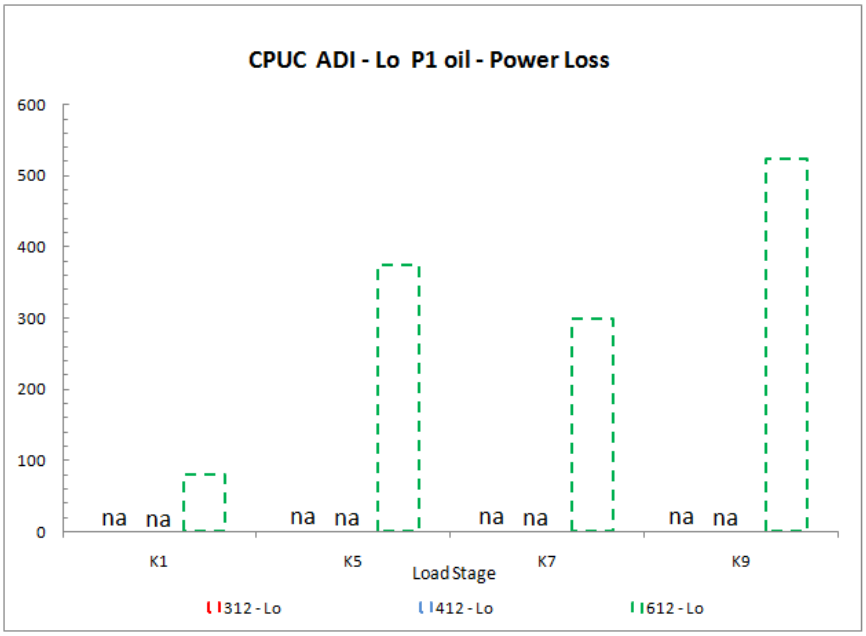

(a)

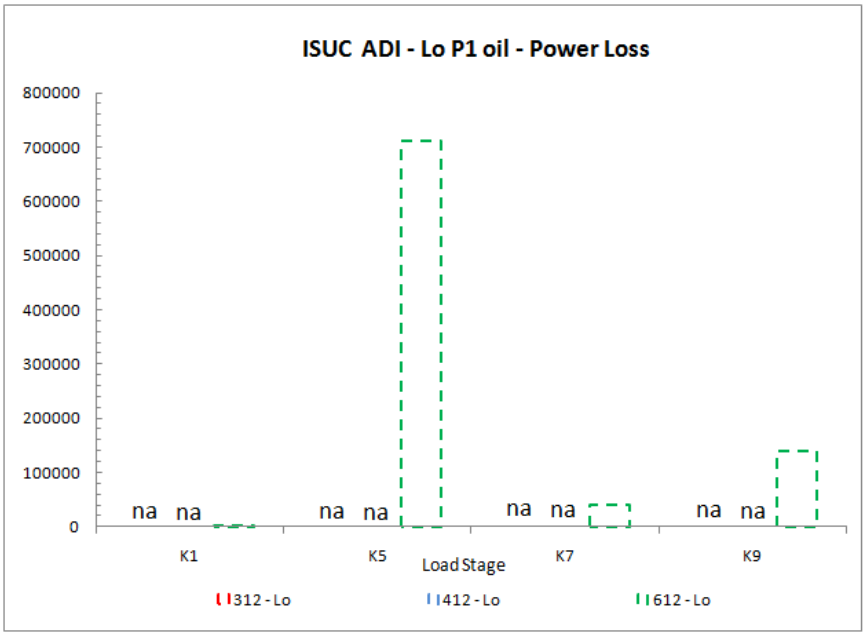

(b)

Figure 4.23.: Ferrography in gear power loss tests: ADI gear (612), P1 lubricant, low oil level.

4.4.2.3. Steel (611) vs ADI (612) gears - lubricant P1 and low oil level

Figure 4.24, displays and compares the wear particles concentration index (CPUC) and the wear severity index (ISUC), for the steel (611) and ADI (612) gears, lubricated with a low oil level.

Figure 4.24a, shows that ADI gear (612) had a higher level of wear particle concentration than any of the steel gears, in almost all the load stages, being the load stage K1 the only exception, since gear 611 CPUC levels were higher than those of gear 612.

The results of the ISUC indexes, show that gear 612 had an higher index than those obtained by the gear 611 in al the load stages. This is presented in the Figure 4.6b.

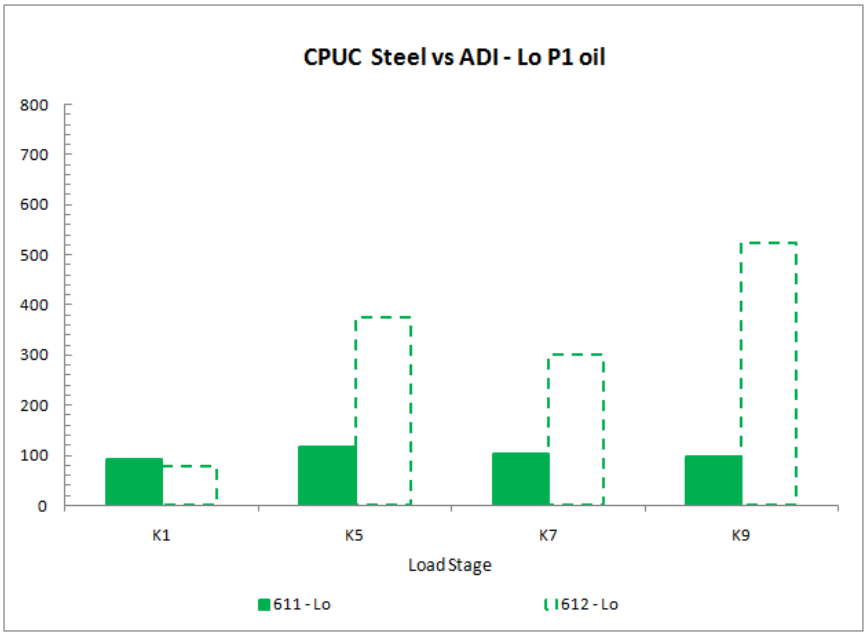

(a)

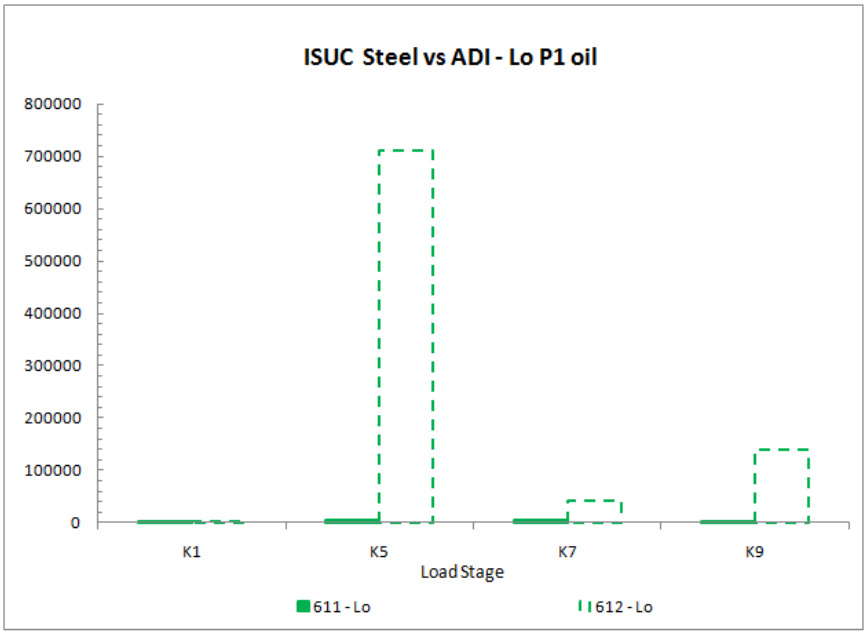

(b)

Figure 4.24.: Ferrography in gear power loss tests: steel vs ADI, with lubricant P1 and low oil level.

4.4.3. Surface Roughness

Table 4.9, Table 4.10 and Table 4.11 show the values for the tooth flank roughness measurements for steel gears 311, 411 and 611, respectively, and Table 4.12 values for the tooth flank measurements for ADI gear 612, all lubricated with P1 PAO based oil and a high oil level.

The values measured for the 610 series (using both materials) are not very reliable since it was very difficult to measure, because of the very small height of the teeth.

The 311 steel gear show a very poor evolution of the tooth flank roughness, both in case of the wheel and the pinion, since all the related parameters increase, between 16% and 190%, being this last one the R_{vk}. The 411 steel gear, they present a good evolution in the case of the wheel since all the parameters decrease, but a poor evolution in the pinion case, since most of the factor increase, from 28% up to 110%. Finally the 611 gear set present an opposite case to the 411 gear set, since the pinion present a good evolution, and the wheel present a poor evolution, being the decrease values from 1% up to 25%, and the increase values from 18% up to 71%.

In the case of the ADI gear 612 showed an decrease in almost all the values of roughness, going from 2% up to 56%, both for the pinion and the wheel. The only values that increase were the R_z and R_{max} on the pinion, and the increase was only of 18%, related to the R_{max} parameter. Concluding a good evolution of the tooth flank roughness in the ADI gear case.

Surface roughness [μm]									
	Probe	Direction	R_a	R_q	R_z	R_{max}	R_{pk}	R_k	R_{vk}
Initial	Pinion	Radial	0.1	0.1	0.53	0.9	0.1	0.2	0.15
Initial	Wheel	Radial	0.12	0.13	0.65	1	0.1	0.35	0.2
Final	Pinion	Radial	0.18	0.23	1.07	1.4	0.12	0.55	0.43
Final	Wheel	Radial	0.2	0.23	1.1	1.4	0.12	0.58	0.4
Pinion roughness evolution (%)			83.33	133.3	100	50.91	16.67	175	188.9
Wheel roughness evolution (%)			71.43	75	69.23	47.37	16.67	66.67	100

Table 4.9.: Tooth flank surface roughness of 20MnCr5 steel gear 311 with P1 gear oil and low oil level.

Surface roughness [μm]									
	Probe	Direction	R_a	R_q	R_z	R_{max}	R_{pk}	R_k	R_{vk}
Initial	Pinion	Radial	0.1	0.15	0.7	1.1	0.15	0.32	0.17
Initial	Wheel	Radial	0.22	0.28	1.37	1.8	0.17	0.67	0.48
Final	Pinion	Radial	0.18	0.23	1.1	1.4	0.13	0.55	0.35
Final	Wheel	Radial	0.17	0.23	1.1	1.5	0.13	0.47	0.45
Pinion roughness evolution (%)			83.33	55.56	57.14	28.13	-11.11	73.68	110
Wheel roughness evolution (%)			-23.08	-17.65	-19.51	-15.6	-20	-30	-6.9

Table 4.10.: Tooth flank surface roughness of 20MnCr5 steel gear 411 with P1 gear oil and low oil level.

Surface roughness [μm]									
	Probe	Direction	R_a	R_q	R_z	R_{max}	R_{pk}	R_k	R_{vk}
Initial	Pinion	Radial	0.28	0.37	1.7	2.2	0.27	0.85	0.52
Initial	Wheel	Radial	0.18	0.22	1.05	1.3	0.12	0.53	0.33
Final	Pinion	Radial	0.28	0.3	1.68	1.9	0.2	0.73	0.53
Final	Wheel	Radial	0.22	0.27	1.4	1.8	0.2	0.73	0.37
Pinion roughness evolution (%)			0	-18.18	-0.98	-14.39	-25	-13.73	3.23
Wheel roughness evolution (%)			18.18	23.08	33.33	36.36	71.43	37.5	10

Table 4.11.: Tooth flank surface roughness of 20MnCr5 steel gear 611 with P1 gear oil and low oil level.

Surface roughness [μm]									
	Probe	Direction	R_a	R_q	R_z	R_{max}	R_{pk}	R_k	R_{vk}
Initial	Pinion	Radial	0.40	0.57	2.60	3.65	0.45	1.27	0.88
Initial	Wheel	Radial	1.38	1.88	10.15	16.93	1.32	4.25	3.32
Final	Pinion	Radial	0.383	0.517	2.667	4.317	0.417	1.1	0.883
Final	Wheel	Radial	0.967	1.45	7.667	12.62	0.933	1.85	3.25
Pinion roughness evolution (%)			-4.167	-8.824	2.564	18.26	-7.407	-13.16	0
Wheel roughness evolution (%)			-30.12	-23.01	-24.47	-25.49	-29.11	-56.47	-2.01

Table 4.12.: Tooth flank surface roughness of ADI gear 612 with P1 gear oil and low oil level.

4.4.4. Mass Loss

The following graphic (Figure 4.25), displays and compares the pinion mass loss during the power loss tests, for steel and ADI gears, lubricated with P1 and low oil level.

The results presented in Figure 4.25, show a lower mass loss for the steel gears.

Gear 612 had the higher mass losses, being this gear manufactured in ADI, this result is due to the release of graphite nodules with the gear use.

Among the steel gears tested, gear 611 has the one with lower mass loss values, followed by gears 311 and 411, being the differences between them very small.

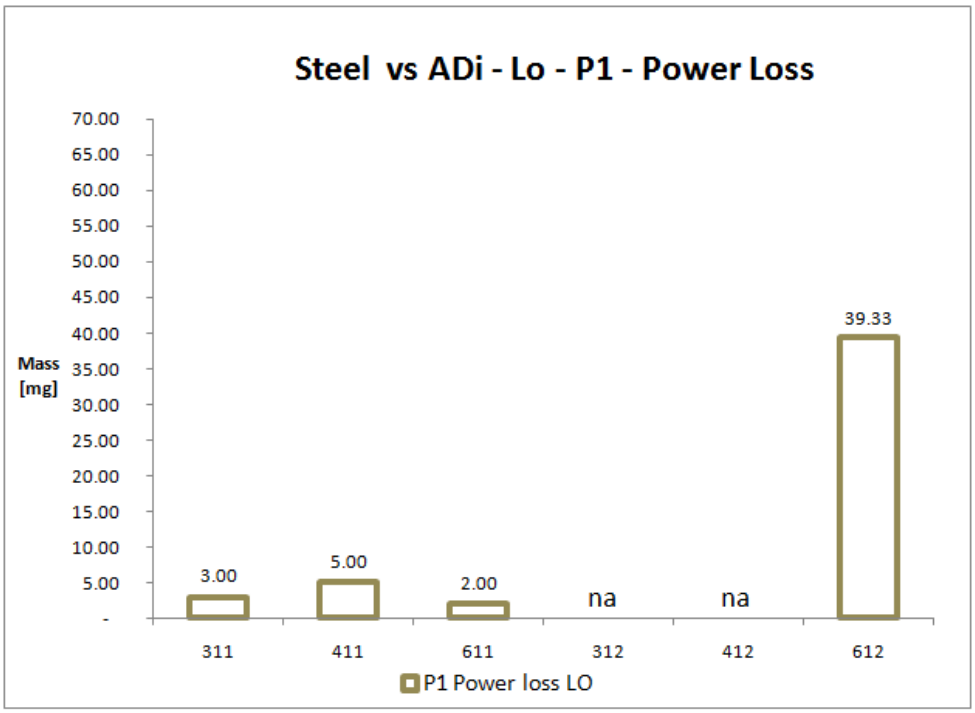

Figure 4.25.: Mass loss in gear power loss tests: steel vs ADI, with lubricant P1 and low oil level.

4.5. Polyalolephine base lubricant oil (P1) gear test and high oil Level

The power loss tests presented in this section were performed by Rui Silva [48] and Cristiano Locateli [9, 49].

4.5.1. Stabilization temperatures

The stabilization temperature is the parameter that will be observed in the following analysis for gear oil P1 and high oil volume. The stabilization temperature is the difference between the maximum oil bath temperature and the room temperature, that is, $\Delta T = T_{oil} - T_{room}$.

4.5.1.1. Steel gear 311, 411 and 611 - lubricant P1 and high oil level

Figure 4.26 presents and compares the stabilization temperatures in function of the reference friction torque, for the steel gears geometries (311,411 and 611), operating with a high oil level. These were performed for all velocities and load stages.

In the results present in the Figure 4.26, it can be observed that, for all load stages and velocities, gear 611 had the best performance.

Gear 611 working at 2000 rpm in load stage K9, had a stabilization temperature that was 30°C lower than the 2 other steel geometries (311 and 411).

In load stages K5 and K7, gear 411 had a lower stabilization temperature than gear 311. In load stage K9, gear 311 had a better performance than gear 411, having in this load stage a lower stabilization temperature. Concluding this way that gear 311 had the worst stabilization temperatures in almost all the load stages, being only overcome by gear 411 in load stage K9.

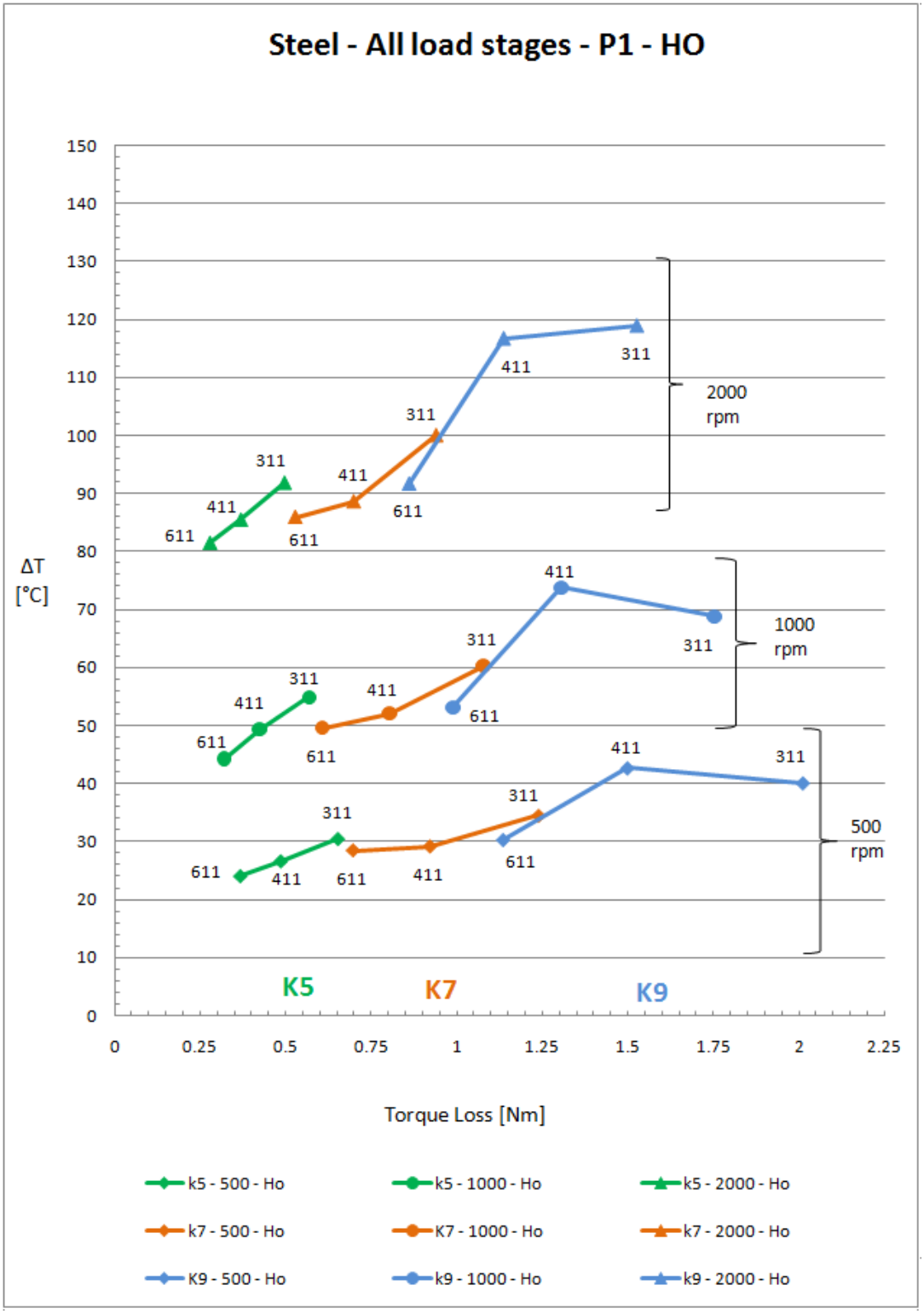

Figure 4.26.: Stabilization temperatures in gear power loss tests: steel gears (311, 411, 611), P1 lubricant, high oil level.

4.5.1.2. ADI gear 312, 412 and 612- lubricant P1 and high oil level

Figure 4.27 shows and compares the stabilization temperatures in function of the reference friction torque loss, for the ADI gears geometries (312, 412 and 612), operating with a high oil level, for all velocities and load stages.

The results presented in Figure 4.27, show that, for all load stages and velocities, gear 612 had the best performance.

At 2000rpm and in the load stage K9, gear 612 stabilization temperature was 50°C lower than those of the other gear sets.

In the lower load stages gear 412 had an average performance, being gear 312 the one with the highest stabilization temperatures. In the higher load stages, gear 312 was better than gear 412. The only handicap of gear 312 was the high reference friction torque loss value.

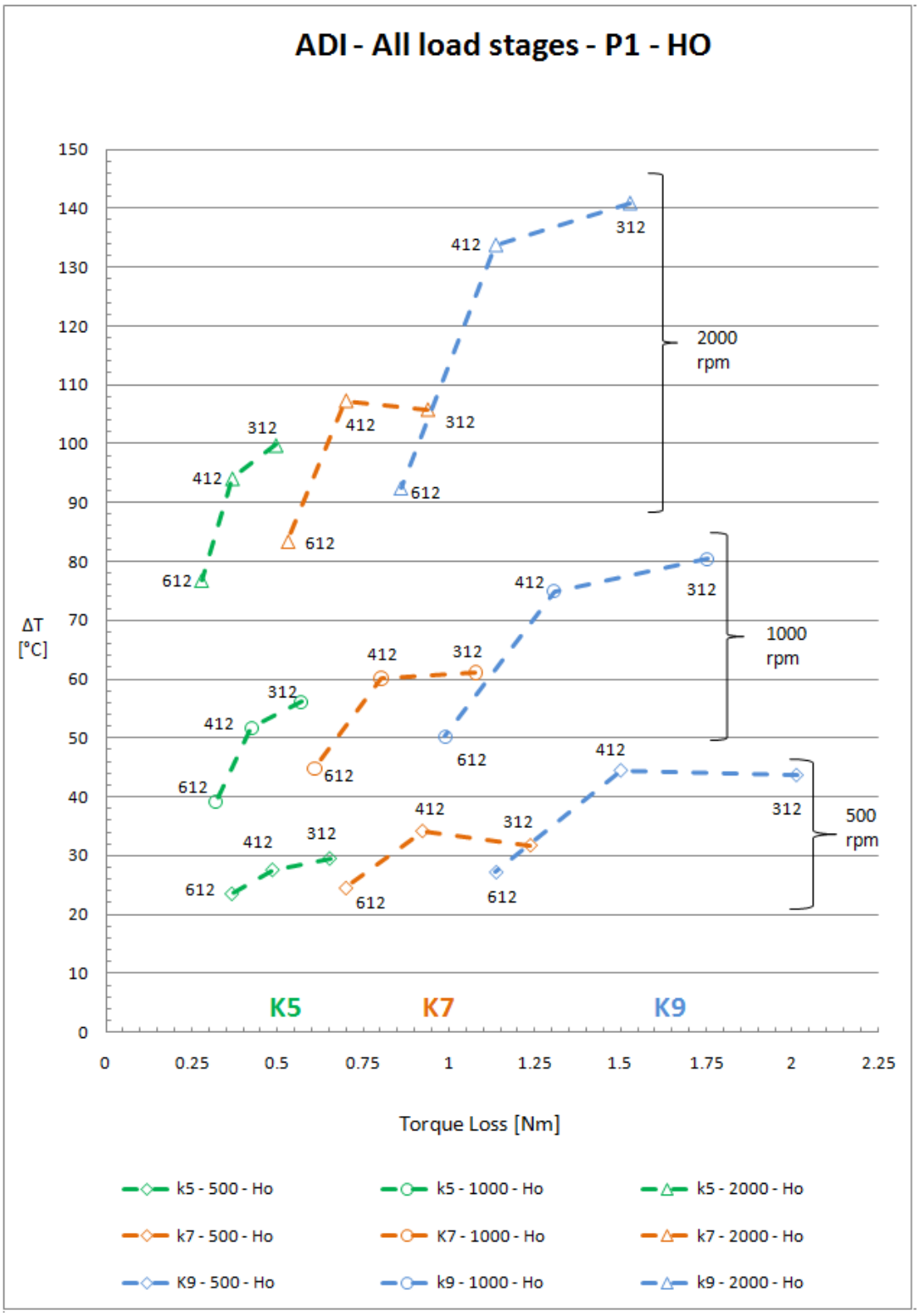

Figure 4.27.: Stabilization temperatures in gear power loss tests: ADI gears (312, 412, 612), P1 lubricant, high oil level.

4.5.1.3. Steel vs ADI gears - lubricant P1 and high oil level

Figure 4.28 shows the comparison of the stabilization temperatures between Steel and Adi gear materials. The stabilization temperatures are presented in function of the reference friction torque loss, lubricated with a high oil level, for all velocities and load stages.

The comparison presented in the Figure 4.28a, shows that gear 312 (ADI) had a higher stabilization temperature, in almost all the load stages and speeds, when compared with gear 311 (Steel).

In load stages K5 and K7, the stabilization temperatures of the gears (311 and 312) are similar, but they start to diverge in load stage K9, and gear 312 stabilization temperature starts to rise again, being worst with the increase in the rotational speed.

The only exception was at 500 rpm, and in the two load stages K5 and K7, that gear 312 was better than gear 311.

Figure 4.28b shows that the two gears, 411 and 412, had similar performances, being gear 411 that had the best stabilization temperatures.

At high speeds and load stages, gear 411 becomes more efficient than gear 412, having a lower stabilization temperature.

The 610 gear geometries (see Figure 4.28c) show a complete opposite case to gear 410 geometries, since gear 612 had a superior performance in almost all operating conditions, being the exception present in load stage K1, were gear 611 had a lower stabilization temperature. However, the performances of the two gears were similar.

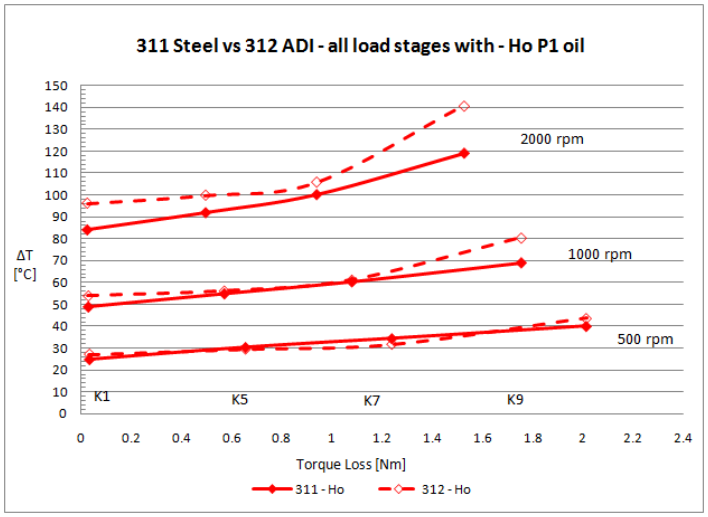

(a)

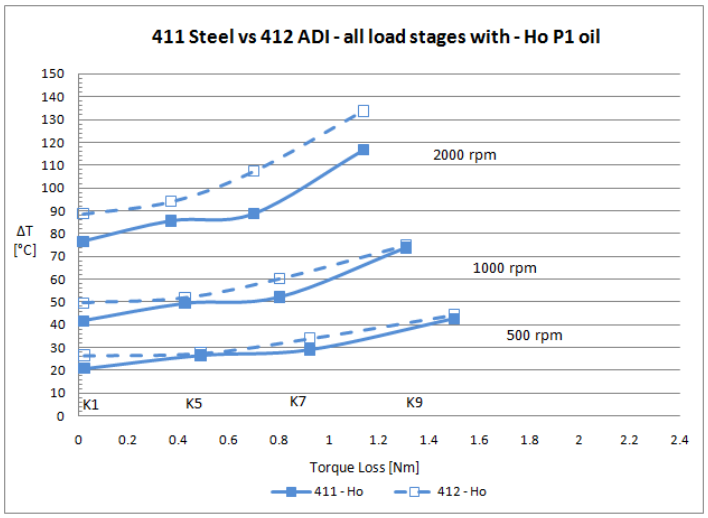

(b)

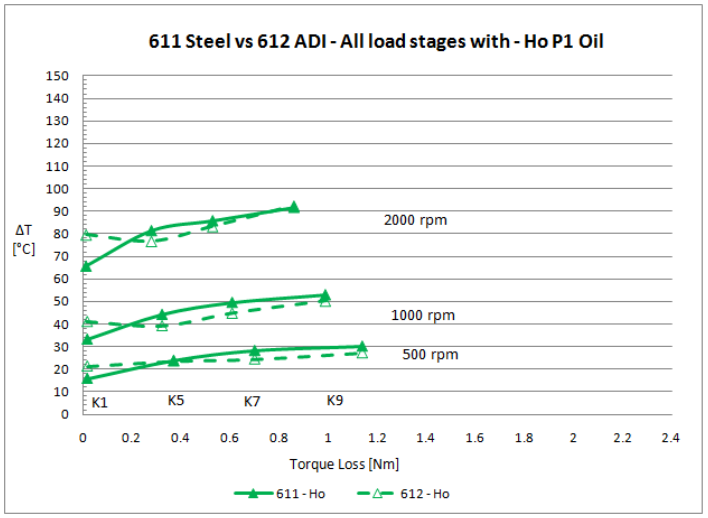

(c)

Figure 4.28.: Stabilization temperatures in gear power loss tests with lubricant P1 and low oil level: a) gear 311 vs 312; b) gear 411 vs 412; c) gear 611 vs 612.

4.5.2. Ferrometry

A summary of the Direct Reading Ferrography results are presented in this section.

4.5.2.1. Steel gears - lubricant P1 and high oil level

The results presented in Figure 4.29, displays and compares the wear particles concentration index (CPUC) and the wear severity index (ISUC), for steel gears lubricated with an high oil level, for each load stage of the power loss tests.

The results presented show that, the wear particle concentration indexes were higher for gear 311 in all load stages.

It can also be seen that, gear 311 had the highest wear severity indexes, showing that its the gear that generates more wear particles and more severe wear.

Gear 411 had average values, but near the ones obtained by gear 611.

Gear 611 had the lowest values of CPUC and ISUC indexes, from all three geometries, in all load stages.

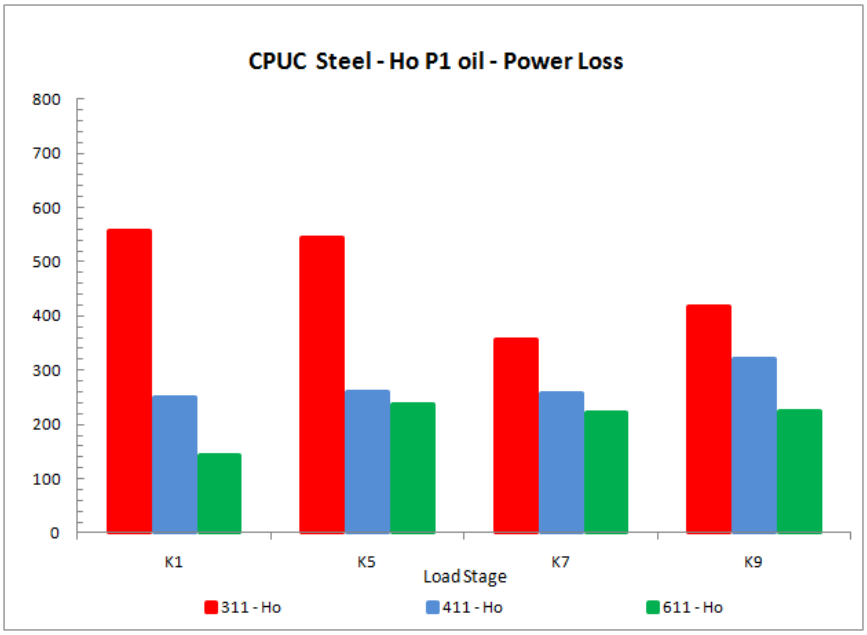

(a)

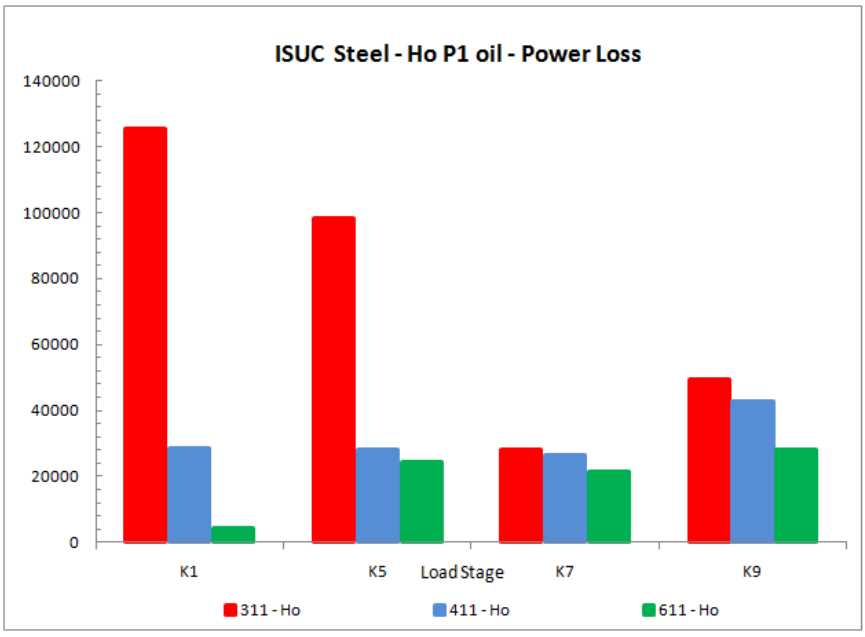

(b)

Figure 4.29.: Ferrography in gear power loss tests: steel gears (311, 411, 611), P1 lubricant, high oil level.

4.5.2.2. ADI gears - lubricant P1 and high oil level

Figure 4.30, displays and compares the wear particles concentration index (CPUC) and the wear severity index (ISUC), for ADI gears operating with an high oil level and in each load stage.

Figures 4.30 shows that, gear 412 presented the highest concentration of particles index (CPUC) and also the highest wear severity index.

Gear 612 had average values of CPUC (see Figure 4.30a) and ISUC (see Figure 4.30b), in load stages, K5, K7 and K9, and in load stage K1 it had values near to those of gear 312.

Gear 312 was the one with the lowest CPUC and ISUC values, being the ADI gear that loses less particles and had the less severe wear.

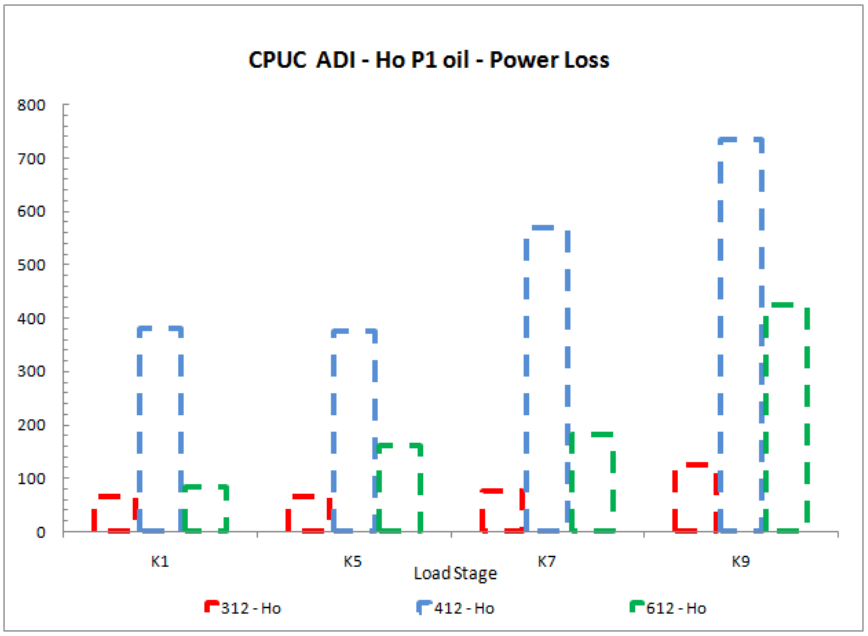

(a)

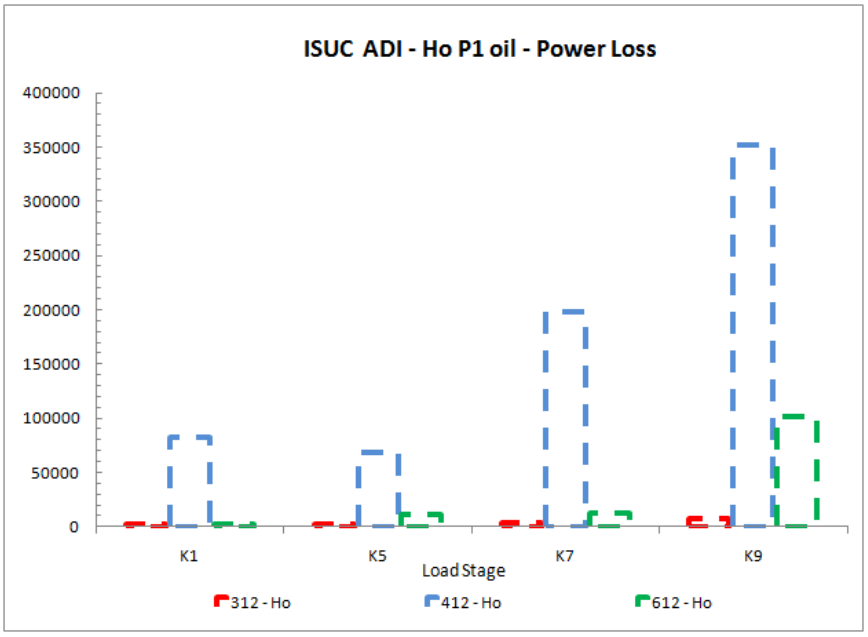

(b)

Figure 4.30.: Ferrography in gear power loss tests: ADI gears (312, 412, 612), P1 lubricant, high oil level.

4.5.2.3. Steel vs ADI gears - lubricant P1 and high oil level

Figure 4.31, displays and compares the wear particles concentration index (CPUC) and the wear severity index (ISUC), for steel and ADI gears, lubricated with an high oil level.

The results are from the all load stages used in the power loss tests and contain results from all gear geometries used.

In load stage K1 and K5, gear 311 had the highest values of CPUC (see Figure 4.31a) and ISUC (see Figure 4.31b), followed by gear 412, 411, 611, 612 and 312.

In load stage K7, gear 412 had the highest values of CPUC and ISUC, followed by gear 311, 411, 611, 612 and 312.

In load stage K9, gear 412 had the highest values of CPUC and ISUC, followed by gear 612, 311, 411, 611 and 312.

Concluding, gear 312 had lower values of CPUC and ISUC, than all other gears.

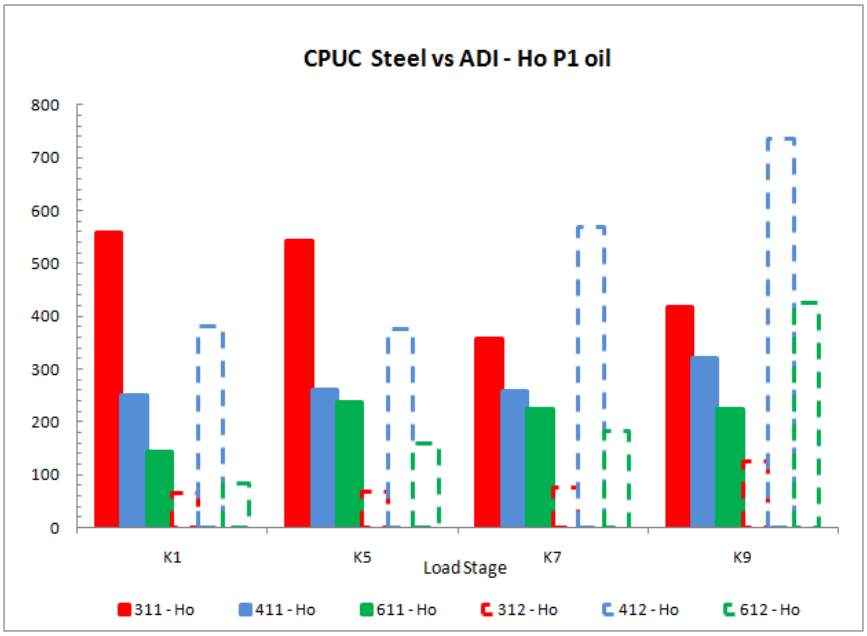

(a)

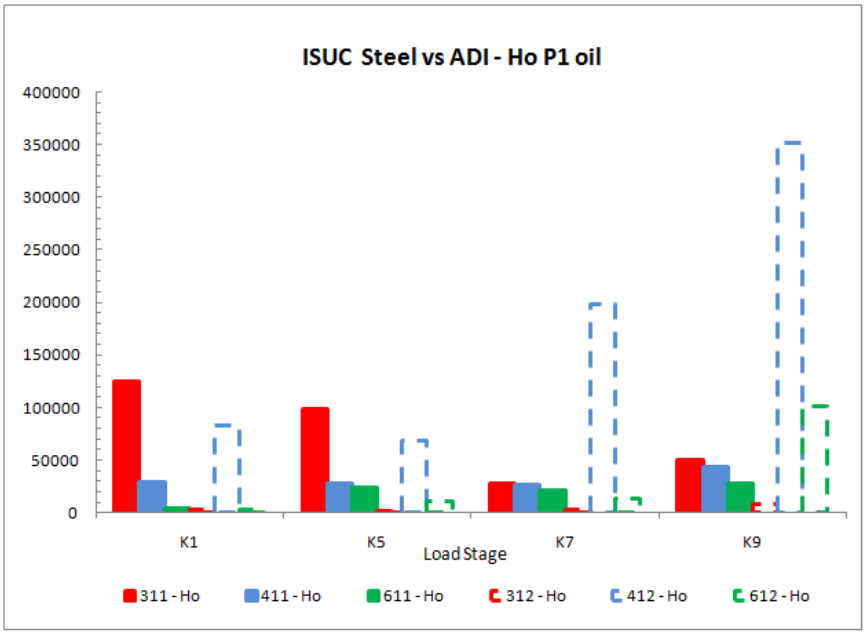

(b)

Figure 4.31.: Ferrography in gear power loss tests: steel vs ADI gears, P1 lubricant, high oil level.

4.5.3. Surface Roughness

Table 4.13 and Table 4.14 shows values of tooth flank roughness measurements for steel gears 311 and 411, respectively. Table 4.15 and Table 4.16 shows values of tooth flank roughness measurements for ADI gears 312 and 412, all lubricated with P1 PAO based oil and a high oil level.

In the case of 610 gears series, it was not possible to perform the roughness measurements because of the small teeth height.

Steel gears 311 and 411 show a very significant evolution of the tooth flank roughness, since almost all of the parameters decreased, some between 1% and 40% both for pinions and wheels. The exception was the R_{vk} that presented some increase.

In the case of the ADI gears 312 and 412 the initial tooth flank roughness values were significantly higher than those of the steel gears.

Gear 312 also showed a very significant evolution of the tooth flank roughness, since almost all parameters decreased between 20% and 50% for wheels and increased between 40% and 180% for gear 312 pinion. There was a decrease of 45% in the R_{vk} parameter, contrasting with the increase of near 490% occurred in the pinion.

Gear 412 had a better evolution, showing a very significant increase of the tooth flank roughness since almost all parameters increased between 20% and 95% for the wheels and showed some increase of 10% and 50% for the R_a and R_q and showing a decrease of almost 30% for the R_k. The R_{vk} increase was slightly lower than in 312 being 150% and 200% for the pinion and wheel respectively.

Surface roughness [μm]									
	Probe	Direction	R_a	R_q	R_z	R_{max}	R_{pk}	R_k	R_{vk}
Initial	Pinion	Radial	0.25	0.32	1.53	1.8	0.24	0.78	0.42
Initial	Wheel	Radial	0.23	0.3	1.5	2.1	0.24	0.71	0.51
Final	Pinion	Radial	0.23	0.31	1.47	2.3	0.12	0.7	0.47
Final	Wheel	Radial	0.18	0.23	1.21	1.6	0.16	0.52	0.38
Pinion roughness evolution (%)			-6.67	-4.17	-3.71	26.88	-49.3	-10.68	10.24
Wheel roughness evolution (%)			-24.29	-23.08	-19.33	-22.37	-32.88	-26.76	-26.62

Table 4.13.: Tooth flank surface roughness of 20MnCr5 steel gear 311 with P1 gear oil and high oil level.

Surface roughness [μm]									
	Probe	Direction	R_a	R_q	R_z	R_{max}	R_{pk}	R_k	R_{vk}
Initial	Pinion	Radial	0.21	0.26	1.3	1.8	0.2	0.66	0.37
Initial	Wheel	Radial	0.2	0.26	1.27	1.6	0.2	0.66	0.31
Final	Pinion	Radial	0.19	0.24	1.28	1.6	0.12	0.56	0.38
Final	Wheel	Radial	0.18	0.23	1.12	1.3	0.12	0.58	0.34
Pinion roughness evolution (%)			-9.68	-8.86	-1.03	-8.17	-38.98	-15.58	3.64
Wheel roughness evolution (%)			-11.48	-10.39	-11.84	-15.7	-41.67	-13.07	9.78

Table 4.14.: Tooth flank surface roughness of 20MnCr5 steel gear 411 with P1 gear oil and high oil level.

Surface roughness [μm]									
	Probe	Direction	R_a	R_q	R_z	R_{max}	R_{pk}	R_k	R_{vk}
Initial	Pinion	Radial	0.23	0.3	1.57	2.28	0.4	0.75	0.3
Initial	Wheel	Radial	0.33	0.43	2.15	3.25	0.3	0.97	0.78
Final	Pinion	Radial	0.53	0.83	4.42	7.03	0.5	1.15	1.77
Final	Wheel	Radial	0.17	0.28	1.72	2.95	0.5	0.48	0.43
Pinion roughness evolution (%)			128.6	177.8	181.9	208	39.13	53.33	488.9
Wheel roughness evolution (%)			-50	-34.62	-20.16	-9.23	45	-50	-44.68

Table 4.15.: Tooth flank surface roughness of ADI gear 312 with P1 gear oil and high oil level.

Surface roughness [μm]									
	Probe	Direction	R_a	R_q	R_z	R_{max}	R_{pk}	R_k	R_{vk}
Initial	Pinion	Radial	0.52	0.62	3.07	4.08	0.6	1.63	0.78
Initial	Wheel	Radial	0.33	0.43	2.42	3.98	0.5	1.08	0.53
Final	Pinion	Radial	0.57	0.92	4.97	8.8	0.4	1.18	1.98
Final	Wheel	Radial	0.53	0.82	4.7	7.87	0.4	1.28	1.62
Pinion roughness evolution (%)			9.68	48.65	61.96	115.5	-43.24	-27.55	153.2
Wheel roughness evolution (%)			60	88.46	94.48	97.49	-25.81	18.46	203.1

Table 4.16.: Tooth flank surface roughness of ADI gear 412 with P1 gear oil and high oil level.

4.5.4. Mass Loss

Figure 4.32, displays and compares the pinion mass loss during the power loss tests, for steel and ADI gears, lubricated with P1 and high oil level. The results for gear geometry 610 in ADI material was not realized, so no values were available to be compared.

Figure 4.32, shows that the ADI gears had higher mass losses than the steel ones, being gear 611 the one that had the nearest values to the ADI gears.

In the gears manufactured in steel material, the 311 gear geometry had the lowest mass losses.

Gear 311 had 10 times less mass loss then gear 312.

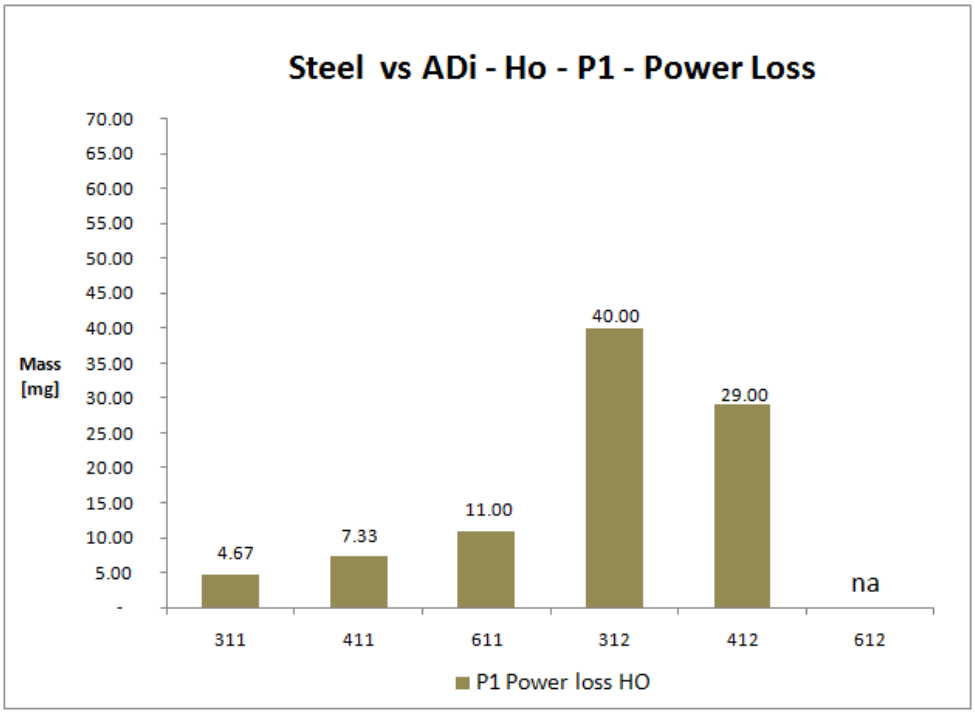

Figure 4.32.: Mass loss in gear power loss tests: steel vs ADI gears, P1 lubricant, high oil level.

4.6. Polyalolephine base lubricant oil gear (P1) test and high vs low oil Level

4.6.1. Stabilization temperatures

Figure 4.33 compares stabilization temperatures generated by the gears, using high and low oil levels. The objective is to understand the influence of oil level on the stabilization temperature.

In the case of the steel gears (see Figure: 4.33a, b and c), whatever the velocity, load stage and gear geometries, a low oil level always generate a lower stabilization temperature.

The difference is mainly dependent on the operating speed: at 500 rpm the differences are very small (-1 to -3°C , in the case of the low oil level), at 1000 rpm, the difference reaches -10°C (in favor of a low oil level) and at 2000 rpm the difference can reach -20°C ate high torque (K9), again in favor of a low oil level.

Working at 2000 rpm the biggest difference was given for the load stages K5 and K7.

In the ADI gears (see Figures: 4.33d, e, f) there is not much to compare, since there is no data available as it was already explain (see subsection 4.4.1.2).

With the available data there can be said that, the performance of gear 612 lubricated with low oil level was better than with high oil (see Figure 4.33f). The difference was higher for the speed of 2000 rpm and low load stage, decreasing as the load increases.

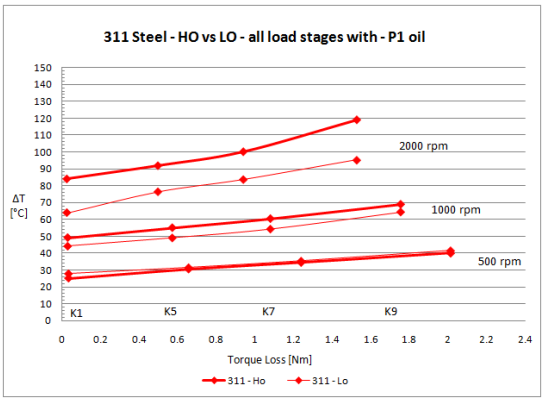

(a)

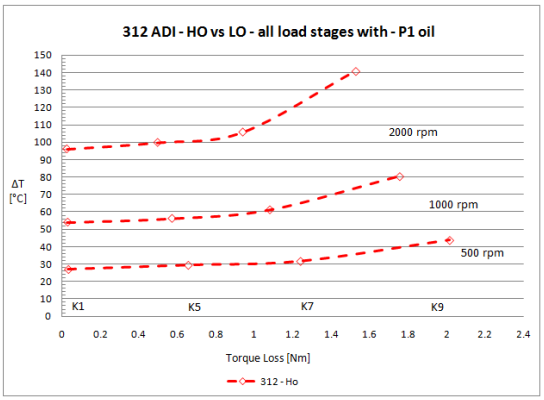

(d)

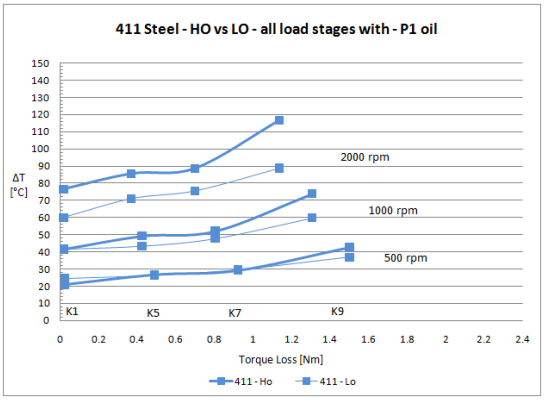

(b)

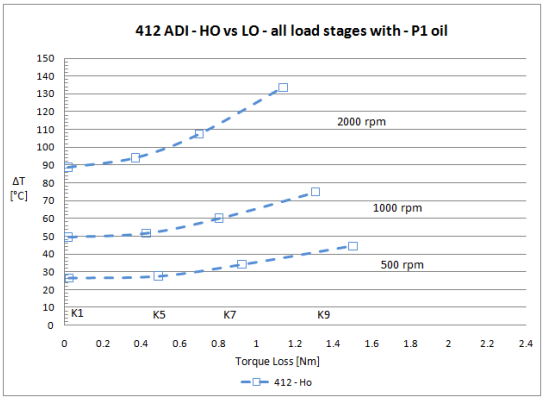

(e)

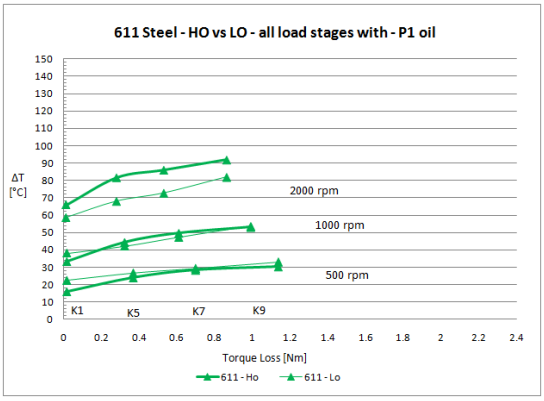

(c)

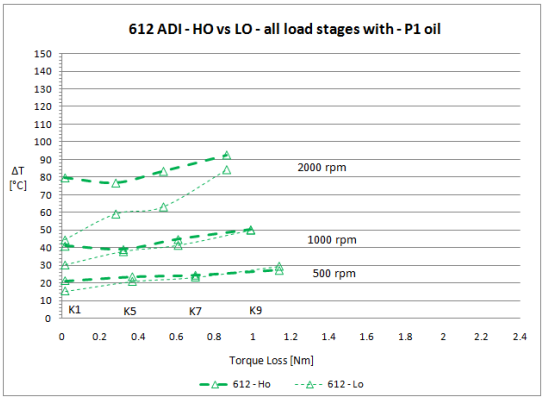

(f)

Figure 4.33.: Stabilization temperatures in gear power loss tests: high vs low oil level, P1 lubricant, steel and ADI gears.

4.6.2. Ferrometry

In the Figures 4.34 and 4.35 are compared the CPUC and ISUC indexes generated by steel and ADI gears lubricated with high and low oil level. The objective is to understand the influence of the oil level on the gears wear.

The CPUC and ISUC values were higher for the steel gears when they work with high oil level, than they were for the same gears working at low oil level.

Gear 311 operating with an high oil level, had the highest level of CPUC (Figure 4.34a) and severe wear (high ISUC) (Figure 4.34b).

In load stage K9 and operating with a low oil level gears 311 and 411 had similar values of CPUC and ISUC.

For ADI, the values of CPUC and ISUC were only established for gear 612 working in high and low oil. In this case, and in the load stage K9, the the high oil level, had the lowest levels of CPUC (Figure 4.35a), but the highest levels of ISUC (Figure 4.35b).

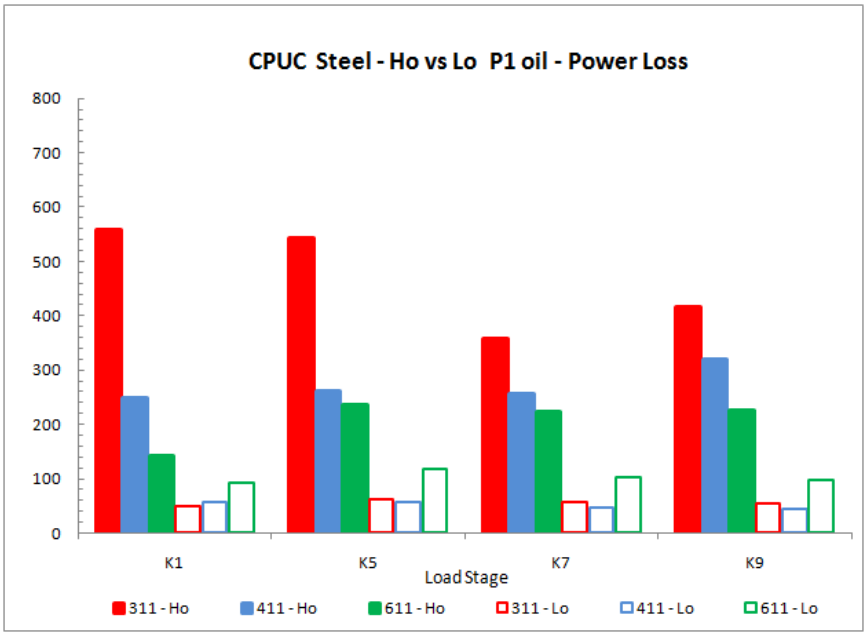

(a)

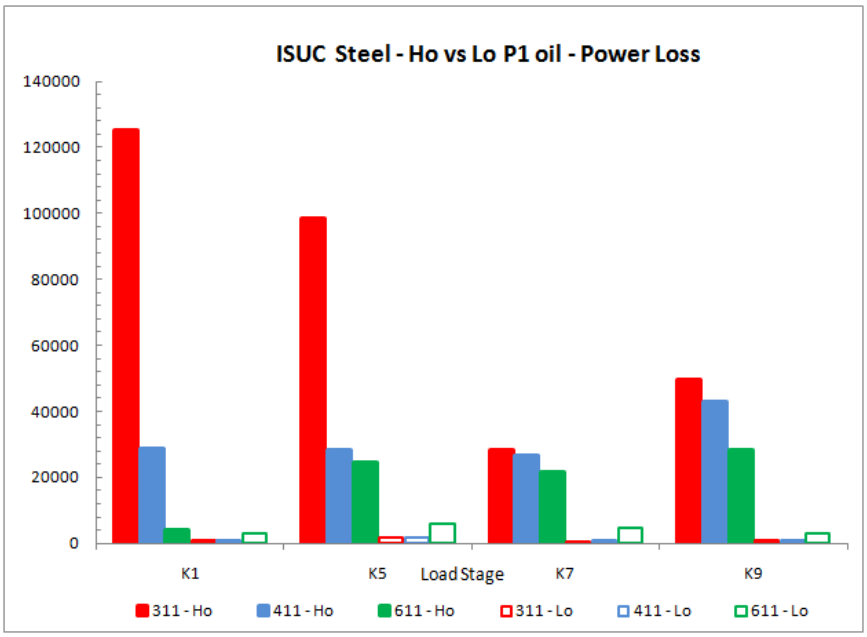

(b)

Figure 4.34.: Ferrography in gear power loss tests: high vs low oil level, P1 lubricant, steel gears.

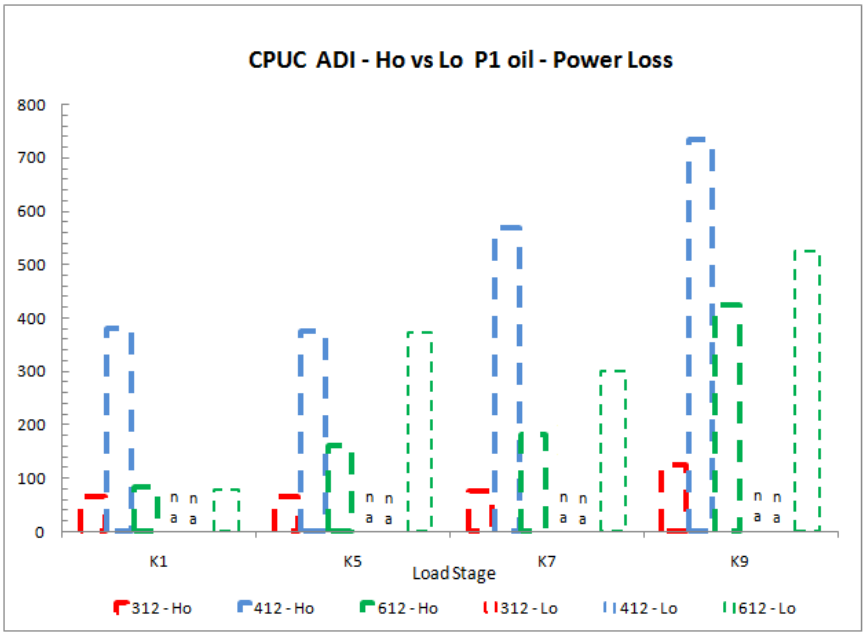

(a)

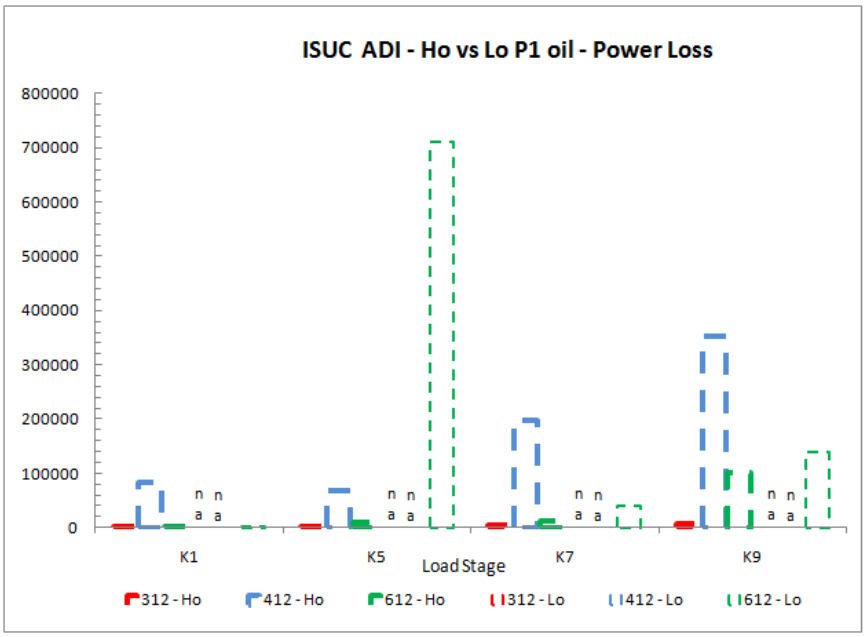

(b)

Figure 4.35.: Ferrography in gear power loss tests: high vs low oil level, P1 lubricant, ADI gears.

4.6.3. Mass Loss

Figure 4.36, displays and compares the pinion mass loss during the power loss tests, for steel and ADI gears, lubricated with P1, high and low oil levels. Some values were not available to be compared.

Figure 4.36, shows that the ADI gears had higher mass losses than the steel ones.

In the gears manufactured in steel material, the 611 lubricated with an low oil level had the lowest mass loss value.

Gears manufactured in steel operating with a low oil level had lower values of mass loss than the same gears lubricated with an high oil level.

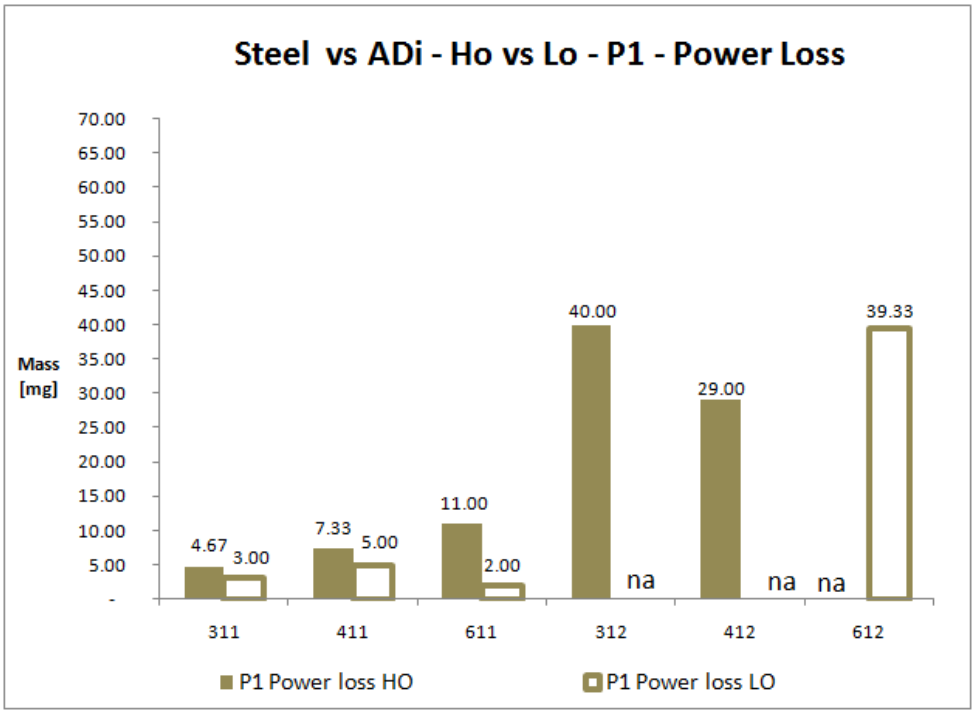

Figure 4.36.: Mass loss in gear power loss tests: high vs low oil level, P1 lubricant, steel and ADI gears.

4.7. Polyalolephine base (P1) vs Ester base (E1) lubricant oil gear test and low oil Level

4.7.1. Stabilization temperatures

The stabilization temperature is the parameter that will be observed in the following analysis . It represents difference between the oil bath temperature and the room temperature, that is, $\Delta T = T_{oil} - T_{room}$, after stabilization, when the power loss inside the FZG gearbox is in equilibrium with the heat flow from the FZG gearbox to the surrounding environment.

The stabilization temperatures were taken after 4 hours of operation at specified operating conditions (torque and speed).

4.7.1.1. Steel gear 311, 411 and 611 - lubricant with low oil level

Figure 4.37 shows and compares the stabilization temperatures of the steel gears (311, 411 and 611), lubricated with gear oils E1 and P1 and low oil level, for all applied torques (K1, K5, K7 and K9) and all operating speeds (500, 1000 and 2000 rpm), in relation to the corresponding reference gear friction torque loss.

Figure 4.37, shows that, operating in the load stages K7 and K9 and at all speeds, the E1 lubricant oil had a better performance than P1, obtaining always the lowest stabilization temperatures.

In load stage K5, at all speeds, gear 311 and 411 presented better stabilization temperatures with E1 instead of P1 (see Figures 4.37a and b).
Gear 611 (see Figure 4.37c) operating at 500 rpm, had a better performance when lubricated with E1 gear oil, however, in every other speed P1 lubricant oil was better.

In load stage K1 and with gear 311, E1 lubricant oil presented lower stabilization temperatures than with P1 lubricant oil.

Gear 411 gear operating at 500 or 1000 rpm, both E1 and P1 have a similar stabilization temperatures, being the difference at 2000 rpm where P1 lubricant oil had lower stabilization temperature.

Gear 611 lubricated with P1 had better performance at 1000 and 2000rpm, however, operating at 500 rpm both lubricants have a similar behaviors.

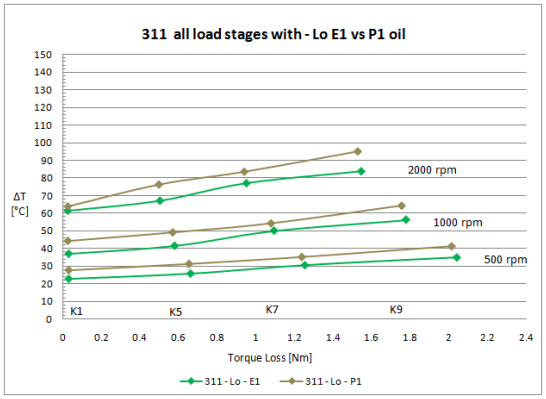

(a)

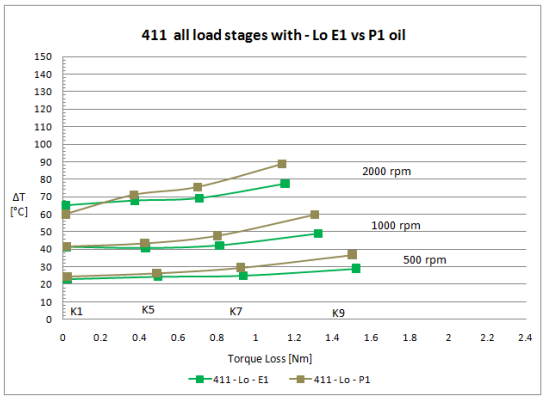

(b)

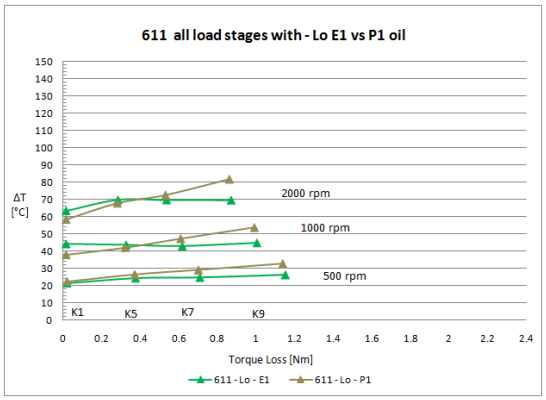

(c)

Figure 4.37.: Stabilization temperatures in gear power loss tests: steel gears (311, 411, 611), P1 and E1 lubricants, low oil level.

4.7.1.2. ADI gear 612 - lubricant with low oil level

Figure 4.38 shows and compares the stabilization temperatures of the ADI gear 612, lubricated with gear oils E1 and P1 and low oil level, for all applied torques (K1, K5, K7 and K9) and all operating speeds (500, 1000 and 2000 rpm), in relation to the corresponding reference gear friction torque loss.

Figure 4.38, shows that gear 612 lubricated with P1 gear oil, had lower stabilization temperatures than those obtained when lubricated with E1 gear oil. At 200 rpm and operating in load stage K9, the difference reaches 30°C .

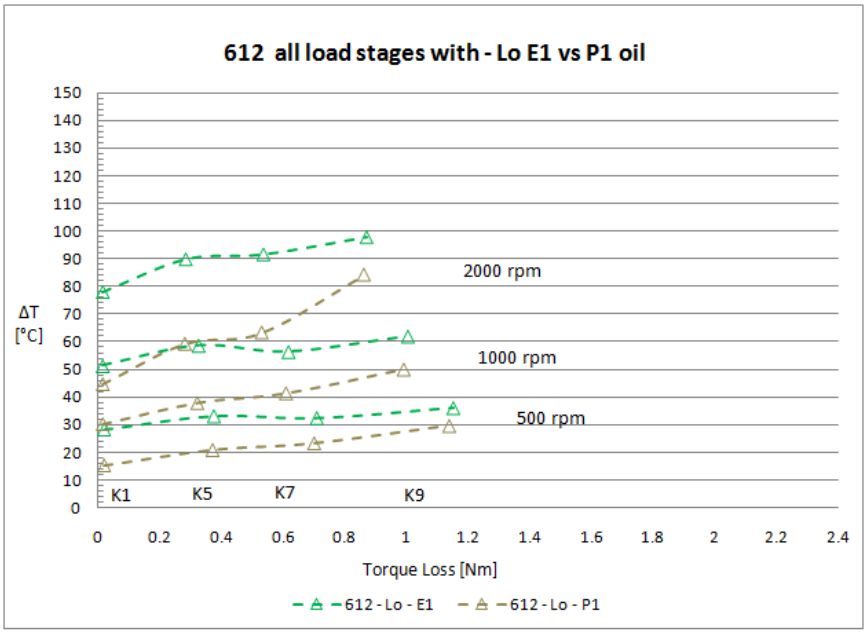

Figure 4.38.: Stabilization temperatures in gear power loss tests: ADI gear (612), P1 and E1 lubricants, low oil level.

4.7.2. Mass Loss

The following graphic (Figure 4.39a), displays and compares the pinion mass loss, of steel gears, at the end of the power loss tests, operating with E1 and P1 lubricant gear oils and low oil level.

Gears 311 and 611, had the lowest mass loss values operating in combination with P1 lubricant oil.
However, operating with gear 411 the lowest mass loss value was found in combination with the E1 lubricant oil.

Figure 4.39b, displays and compares the pinion mass loss, of ADI gears, at the end of the power loss tests, operating with E1 and P1 lubricant gear oils and low oil level.

Gear 612, have lower mass losses when combined with P1 lubricant oil, being the difference to the E1 lubricant oil of 11 mg.

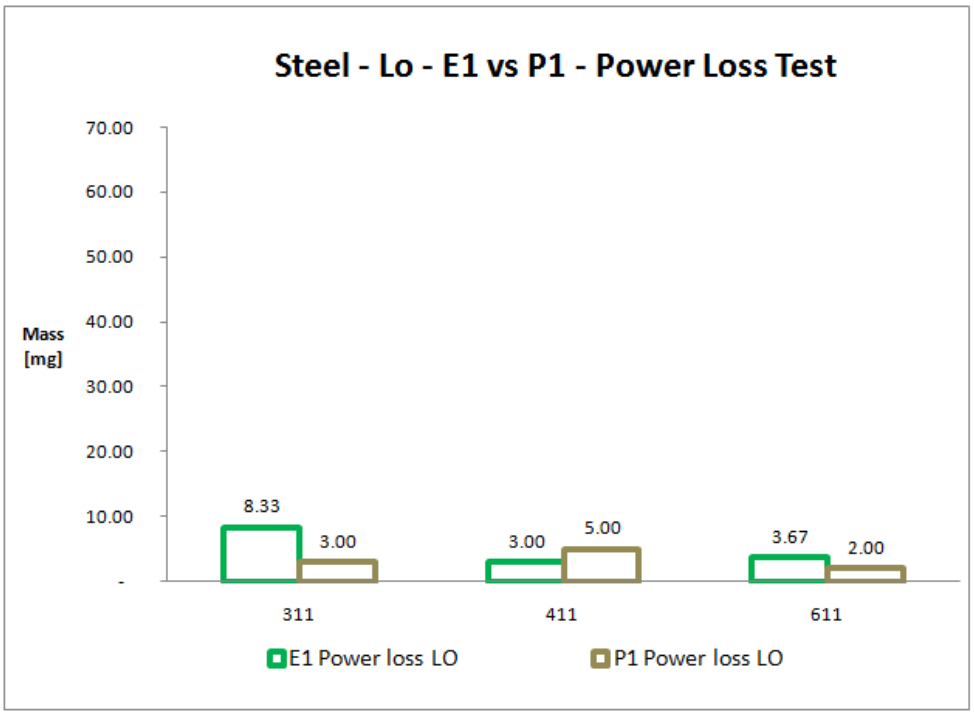

(a)

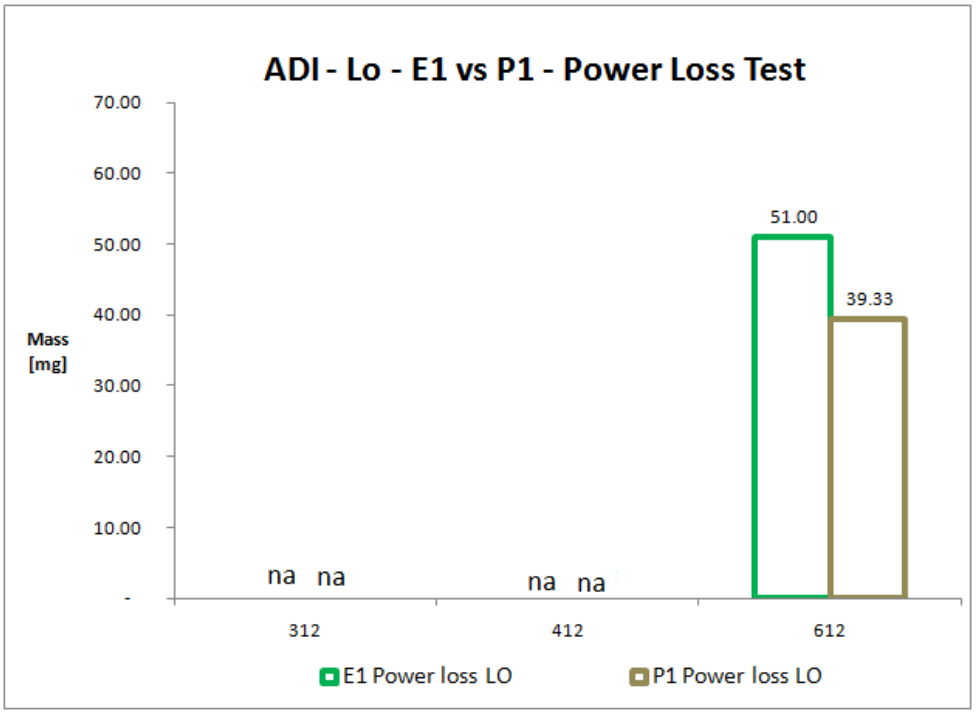

(b)

Figure 4.39.: Mass loss in gear power loss tests: a) steel and b) ADI gears, E1 vs P1 gear oils, and low oil level.

4.8. Polyalolephine base (P1) vs Ester base (E1) lubricant oil gear test and high oil Level

4.8.1. Stabilization temperatures

4.8.1.1. Steel gear 311, 411 and 611 - lubricant with high oil level

Figure 4.40 shows and compares the stabilization temperatures of the steel gears (311, 411 and 611), lubricated with gear oils E1 and P1 and high oil level, for all applied torques (K1, K5, K7 and K9) and all operating speeds (500, 1000 and 2000 rpm), in relation to the corresponding reference gear friction torque loss.

Figure 4.40a, shows that, E1 lubricant oil had a better performance in almost all load stages when combined with gear 311. The exception was load stage K5 operating at 2000 rpm, in which lubricant P1 had a slightly lower stabilization temperature than in the other load stages and speeds.

Gear 411 lubricated P1 gear oil, presented the lowest stabilization temperatures operating in load stages K1, K5 and K7. The highest difference between E1 and P1 was at 2000 rpm (see Figure 4.40b). In load stage K9, lubricant E1 had a better performance than P1, at all speeds.

The combination, gear 611 and P1 lubricant oil, had the best performance operating at 500 or 1000 rpm and in load stages K1 and K9, however being the worst combination in the load stages K5 and K7, at the same speeds. (see Figure 4.40c)

Operating at 2000 rpm, the combination 611 and P1 oil, had a better performance, for all load stages, being the biggest difference of -30 °C when compared to the same gear lubricated with E1 lubricant oil.

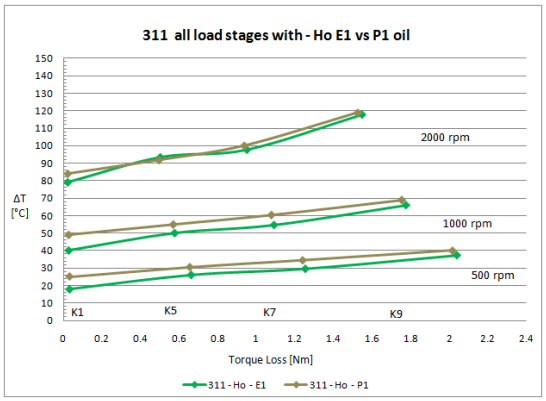

(a)

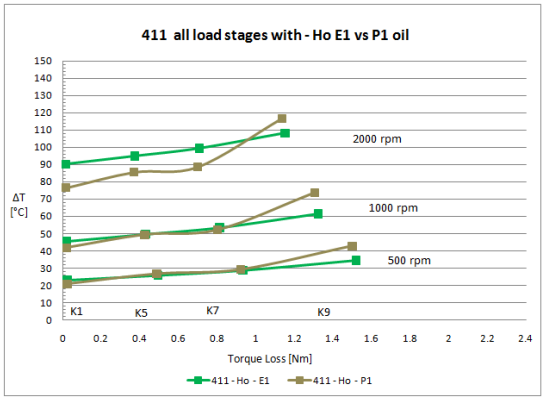

(b)

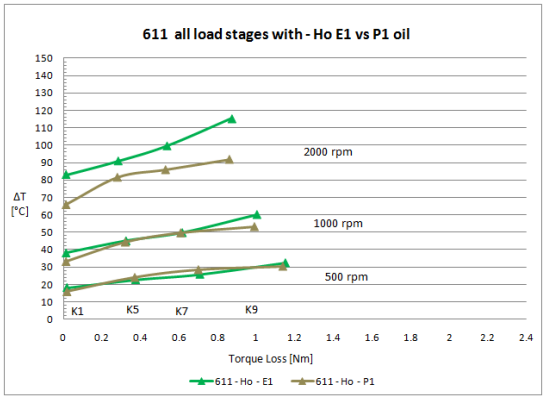

(c)

Figure 4.40.: Stabilization temperatures in gear power loss tests: steel gears (311, 411, 611), P1 and E1 lubricants, high oil level.

4.8.1.2. ADI gear 312, 412 and 612- lubricant with low oil level

Figure 4.41 shows and compares the stabilization temperatures of the ADI gears (312, 412 and 612), lubricated with gear oils E1 and P1 and high oil level, for all applied torques (K1, K5, K7 and K9) and all operating speeds (500, 1000 and 2000 rpm), in relation to the corresponding reference gear friction torque loss.

The combination, gear 312 and P1 lubricant oil, had the best performance operating in the load stages K7 and K9, at all speeds. However being this the worst combination for the load stages K1 and K5, at the same speeds.

Gear 312 lubricated with E1 oil, was the solution that had the lowest stabilization temperatures in this case.(see Figure 4.41a)

Both combination of gear 412 or 612 with the E1 lubricant oil, had a better performance in almost all load stages and speeds, than if there was used P1 lubricant oil.

The only exception was, gear 412 operating at 2000 rpm in K1 load stage. In this case the P1 lubricant oil presented the lowest stabilization temperature.(see Figure 4.41a and Figure 4.41a for the 412 and 612 gears respectively)

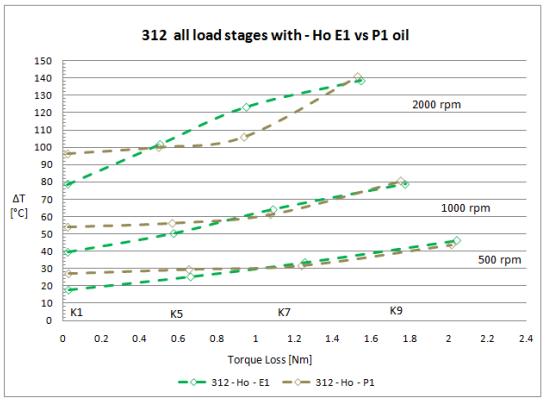

(a)

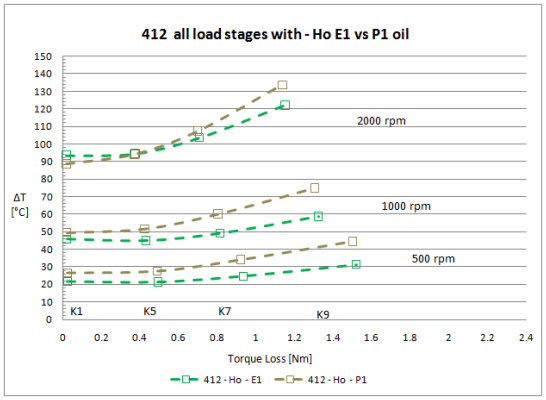

(b)

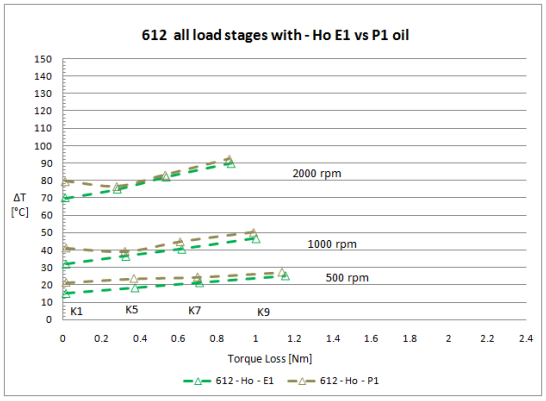

(c)

Figure 4.41.: Stabilization temperatures in gear power loss tests: ADI gears (312, 412, 612), P1 and E1 lubricants, high oil level.

4.8.2. Mass Loss

The following results (Figure 4.42a), displays and compares the pinion mass loss during the power loss tests, for E1 and P1 lubricant oils, with the use of steel gears and high oil level.

Using gears 311 or 411, the lowest mass loss values were found in combination with the P1 lubricant oil.

However with gear 611, the case reverses it self and the lowest mass loss values were found in combination with the E1 lubricant oil.

The results (Figure 4.42b), show the pinion mass loss during the power loss tests, for E1 and P1 lubricant oils, with the use of ADI gears and high oil level.

Gear 312 had the lowest values of mass loss in combination with P1 lubricant oil.

In the case of the gear 412, the mass loss values were the same, combining with P1 or E1 lubricant oil.

The mass loss values of gear 612 using lubricant oil P1, were not available, so the comparison was not realized.

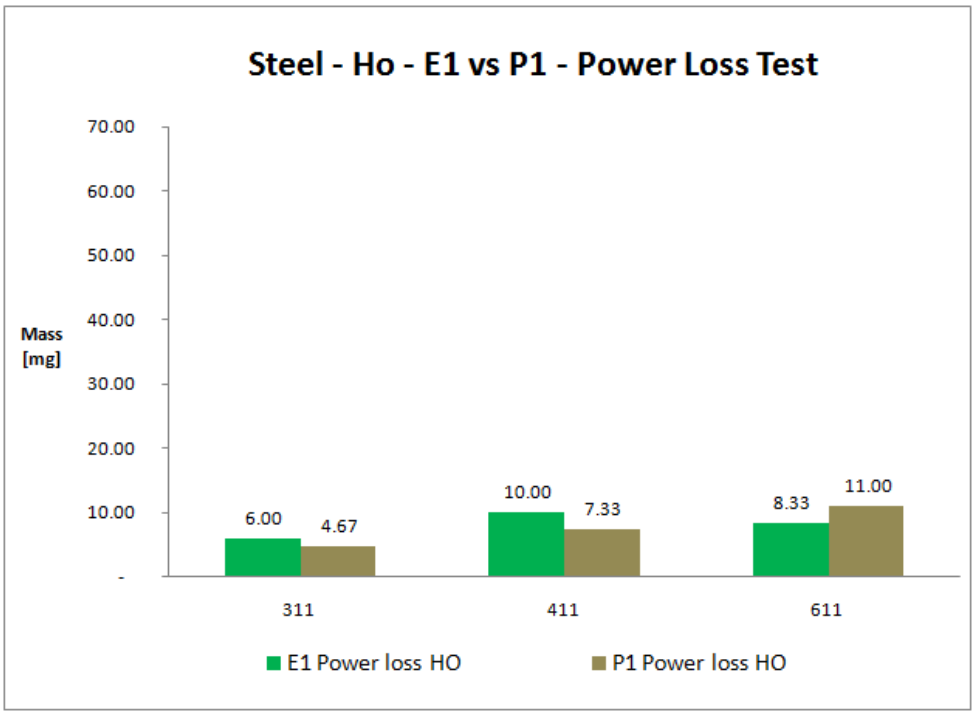

(a)

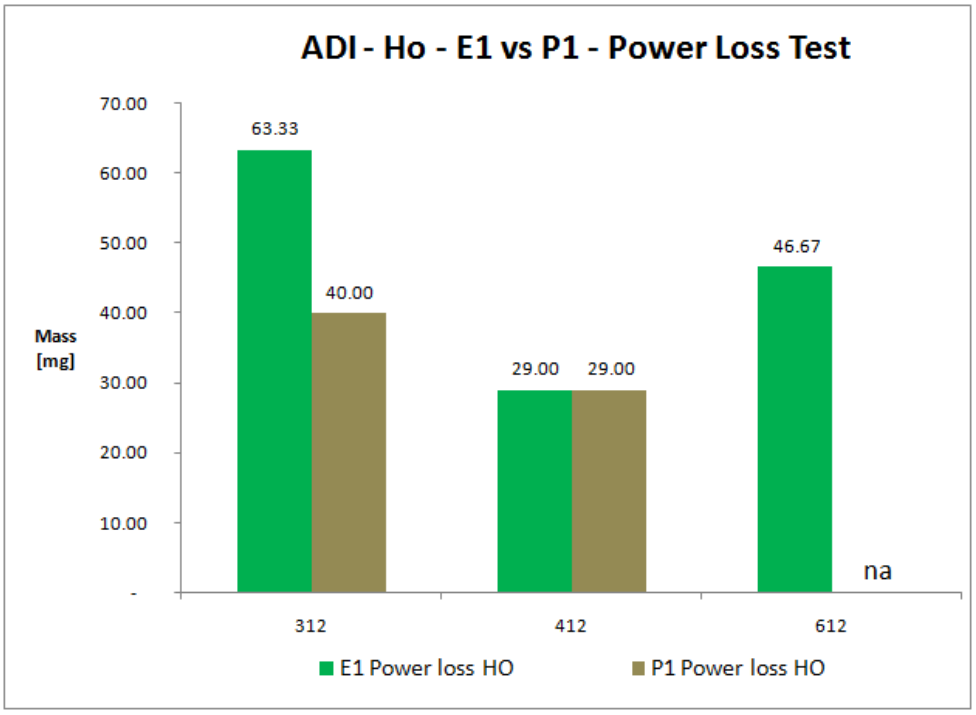

(b)

Figure 4.42.: Mass loss in gear power loss tests: a) steel and b) ADI gears, E1 vs P1 gear oils, and high oil level.

4.9. No load test - Churning loss

The "no load" tests were performed in the K1 load stage. Being this test performed with the lower value of torque applied, was ideal to evaluate the contribution of the "no load" losses, to the total losses of the system.

The study was made using the available gears, the two oils (E1 and P1) and the two oil levels, using wheel speed between 500 rpm to 2500rpm. The churning loss tests (also know as "no load") were performed before the power losses tests and as well as, the power loss tests, with the churning loss test some gears were not tested due to some technical problems.
Figure 4.43, shows the results to the churning loss tests, and compares the behavior of the steel and ADI gears to the test conditions.

Figure 4.43a, shows that, gear 311 had the lowest stabilization temperatures when operating with a low oil level, and between the two results the P1 lubricant oil had the best performance. Operating with high oil level P1 lubricant oil was also better than the E1.

Gear 411, had lower stabilization temperatures also with low oil level. For low speeds and low oil level both lubricants, E1 and P1, had the same behavior, but at high speeds (above 1500 rpm), P1 lubricant oil had lower stabilization temperatures.(see Figure 4.43b)
In the case of gear 611, the stabilization temperatures were lower when combined with P1 lubricant oil and low oil level (see Figure 4.43c). Operating with high oil level, the behavior of the two lubricant oils were similar, but for low speeds (from 500 to 1500 rpm) E1 lubricant oil was better than P1 lubricant, being P1 lubricant oil better when operating at high speeds (from 1500 to 2500 rpm).

The stabilization temperatures in the case of gear 612 were lower when combined with P1 lubricant oil and low oil level, being even the combination of gear 612 with P1 and high oil level better than those of the combination of the 612 with the E1 and low oil level (see Figure 4.43d).

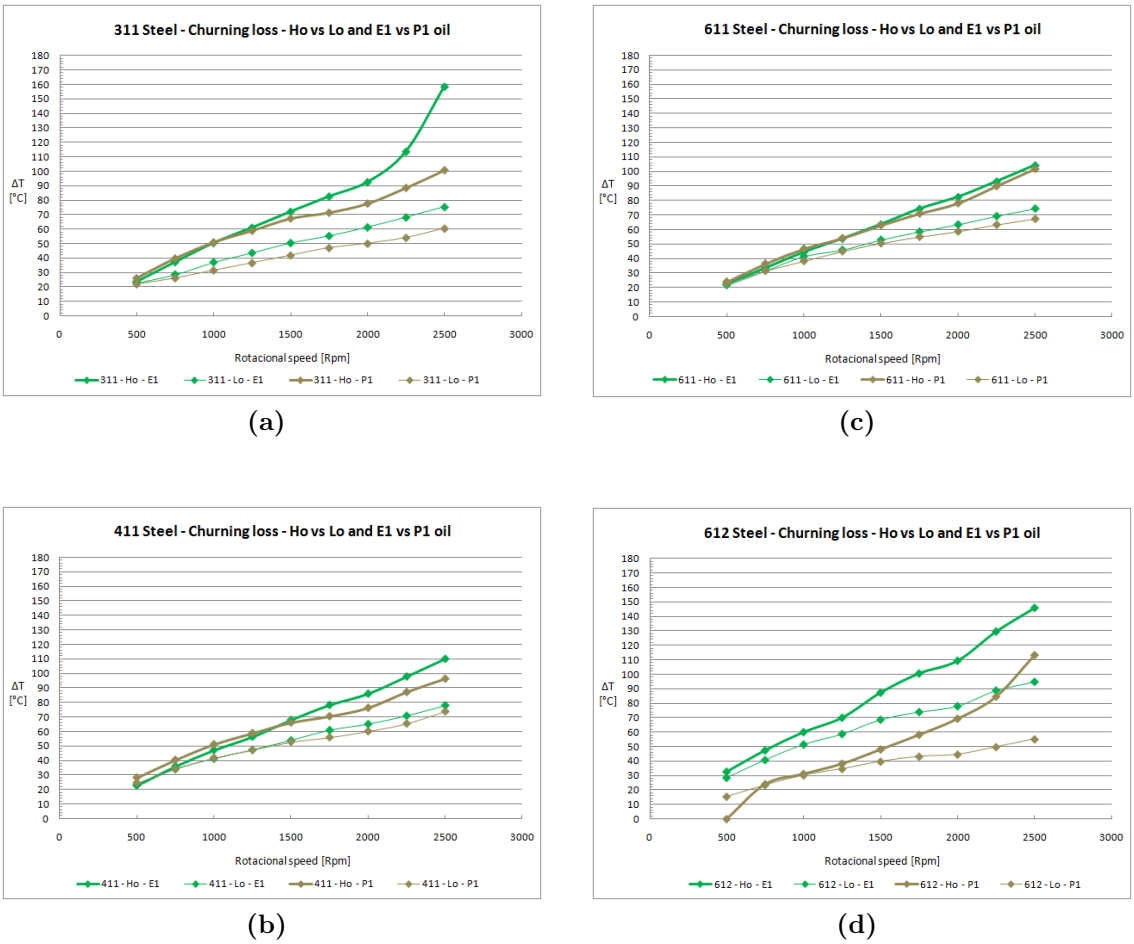

Figure 4.43.: Stabilization temperatures in gear churning loss tests: steel and ADI gears (311, 411, 611 and 612), P1 and E1 lubricant oils, high and low oil levels.

5. Conclusions and Future work

Analyzing the experimental results several conclusions can be draw regarding the behavior of the Steel and ADI performance when tested with a Ester base oil (E1) and a Polyalphaolephine oil (P1) in two oil levels (high and low).

5.1. Conclusion

I) Both 611 or 612 gears have a similar performance working with E1 or P1 lubricant oil.

II) The steel gears have always lower mass losses and lower CPUC and ISUC values when compared with the ADI gears, using both high and low oil levels and E1 and P1 lubricants.

III) Generally low oil level and P1 lubricant has better results with ADI gears and E1 has the better results with steel gears.

IV) Being the main objective of this research, whether there is an advantage in reducing the module of gears and if that causes fewer losses, it can be concluded that there is an advantage, since it has been proved that the 610 gear geometry has best results.

V) The other objective was to study the influence of the high and low oil, and in this matter it was proved that working with low oil presents better results, whatever the lubricant used.

5.2. Future work

In this field of research further work could be done, for example:

1. Modify the gears width, in order to test the same safety coefficients in all three geometries. To make it possible its also necessary to remove the pressure pads and use a proper helical gearbox;

2. Apply an computerized energetic model to the behavior of the gearbox;

3. Realize endurance tests in the same conditions already tested.

Bibliography

[1] G. Henriot, *Engrenages conception, fabrication, mise en oeuvre.* Dunod, 1999, v7e ed.

[2] J. Seabra, *Engrenagens - Lubrificação, Rendimento E Avarias.* Seabra-SMAp-DEMEGI-FEUP, 2005.

[3] J. Seabra, A. Campos, and A. Sottomayor, *Lubrificação Elastohidrodinâmica.* FEUP, 2002.

[4] D. M. Pirro and A. A. Wessol, *Lubrication fundamentals.* Marcel Dekker, 2001.

[5] S. I. P. C. Limited, *The lubrication of industrial gears.* Shell, 1964.

[6] B. R. Hohn and K. Michaelis, "Influence of oil temperature on gear failures," *Tribology International*, vol. 37, no. 2, pp. 103–109, 2004.

[7] N. F. R. Cardoso, *Mechanical performance of biodegradable, low toxicity ester based industrial gear oils.* PhD thesis, Universidade do Porto. Faculdade de Engenharia, 2007.

[8] B.-R. Höhn, K. Michaelis, and A. Wimmer, "Low loss. gears," *Gear Technology*, pp. 28–35, 2007.

[9] L. Magalhães, R. Martins, C. Locateli, and J. Seabra, "Influence of tooth profile and oil formulation on gear power loss," *Tribology International*, vol. In Press, Accepted Manuscript.

[10] T. Cousseau, "Análise comparativa do comportamento de massas lubrificantes num rolamento axial de esferas," Master's thesis, Universidade do Porto. Faculdade de Engenharia, 2009.

[11] L. Magalhães, R. Martins, J. Seabra, and R. Gonçalves, "Low torque loss gears: Austempered ductile iron vs carburized steel,"

[12] R. Martins, J. Seabra, and L. Magalhaes, "Austempered ductile iron (adi) gears: Power loss, pitting and micropitting," *Wear*, vol. 264, no. 9-10, pp. 838–849, 2008.

[13] R. Martins, N. Cardoso, H. Bock, A. Igartua, and J. Seabra, "Power loss performance of high pressure nitrided steel gears," *Tribology International*, vol. 42, no. 11-12, pp. 1807–1815, 2009.

[14] B.-R. Hohn, K. Michaelis, and T. Vollmer, "Thermal rating of gear drives: Balance between power loss and heat dissipation," *AGMA Technical Paper*, 1996.

[15] L. A. Ferreira, *Tribologia notas de curso lubrificação e lubrificantes*. Publindústria, 2000.

[16] A. Z. Szeri, *Tribology friction, lubrication, and wear*. Hemisphere Publishing Corporation, 1980.

[17] P. Velex and M. Maatar, "An analytical expression for the time-varying contact length in perfect cylindrical gears: Some possible aplications in gears dynamics," *Mechanical Design*, December 1996.

[18] E. Höglund, "Influence of lubricant properties on elastohydrodynamic lubrication," *Wear*, vol. 232, pp. 176 – 184, 1999.

[19] D. Dowson and G. R. Higginson, *Elastohydrodinamic lubrication*. S. I. Editon, Pergamon Press Ltd., 1977.

[20] B.-R. Höhn, K. Michaelis, and H.-P. Otto, "Influence of immersion depth of dip lubricated gears on power loss, bulk temperature and scuffing load carrying capacity," *International Journal of Mechanics and Materials in Design*, vol. 4, pp. 145–156, 2008.

[21] H. S. Cheng, "Lubrication regimes," *Materials Park, OH: ASM International*, pp. 89–97, 1992.

[22] *Lubrication theory and its application*. Bp trading limited, London, 1969.

[23] R. Martins, N. Cardoso, and J. Seabra, "Gear power loss performance of biodegradable low-toxicity ester-based oils," *Proceedings of the Institution of Mechanical Engineers Part J-Journal of Engineering Tribology*, vol. 222, no. J3, pp. 431–440, 2008.

[24] J. J. O'Connor, *Standard handbook of lubrication engineering*. McGraw Hill, 1968.

[25] R. P. Carreteiro and P. N. A. Belmiro, *Lubrificantes & lubrificação industrial*. Interciência, 2006.

[26] S. I. P. C. Limited, *The application of lubricants*. Shell, 1965.

[27] B. Bhushan, ed., *Modern Tribology handbook - Principles of Tribology*, vol. 1. CRC Press, 2001.

[28] T. Mang and W. Dresel, *Lubricants and lubrications*. Wiley-VCH, 2001.

[29] M. J. D. d. Castro, *Gripagem de engrenagens FZG lubrificadas com óleos base Novos critérios de gripagem globais e locais*. FEUP, 2004.

[30] B. Bhushan, ed., *Modern Tribology handbook - Materials, coatings, and industrial applications*, vol. 2. CRC Press, 2001.

[31] C. Changenet, X. Oviedo-Marlot, and P. Velex, "Power loss predictions in geared transmissions using thermal networks-applications to a six-speed manual gearbox," *Journal of Mechanical Design*, vol. Volume 128, pp. Issue 3, 618 (8 pages), May 2006.

[32] Y. Diab, F. Ville, and P. Velex, "Prediction of power losses due to tooth friction in gears," *Tribology Transactions*, pp. 260–270, 2006.

[33] C. Changenet and M. Pasquier, "Power losses and heat exchange in reduction gears: Numerical and experimental results," *VDI Berichte*, vol. 2, no. 1665, pp. 603–613, 2002.

[34] A. J. Wimmer, *Lastverluste von Stirnradverzahnungen: Konstruktive Einflüsse, Wirkungsgradmaximierung, Tribologie (Load loss of helical gears: Constructive influences, efficiency maximization, Tribology)*. PhD thesis, Technische Universität München, 2005.

[35] P. Eschmann, *Ball and roller bearings - Theory, design and applications*. 1985.

[36] R. Martins, J. Seabra, A. Brito, C. Seyfert, and A. Luther, R.and Igartua, "Friction coefficient in fzg gears lubricated with industrial gear oils:biodegradable ester vs. mineral oil," *Tribology International*, vol. 39, no. 6, pp. 512–521, 2006.

[37] H. Winter and K. Michaelis, "Investigations on the thermal balance of gear drives," in *Fifth World Congress on Theory of Machines and Mechanisms*, American Society of Mechanical Engineers, 1979.

[38] L. Magalhães, R. Martins, C. Locateli, and J. Seabra, "Influence of tooth profile on gear power loss," in *IRF2009 Integrity Reliability Failure - Challenges and Opportunities, Third International Conference* (A. M. J. F. Silva Gomes, ed.), (Faculty of Engineering, University of Porto, Porto, Portugal), pp. 189–190, INEGI, 2009.

[39] B. R. Hohn, P. Oster, and U. Schrade, "Studies on the micropitting resistance of case-carburised gears - industrialapplication of the new calculation method," *VDI Berichte*, no. 1904 II, pp. 1287–1307, 2005.

[40] B. R. Hohn, K. Michaelis, and A. Wimmer, "Gearboxes with minimised power loss," *VDI Berichte*, vol. 1904 II, pp. 1451–1465, 2005.

[41] H. Winter and K. Michaelis, "Fzg gear test rig - desciption and test possibilities," *In: Coordinate European Council Second International Symposium on The performanceEvaluation of Automotive Fuels and Lubricants*, 1985.

[42] R. Martins, P. Moura, and J. Seabra, "Power loss in fzg gears: Mineral oil vs. biodegradable ester and carburizedsteel vs. austempered ductile iron vs. mos2-ti coated steel," *VDI Berichte*, no. 1904 II, pp. 1467–1486, 2005.

[43] L. Magalhães, *Caracterização tribológica de um ferro nodular austemperado em ensaios disco-disco e de engrenagens FZG*. PhD thesis, Faculdade de Engenharia, Universidade do Porto, 2003.

[44] J. Magalhães, L. Seabra, "Wear and scuffing of austempered ductile iron gears," *WEAR*, vol. 215, no. 1-2, pp. 237–246, 1998.

[45] L. Mummery, *Surface Texture Analysis: The Handbook*. Hommelwerke GmbH, 1990.

[46] T. Hunt, *Handbook of Wear Debris Analysis and Particle Detection in Liquids*. 1993.

[47] J. Denis, J. Briant, and J.-C. Hipeaux, *Physico-Chimie des Lubrifiants - Analyses et Essais*. Éditions Technip, 1997.

[48] R. M. L. d. Silva, "Low power loss gears: Influence of design, materials and oil formulation," Master's thesis, FEUP, 2010.

[49] L. Magalhães, R. Martins, C. Locateli, and J. Seabra, "Influence of tooth profile on gear power loss," *Industrial Lubrication and Tribology*, to be published.

A. Appendix

A.1. Power Loss Data Sheets

FZG Gear Power Loss Test

TEST DATA SHEET

inegi Instituto de Engenharia Mecânica e Gestão Industrial

CETRIB Unidade de Tribologia, Vibrações e Manutenção Industrial

Test Ref.: CL HO
Gear Ref.: 311
Side: B

Oil ref.: E1
Date: 10-09-2010
Material: 20MnCr5 + Case Hardened

Stabilisation temperature [ºC]		
	High Oil	
KFZG	Oil	Env.
500	54.5	30.6
750	68.4	31
1000	80.5	29.9
1250	89.9	28.7
1500	101.6	29.4
1750	111.9	29.2
2000	121.6	29
2250	144.1	30.4
2500	189.2	30.6

	Oil Analysis - Ferrometry
	High Oil
Hours	36
d	1
DL	51
DS	21.9
CPUC	72.9
ISUC	2121.4

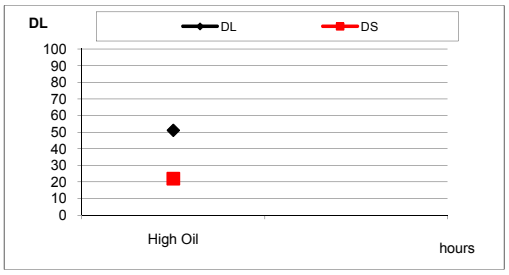

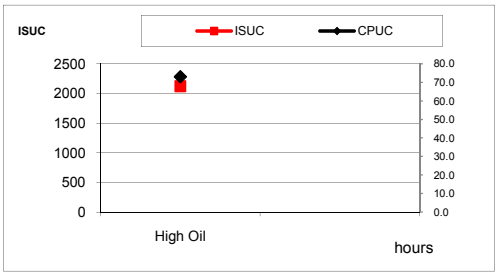

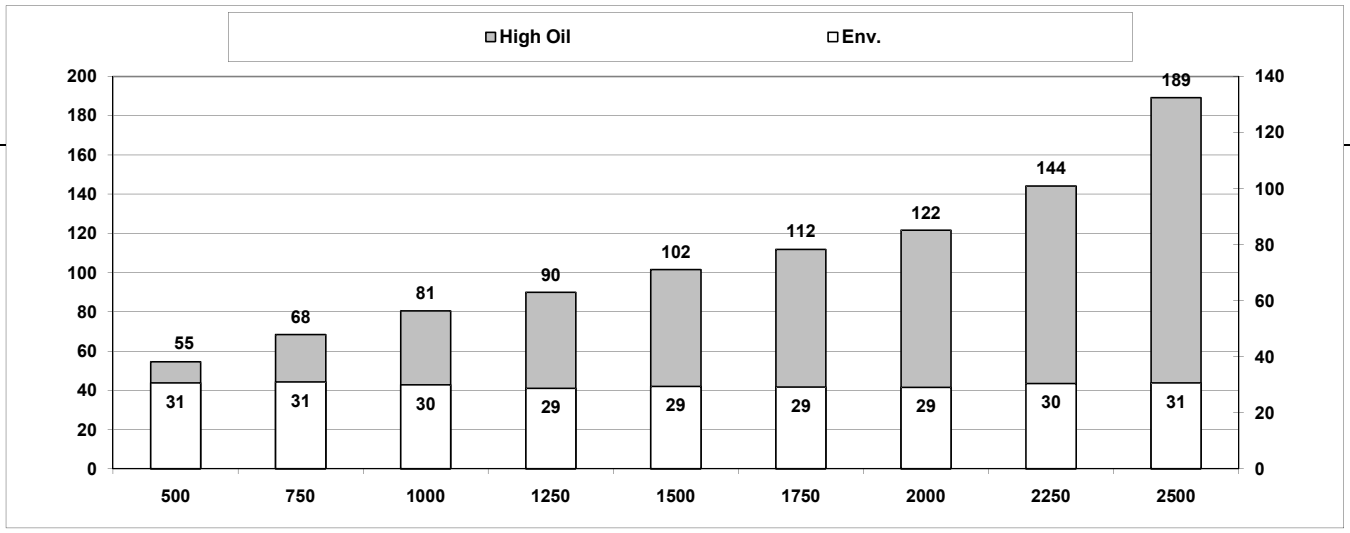

FZG Gear Power Loss Test

TEST DATA SHEET

Test Ref.:	CL HO	**Oil ref.:**	E1
Gear Ref.:	311	**Date:**	10-09-2010
Side:	B	**Material:**	20MnCr5 + Case Hardened

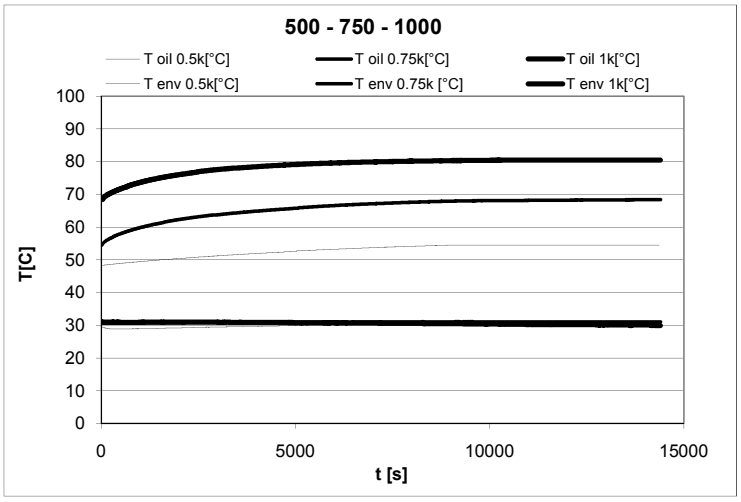

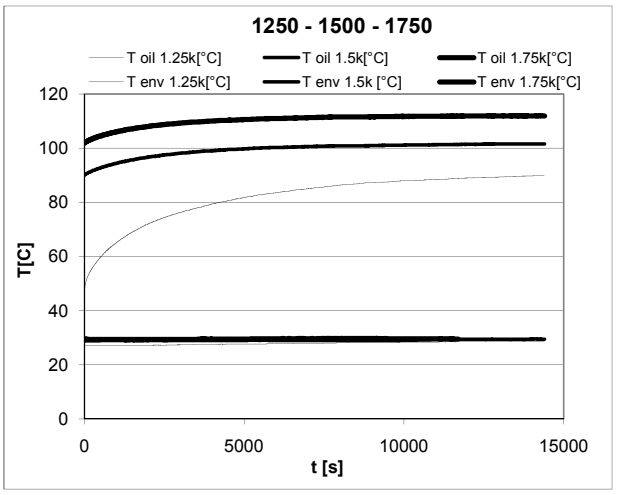

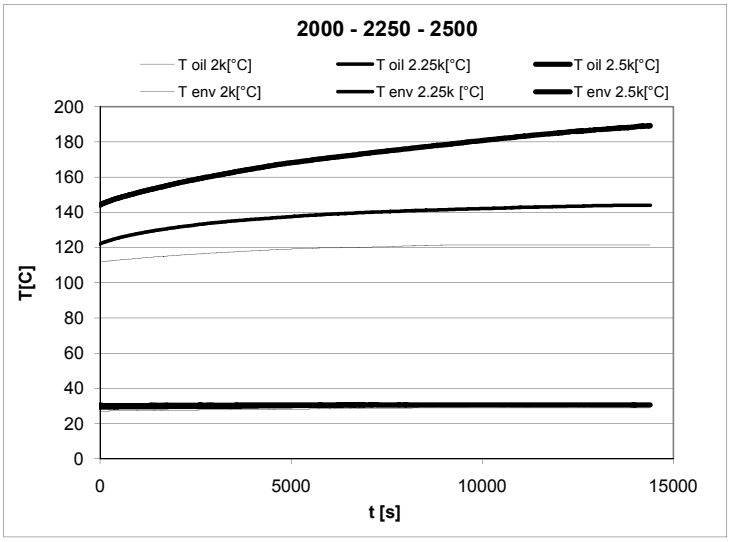

FZG Gear Power Loss Test

TEST DATA SHEET

Test Ref.: CL LO
Gear Ref.: 311
Side: B

Oil ref.: E1
Date: 10-09-2010
Material: 20MnCr5 + Case Hardened

Stabilisation temperature [ºC]		
	Low Oil	
KFZG	Oil	Env.
500	50	27.2
750	56.4	27.9
1000	64.4	27.4
1250	70.6	27.1
1500	78.4	28
1750	82.3	27
2000	88.5	27.2
2250	96.4	28.2
2500	103	27.6

	Oil Analysis - Ferrometry
	Low Oil
Hours	36
d	1
DL	53
DS	34.5
CPUC	87.5
ISUC	1618.8

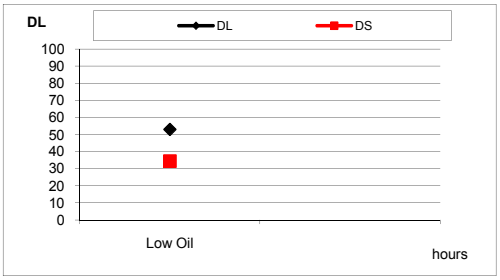

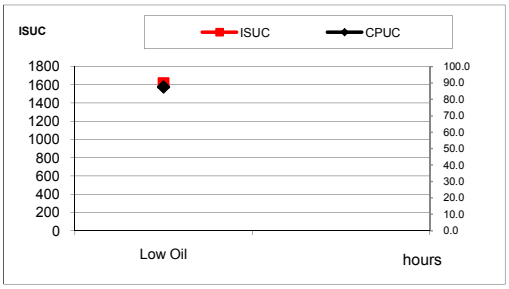

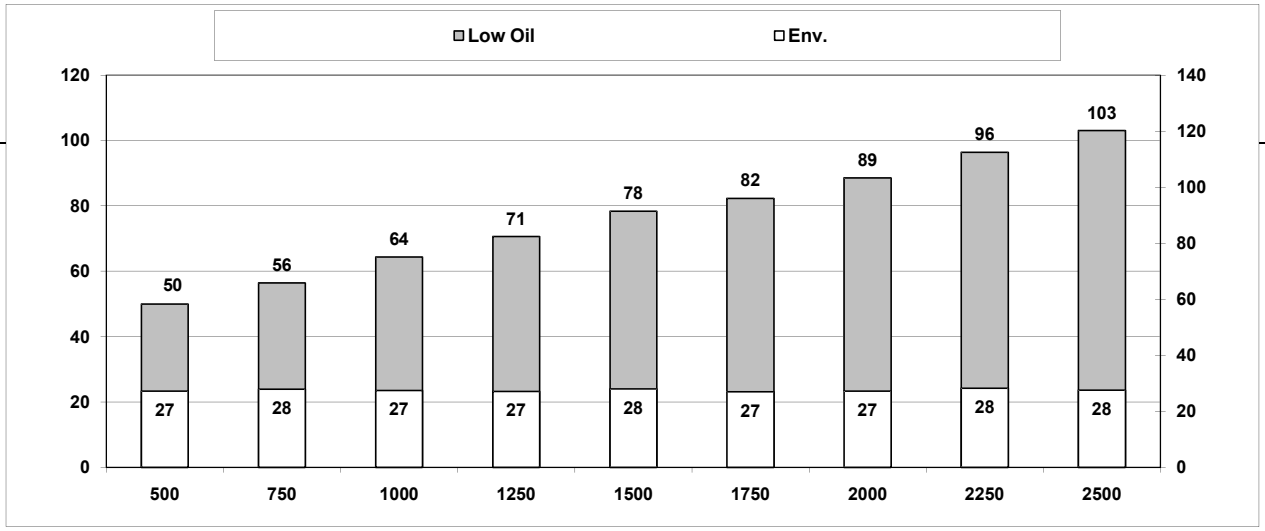

FZG Gear Power Loss Test

TEST DATA SHEET

Test Ref.:	CL LO	**Oil ref.:**	E1
Gear Ref.:	311	**Date:**	10-09-2010
Side:	B	**Material:**	20MnCr5 + Case Hardened

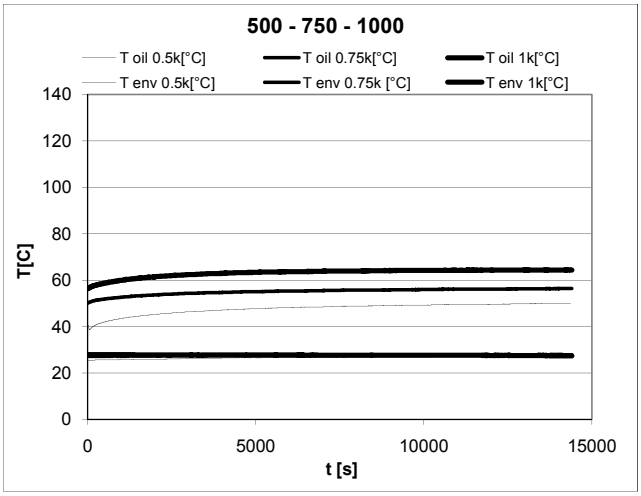

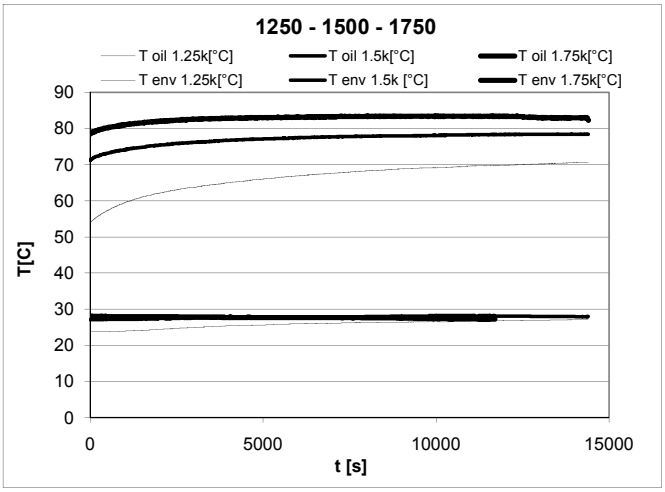

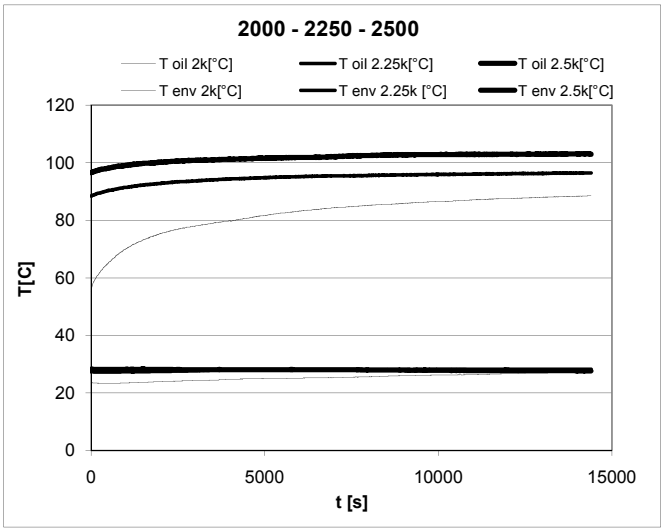

FZG Gear Power Loss Test

TEST DATA SHEET

inegi Instituto de Engenharia Mecânica e Gestão Industrial

CETRIB Unidade de Tribologia, Vibrações e Manutenção Industrial

Test Ref.:	CL HO & LO	**Oil ref.:**	E1
Gear Ref.:	311	**Date:**	10-09-2010
Side:	B	**Material:**	20MnCr5 + Case Hardened

Stabilisation temperature [°C]				
	High Oil		Low Oil	
KFZG	Oil	Env.	Oil	Env.
500	54.5	30.6	50	27.2
750	68.4	31	56.4	27.9
1000	80.5	29.9	64.4	27.4
1250	89.9	28.7	70.6	27.1
1500	101.6	29.4	78.4	28
1750	111.9	29.2	82.3	27
2000	121.6	29	88.5	27.2
2250	144.1	30.4	96.4	28.2
2500	189.2	30.6	103	27.6

	Oil Analysis - Ferrometry	
	High Oil	Low Oil
Hours	36	36
d	1	1
DL	51	53
DS	21.9	34.5
CPUC	72.9	87.5
ISUC	2121.4	1618.8

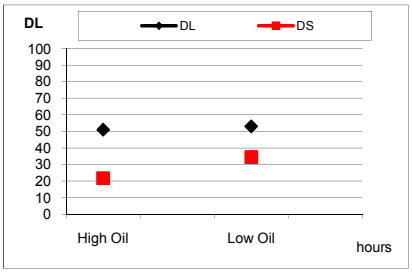

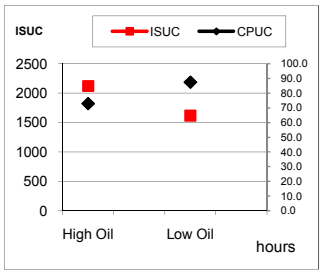

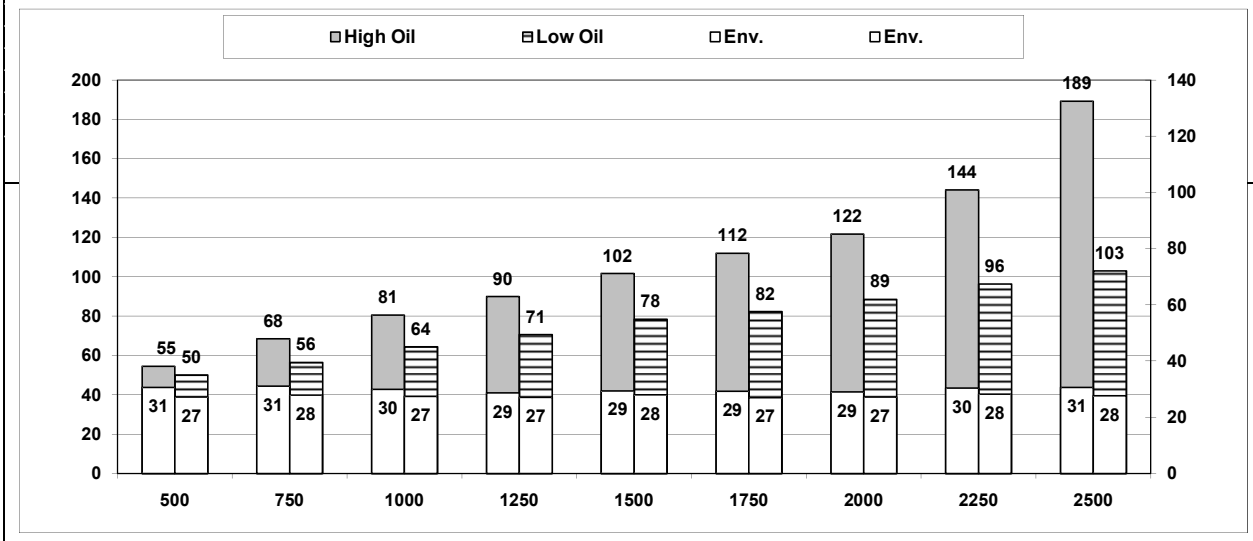

FZG Gear Power Loss Test

TEST DATA SHEET

Test Ref.: PL LO
Gear Ref.: 311
Side: B

Oil ref.: E1
Date: 28-09-2010
Material: 20MnCr5 + Case Hardened

Stabilisation temperature [ºC]						
	500 rpm		1000 rpm		2000 rpm	
KFZG	Oil	Env.	Oil	Env.	Oil	Env.
K1	50	27.2	64.4	27.4	88.5	27.2
K5	52.2	26.4	68.8	27.3	94.7	27.7
K7	56.2	25.6	76.4	26.4	103.4	26.4
K9	59	24	81.8	25.6	109.4	25.6

Mass loss [mg]	
	running in+k9
pinion	8

	Oil analysis - Ferrometry			
	k1	k5	k7	k9
Hours	12	24	36	48
d	1	1	1	1
DL	53	67.8	62.7	58.1
DS	34.5	42.3	31.3	32
CPUC	87.5	110.1	94.0	90.1
ISUC	1618.8	2807.6	2951.6	2351.6

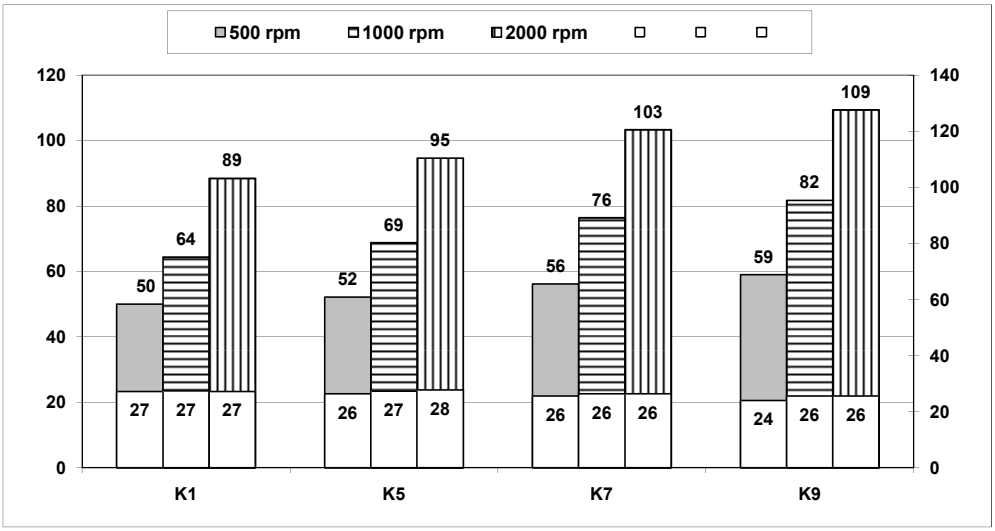

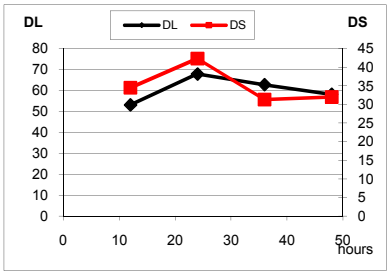

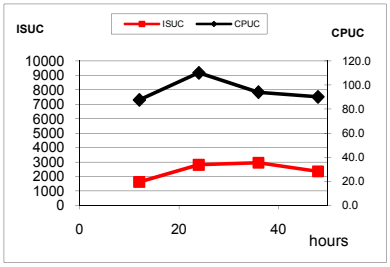

Pinion surface roughness [µm]												
		direction	Ra	Rq	Rz	Rmax	Rpk	Rk	Rvk	Mr1	Mr2	Vo
Initial	Pinion	radial	0.20	0.20	0.90	1.10	0.2	0.50	0.35	6.00	85.1	6.5
	Wheel	radial	0.12	0.17	0.78	1.35	0.1	0.32	0.28	6.58	84.4	5.6
Final	Pinion	radial	0.12	0.15	0.72	1.05	0.1	0.33	0.27	8.00	84.5	5.1
	Wheel	radial	0.30	0.35	1.43	1.90	0.2	0.88	0.57	7.28	84.4	11.6

FZG Gear Power Loss Test

TEST DATA SHEET

Test Ref.:	PL LO	**Oil ref.:**	E1
Gear Ref.:	311	**Date:**	28-09-2010
Side:	B	**Material:**	20MnCr5 + Case Hardened

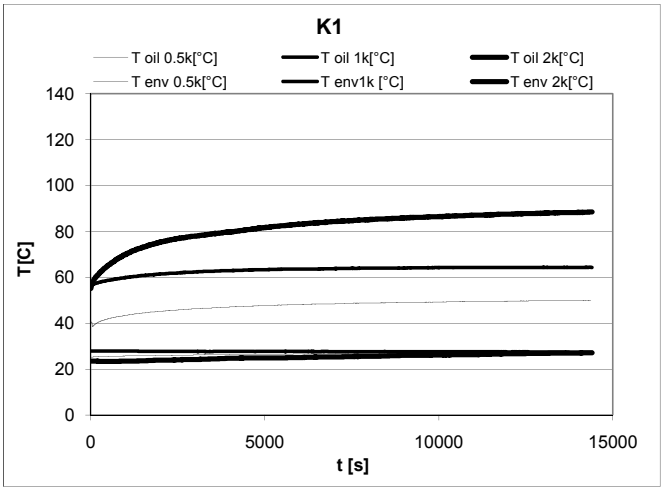

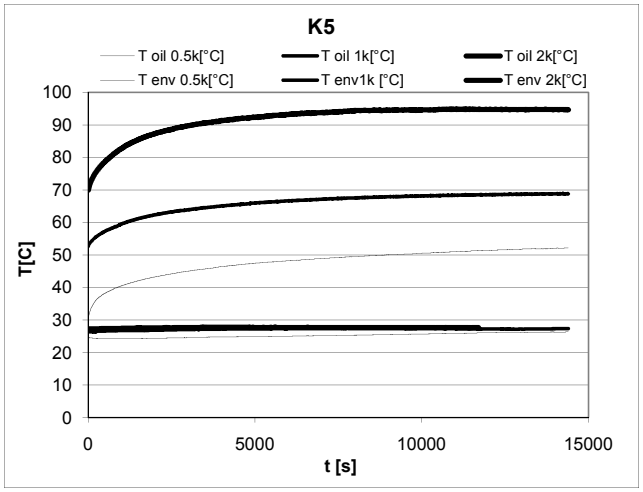

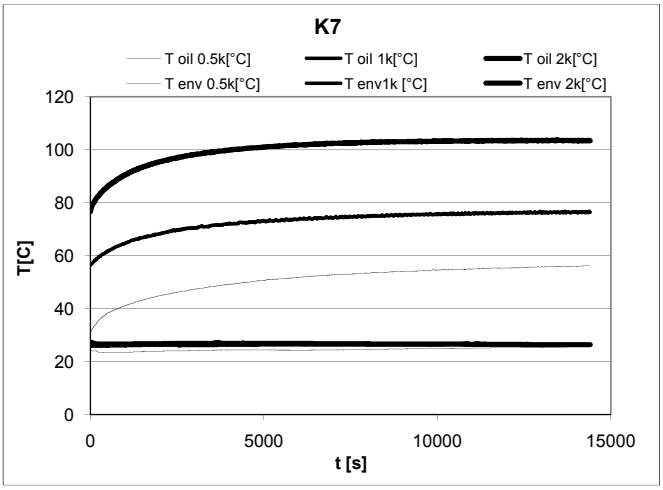

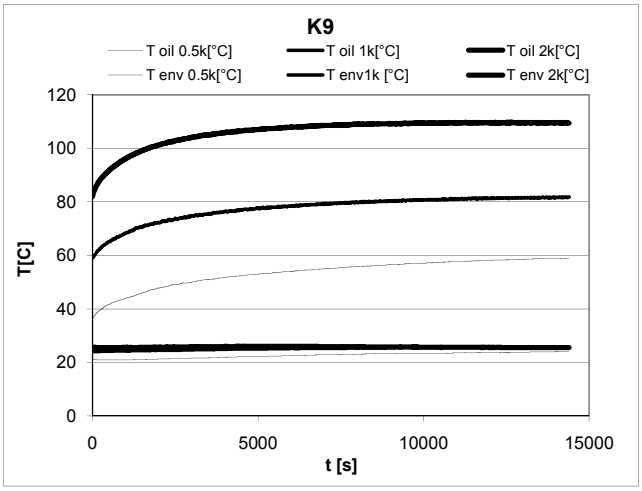

FZG Gear Power Loss Test

TEST DATA SHEET

Test Ref.: CL HO
Gear Ref.: 411
Side: B

Oil ref.: E1
Date: 28-09-2010
Material: 20MnCr5 + Case Hardened

Stabilisation temperature [ºC]		
	High Oil	
KFZG	Oil	Env.
500	47.9	25.2
750	61.5	25.6
1000	72.6	25.5
1250	81.6	25.3
1500	93.9	26
1750	103.5	25.3
2000	112	26
2250	125.4	27.6
2500	137.5	27.5

	Oil Analysis - Ferrometry
	High Oil
Hours	36
d	1
DL	45.5
DS	15.9
CPUC	61.4
ISUC	1817.4

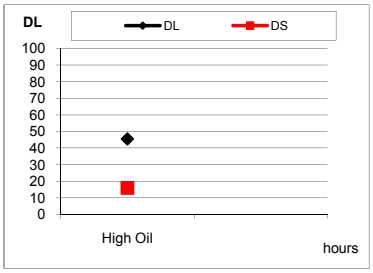

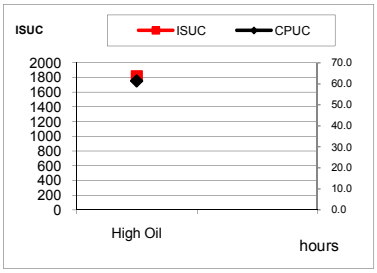

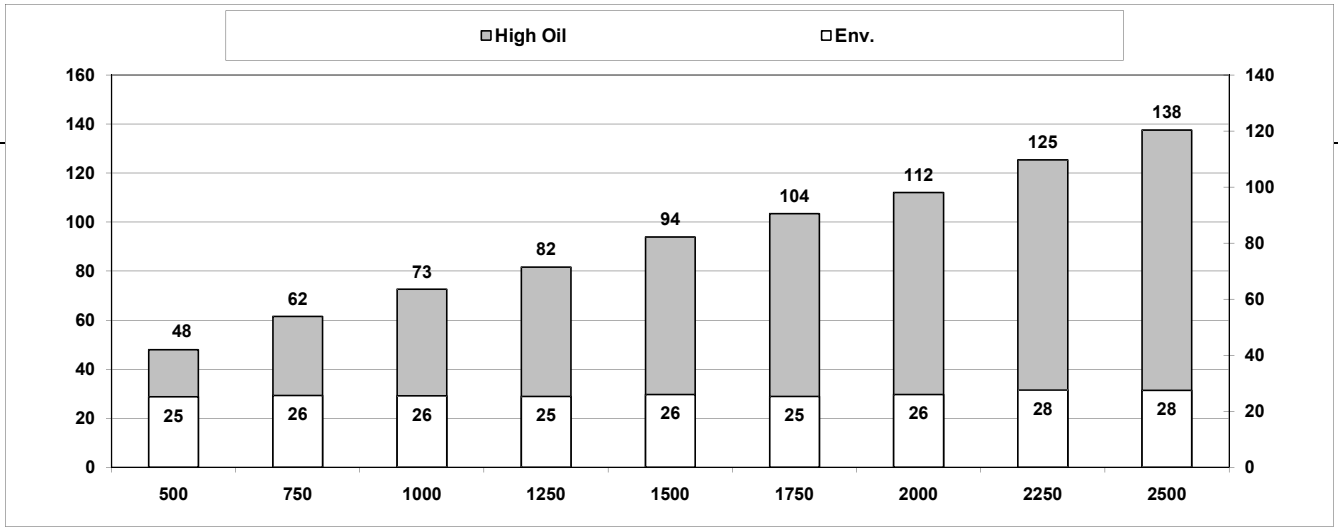

FZG Gear Power Loss Test

TEST DATA SHEET

Test Ref.:	CL HO	**Oil ref.:**	E1
Gear Ref.:	411	**Date:**	28-09-2010
Side:	B	**Material:**	20MnCr5 + Case Hardened

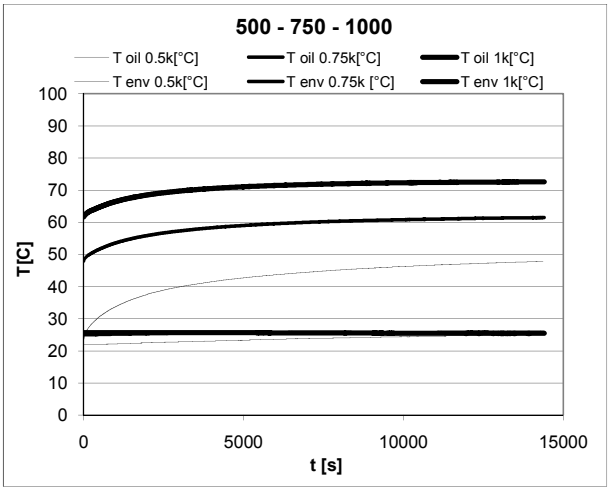

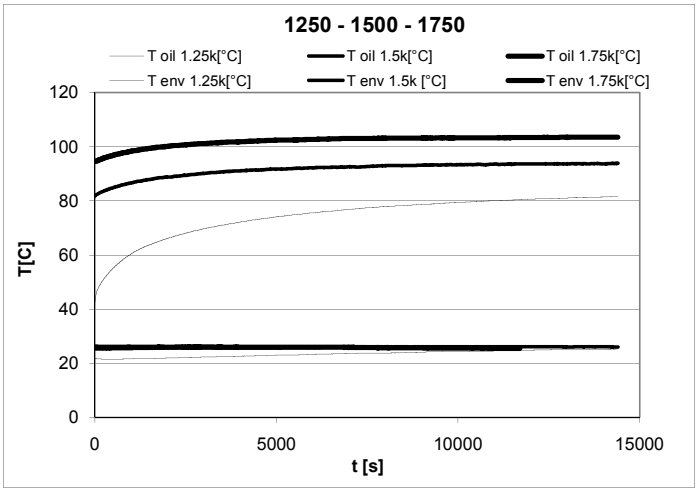

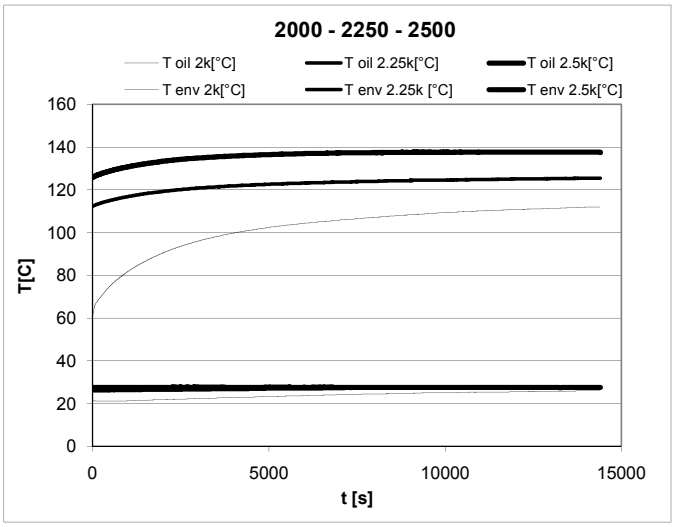

FZG Gear Power Loss Test

TEST DATA SHEET

inegi
Instituto de Engenharia Mecânica e Gestão Industrial

CETRIB
Unidade de Tribologia, Vibrações e Manutenção Industrial

Test Ref.: CL LO
Gear Ref.: 411
Side: B

Oil ref.: E1
Date: 28-09-2010
Material: 20MnCr5 + Case Hardened

Stabilisation temperature [ºC]		
	Low Oil	
KFZG	Oil	Env.
500	46.2	23.2
750	58	24
1000	64.9	23.6
1250	70.2	22.9
1500	78.8	24.9
1750	86	25.1
2000	91.2	26.1
2250	98.4	27.6
2500	105.3	27.4

Oil Analysis - Ferrometry	
	Low Oil
Hours	36
d	1
DL	35
DS	15.5
CPUC	50.5
ISUC	984.8

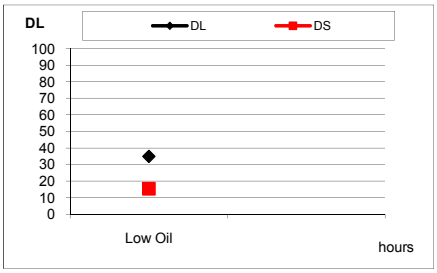

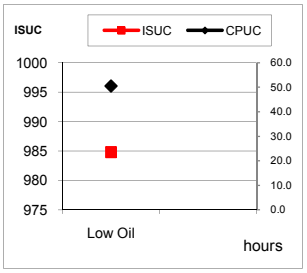

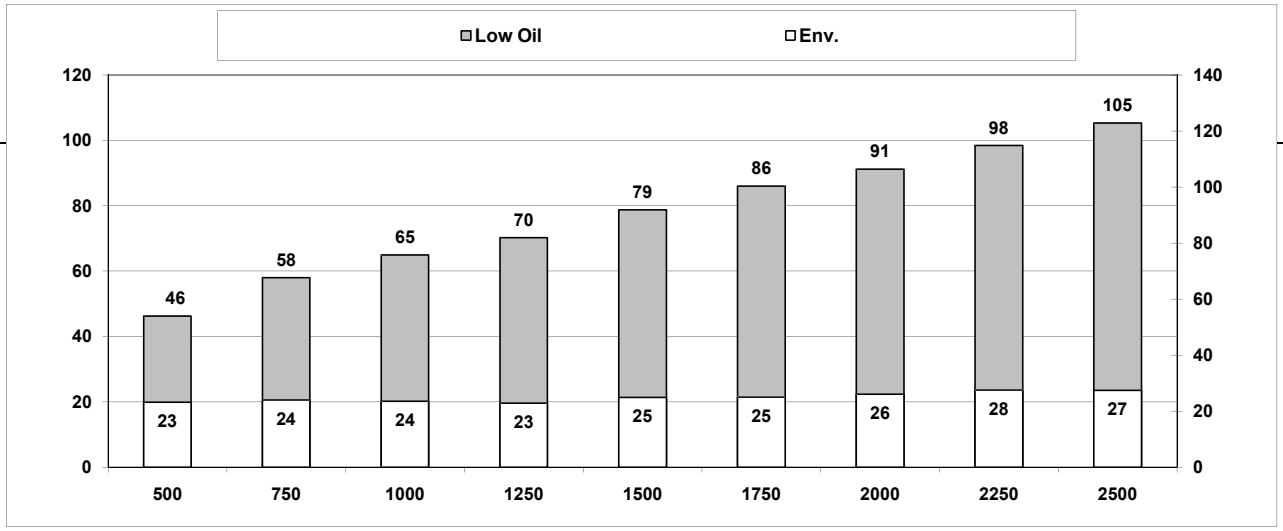

FZG Gear Power Loss Test

TEST DATA SHEET

Test Ref.:	CL LO	**Oil ref.:**	E1
Gear Ref.:	411	**Date:**	28-09-2010
Side:	B	**Material:**	20MnCr5 + Case Hardened

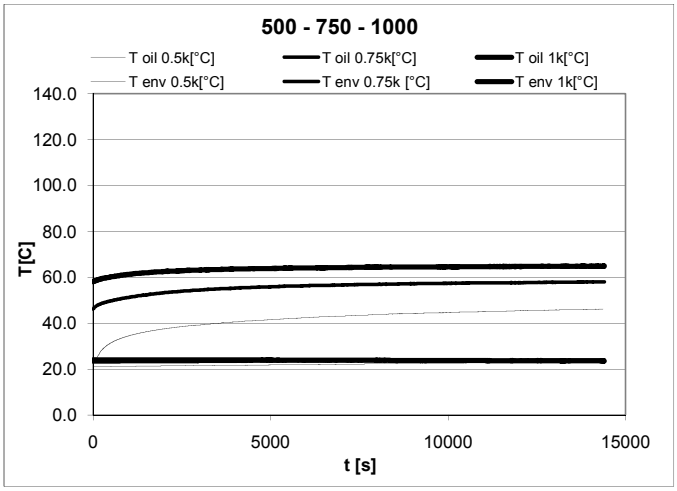

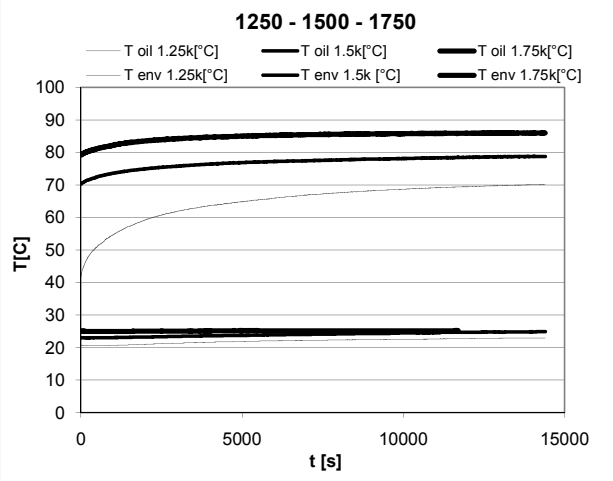

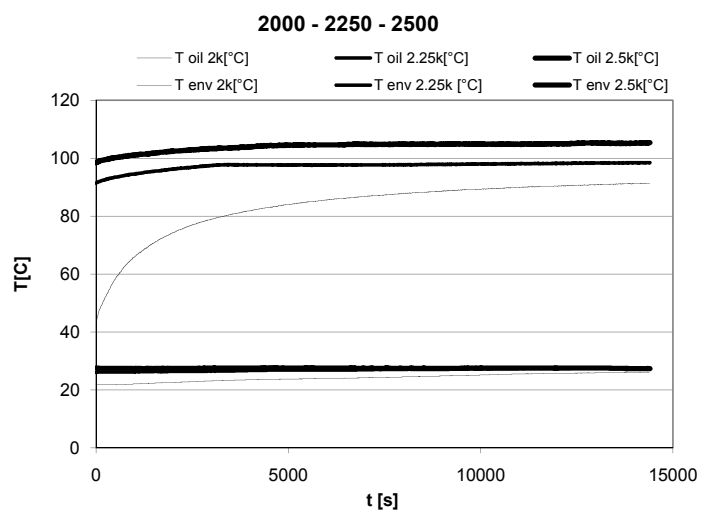

FZG Gear Power Loss Test

TEST DATA SHEET

inegi Instituto de Engenharia Mecânica e Gestão Industrial

CETRIB Unidade de Tribologia, Vibrações e Manutenção Industrial

Test Ref.:	CL HO & LO	**Oil ref.:**	E1
Gear Ref.:	411	**Date:**	28-09-2010
Side:	B	**Material:**	20MnCr5 + Case Hardened

Stabilisation temperature [°C]				
	High Oil		Low Oil	
KFZG	Oil	Env.	Oil	Env.
500	47.9	25.2	46.2	23.2
750	61.5	25.6	58	24
1000	72.6	25.5	64.9	23.6
1250	81.6	25.3	70.2	22.9
1500	93.9	26	78.8	24.9
1750	103.5	25.3	86	25.1
2000	112	26	91.2	26.1
2250	125.4	27.6	98.4	27.6
2500	137.5	27.5	105.3	27.4

	Oil Analysis - Ferrometry	
	High Oil	Low Oil
Hours	36	36
d	1	1
DL	45.5	35
DS	15.9	15.5
CPUC	61.4	50.5
ISUC	1817.4	984.8

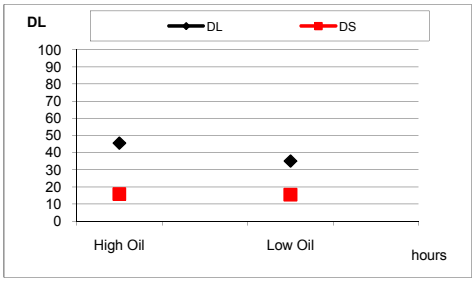

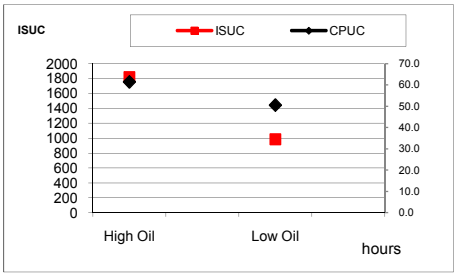

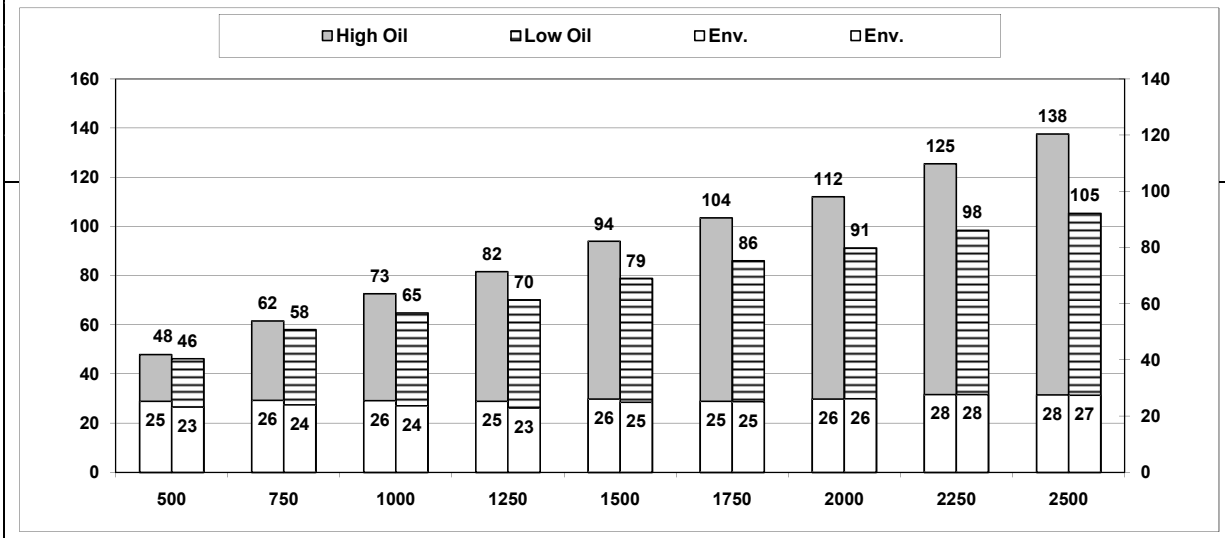

FZG Gear Power Loss Test

TEST DATA SHEET

Test Ref.:	PL LO	**Oil ref.:**	E1
Gear Ref.:	411	**Date:**	28-09-2010
Side:	B	**Material:**	20MnCr5 + Case Hardened

Stabilisation temperature [ºC]						
	500 rpm		1000 rpm		2000 rpm	
KFZG	Oil	Env.	Oil	Env.	Oil	Env.
K1	46.2	23.2	64.9	23.6	91.2	26.1
K5	48.4	24	66.3	25.7	94.1	26.3
K7	50.3	25.3	69	26.8	95.9	26.7
K9	55.1	26.1	76.1	27.1	104.4	27.1

Mass loss [mg]	
	running in+k9
pinion	3

	Oil analysis - Ferrometry			
	k1	**k5**	**k7**	**k9**
Hours	12	24	36	48
d	1	1	1	1
DL	35	46.6	48	57.2
DS	15.5	23.4	19.7	26.4
CPUC	50.5	70.0	67.7	83.6
ISUC	984.8	1624.0	1915.9	2574.9

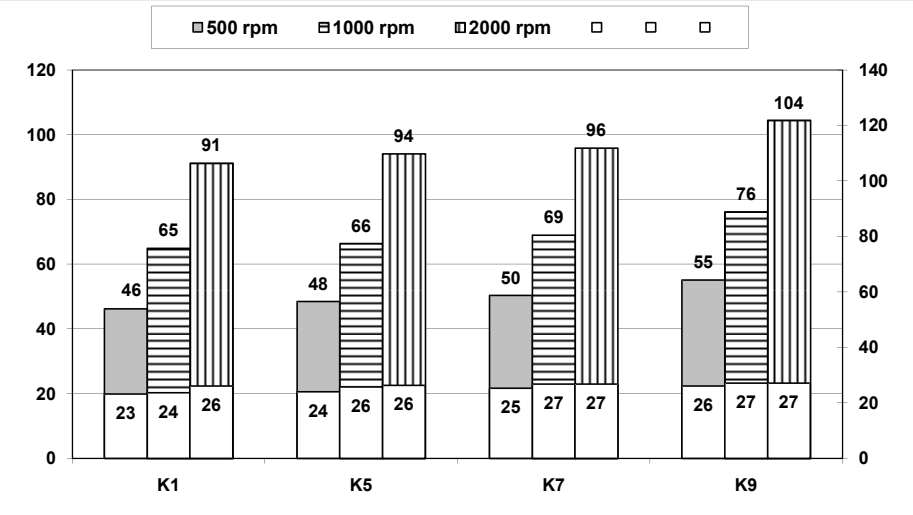

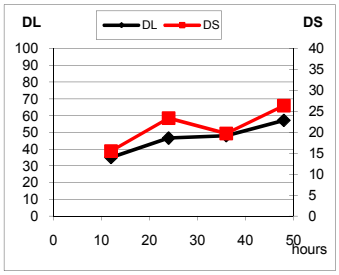

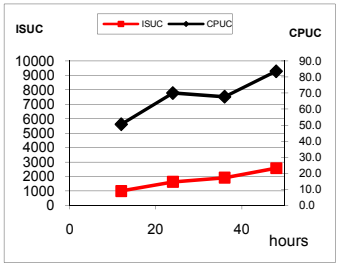

Pinion surface roughness [µm]												
		direction	**Ra**	**Rq**	**Rz**	**Rmax**	**Rpk**	**Rk**	**Rvk**	**Mr1**	**Mr2**	**Vo**
Initial	Pinion	radial	0.25	0.32	1.53	2.02	0.3	0.73	0.50	7.57	83.0	10.4
	Wheel	radial	0.15	0.22	1.08	1.43	0.1	0.47	0.33	7.32	84.0	6.8
Final	Pinion	radial	0.18	0.22	0.93	1.20	0.1	0.55	0.30	9.52	85.8	6.6
	Wheel	radial	0.17	0.20	0.95	1.23	0.2	0.50	0.30	8.52	84.0	6.4

FZG Gear Power Loss Test

TEST DATA SHEET

Test Ref.:	PL LO	**Oil ref.:**	E1
Gear Ref.:	411	**Date:**	28-09-2010
Side:	B	**Material:**	20MnCr5 + Case Hardened

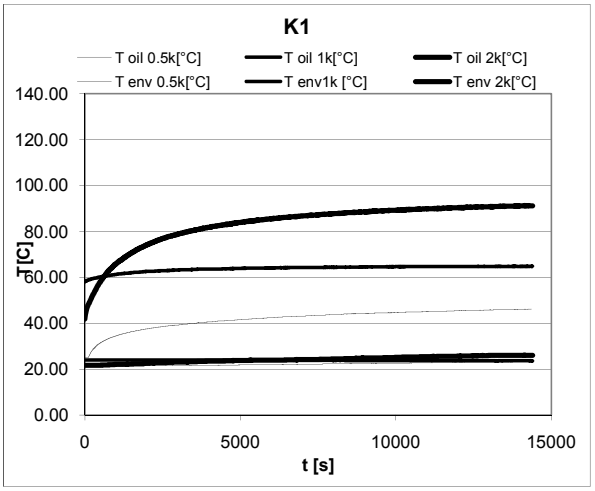

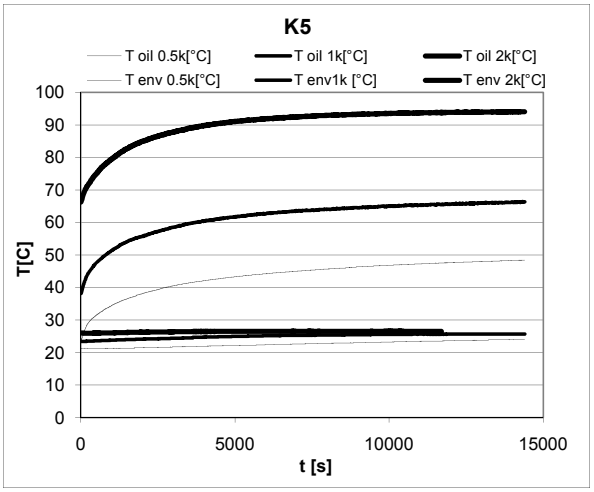

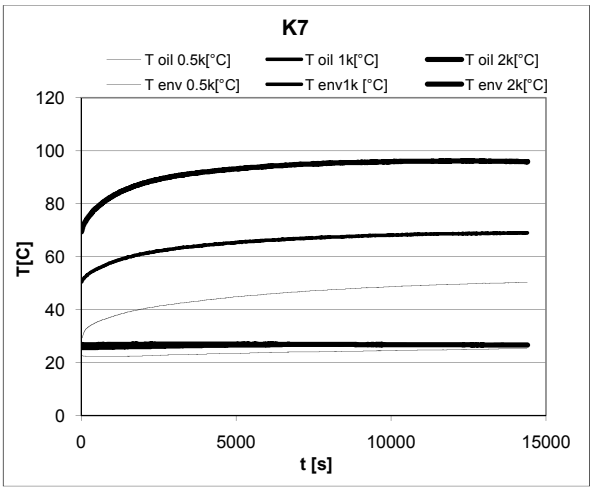

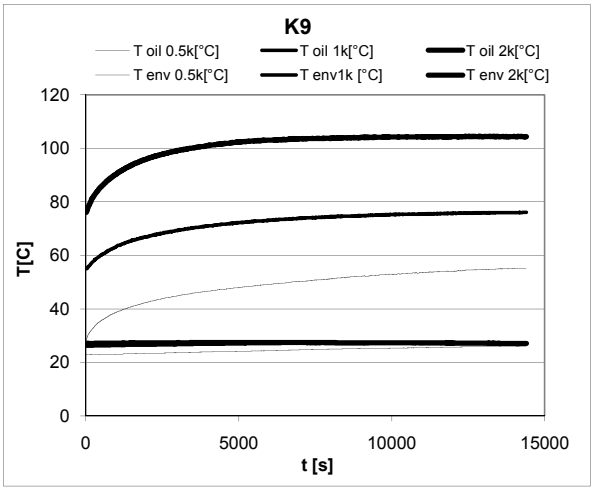

FZG Gear Power Loss Test

TEST DATA SHEET

inegi
Instituto de Engenharia Mecânica e Gestão Industrial

CETRIB
Unidade de Tribologia, Vibrações e Manutenção Industrial

Test Ref.: CL HO
Gear Ref.: 611
Side: B

Oil ref.: E1
Date: 28-09-2010
Material: 20MnCr5 + Case Hardened

Stabilisation temperature [ºC]		
	High Oil	
KFZG	Oil	Env.
500	46.7	24.4
750	58.6	25.2
1000	68.9	24.5
1250	76.7	23
1500	88.8	25.2
1750	98.8	24.5
2000	107.3	24.8
2250	120.1	26.9
2500	130.3	25.9

	Oil Analysis - Ferrometry
	High Oil
Hours	36
d	1
DL	30.4
DS	11.1
CPUC	41.5
ISUC	801.0

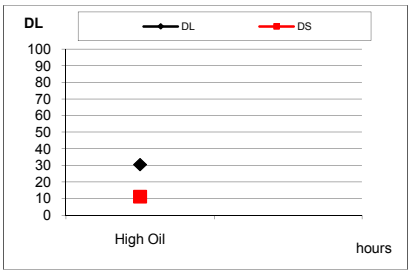

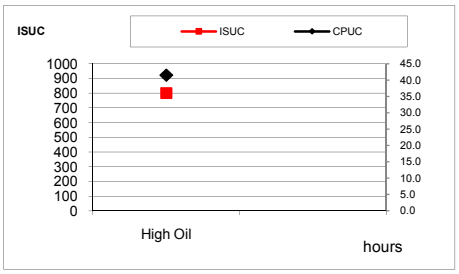

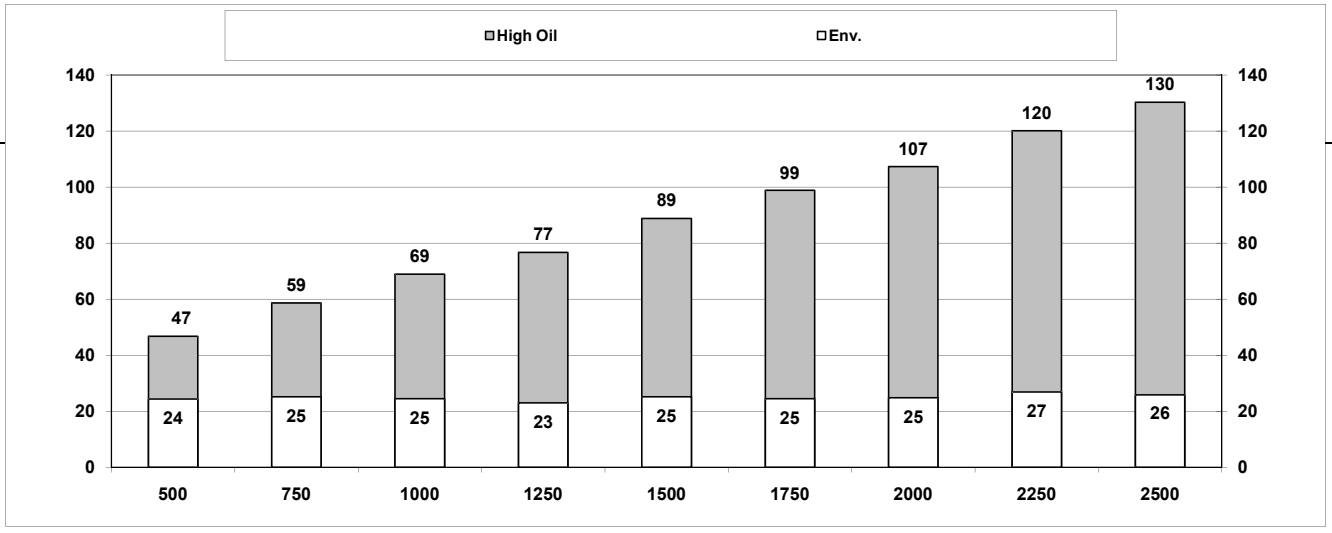

FZG Gear Power Loss Test

TEST DATA SHEET

Test Ref.:	CL HO	**Oil ref.:**	E1
Gear Ref.:	611	**Date:**	28-09-2010
Side:	B	**Material:**	20MnCr5 + Case Hardened

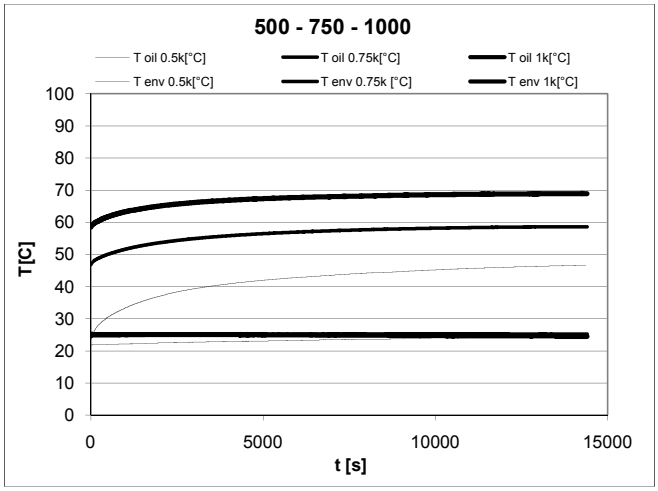

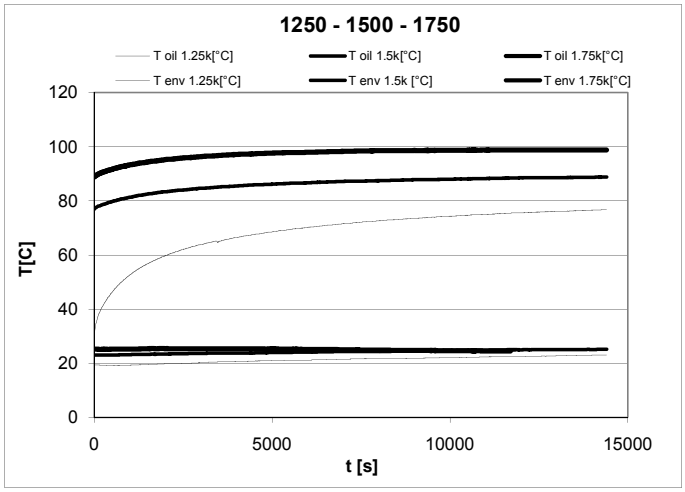

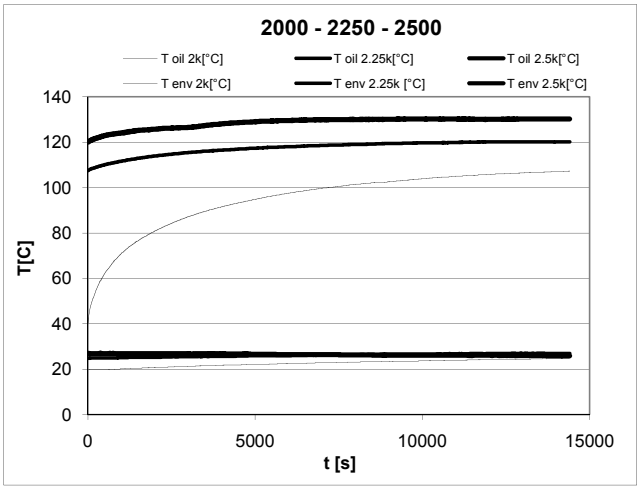

FZG Gear Power Loss Test

TEST DATA SHEET

inegi
Instituto de Engenharia Mecânica e Gestão Industrial
CETRIB
Unidade de Tribologia, Vibrações e Manutenção Industrial

Test Ref.: CL LO
Gear Ref.: 611
Side: B

Oil ref.: E1
Date: 28-09-2010
Material: 20MnCr5 + Case Hardened

Stabilisation temperature [°C]		
	Low Oil	
KFZG	Oil	Env.
500	44.6	23
750	56	24.5
1000	65.1	23.6
1250	70	24.1
1500	78.4	25.6
1750	83.1	24.7
2000	87.2	23.9
2250	94.8	25.7
2500	99.6	25.3

Oil Analysis - Ferrometry	
	Low Oil
Hours	36
d	1
DL	30.7
DS	11.5
CPUC	42.2
ISUC	810.2

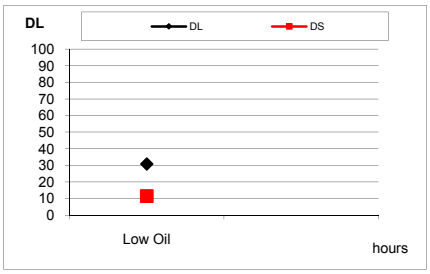

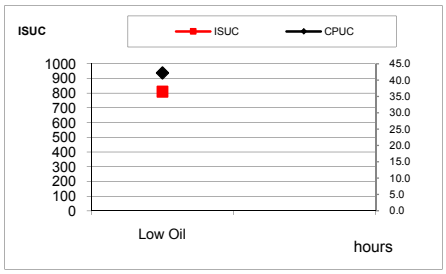

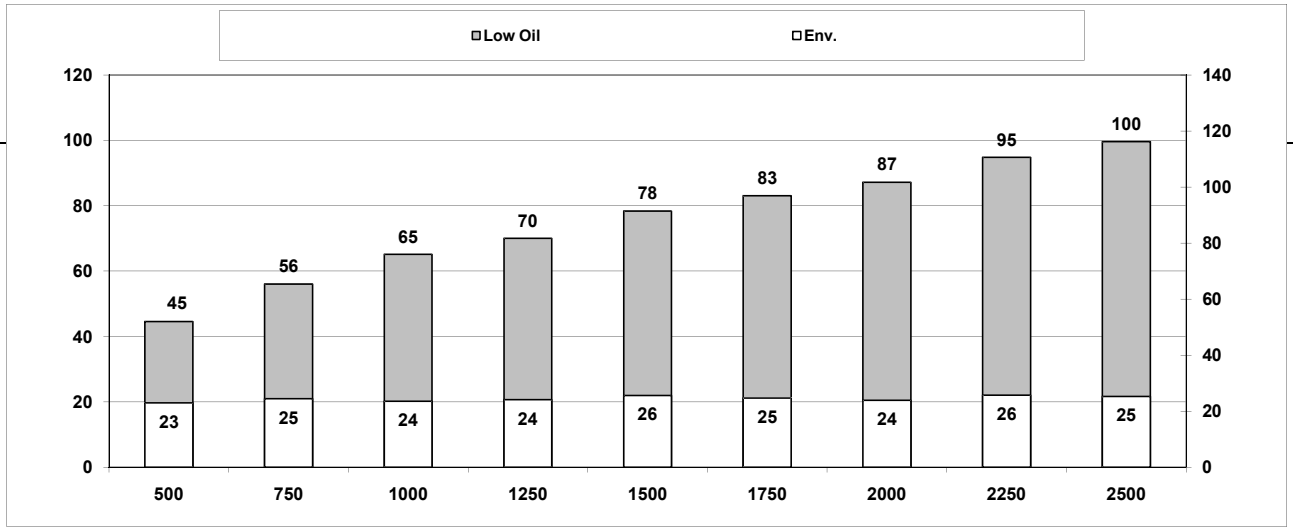

FZG Gear Power Loss Test

TEST DATA SHEET

Test Ref.:	CL LO	**Oil ref.:**	E1
Gear Ref.:	611	**Date:**	28-09-2010
Side:	B	**Material:**	20MnCr5 + Case Hardened

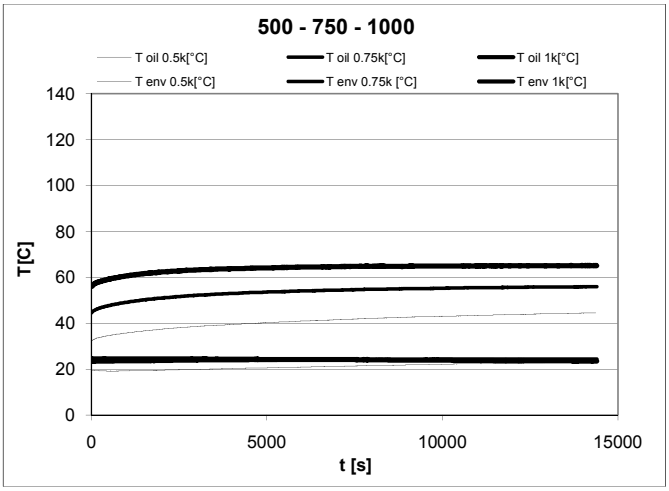

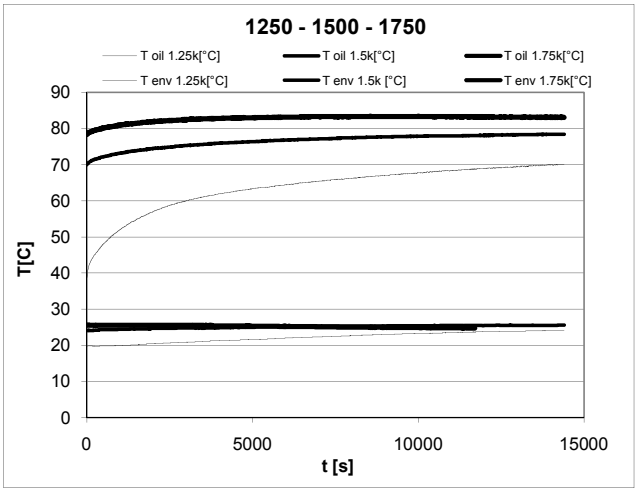

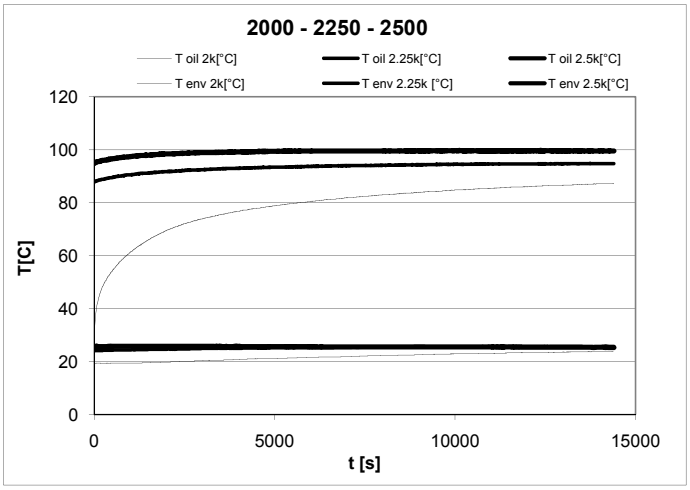

FZG Gear Power Loss Test

TEST DATA SHEET

inegi Instituto de Engenharia Mecânica e Gestão Industrial

CETRIB Unidade de Tribologia, Vibrações e Manutenção Industrial

Test Ref.:	CL HO & LO	**Oil ref.:**	E1
Gear Ref.:	611	**Date:**	28-09-2010
Side:	B	**Material:**	20MnCr5 + Case Hardened

Stabilisation temperature [ºC]				
	High Oil		Low Oil	
KFZG	Oil	Env.	Oil	Env.
500	46.7	24.4	44.6	23
750	58.6	25.2	56	24.5
1000	68.9	24.5	65.1	23.6
1250	76.7	23	70	24.1
1500	88.8	25.2	78.4	25.6
1750	98.8	24.5	83.1	24.7
2000	107.3	24.8	87.2	23.9
2250	120.1	26.9	94.8	25.7
2500	130.3	25.9	99.6	25.3

	Oil Analysis - Ferrometry	
	High Oil	Low Oil
Hours	36	36
d	1	1
DL	30.4	30.7
DS	11.1	11.5
CPUC	41.5	42.2
ISUC	801.0	810.2

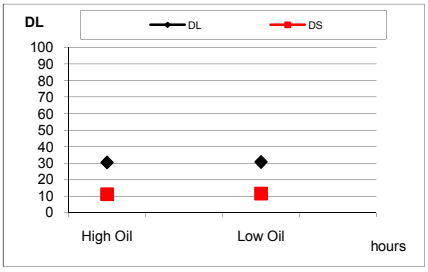

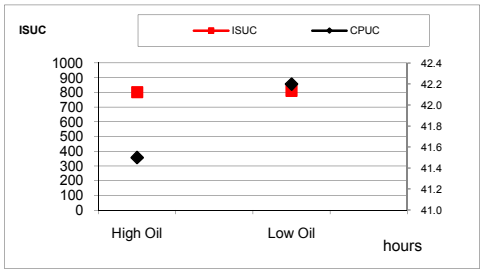

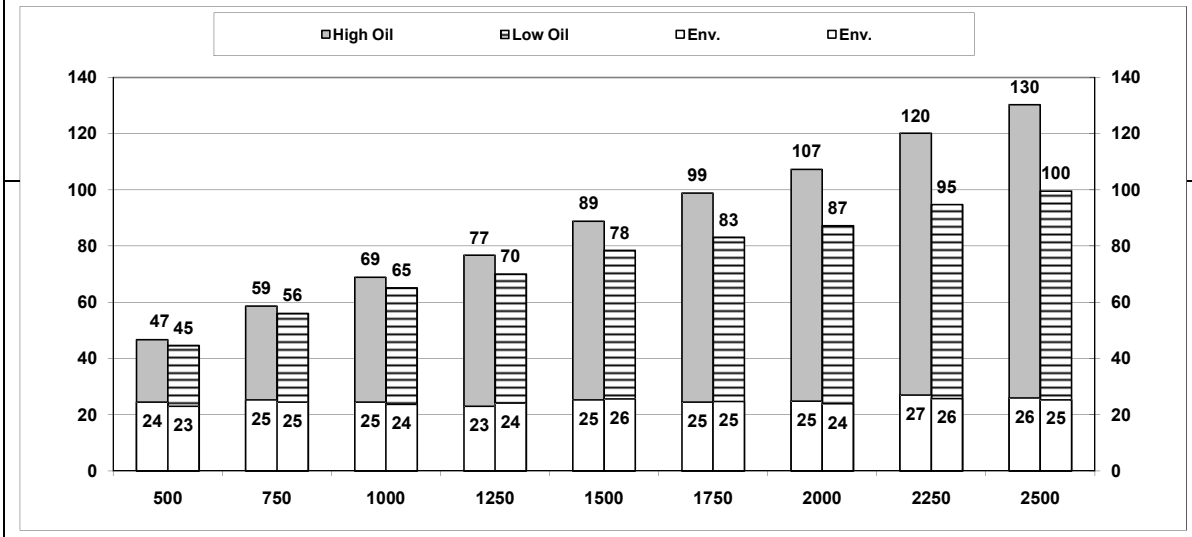

FZG Gear Power Loss Test

TEST DATA SHEET

inegi Instituto de Engenharia Mecânica e Gestão Industrial

CETRIB Unidade de Tribologia, Vibrações e Manutenção Industrial

Test Ref.:	PL LO	**Oil ref.:**	E1
Gear Ref.:	611	**Date:**	29-09-2010
Side:	B	**Material:**	20MnCr5 + Case Hardened

Stabilisation temperature [ºC]						
	500 rpm		1000 rpm		2000 rpm	
KFZG	Oil	Env.	Oil	Env.	Oil	Env.
K1	44.6	23	68.9	24.5	87.2	23.9
K5	47.4	22.9	68.2	24.4	93.9	24.2
K7	47	22.1	66.8	23.7	93.6	24
K9	49.5	23.1	69.3	24.3	94.4	24.9

Oil analysis - Ferrometry				
	k1	k5	k7	k9
Hours	12	24	36	48
d	1	1	1	1
DL	30.7	40.7	43.2	47.9
DS	11.5	16.7	18.3	19.1
CPUC	42.2	57.4	61.5	67.0
ISUC	810.2	1377.6	1531.4	1929.6

Mass loss [mg]	
	running in+k9
pinion	4

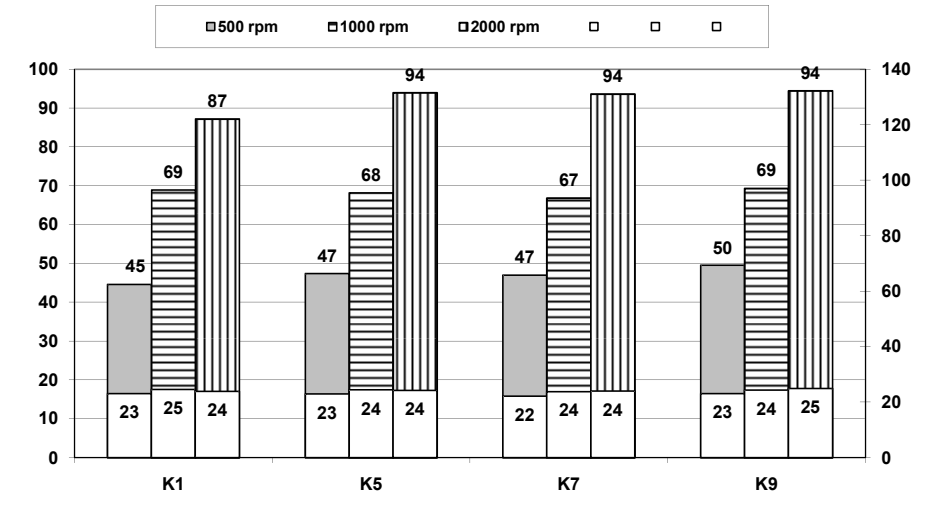

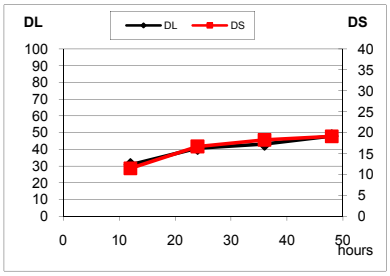

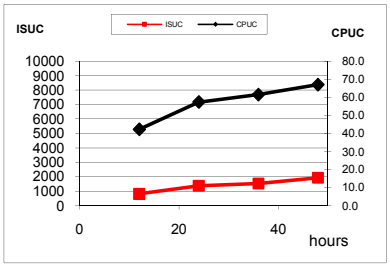

Pinion surface roughness [µm]												
		direction	Ra	Rq	Rz	Rmax	Rpk	Rk	Rvk	Mr1	Mr2	Vo
Initial	Pinion	radial	0.12	0.17	0.75	1.22	0.1	0.28	0.40	6.95	81.0	6.9
	Wheel	radial	0.13	0.20	0.98	1.33	0.1	0.42	0.32	6.12	83.7	6.3
Final	Pinion	radial	0.22	0.33	1.13	1.98	0.3	0.50	0.68	8.25	80.6	11.7
	Wheel	radial	0.28	0.35	1.50	2.03	0.3	0.82	0.53	6.90	84.3	11.3

FZG Gear Power Loss Test

TEST DATA SHEET

Test Ref.:	PL LO	**Oil ref.:**	E1
Gear Ref.:	611	**Date:**	29-09-2010
Side:	B	**Material:**	20MnCr5 + Case Hardened

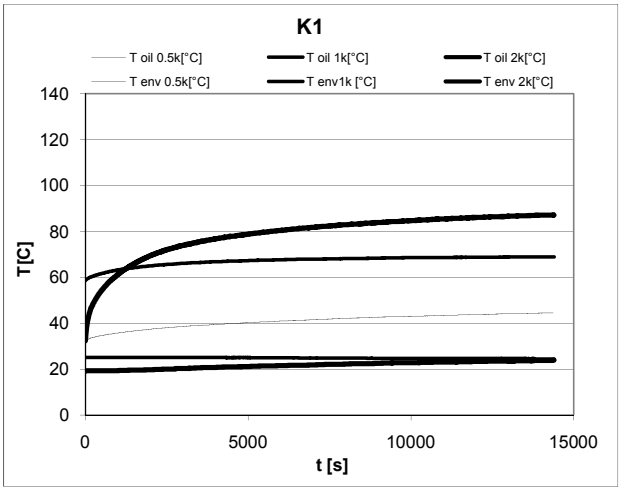

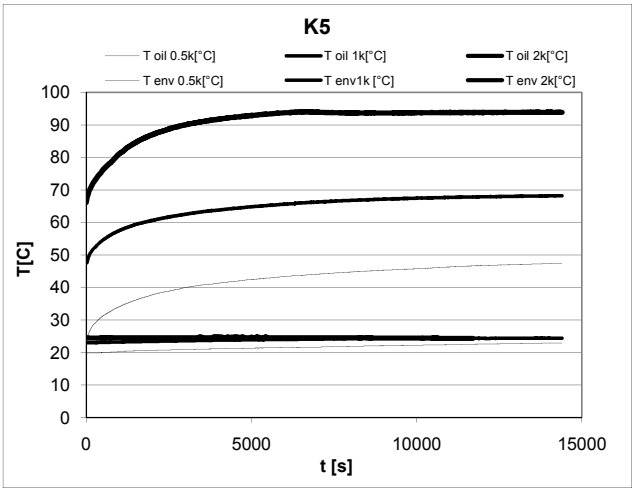

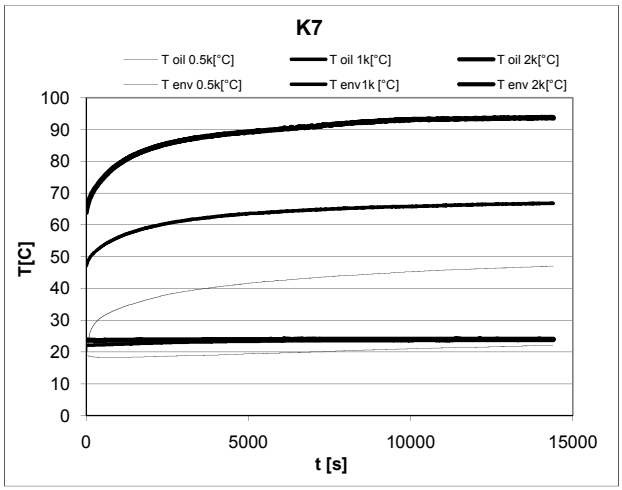

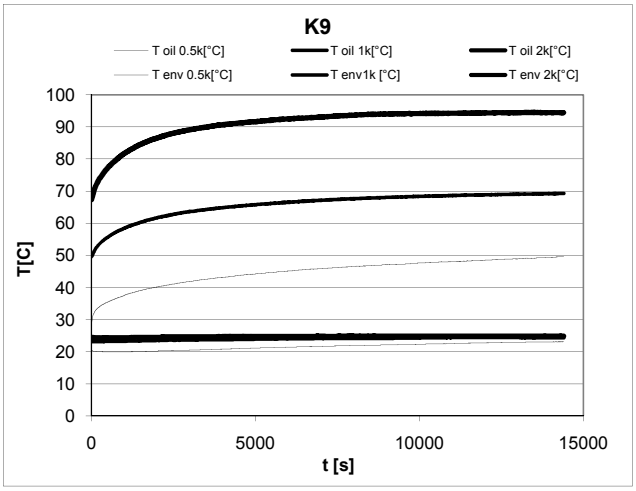

FZG Gear Power Loss Test

TEST DATA SHEET

Test Ref.: CL HO
Gear Ref.: 612 G
Side: B

Oil ref.: P1
Date: 06-12-2010
Material: ADI

Stabilisation temperature [ºC]		
	High Oil	
KFZG	Oil	Env.
500	0	0
750	46.5	22.4
1000	55.2	24
1250	59.3	21.1
1500	69.7	21.6
1750	80.4	22.2
2000	91.3	22
2250	108	23.5
2500	137.3	24.1

Oil Analysis - Ferrometry	
	High Oil
Hours	36
d	
DL	
DS	
CPUC	
ISUC	

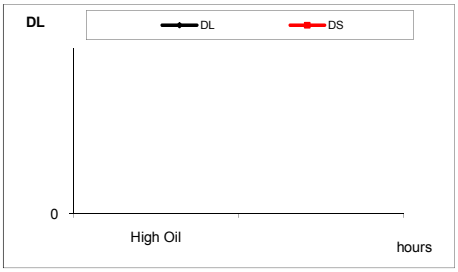

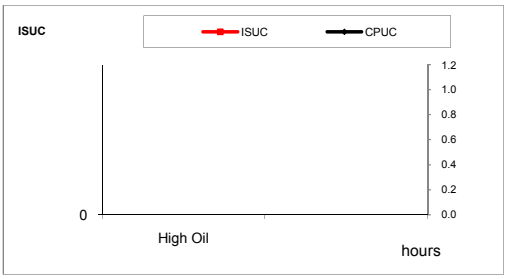

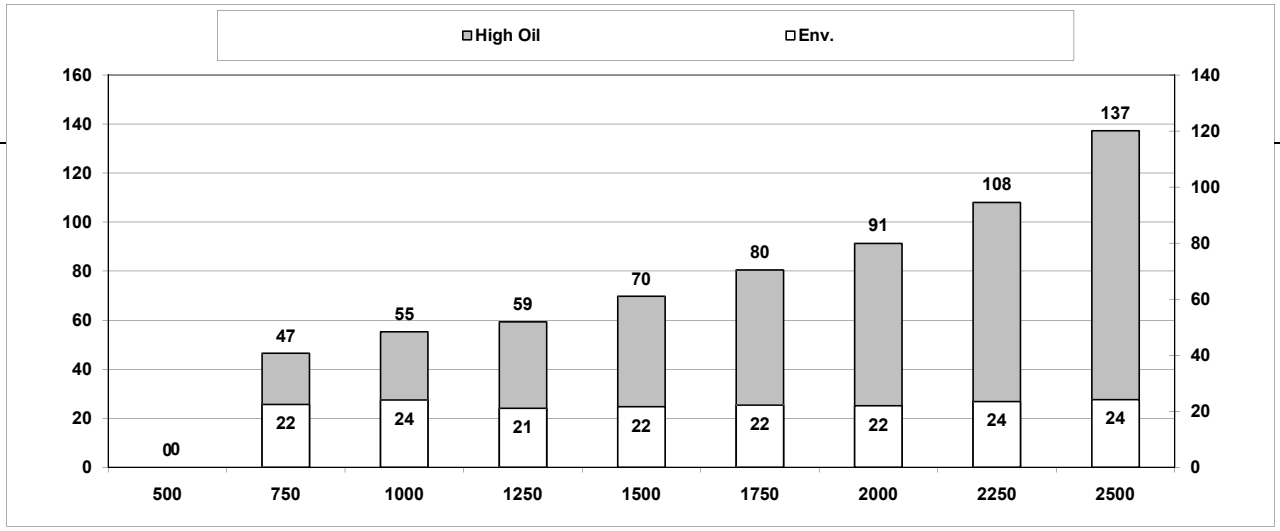

FZG Gear Power Loss Test

TEST DATA SHEET

Test Ref.:	CL HO	**Oil ref.:**	P1
Gear Ref.:	612 G	**Date:**	06-12-2010
Side:	B	**Material:**	ADI

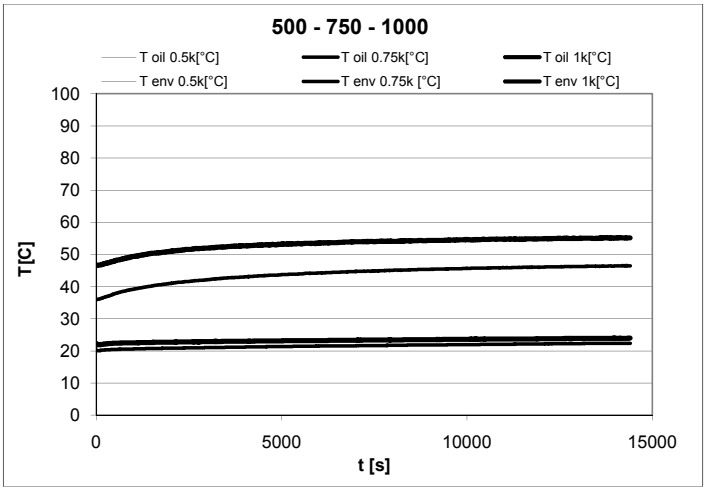

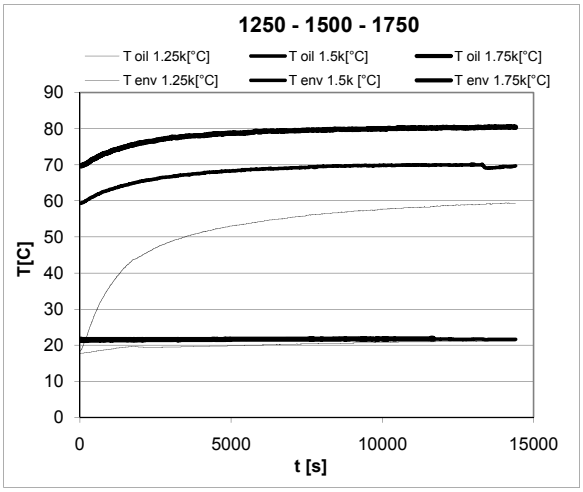

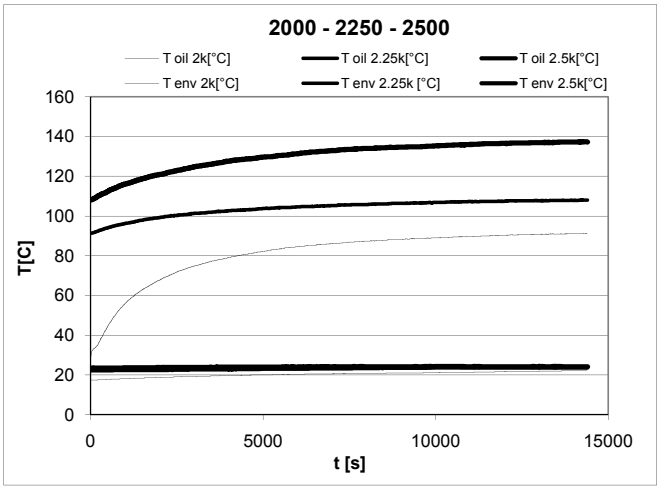

FZG Gear Power Loss Test

TEST DATA SHEET

inegi
Instituto de Engenharia Mecânica e Gestão Industrial
CETRIB
Unidade de Tribologia, Vibrações e Manutenção Industrial

Test Ref.: CL LO
Gear Ref.: 612 G
Side: B

Oil ref.: P1
Date: 06-12-2010
Material: ADI

Stabilisation temperature [ºC]		
	Low Oil	
KFZG	Oil	Env.
500	33.8	18.5
750	42.8	19.4
1000	50.3	20.1
1250	55.9	21.3
1500	62.1	22.4
1750	66.2	23
2000	64.7	20.1
2250	70.9	21.1
2500	76.1	20.9

	Oil Analysis - Ferrometry
	Low Oil
Hours	36
d	1
DL	54.3
DS	25.2
CPUC	79.5
ISUC	2.30E+03

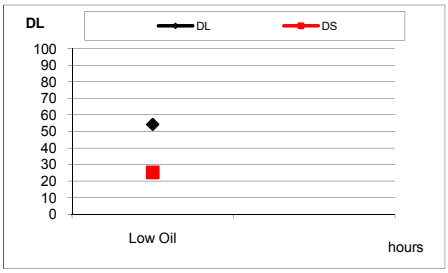

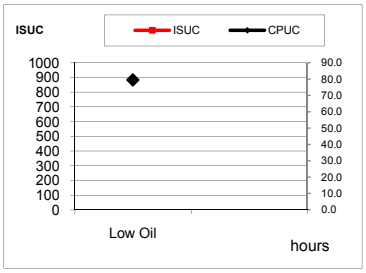

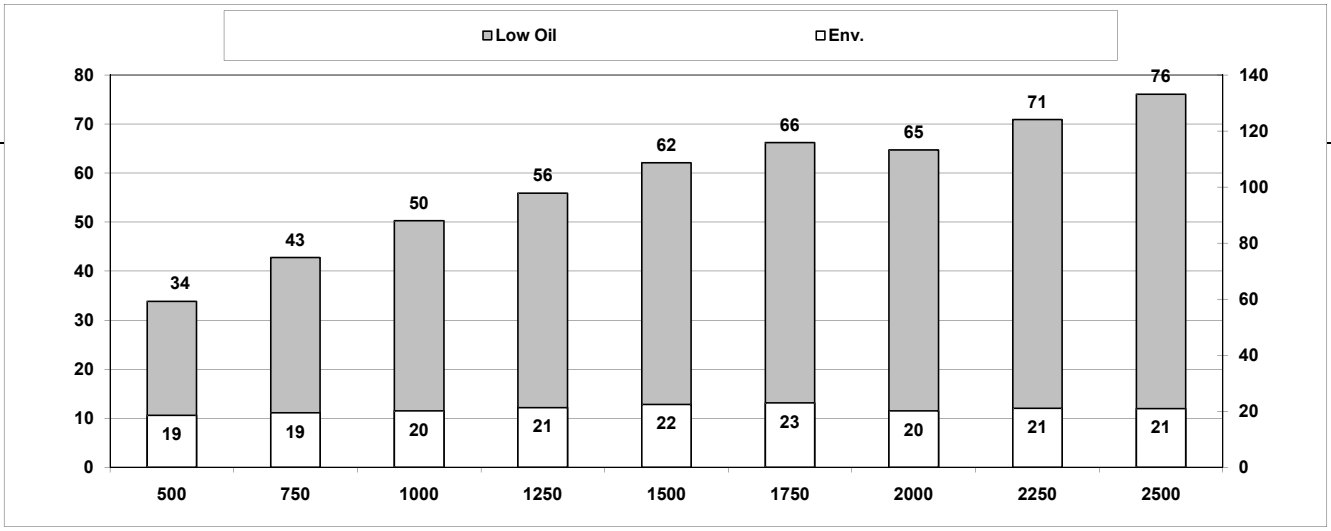

FZG Gear Power Loss Test

TEST DATA SHEET

Test Ref.:	CL LO	**Oil ref.:**	P1
Gear Ref.:	612 G	**Date:**	06-12-2010
Side:	B	**Material:**	ADI

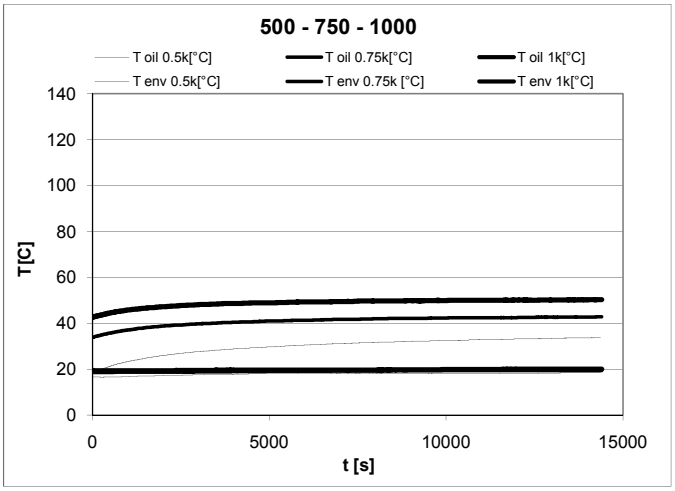

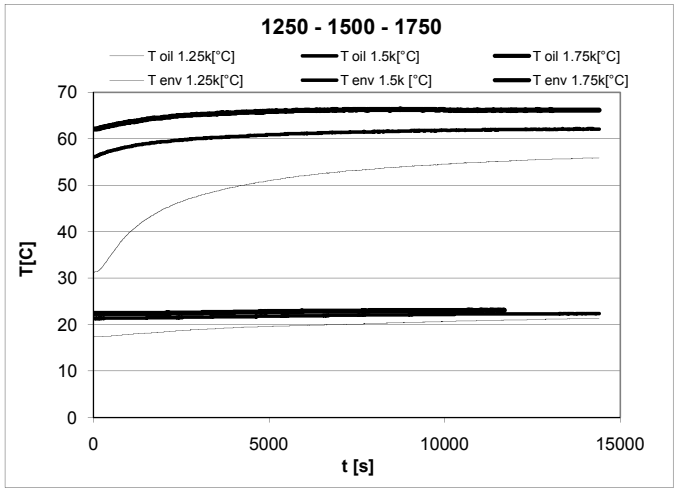

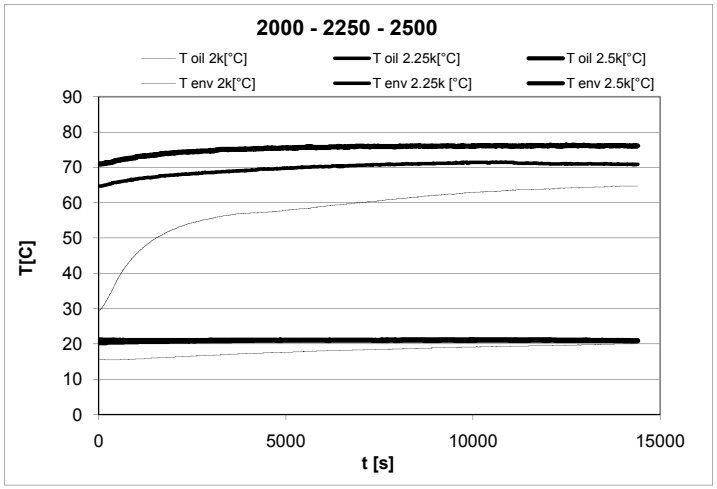

FZG Gear Power Loss Test

TEST DATA SHEET

inegi Instituto de Engenharia Mecânica e Gestão Industrial

CETRIB Unidade de Tribologia, Vibrações e Manutenção Industrial

Test Ref.:	CL HO & LO	**Oil ref.:**	P1
Gear Ref.:	612 G	**Date:**	06-12-2010
Side:	B	**Material:**	ADI

Stabilisation temperature [ºC]				
	High Oil		Low Oil	
KFZG	Oil	Env.	Oil	Env.
500	0	0	33.8	18.5
750	46.5	22.4	42.8	19.4
1000	55.2	24	50.3	20.1
1250	59.3	21.1	55.9	21.3
1500	69.7	21.6	62.1	22.4
1750	80.4	22.2	66.2	23
2000	91.3	22	64.7	20.1
2250	108	23.5	70.9	21.1
2500	137.3	24.1	76.1	20.9

	Oil Analysis - Ferrometry	
	High Oil	Low Oil
Hours	36	36
d	0	1
DL	0	54.3
DS	0	25.2
CPUC	0.0	79.5
ISUC	0.0	2.30E+03

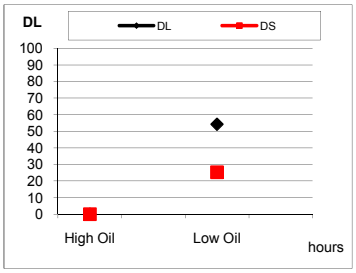

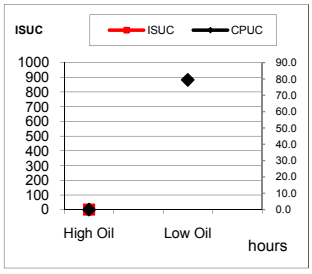

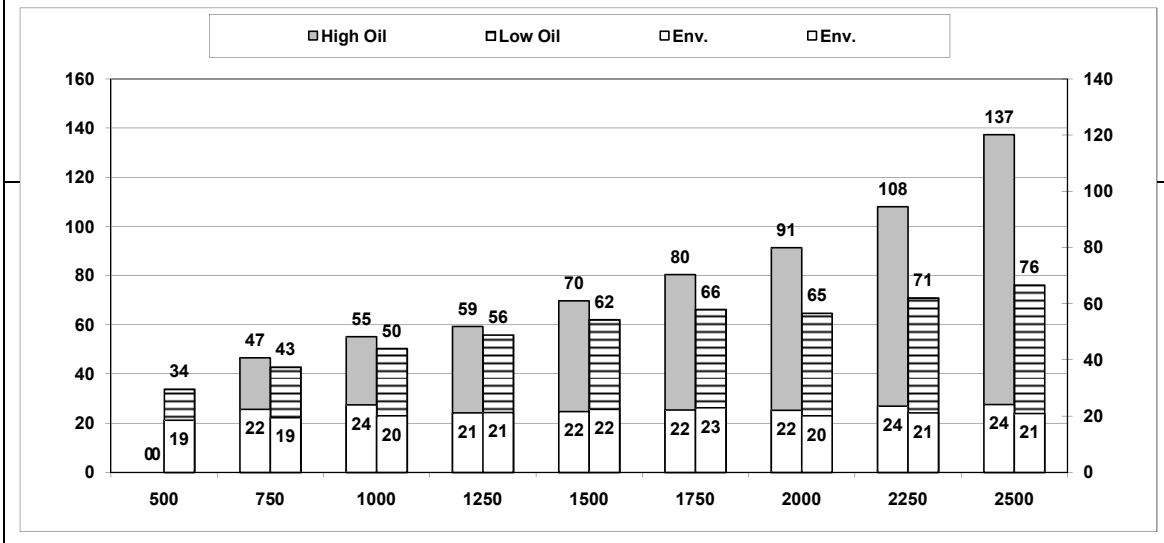

FZG Gear Power Loss Test

TEST DATA SHEET

inegi
Instituto de Engenharia Mecânica e Gestão Industrial
CETRIB

Test Ref.:	PL LO	**Oil ref.:**	P1
Gear Ref.:	612 G	**Date:**	14-12-2010
Side:	B	**Material:**	ADI

Stabilisation temperature [ºC]						
	500 rpm		1000 rpm		2000 rpm	
KFZG	Oil	Env.	Oil	Env.	Oil	Env.
K1	33.8	18.5	50.3	20.1	64.7	20.1
K5	37.4	16.6	55.7	17.8	76.9	17.7
K7	39	15.8	58.4	17	80.6	17.4
K9	47.3	17.9	69.1	19	104	19.9

Mass loss [mg]	
	running in+k9
pinion	39

Oil analysis - Ferrometry				
	k1	**k5**	**k7**	**k9**
Hours	12	24	36	48
d	1	0.1	0.1	0.1
DL	54.3	28.1	21.9	39.9
DS	25.2	9.2	8.1	12.5
CPUC	79.5	374.0	300.0	524.0
ISUC	2.30E+03	7.10E+05	4.10E+04	1.40E+05

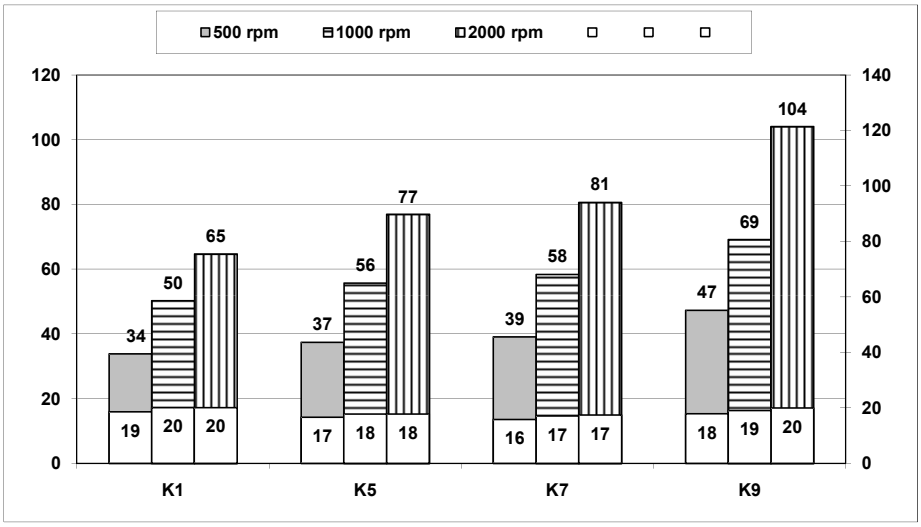

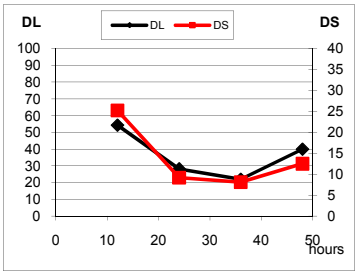

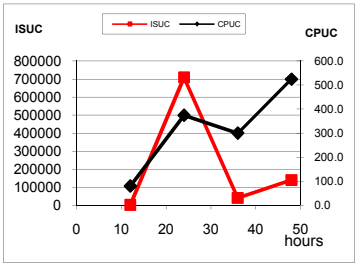

Pinion surface roughness [µm]												
		direction	**Ra**	**Rq**	**Rz**	**Rmax**	**Rpk**	**Rk**	**Rvk**	**Mr1**	**Mr2**	**Vo**
Initial	Pinion	radial	0.40	0.57	2.60	3.65	0.5	1.27	0.88	7.17	83.5	17.4
	Wheel	radial	1.38	1.88	10.15	16.93	1.3	4.25	3.32	8.97	87.3	67.4
Final	Pinion	radial	0.38	0.52	2.67	4.32	0.4	1.10	0.88	5.68	84.2	17.4
	Wheel	radial	0.97	1.45	7.67	12.62	0.9	1.85	3.25	9.83	79.9	53.0

FZG Gear Power Loss Test

TEST DATA SHEET

Test Ref.:	PL LO	**Oil ref.:**	P1
Gear Ref.:	612 G	**Date:**	14-12-2010
Side:	B	**Material:**	ADI

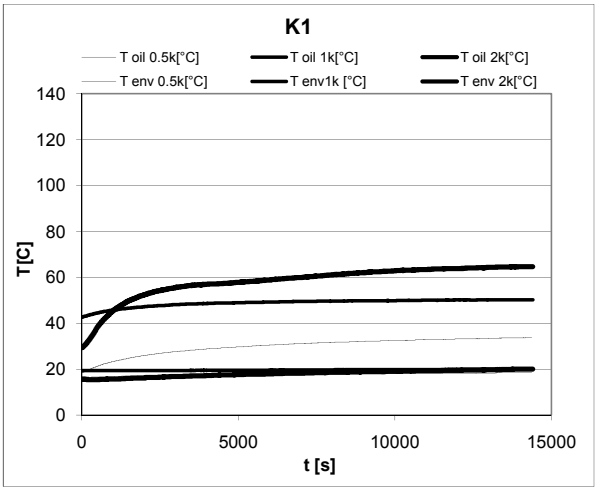

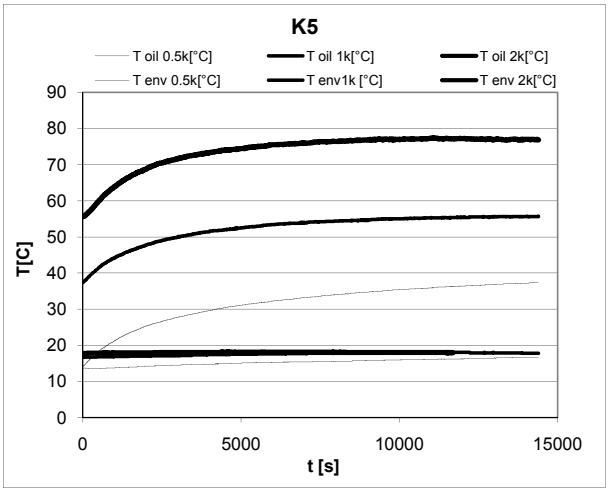

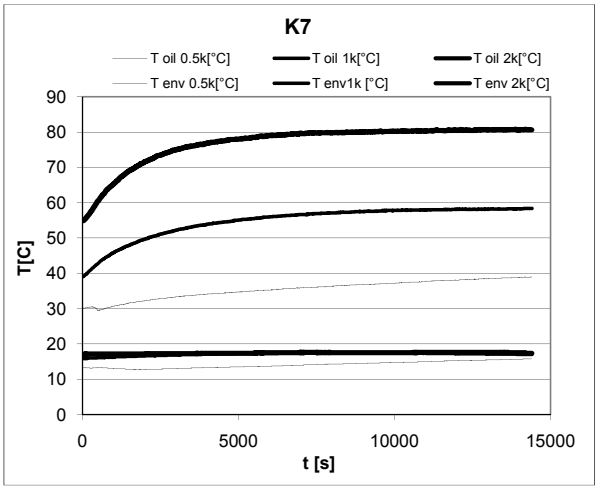

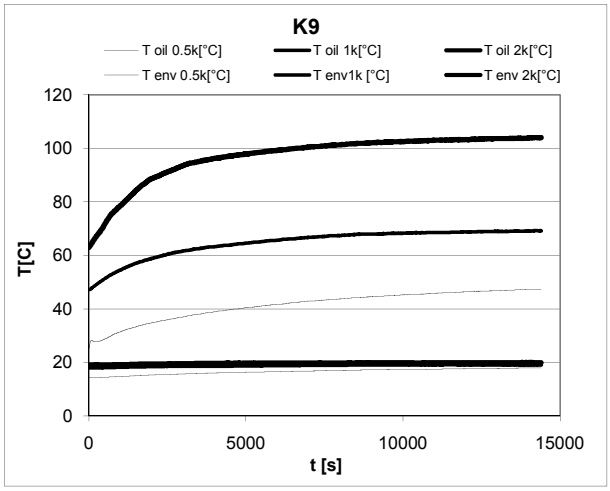

FZG Gear Power Loss Test

TEST DATA SHEET

inegi
Instituto de Engenharia Mecânica e Gestão Industrial

CETRIB
Unidade de Tribologia, Vibrações e Manutenção Industrial

Test Ref.:	CL HO	**Oil ref.:**	E1
Gear Ref.:	612 H	**Date:**	02-11-2010
Side:	B	**Material:**	ADI

Stabilisation temperature [ºC]

	High Oil	
KFZG	Oil	Env.
500	55.1	22.3
750	70.7	23.2
1000	82.9	22.8
1250	93.5	23.5
1500	112.3	25
1750	125.8	25.3
2000	136.2	27
2250	157.8	28.5
2500	174.2	28.6

Oil Analysis - Ferrometry

	High Oil
Hours	36
d	1
DL	41.2
DS	12.3
CPUC	53.5
ISUC	1500.0

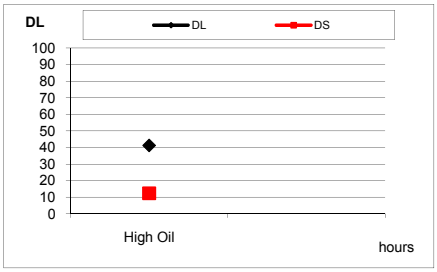

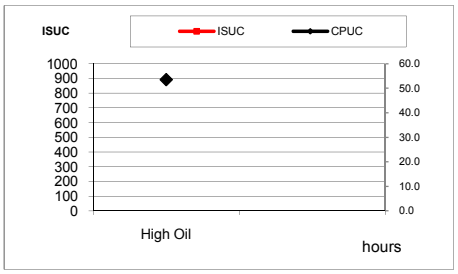

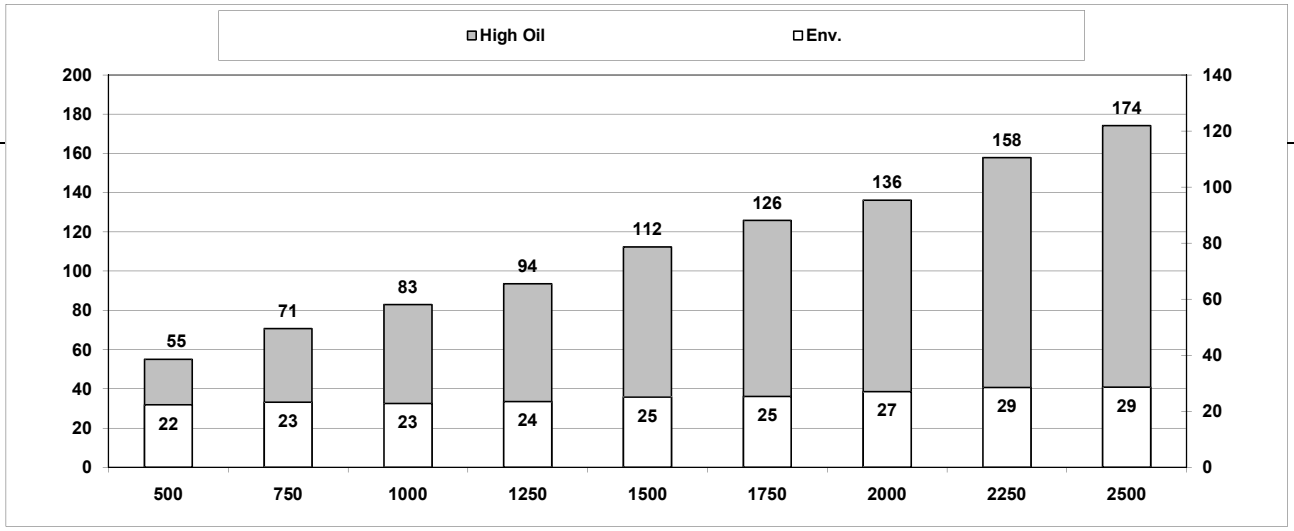

FZG Gear Power Loss Test

TEST DATA SHEET

Test Ref.:	CL HO	**Oil ref.:**	E1
Gear Ref.:	612 H	**Date:**	02-11-2010
Side:	B	**Material:**	ADI

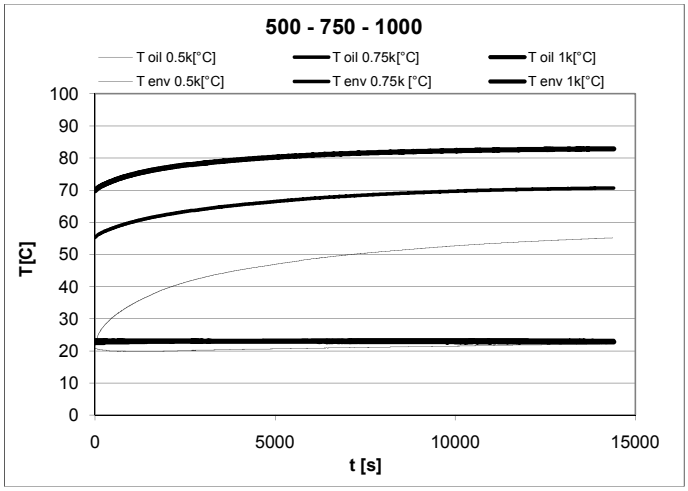

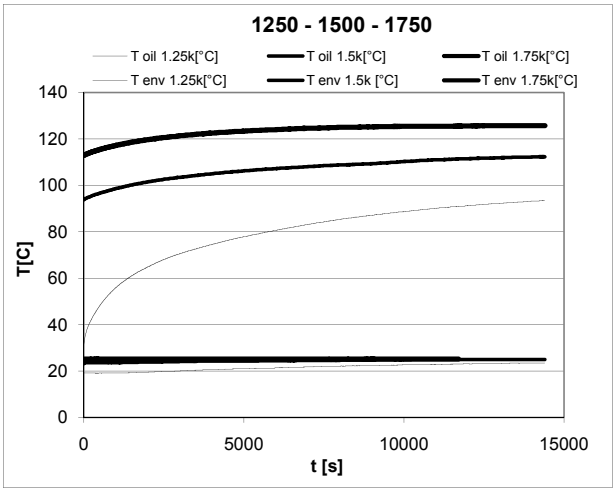

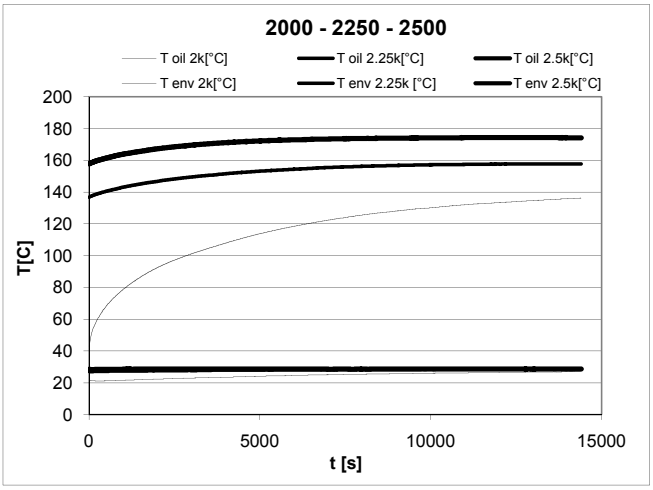

FZG Gear Power Loss Test

TEST DATA SHEET

inegi
Instituto de Engenharia Mecânica e Gestão Industrial
CETRIB
Unidade de Tribologia, Vibrações e Manutenção Industrial

Test Ref.:	CL LO	**Oil ref.:**	E1
Gear Ref.:	612 H	**Date:**	02-11-2010
Side:	B	**Material:**	ADI

Stabilisation temperature [ºC]		
	Low Oil	
KFZG	Oil	Env.
500	53.4	25.1
750	66	25.4
1000	76.1	24.8
1250	79.6	21.1
1500	90.1	21.7
1750	95.9	22.2
2000	100.1	22.3
2250	111.9	23.3
2500	117.6	23

Oil Analysis - Ferrometry	
	Low Oil
Hours	36
d	1
DL	38.9
DS	18.5
CPUC	57.4
ISUC	12000.0

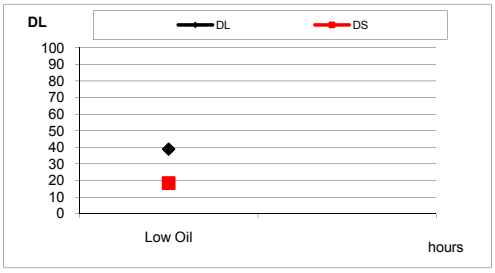

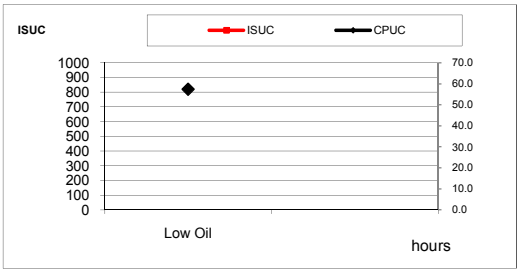

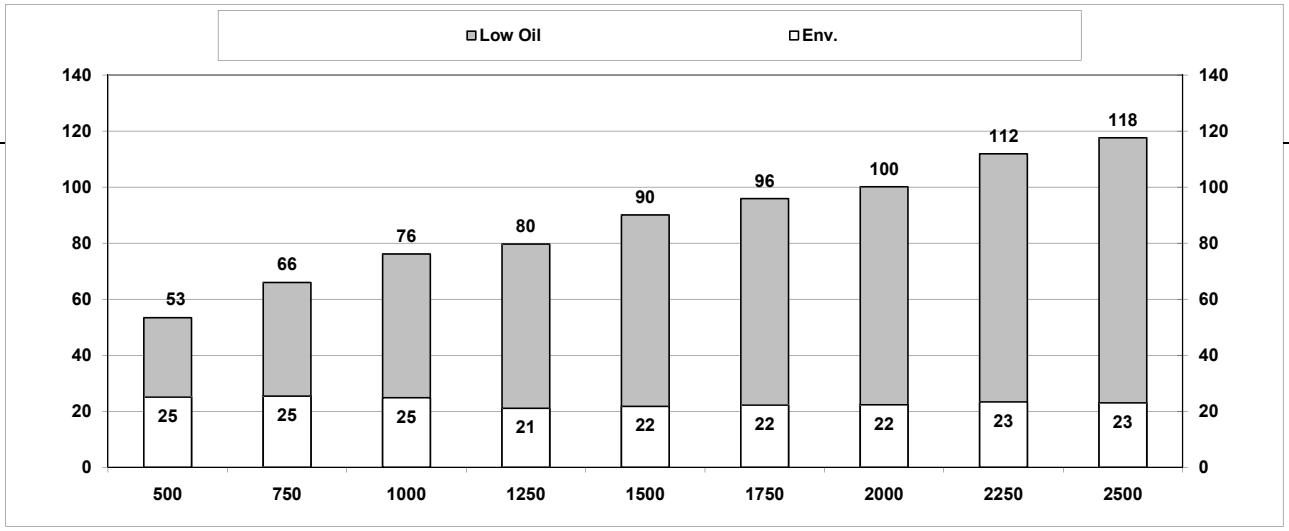

FZG Gear Power Loss Test

TEST DATA SHEET

Test Ref.:	CL LO	**Oil ref.:**	E1
Gear Ref.:	612 H	**Date:**	02-11-2010
Side:	B	**Material:**	ADI

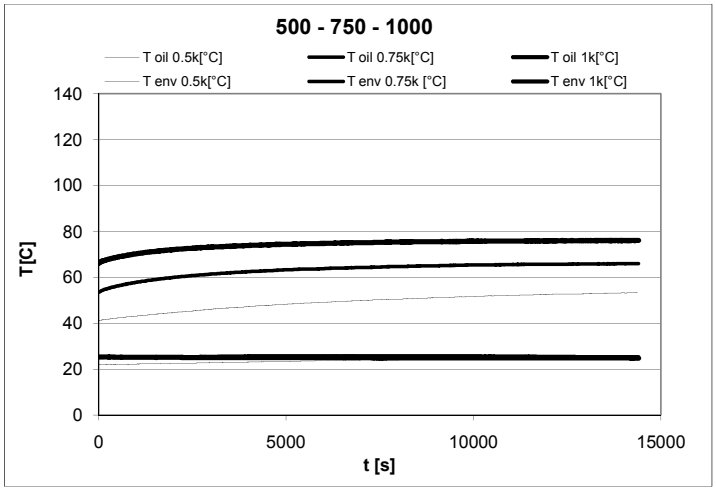

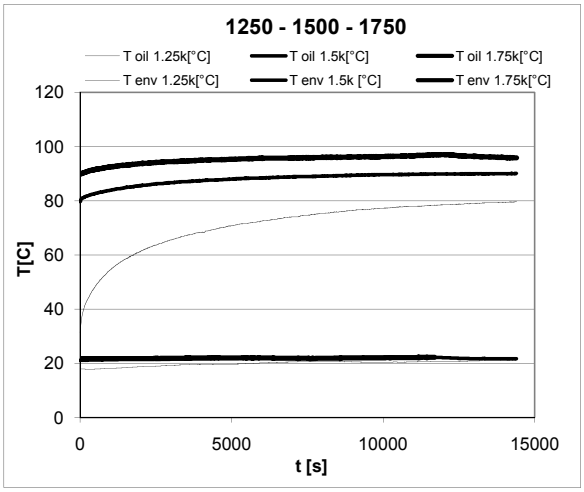

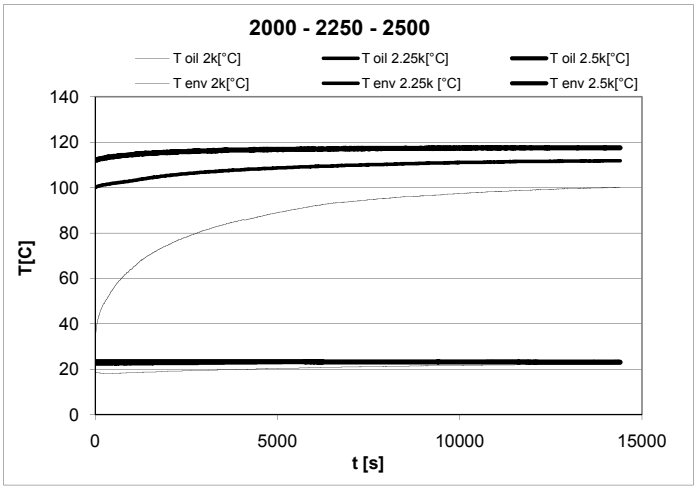

FZG Gear Power Loss Test

TEST DATA SHEET

inegi Instituto de Engenharia Mecânica e Gestão Industrial

CETRIB Unidade de Tribologia, Vibrações e Manutenção Industrial

Test Ref.: CL HO & LO
Gear Ref.: 612 H
Side: B

Oil ref.: E1
Date: 02-11-2010
Material: ADI

Stabilisation temperature [ºC]				
	High Oil		Low Oil	
KFZG	Oil	Env.	Oil	Env.
500	55.1	22.3	53.4	25.1
750	70.7	23.2	66	25.4
1000	82.9	22.8	76.1	24.8
1250	93.5	23.5	79.6	21.1
1500	112.3	25	90.1	21.7
1750	125.8	25.3	95.9	22.2
2000	136.2	27	100.1	22.3
2250	157.8	28.5	111.9	23.3
2500	174.2	28.6	117.6	23

	Oil Analysis - Ferrometry	
	High Oil	Low Oil
Hours	36	36
d	1	1
DL	41.2	38.9
DS	12.3	18.5
CPUC	53.5	57.4
ISUC	1500.0	1.20E+04

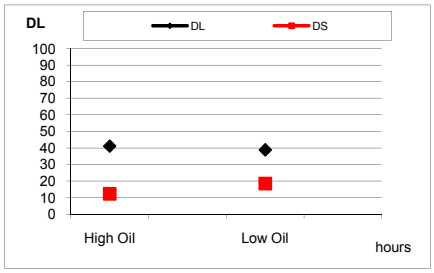

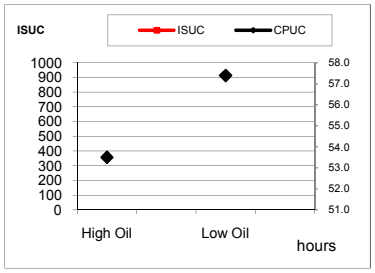

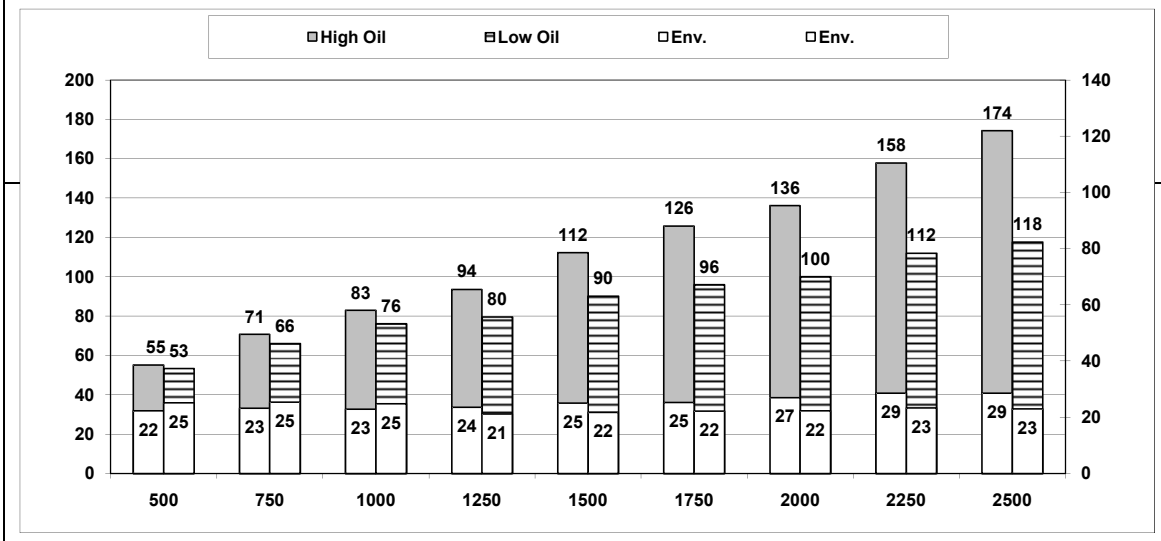

FZG Gear Power Loss Test

TEST DATA SHEET

inegi Instituto de Engenharia Mecânica e Gestão Industrial

CETRIB Unidade de Tribologia, Vibrações e Manutenção Industrial

Test Ref.:	PL LO	**Oil ref.:**	E1
Gear Ref.:	612 H	**Date:**	15-11-2010
Side:	B	**Material:**	ADI

Stabilisation temperature [ºC]

	500 rpm		1000 rpm		2000 rpm	
KFZG	Oil	Env.	Oil	Env.	Oil	Env.
K1	53.4	25.1	76.1	24.8	100.1	22.3
K5	55.5	22.4	81.7	23	113.5	23.7
K7	51.4	19	76.8	20.4	112.7	21.1
K9	55.3	19.3	83	21	120	22.1

Oil analysis - Ferrometry

	k1	k5	k7	k9
Hours	12	24	36	48
d	1	1	1	0.1
DL	38.9	57	74.8	44.7
DS	18.5	26.4	31	16.9
CPUC	57.4	83.4	105.8	616.0
ISUC	1.20E+04	2.60E+03	4.60E+03	1.70E+05

Mass loss [mg]

	running in+k9
pinion	51

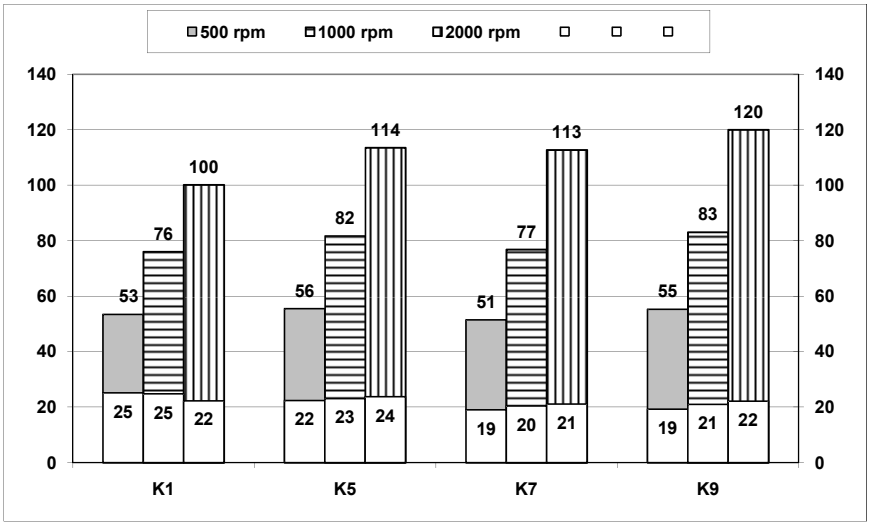

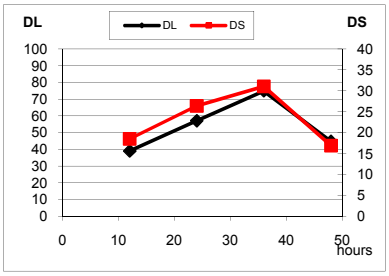

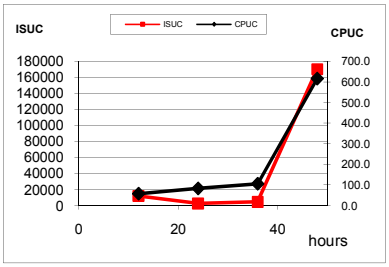

Pinion surface roughness [µm]

		direction	Ra	Rq	Rz	Rmax	Rpk	Rk	Rvk	Mr1	Mr2	Vo
Initial	Pinion	radial	0.47	0.60	2.87	3.72	0.5	1.38	0.87	8.57	85.7	18.2
	Wheel	radial	0.40	0.55	2.87	4.30	0.6	1.18	0.82	11.38	83.8	16.8
Final	Pinion	radial	0.32	0.38	1.95	2.47	0.5	1.00	0.38	9.10	87.0	9.7
	Wheel	radial	0.40	0.53	2.65	3.55	0.6	1.22	0.68	8.17	85.2	15.4

FZG Gear Power Loss Test

TEST DATA SHEET

Test Ref.:	PL LO	**Oil ref.:**	E1
Gear Ref.:	612 H	**Date:**	15-11-2010
Side:	B	**Material:**	ADI

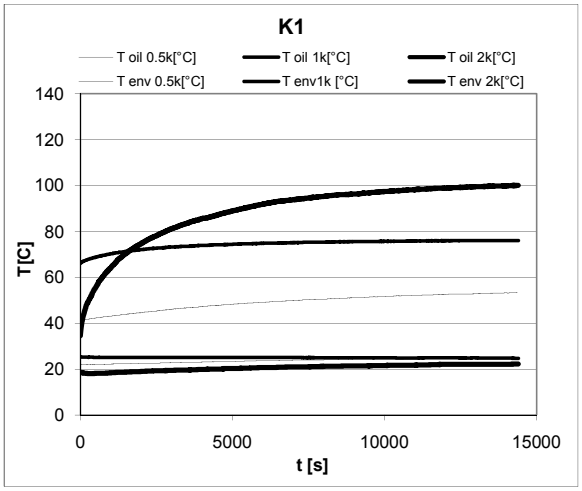

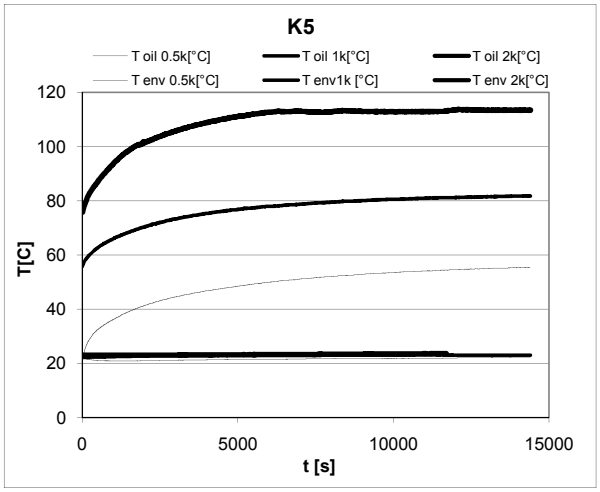

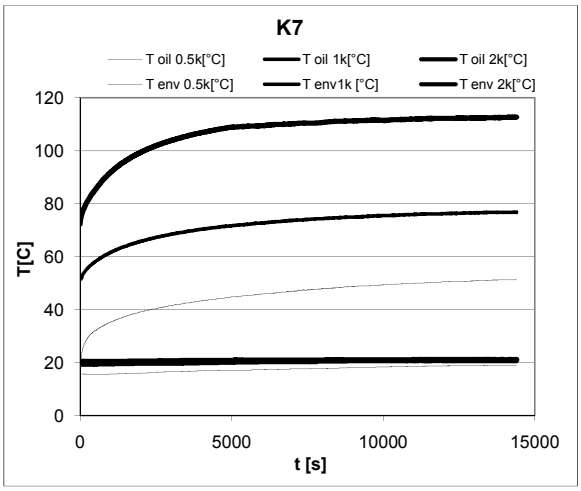

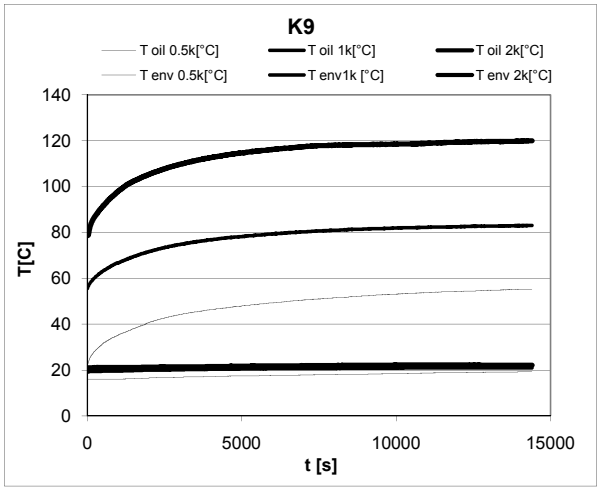

A.2. Power Loss oil Reports

Relatório
de
Análise de Lubrificantes

Análise nº: Tipo de análise: Confidencialidade:	57 -61 / 10 Ferrometria e Ferrografia Analítica 1
Cliente: Morada: Telefone / Fax:	INEGI - Cetrib Porto
Equipamento: Lubrificante: Dossier:	FZG (20MnCr5 – 311 Labo B) Bio-GearOil (E2) /
Nº de páginas: Data:	5 14/10/10
Responsável: Rúbrica:	Beatriz Graça – Jorge Seabra

Os resultados apresentados referem-se exclusivamente às amostras ensaiadas.
Este documento não pode ser reproduzido, total ou parcialmente, sem a autorização por escrito do INEGI.

OBJECTIVO

Análise de cinco amostras de óleo lubrificante E2 resultantes de ensaios na Máquina FZG com engrenagens de aço (20MnCr5), para avaliação do desgaste presente.

As amostras analisadas foram as seguintes:

Ensaio	Estágio	Análises efectuadas	
		Ferrometria	Ferrografia Analítica
PLoss HO	Chap. K1	X	X
PLoss LO	Chap. K1	X	X
PLoss LO	K5	X	X
PLoss LO	K7	X	X
PLoss LO	K9	X	X

RESULTADOS DAS ANÁLISES

Nas páginas seguintes são apresentados os resultados referentes às análises de Ferrometria (DR III) e Ferrografia Analítica (FM III).

Os resultados apresentados referem-se exclusivamente às amostras ensaiadas.
Este documento não pode ser reproduzido, total ou parcialmente, sem a autorização por escrito do INEGI.

	CLIENTE: ***INEGI***			MÁQUINA: Máquina de Ensaios FZG			
	MORADA: Porto			Ref. ÓLEO: Bio-GearOil (E2)			
	DATA: 13/10/10			ENSAIOS FZG - 20MnCr5 Gears 311 Lado B			
IDENTIFICAÇÃO							
Ensaio:	PL Chap.	PL Chap.	PLoss	PLoss	PLoss		
Data amostra:	Set-10	Set-10	Set-10	Set-10	Set-10		
Análise nº:	57/10	58/10	59/10	60/10	61/10		
Estágio:	K1	K1	K5	K7	K9		
Lubrificante:	High Oil	Low Oil	Low Oil	Low Oil	Low Oil		
FERROMETRIA							
d:	1	1	1	1	1		
DL:	51,0	53,0	67,8	62,7	58,1		
DS:	21,9	34,5	42,3	31,3	32,0		
CPUC:	72,9	87,5	110,1	94,0	90,1		
ISUC:	2121,4	1618,8	2807,6	2951,6	2351,6		
FERROGRAFIA:							
Desgaste normal							
Desgaste severo							
Desgaste abrasão							
Desgaste combinado							
Desgaste fadiga							
Esferas Metálicas							
Ligas não ferrosas							
Óxidos de ferro							
Minerais/Orgânicos							
OILVIEW:							
Índice OilLife:							
Índice Oxidação:							
Índice Contaminação:							
Índice Ferromagnético:							
Grandes Contaminantes:							
Constante Dieléctrica:							
FILTRAGEM							
(Nº Partículas/10 ml)							
5 - 15 µm							
15 - 25 µm							
25 - 50 µm							
50 - 100 µm							
> 100 µm							
VISCOSIDADE							
(cSt a 40° C):							
ACIDEZ (TAN)							
(mg KOH)							
P. INFLAMAÇÃO							
(° C)							
DIAGNÓSTICO:							

LEGENDA	**DL** - Índice de partículas grandes		Não existe
	DS - Índice de partículas pequenas	**f**	Fraco
	CPUC - Concentração part. de desgaste	**M**	Médio
	ISUC - Índice Severidade de Desgaste	**F**	Forte

231

Os resultados apresentados referem-se exclusivamente às amostras ensaiadas.
Este documento não pode ser reproduzido, total ou parcialmente, sem a autorização por escrito do INEGI.

CLIENTE: *INEGI*	MÁQUINA: Máquina de Ensaios FZG
MORADA: Porto	Ref. ÓLEO: Bio-GearOil (E2) Chap. High Oil
DATA: 13/10/10	ENSAIOS FZG - Steel Gears 311 K1

Fotografia 1

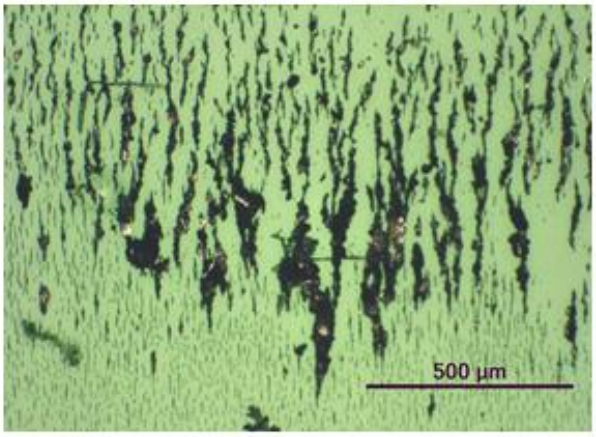

Ampliação: x 100 Diluição: 1
Localização: Núcleo Luz: Branca / Verde

Observações: Presença significativa de particulas ferrosas de pequenas e grandes dimensões.

Fotografia 2

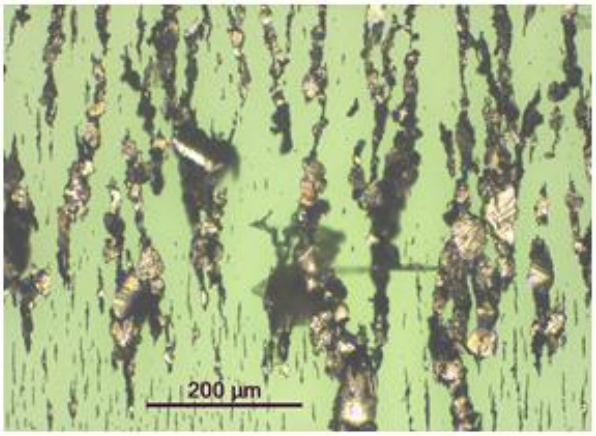

Ampliação: x 200 Diluição: 1
Localização: Núcleo Luz: Branca / Verde

Observações: Ampliação da Fotografia 1. Presença de particulas ferrosas de grandes dimensões e algumas oxidadas.

Fotografia 3

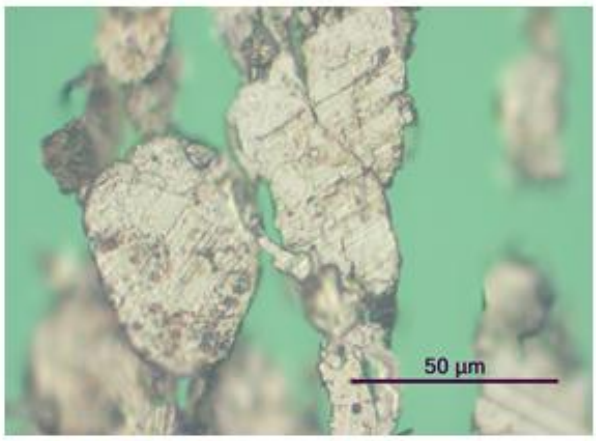

Ampliação: x 1000 Diluição: 1
Localização: Núcleo Luz: Branca / Verde

Observações: Ampliação da Fotografia 2. Particulas ferrosas laminares, tipica de desgaste combinado (fadiga+escorrefgamento).

Fotografia 4

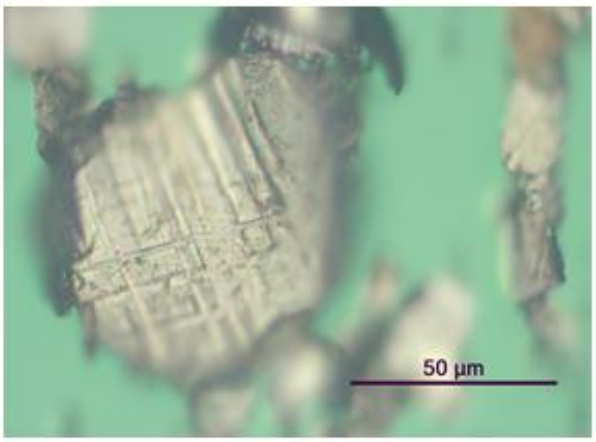

Ampliação: x 1000 Diluição: 1
Localização: Núcleo Luz: Branca / Verde

Observações: Particula laminar, tipica de desgaste combinado e de grandes dimensões.

Os resultados apresentados referem-se exclusivamente às amostras ensaiadas.
Este documento não pode ser reproduzido, total ou parcialmente, sem a autorização por escrito do INEGI.

CLIENTE: ***INEGI***	MÁQUINA: Máquina de Ensaios FZG
MORADA: Porto	Ref. ÓLEO: Bio-GearOil (E2) Chap. Low Oil
DATA: 13/10/10	ENSAIOS FZG - Steel Gears 311 K1

Fotografia 5

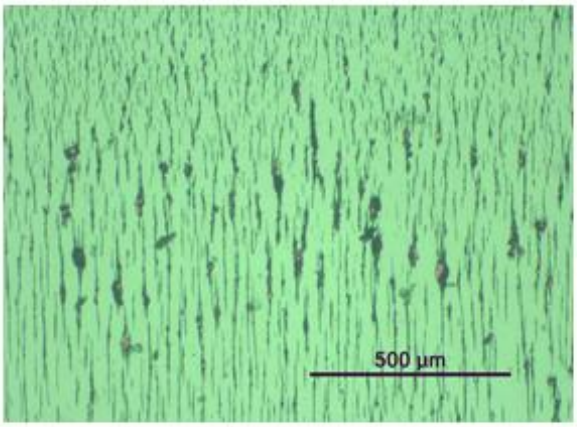

Ampliação: x 100 Diluição: 1
Localização: Núcleo Luz: Branca / Verde

Observações: Presença de particulas ferrosas de pequenas dimensões e algumas de grandes dimensões.

Fotografia 6

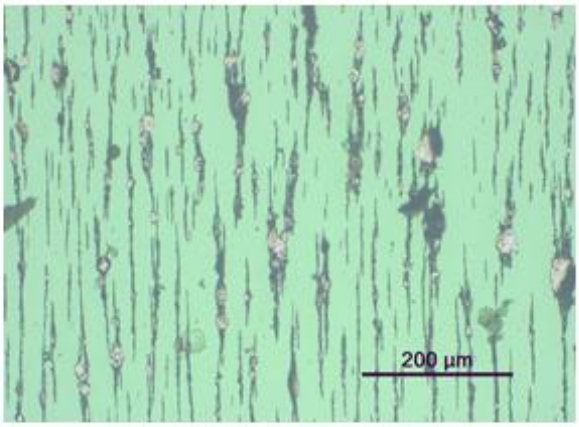

Ampliação: x 200 Diluição: 1
Localização: Núcleo Luz: Branca / Verde

Observações: Ampliação da Fotografia 5. Presença de particulas ferrosas de pequenas e grandes dimensões.

Fotografia 7

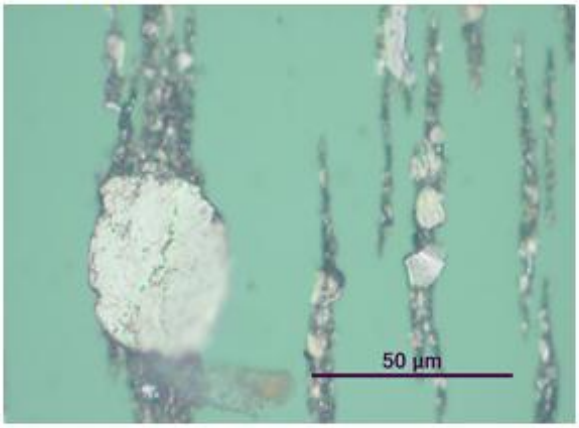

Ampliação: x 1000 Diluição: 1
Localização: Núcleo Luz: Branca / Verde

Observações: Ampliação da Fotografia 6. Particula ferrosa de desgaste de fadiga com grandes dimensões.

Fotografia 8

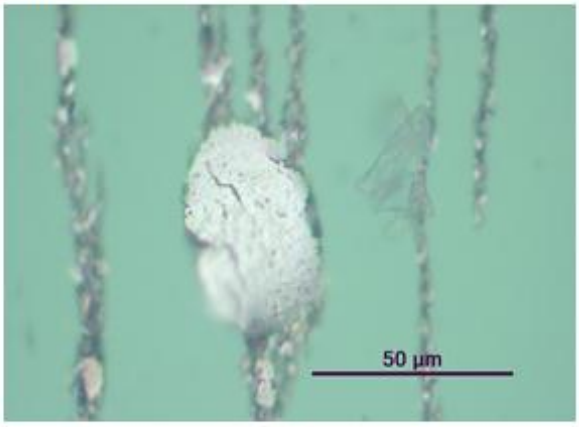

Ampliação: x 1000 Diluição: 1
Localização: Núcleo Luz: Branca / Verde

Observações: Ampliação da Fotografia 6. Particula ferrosa de desgaste de fadiga com grandes dimensões.

Os resultados apresentados referem-se exclusivamente às amostras ensaiadas.
Este documento não pode ser reproduzido, total ou parcialmente, sem a autorização por escrito do INEGI.

CLIENTE: *INEGI*	MÁQUINA: Máquina de Ensaios FZG
MORADA: Porto	Ref. ÓLEO: Bio-GearOil (E2)
DATA: 13/10/10	ENSAIOS FZG - Steel Gears 311 K5

Fotografia 9

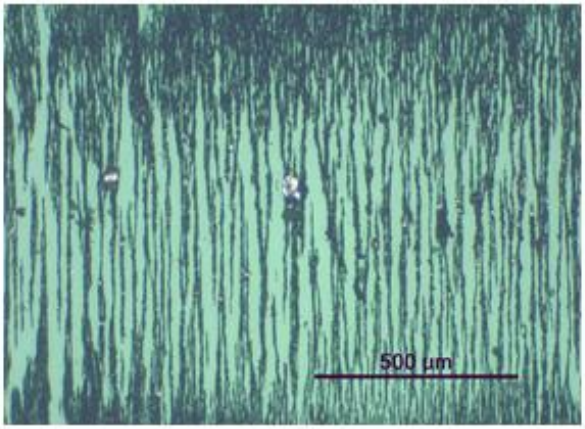

Ampliação: x 100 Diluição: 1
Localização: Núcleo Luz: Branca / Verde

Observações: Presença significativa de particulas ferrosas de pequenas dimensões e algumas de grandes dimensões.

Fotografia 10

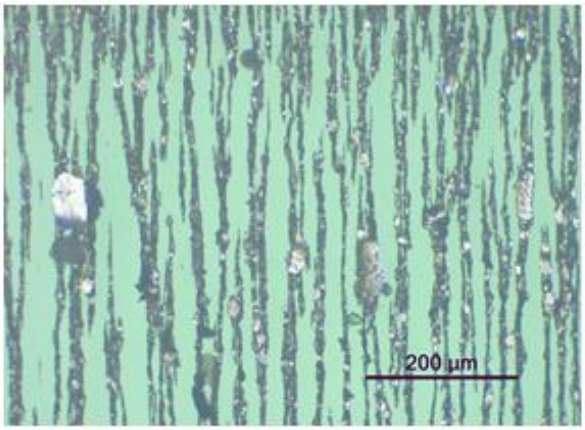

Ampliação: x 200 Diluição: 1
Localização: Núcleo Luz: Branca / Verde

Observações: Ampliação da Fotografia 9.
Presença de poucas particulas ferrosas de grandes dimensões.

Fotografia 11

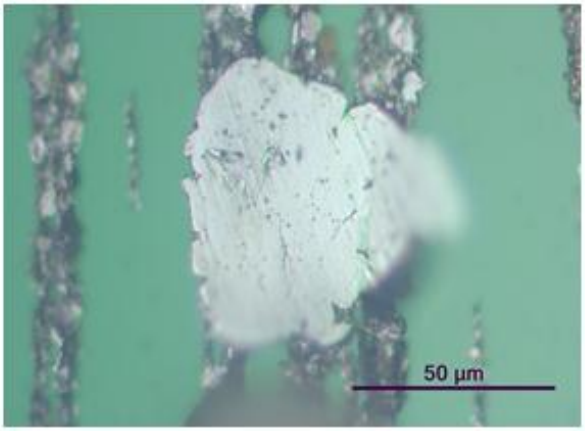

Ampliação: x 1000 Diluição: 1
Localização: Núcleo Luz: Branca / Verde

Observações: Ampliação da Fotografia 10.
Particula ferrosa de desgaste de fadiga com grandes dimensões.

Fotografia 12

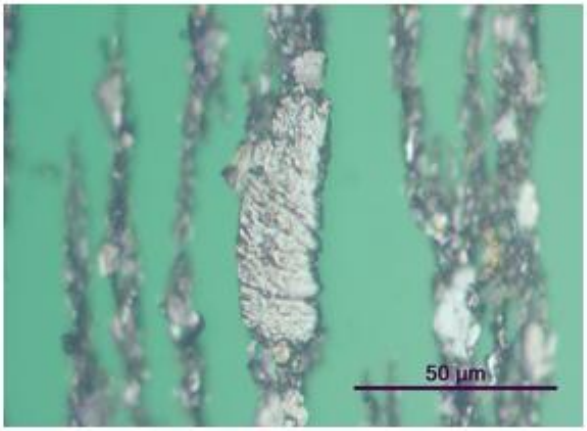

Ampliação: x 1000 Diluição: 1
Localização: Núcleo Luz: Branca / Verde

Observações: Ampliação da Fotografia 10.
Particula ferrosa de desgaste de abrasão com grandes dimensões.

234

Os resultados apresentados referem-se exclusivamente às amostras ensaiadas.
Este documento não pode ser reproduzido, total ou parcialmente, sem a autorização por escrito do INEGI.

CLIENTE: ***INEGI***	MÁQUINA: Máquina de Ensaios FZG
MORADA: Porto	Ref. ÓLEO: Bio-GearOil (E2) Low Oil
DATA: 13/10/10	ENSAIOS FZG - Steel Gears 311 K7

Fotografia 13

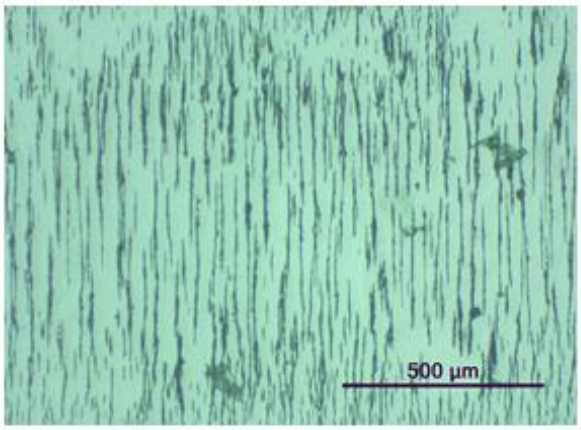

Ampliação: x 100 Diluição: 1
Localização: Núcleo Luz: Branca / Verde

Observações: Presença significativa de particulas ferrosas de pequenas dimensões.

Fotografia 14

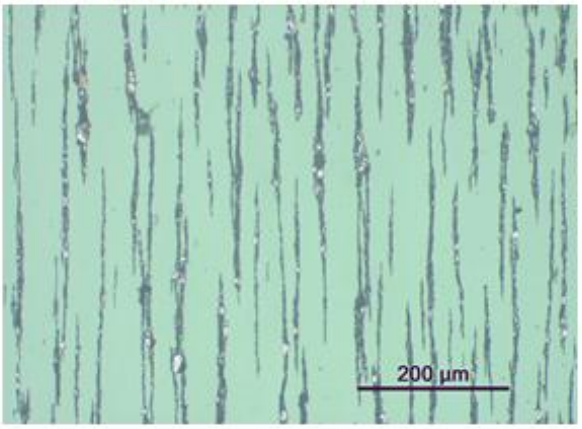

Ampliação: x 200 Diluição: 1
Localização: Núcleo Luz: Branca / Verde

Observações: Ampliação da Fotografia 13. Presença significativa de particulas ferrosas de pequenas dimensões. Ausencia de particulas de grandes dimensões.

Fotografia 15

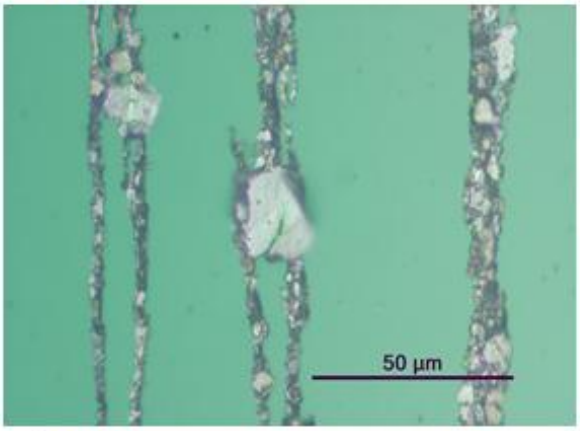

Ampliação: x 1000 Diluição: 1
Localização: Núcleo Luz: Branca / Verde

Observações: Ampliação da Fotografia 14. Particulas ferrosas de pequenas dimensões e algumas de média dimensão.

Fotografia 16

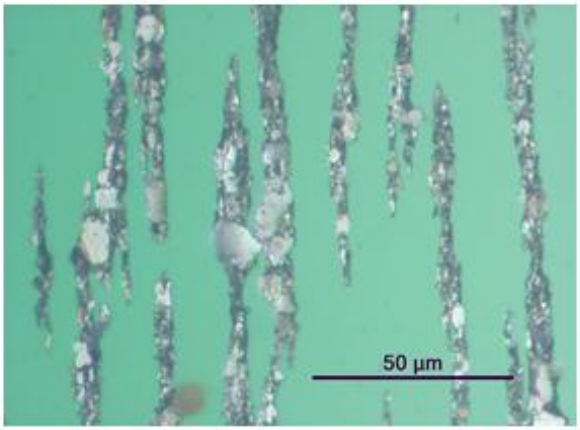

Ampliação: x 1000 Diluição: 1
Localização: Núcleo Luz: Branca / Verde

Observações: Ampliação da Fotografia 14. Partículas ferrosas de pequenas dimensões.

235

Este documento não pode ser reproduzido, total ou parcialmente, sem a autorização por escrito do INEGI.

CLIENTE: *INEGI*	MÁQUINA: Máquina de Ensaios FZG
MORADA: Porto	Ref. ÓLEO: Bio-GearOil (E2) Low Oil
DATA: 13/10/10	ENSAIOS FZG - Steel Gears 311 K9

Fotografia 17

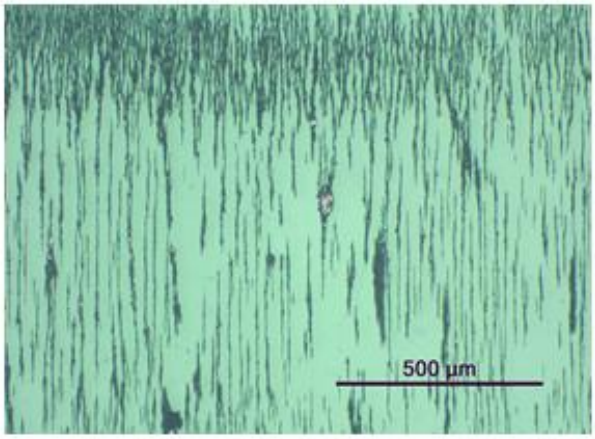

Ampliação: x 100 Diluição: 1
Localização: Núcleo Luz: Branca / Verde

Observações: Presença significativa de partículas ferrosas de pequenas dimensões.

Fotografia 18

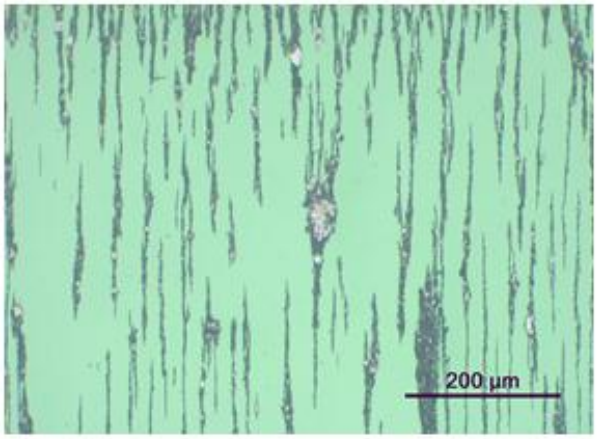

Ampliação: x 200 Diluição: 1
Localização: Núcleo Luz: Branca / Verde

Observações: Ampliação da Fotografia 17. Presença significativa de partículas ferrosas de pequenas dimensões. Presença de poucas de grandes dimensões.

Fotografia 19

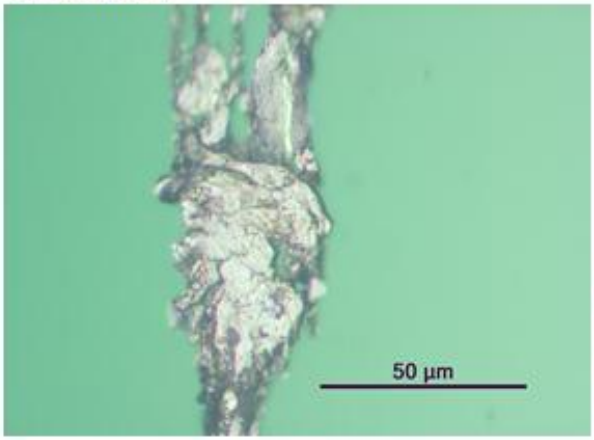

Ampliação: x 1000 Diluição: 1
Localização: Núcleo Luz: Branca / Verde

Observações: Ampliação da Fotografia 14. Particula ferrosa de grandes dimensões típica de desgaste de abrasão.

236

Fotografia 20

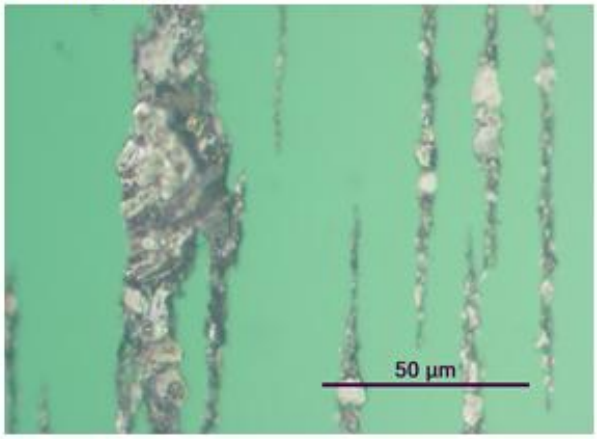

Ampliação: x 1000 Diluição: 1
Localização: Núcleo Luz: Branca / Verde

Observações: Ampliação da Fotografia 14. Partículas ferrosas de grandes dimensões típicas de desgaste de abrasão.

Os resultados apresentados referem-se exclusivamente às amostras ensaiadas.
Este documento não pode ser reproduzido, total ou parcialmente, sem a autorização por escrito do INEGI.

Relatório
de
Análise de Lubrificantes

Análise nº: Tipo de análise: Confidencialidade:	62 -66 / 10 Ferrometria e Ferrografia Analítica 1
Cliente: Morada: Telefone / Fax:	INEGI - Cetrib Porto
Equipamento: Lubrificante: Dossier:	FZG (20MnCr5 – 411 Labo B) Bio-GearOil (E2) /
Nº de páginas: Data:	5 27/10/10
Responsável: Rúbrica:	Beatriz Graça – Jorge Seabra

Os resultados apresentados referem-se exclusivamente às amostras ensaiadas.
Este documento não pode ser reproduzido, total ou parcialmente, sem a autorização por escrito do INEGI.

OBJECTIVO

Análise de cinco amostras de óleo lubrificante E2 resultantes de ensaios na Máquina FZG com engrenagens de aço (20MnCr5), para avaliação do desgaste presente.

As amostras analisadas foram as seguintes:

Ensaio	Estágio	Análises efectuadas	
		Ferrometria	Ferrografia Analítica
PLoss HO	Chap. K1	X	X
PLoss LO	Chap. K1	X	X
PLoss LO	K5	X	X
PLoss LO	K7	X	X
PLoss LO	K9	X	X

RESULTADOS DAS ANÁLISES

Nas páginas seguintes são apresentados os resultados referentes às análises de Ferrometria (DR III) e Ferrografia Analítica (FM III).

Os resultados apresentados referem-se exclusivamente às amostras ensaiadas.
Este documento não pode ser reproduzido, total ou parcialmente, sem a autorização por escrito do INEGI.

	CLIENTE: ***INEGI***			MÁQUINA: Máquina de Ensaios FZG			
	MORADA: Porto			Ref. ÓLEO: Bio-GearOil (E2)			
	DATA: 22/10/10			ENSAIOS FZG - 20MnCr5 Gears 411 Lado B			
IDENTIFICAÇÃO							
Ensaio:	PL Chap.	PL Chap.	PLoss	PLoss	PLoss		
Data amostra:	Out-10	Out-10	Out-10	Out-10	Out-10		
Análise nº:	62/10	63/10	64/10	65/10	66/10		
Estágio:	K1	K1	K5	K7	K9		
Lubrificante:	High Oil	Low Oil	Low Oil	Low Oil	Low Oil		
FERROMETRIA							
d:	1	1	1	1	1		
DL:	45,5	35,0	46,6	48,0	57,2		
DS:	15,9	15,5	23,4	19,7	26,4		
CPUC:	61,4	50,5	70,0	67,7	83,6		
ISUC:	1817,4	984,8	1624,0	1915,9	2574,9		
FERROGRAFIA:							
Desgaste normal							
Desgaste severo							
Desgaste abrasão							
Desgaste combinado							
Desgaste fadiga							
Esferas Metálicas							
Ligas não ferrosas							
Óxidos de ferro							
Minerais/Orgânicos							
OILVIEW:							
Índice OilLife:							
Índice Oxidação:							
Índice Contaminação:							
Índice Ferromagnético:							
Grandes Contaminantes:							
Constante Dieléctrica:							
FILTRAGEM							
(Nº Partículas/10 ml)							
5 - 15 µm							
15 - 25 µm							
25 - 50 µm							
50 - 100 µm							
> 100 µm							
VISCOSIDADE							
(cSt a 40° C):							
ACIDEZ (TAN)							
(mg KOH)							
P. INFLAMAÇÃO							
(° C)							
DIAGNÓSTICO:							

LEGENDA	**DL** - Índice de partículas grandes		Não existe
	DS - Índice de partículas pequenas	**f**	Fraco
	CPUC - Concentração part. de desgaste	**M**	Médio
	ISUC - Índice Severidade de Desgaste	**F**	Forte

Os resultados apresentados referem-se exclusivamente às amostras ensaiadas.
Este documento não pode ser reproduzido, total ou parcialmente, sem a autorização por escrito do INEGI.

CLIENTE: ***INEGI***	MÁQUINA: Máquina de Ensaios FZG
MORADA: Porto	Ref. ÓLEO: Bio-GearOil (E2) Chap. High Oil
DATA: 22/10/10	ENSAIOS FZG - Gears 411 Lado B - K1

Fotografia 1

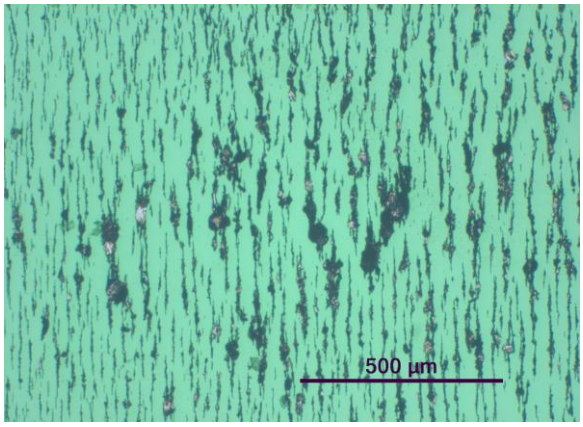

Ampliação: x 100 Diluição: 1
Localização: Núcleo Luz: Branca / Verde

Observações: Presença de partículas ferrosas de pequenas dimensões e grandes dimensões.

Fotografia 2

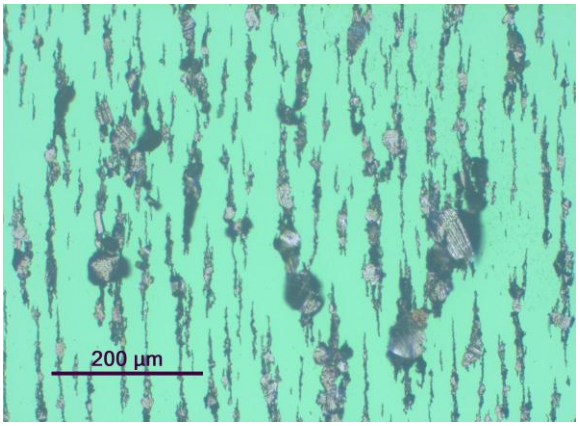

Ampliação: x 200 Diluição: 1
Localização: Núcleo Luz: Branca / Verde

Observações: Ampliação da Fotografia 1. Presença de partículas ferrosas de grandes dimensões e oxidadas

Fotografia 3

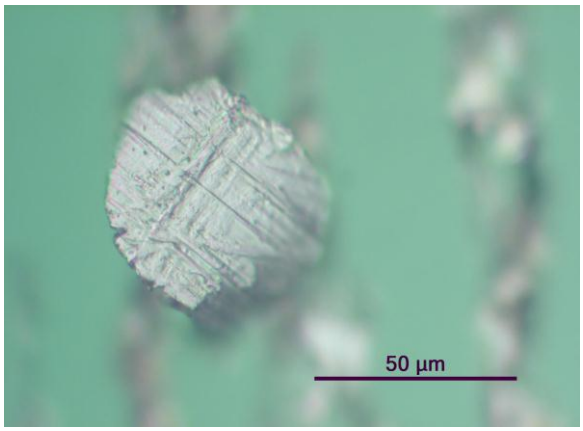

Ampliação: x 1000 Diluição: 1
Localização: Núcleo Luz: Branca / Verde

Observações: Ampliação da Fotografia 2. Partícula ferrosa laminar, típica de desgaste combinado (fadiga + escorregamento).

Fotografia 4

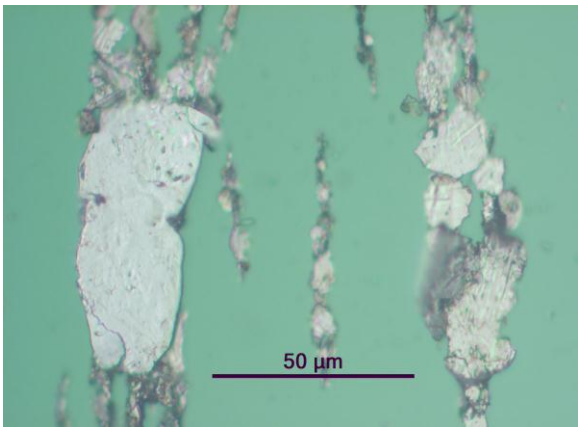

Ampliação: x 1000 Diluição: 1
Localização: Núcleo Luz: Branca / Verde

Observações: Partículas laminares típicas de desgaste de fadiga.

240

Os resultados apresentados referem-se exclusivamente às amostras ensaiadas.
Este documento não pode ser reproduzido, total ou parcialmente, sem a autorização por escrito do INEGI.

CLIENTE: ***INEGI***	MÁQUINA: Máquina de Ensaios FZG
MORADA: Porto	Ref. ÓLEO: Bio-GearOil (E2) Chap. Low Oil
DATA: 22/10/10	ENSAIOS FZG - Gears 411 Lado B - K1

Fotografia 5

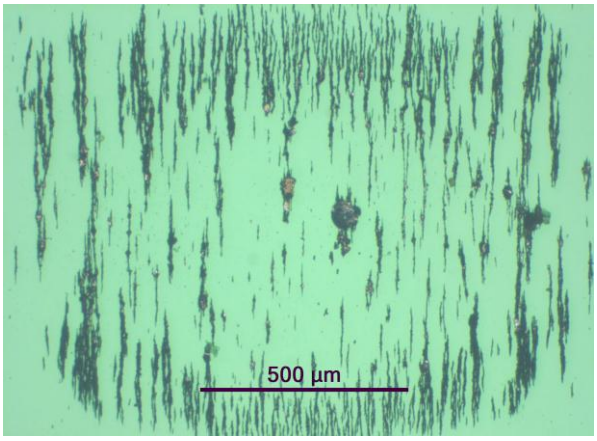

Ampliação: x 100 Diluíção: 1
Localização: Núcleo Luz: Branca / Verde

Observações: Presença de partículas ferrosas de pequenas e algumas de grandes dimensões.

Fotografia 6

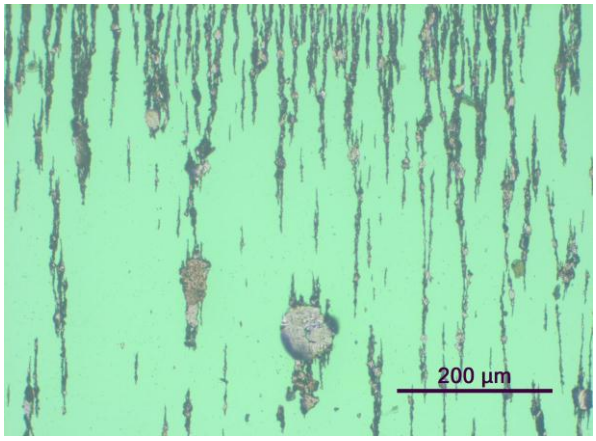

Ampliação: x 200 Diluíção: 1
Localização: Núcleo Luz: Branca / Verde

Observações: Ampliação da Fotografia 5. Presença de partículas ferrosas de pequenas e algumas de grandes dimensões.

Fotografia 7

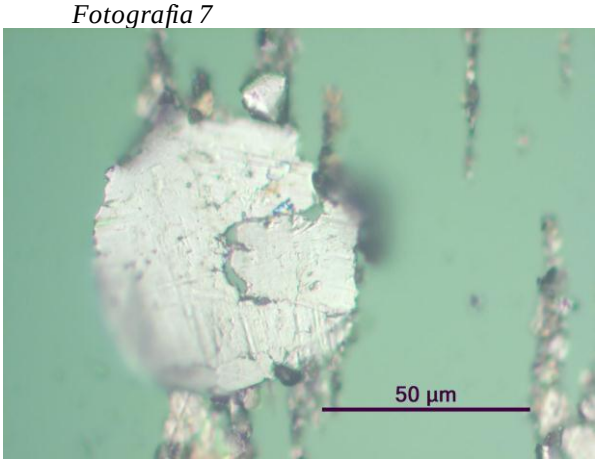

Ampliação: x 1000 Diluíção: 1
Localização: Núcleo Luz: Branca / Verde

Observações: Ampliação da Fotografia 6. Partícula ferrosa de desgaste de fadiga com grandes dimensões.

Fotografia 8

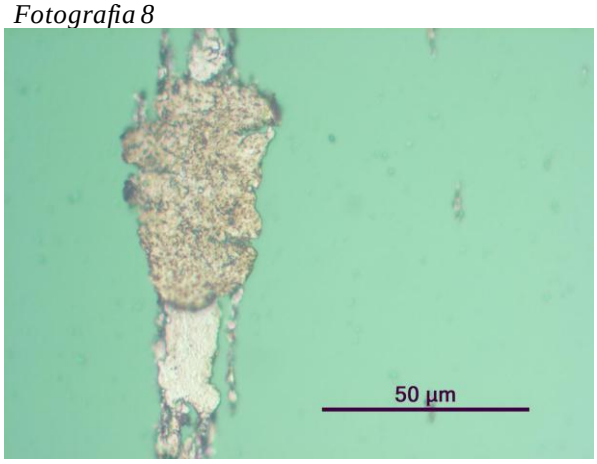

Ampliação: x 1000 Diluíção: 1
Localização: Núcleo Luz: Branca / Verde

Observações: Ampliação da Fotografia 6. Partícula ferrosa de desgaste de fadiga com grandes dimensões e ligeiramente oxidada.

Os resultados apresentados referem-se exclusivamente às amostras ensaiadas.
Este documento não pode ser reproduzido, total ou parcialmente, sem a autorização por escrito do INEGI.

CLIENTE: ***INEGI***	MÁQUINA: Máquina de Ensaios FZG
MORADA: Porto	Ref. ÓLEO: Bio-GearOil (E2)
DATA: 22/10/10	ENSAIOS FZG - Gears 411 Lado B - K5

Fotografia 9

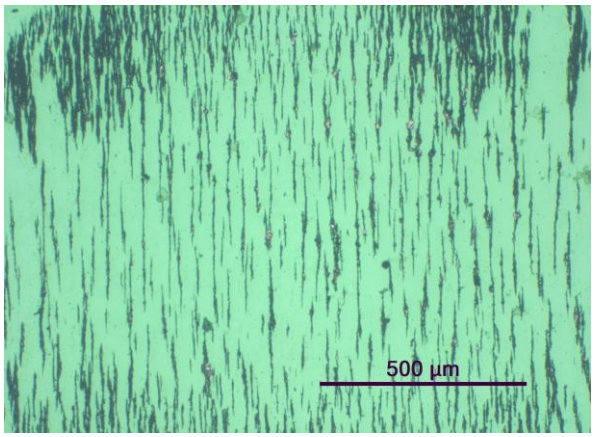

Ampliação: x 100 Diluição: 1
Localização: Núcleo Luz: Branca / Verde

Observações: Presença de partículas ferrosas de pequenas dimensões e poucas de grandes dimensões.

Fotografia 10

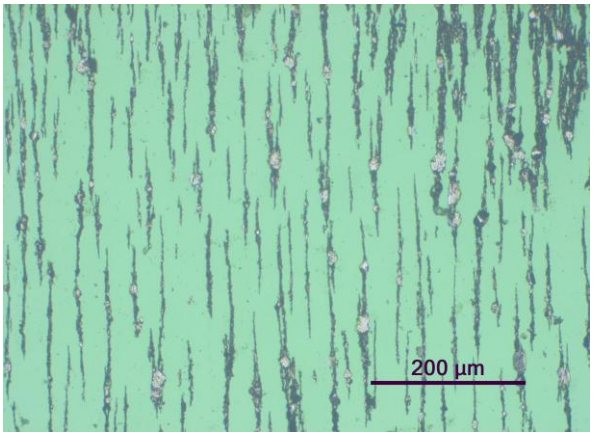

Ampliação: x 200 Diluição: 1
Localização: Núcleo Luz: Branca / Verde

Observações: Ampliação da Fotografia 9. Presença de poucas partículas ferrosas de grandes dimensões.

Fotografia 11

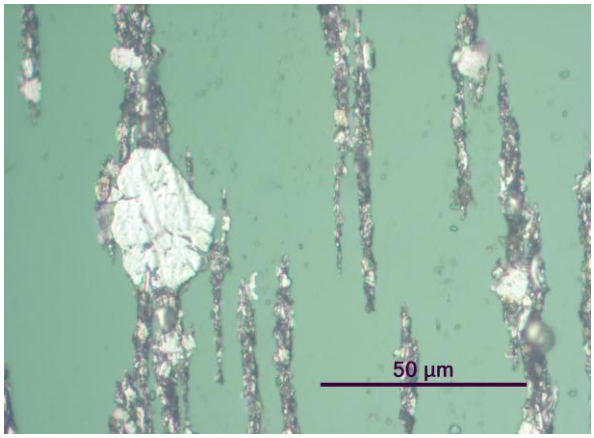

Ampliação: x 1000 Diluição: 1
Localização: Núcleo Luz: Branca / Verde

Observações: Ampliação da Fotografia 10. Partícula ferrosa de desgaste de fadiga com grandes dimensões.

Fotografia 12

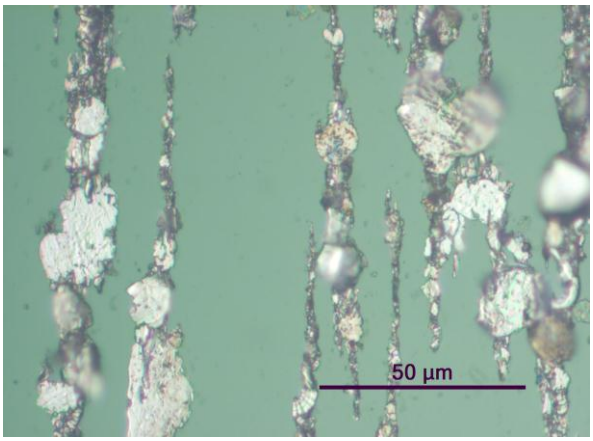

Ampliação: x 1000 Diluição: 1
Localização: Núcleo Luz: Branca / Verde

Observações: Ampliação da Fotografia 10. Partículas ferrosas de desgaste de fadiga de médias dimensões.

242

Os resultados apresentados referem-se exclusivamente às amostras ensaiadas.
Este documento não pode ser reproduzido, total ou parcialmente, sem a autorização por escrito do INEGI.

CLIENTE: ***INEGI***	MÁQUINA: Máquina de Ensaios FZG
MORADA: Porto	Ref. ÓLEO: Bio-GearOil (E2) Low Oil
DATA: 22/10/10	ENSAIOS FZG - Gears 411 Lado B - K7

Fotografia 13

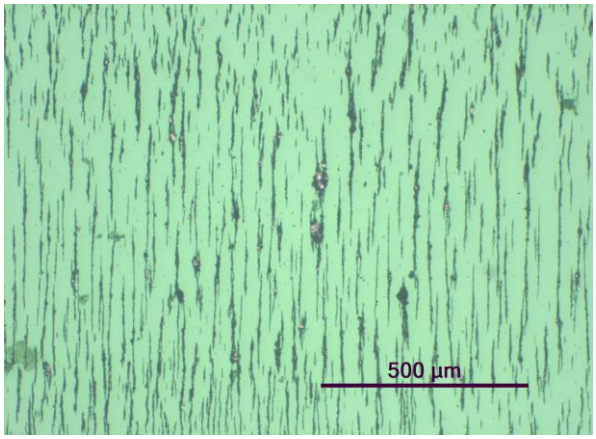

Ampliação: x 100 Diluição: 1
Localização: Núcleo Luz: Branca / Verde

Observações: Presença de partículas ferrosas de pequenas dimensões e algumas de grandes dimensões.

Fotografia 14

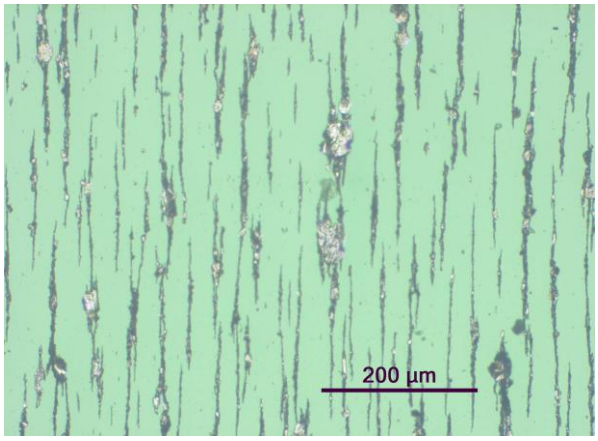

Ampliação: x 200 Diluição: 1
Localização: Núcleo Luz: Branca / Verde

Observações: Ampliação da Fotografia 13. Presença de partículas ferrosas de pequenas dimensões e algumas de grandes dimensões.

Fotografia 15

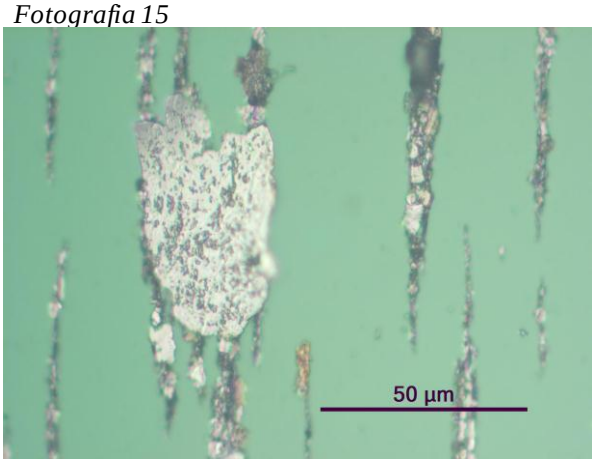

Ampliação: x 1000 Diluição: 1
Localização: Núcleo Luz: Branca / Verde

Observações: Ampliação da Fotografia 14. Partícula ferrosa de desgaste de fadiga com grandes dimensões.

Fotografia 16

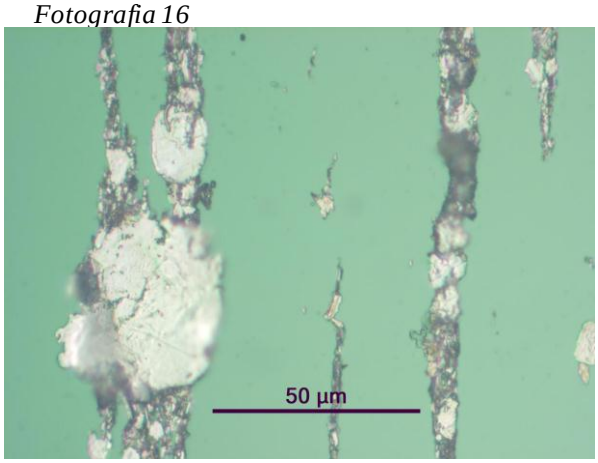

Ampliação: x 1000 Diluição: 1
Localização: Núcleo Luz: Branca / Verde

Observações: Ampliação da Fotografia 14. Partícula ferrosa de desgaste de fadiga com grandes dimensões.

Os resultados apresentados referem-se exclusivamente às amostras ensaiadas.
Este documento não pode ser reproduzido, total ou parcialmente, sem a autorização por escrito do INEGI.

CLIENTE: ***INEGI***	MÁQUINA: Máquina de Ensaios FZG
MORADA: Porto	Ref. ÓLEO: Bio-GearOil (E2) Low Oil
DATA: 22/10/10	ENSAIOS FZG - Gears 411 Lado B - K9

Fotografia 17

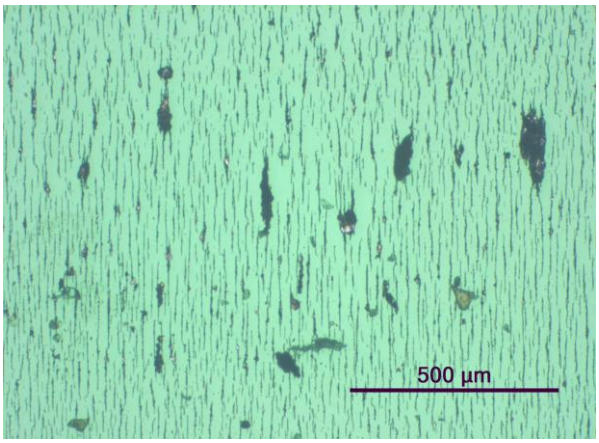

Ampliação: x 100 Diluição: 1
Localização: Núcleo Luz: Branca / Verde

Observações: Presença de partículas ferrosas de pequenas dimensões e grandes dimensões.

Fotografia 18

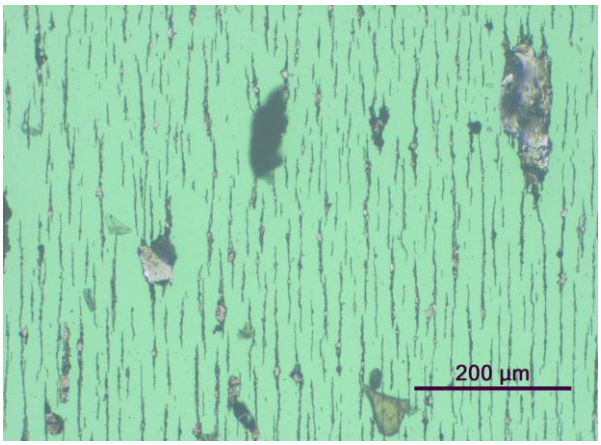

Ampliação: x 200 Diluição: 1
Localização: Núcleo Luz: Branca / Verde

Observações: Ampliação da Fotografia 17. Presença de partículas ferrosas de pequenas dimensões e grandes dimensões, algumas severamente oxidadas.

Fotografia 19

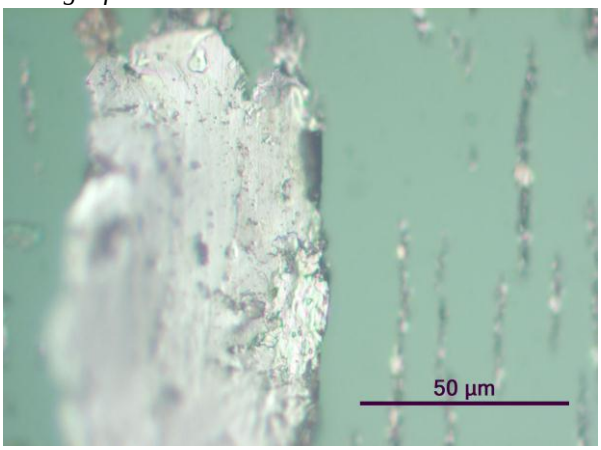

Ampliação: x 1000 Diluição: 1
Localização: Núcleo Luz: Branca / Verde

Observações: Ampliação da Fotografia 17. Partícula ferrosa de muito grandes dimensões (200µm) típica de desgaste de fadiga.

Fotografia 20

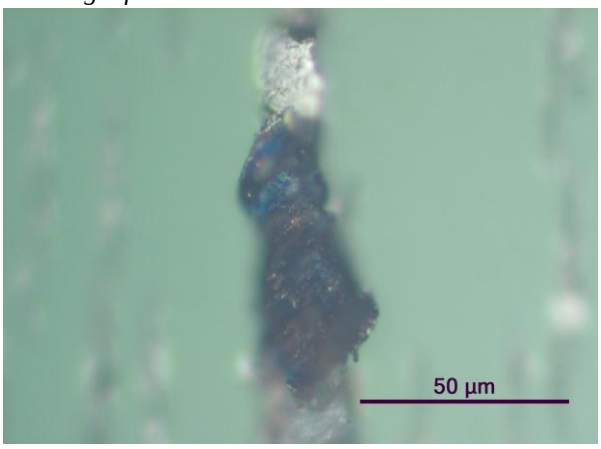

Ampliação: x 1000 Diluição: 1
Localização: Núcleo Luz: Branca / Verde

Observações: Ampliação da Fotografia 17. Partícula ferrosa de grandes dimensões e termicamente oxidada.

Os resultados apresentados referem-se exclusivamente às amostras ensaiadas.
Este documento não pode ser reproduzido, total ou parcialmente, sem a autorização por escrito do INEGI.

Relatório
de
Análise de Lubrificantes

Análise nº: Tipo de análise: Confidencialidade:	69 74 / 10 Ferrometria e Ferrografia Analítica 1
Cliente: Morada: Telefone / Fax:	INEGI - Cetrib Porto
Equipamento: Lubrificante: Dossier:	FZG (20MnCr5 – 611 Labo B) Bio-GearOil (E2) /
Nº de páginas: Data:	5 03/11/10
Responsável: Rúbrica:	Beatriz Graça – Jorge Seabra

Os resultados apresentados referem-se exclusivamente às amostras ensaiadas.
Este documento não pode ser reproduzido, total ou parcialmente, sem a autorização por escrito do INEGI.

OBJECTIVO

Análise de cinco amostras de óleo lubrificante E2 resultantes de ensaios na Máquina FZG com engrenagens de aço (20MnCr5), para avaliação do desgaste presente.

Algumas amostras - K5*, K7* e K9*, foram recolhidas a meio do ensaio para avaliar o efeito da sedimentação das partículas.

As amostras analisadas foram as seguintes:

Ensaio	Estágio	Análises efectuadas	
		Ferrometria	Ferrografia Analítica
PLoss HO	Chap. K1	X	X
PLoss LO	Chap. K1	X	X
PLoss LO	K5*	X	X
PLoss LO	K7*	X	X
PLoss LO	K9*	X	X
PLoss LO	K9	X	X

RESULTADOS DAS ANÁLISES

Nas páginas seguintes são apresentados os resultados referentes às análises de Ferrometria (DR III) e Ferrografia Analítica (FM III).

Os resultados apresentados referem-se exclusivamente às amostras ensaiadas.
Este documento não pode ser reproduzido, total ou parcialmente, sem a autorização por escrito do INEGI.

	CLIENTE: ***INEGI***			MÁQUINA: Máquina de Ensaios FZG			
	MORADA: Porto			Ref. ÓLEO: Bio-GearOil (E2)			
	DATA: 02/11/10			ENSAIOS FZG - 20MnCr5 Gears 611 Lado B			
IDENTIFICAÇÃO							
Ensaio:	PL Chap.	PL Chap.	Ploss*	Ploss*	Ploss*	Ploss	
Data amostra:	Out-10	Out-10	Out-10	Out-10	Out-10	Out-10	
Análise nº:	69/10	70/10	71/10	72/10	73/10	74/10	
Estágio:	K1	K1	K5	K7	K9	K9	
Lubrificante:	High Oil	Low Oil	Low Oil	Low Oil	Low Oil	Low Oil	
FERROMETRIA							
d:	1	1	1	1	1	1	
DL:	30,4	30,7	40,7	43,2	47,9	40,2	
DS:	11,1	11,5	16,7	18,3	19,1	18,1	
CPUC:	41,5	42,2	57,4	61,5	67,0	58,3	
ISUC:	801,0	810,2	1377,6	1531,4	1929,6	1288,4	
FERROGRAFIA:							
Desgaste normal							
Desgaste severo							
Desgaste abrasão							
Desgaste combinado							
Desgaste fadiga							
Esferas Metálicas							
Ligas não ferrosas							
Óxidos de ferro							
Minerais/Orgânicos							
OILVIEW:							
Índice OilLife:							
Índice Oxidação:							
Índice Contaminação:							
Índice Ferromagnético:							
Grandes Contaminantes:							
Constante Dieléctrica:							
FILTRAGEM							
(Nº Partículas/10 ml)							
5 - 15 µm							
15 - 25 µm							
25 - 50 µm							
50 - 100 µm							
> 100 µm							
VISCOSIDADE							
(cSt a 40° C):							
ACIDEZ (TAN)							
(mg KOH)							
P. INFLAMAÇÃO							
(° C)							

DIAGNÓSTICO:

Ploss* - Amostra recolhida a meio do ensaio.

LEGENDA			
DL - Índice de partículas grandes		Não existe	
DS - Índice de partículas pequenas	f	Fraco	
CPUC - Concentração part. de desgaste	M	Médio	
ISUC - Índice Severidade de Desgaste	F	Forte	247

Os resultados apresentados referem-se exclusivamente às amostras ensaiadas.
Este documento não pode ser reproduzido, total ou parcialmente, sem a autorização por escrito do INEGI.

CLIENTE: ***INEGI***	MÁQUINA: Máquina de Ensaios FZG
MORADA: Porto	Ref. ÓLEO: Bio-GearOil (E2) Chap. High Oil
DATA: 02/11/10	ENSAIOS FZG - Gears 611 Lado B - K1

Fotografia 1

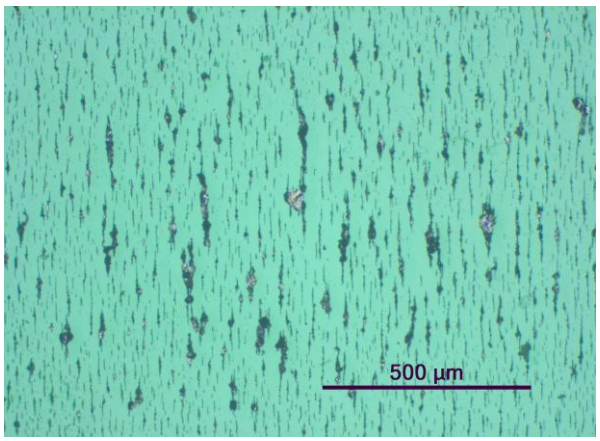

Ampliação: x 100 Diluição: 1
Localização: Núcleo Luz: Branca / Verde

Observações: Presença de partículas ferrosas de pequenas e grandes dimensões.

Fotografia 2

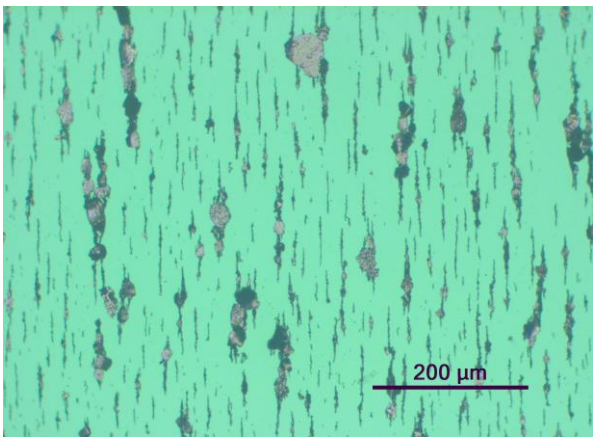

Ampliação: x 200 Diluição: 1
Localização: Núcleo Luz: Branca / Verde

Observações: Ampliação da Fotografia 1. Presença de partículas ferrosas, algumas de grandes dimensões.

Fotografia 3

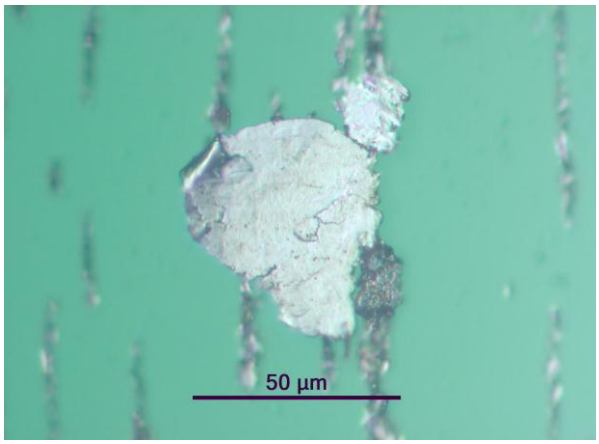

Ampliação: x 1000 Diluição: 1
Localização: Núcleo Luz: Branca / Verde

Observações: Ampliação da Fotografia 2. Partícula ferrosa laminar, típica de desgaste de fadiga.

Fotografia 4

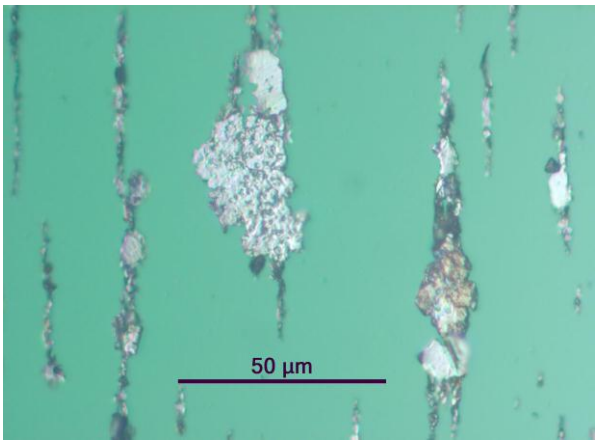

Ampliação: x 1000 Diluição: 1
Localização: Núcleo Luz: Branca / Verde

Observações: Ampliação da Fotografia 2. Partículas laminares típicas de desgaste de fadiga, algumas oxidadas.

248

Os resultados apresentados referem-se exclusivamente às amostras ensaiadas.
Este documento não pode ser reproduzido, total ou parcialmente, sem a autorização por escrito do INEGI.

CLIENTE: ***INEGI***	MÁQUINA: Máquina de Ensaios FZG
MORADA: Porto	Ref. ÓLEO: Bio-GearOil (E2) Chap. Low Oil
DATA: 02/11/10	ENSAIOS FZG - Gears 611 Lado B - K1

Fotografia 5

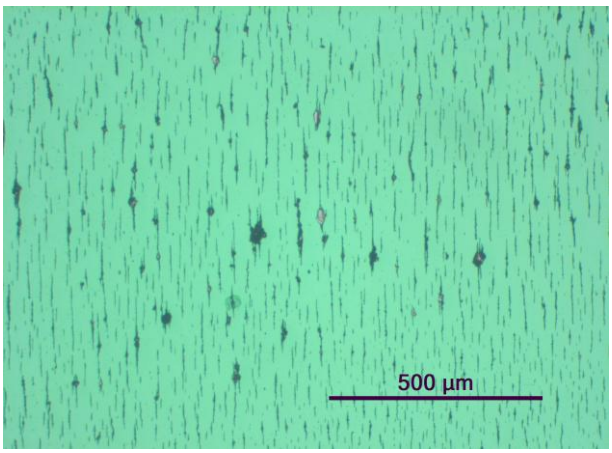

Ampliação: x 100 Diluição: 1
Localização: Núcleo Luz: Branca / Verde

Observações: Presença de partículas ferrosas de pequenas e algumas de grandes dimensões.

Fotografia 6

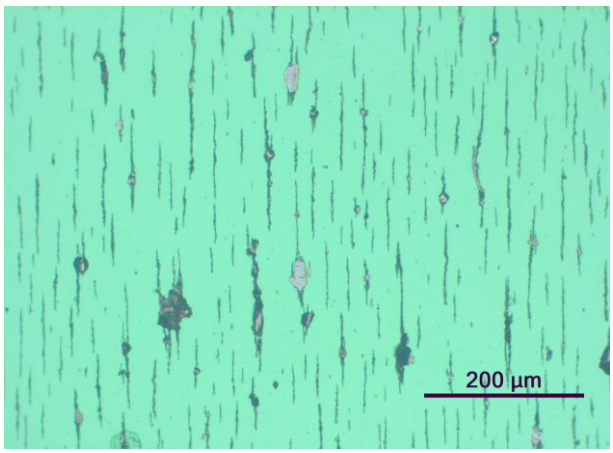

Ampliação: x 200 Diluição: 1
Localização: Núcleo Luz: Branca / Verde

Observações: Ampliação da Fotografia 5. Presença de partículas ferrosas de pequenas e algumas de grandes dimensões.

Fotografia 7

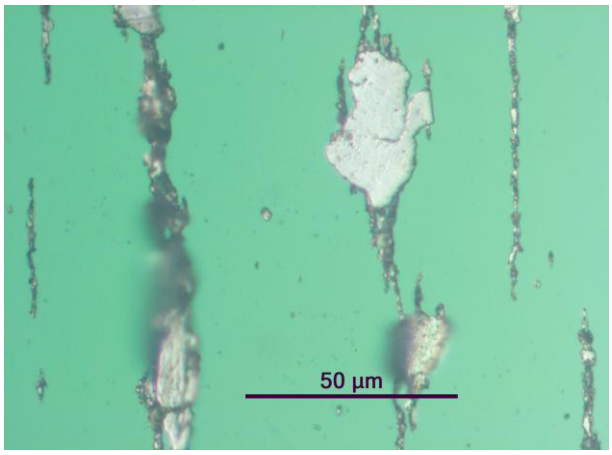

Ampliação: x 1000 Diluição: 1
Localização: Núcleo Luz: Branca / Verde

Observações: Ampliação da Fotografia 6. Partículas ferrosas de desgaste de fadiga com grandes dimensões.

Fotografia 8

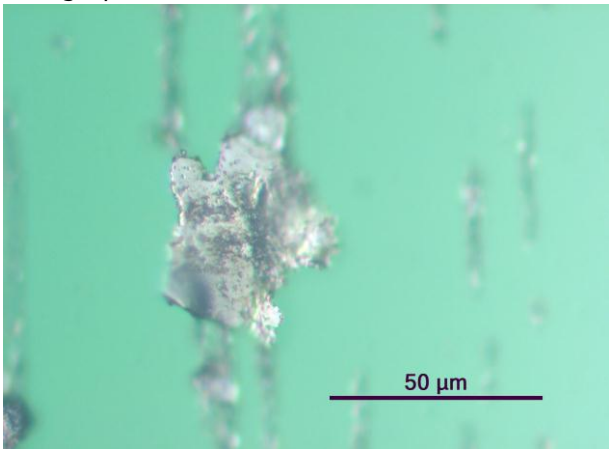

Ampliação: x 1000 Diluição: 1
Localização: Núcleo Luz: Branca / Verde

Observações: Ampliação da Fotografia 6. Partícula ferrosa de desgaste com grandes dimensões e ligeiramente oxidada.

Os resultados apresentados referem-se exclusivamente às amostras ensaiadas.
Este documento não pode ser reproduzido, total ou parcialmente, sem a autorização por escrito do INEGI.

CLIENTE: ***INEGI***	MÁQUINA: Máquina de Ensaios FZG
MORADA: Porto	Ref. ÓLEO: Bio-GearOil (E2)
DATA: 02/11/10	ENSAIOS FZG - Gears 611 Lado B - K5*

Fotografia 9

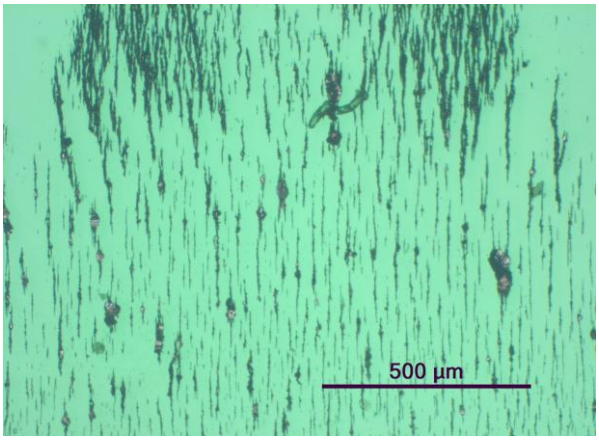

Ampliação: x 100 Diluição: 1
Localização: Núcleo Luz: Branca / Verde

Observações: Presença de partículas ferrosas de pequenas dimensões e de grandes dimensões.

Fotografia 10

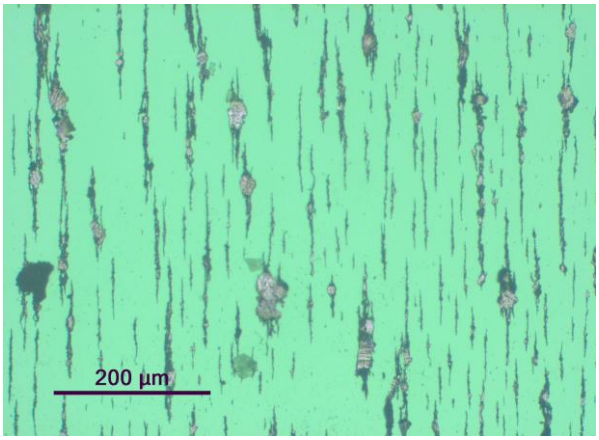

Ampliação: x 200 Diluição: 1
Localização: Núcleo Luz: Branca / Verde

Observações: Ampliação da Fotografia 9. Presença de partículas ferrosas, algumas de grandes dimensões.

Fotografia 11

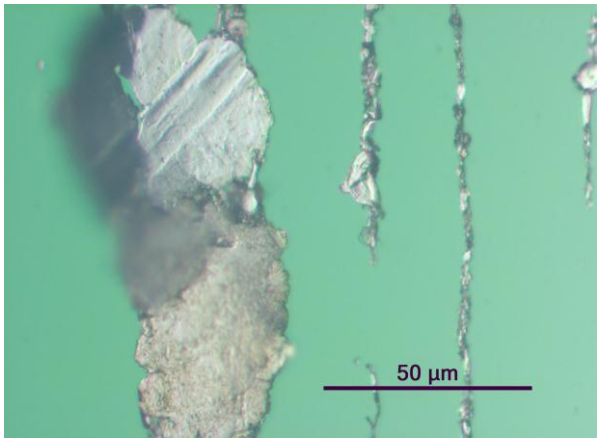

Ampliação: x 1000 Diluição: 1
Localização: Núcleo Luz: Branca / Verde

Observações: Ampliação da Fotografia 10. Partículas ferrosas de desgaste de fadiga e de grandes dimensões.

250

Fotografia 12

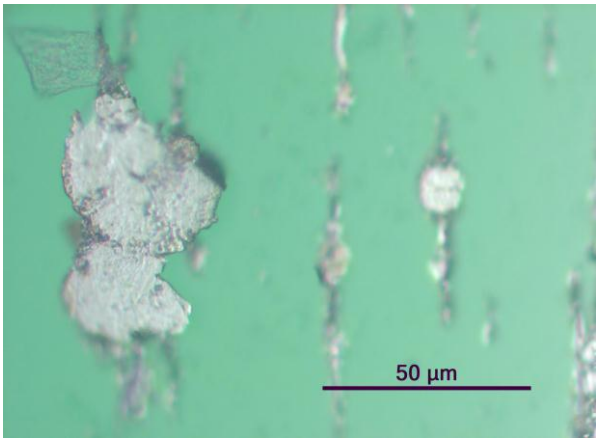

Ampliação: x 1000 Diluição: 1
Localização: Núcleo Luz: Branca / Verde

Observações: Ampliação da Fotografia 10. Partículas ferrosas de desgaste de fadiga de grandes dimensões.

Os resultados apresentados referem-se exclusivamente às amostras ensaiadas.
Este documento não pode ser reproduzido, total ou parcialmente, sem a autorização por escrito do INEGI.

CLIENTE: ***INEGI***	MÁQUINA: Máquina de Ensaios FZG
MORADA: Porto	Ref. ÓLEO: Bio-GearOil (E2) Low Oil
DATA: 02/11/10	ENSAIOS FZG - Gears 611 Lado B - K7*

Fotografia 13

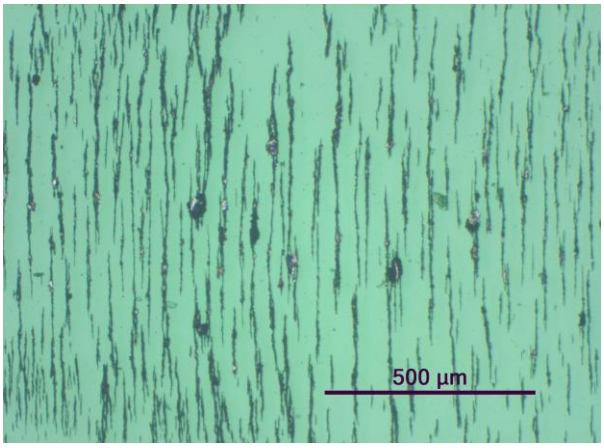

Ampliação: x 100 Diluição: 1
Localização: Núcleo Luz: Branca / Verde

Observações: Presença de partículas ferrosas de pequenas dimensões e algumas de grandes dimensões.

Fotografia 14

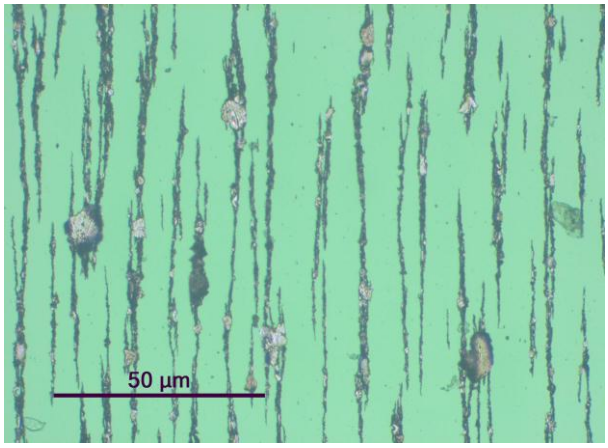

Ampliação: x 200 Diluição: 1
Localização: Núcleo Luz: Branca / Verde

Observações: Ampliação da Fotografia 13. Presença de partículas ferrosas de pequenas dimensões e algumas de grandes dimensões.

Fotografia 15

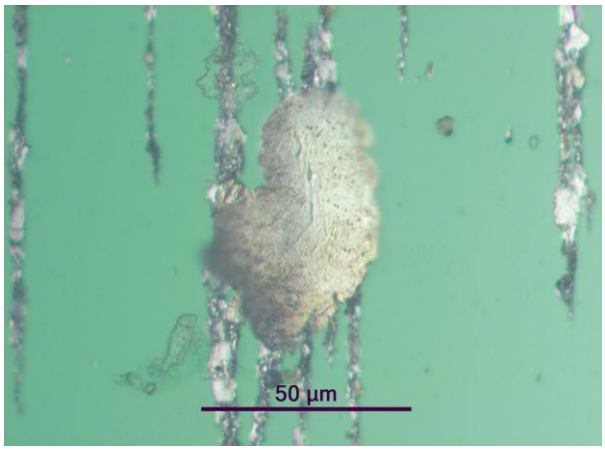

Ampliação: x 1000 Diluição: 1
Localização: Núcleo Luz: Branca / Verde

Observações: Ampliação da Fotografia 14. Partícula ferrosa de desgaste de fadiga com grandes dimensões e ligeiramente oxidada.

Fotografia 16

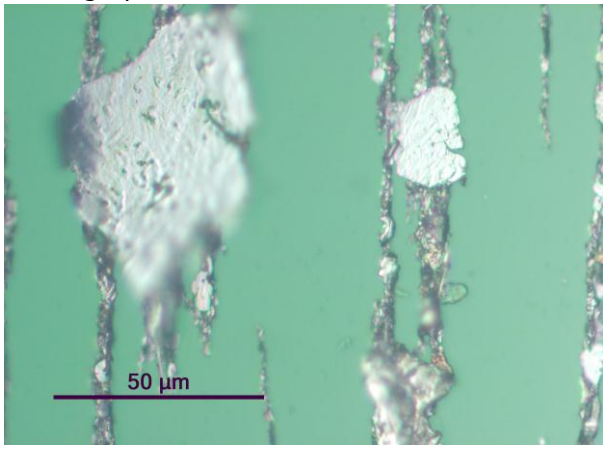

Ampliação: x 1000 Diluição: 1
Localização: Núcleo Luz: Branca / Verde

Observações: Ampliação da Fotografia 14. Partícula ferrosa de desgaste de fadiga com grandes dimensões.

Os resultados apresentados referem-se exclusivamente às amostras ensaiadas.
Este documento não pode ser reproduzido, total ou parcialmente, sem a autorização por escrito do INEGI.

CLIENTE: ***INEGI***	MÁQUINA: Máquina de Ensaios FZG
MORADA: Porto	Ref. ÓLEO: Bio-GearOil (E2) Low Oil
DATA: 02/11/10	ENSAIOS FZG - Gears 611 Lado B - K9*

Fotografia 17

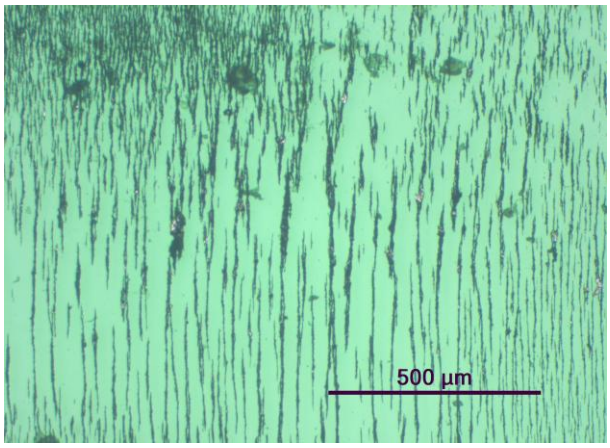

Ampliação: x 100 Diluição: 1
Localização: Núcleo Luz: Branca / Verde

Observações: Presença de partículas ferrosas de pequenas dimensões e algumas de grandes dimensões.

Fotografia 18

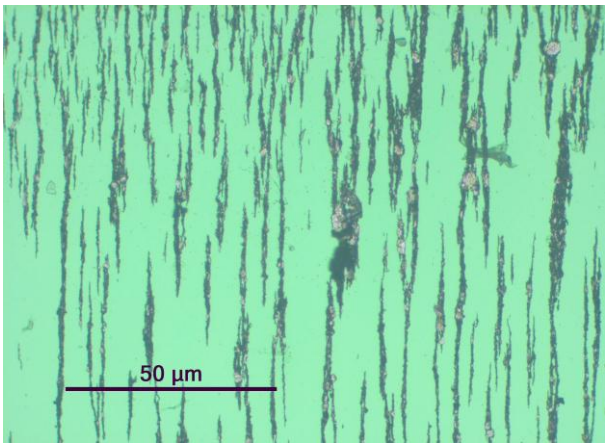

Ampliação: x 200 Diluição: 1
Localização: Núcleo Luz: Branca / Verde

Observações: Ampliação da Fotografia 17. Presença de partículas ferrosas de pequenas dimensões e algumas de grandes dimensões.

Fotografia 19

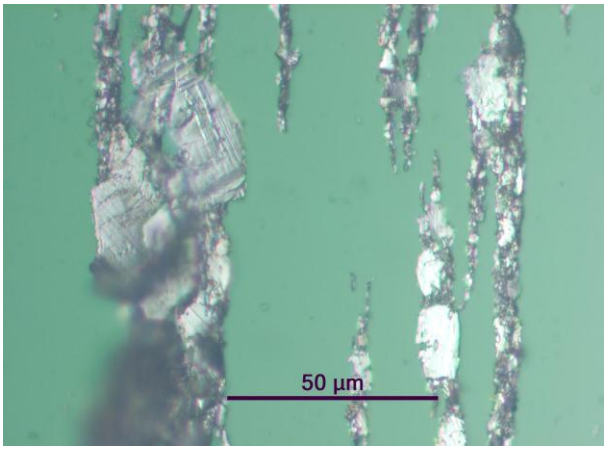

Ampliação: x 1000 Diluição: 1
Localização: Núcleo Luz: Branca / Verde

Observações: Ampliação da Fotografia 17. Partículas ferrosas de grandes dimensões e alguns óxidos termicos.

Fotografia 20

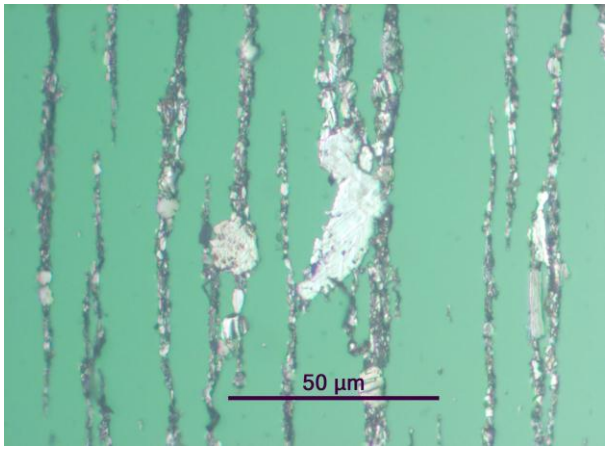

Ampliação: x 1000 Diluição: 1
Localização: Núcleo Luz: Branca / Verde

Observações: Ampliação da Fotografia 17. Partículas ferrosas de médias e grandes dimensões.

252

Os resultados apresentados referem-se exclusivamente às amostras ensaiadas.
Este documento não pode ser reproduzido, total ou parcialmente, sem a autorização por escrito do INEGI.

Relatório
de
Análise de Lubrificantes

Análise nº: Tipo de análise: Confidencialidade:	77, 83-87 / 10 Ferrometria e Ferrografia Analítica 1
Cliente: Morada: Telefone / Fax:	INEGI - Cetrib Porto
Equipamento: Lubrificante: Dossier:	FZG (ADI – 612) E2 /
Nº de páginas: Data:	7 22/12/10
Responsável: Rúbrica:	Beatriz Graça – Jorge Seabra

Os resultados apresentados referem-se exclusivamente às amostras ensaiadas.
Este documento não pode ser reproduzido, total ou parcialmente, sem a autorização por escrito do INEGI.

OBJECTIVO

Análise de cinco amostras de óleo lubrificante E2 resultantes de ensaios na Máquina FZG com engrenagens de ADI, para avaliação do desgaste presente.

As amostras analisadas foram as seguintes:

Amostra Nº	Ciclos	Análises efectuadas	
		Ferrometria	Ferrografia Analítica
K1 HO	-	X	X
K1 LO	-	X	X
K5*	-	X	X
K7	-	X	-
K9*	-	X	X
K9 Fim			

** - Amostras recolhidas no final do 1º ciclo de ensaio (1000 rpm) do correspondente estágio de carga.*

RESULTADOS DAS ANÁLISES

Nas páginas seguintes são apresentados os resultados referentes às análises de Ferrometria (DR III) e Ferrografia Analítica (FM III).

Os resultados apresentados referem-se exclusivamente às amostras ensaiadas.
Este documento não pode ser reproduzido, total ou parcialmente, sem a autorização por escrito do INEGI.

	CLIENTE: ***INEGI***			MÁQUINA: Máquina de Ensaios FZG			
	MORADA: Porto			Ref. ÓLEO: E2 - 612			
	DATA: 22/12/10			ENSAIOS FZG - ADI Gears			
IDENTIFICAÇÃO							
Amostra nº:	K1 HO	K1 LO	K5*	K7	K9	K9*	
Data amostra:	Dez-10	Dez-10	Dez-10	Dez-10	Dez-10	Dez-10	
Análise nº:	77/10	83/10	84/10	85/10	86/10	87/10	
Ciclos/Máquina:	-	-	-	-	-		
Ciclos/Óleo:	-	-	-	-	-		
FERROMETRIA							
d:	1	1	1	1	0,1	0,1	
DL:	41,2	38,9	57,0	74,8	44,7	25,7	
DS:	12,3	18,5	26,4	31,0	16,9	11,0	
CPUC:	53,5	57,4	83,4	105,8	616,0	367,0	
ISUC:	1,5E+03	1,2E+03	2,6E+03	4,6E+03	1,7E+05	5,4E+04	
FERROGRAFIA:							
Desgaste normal							
Desgaste severo							
Desgaste abrasão							
Desgaste combinado							
Desgaste fadiga							
Esferas Metálicas							
Ligas não ferrosas							
Óxidos de ferro							
Minerais/Orgânicos							
OILVIEW:							
Índice OilLife:							
Índice Oxidação:							
Índice Contaminação:							
Índice Ferromagnético:							
Grandes Contaminantes:							
Constante Dieléctrica:							
FILTRAGEM							
(Nº Partículas/10 ml)							
5 - 15 µm							
15 - 25 µm							
25 - 50 µm							
50 - 100 µm							
> 100 µm							
VISCOSIDADE							
(cSt a 40° C):							
ACIDEZ (TAN)							
(mg KOH)							
P. INFLAMAÇÃO							
(° C)							
DIAGNÓSTICO:							

LEGENDA	**DL** - Índice de partículas grandes		Não existe
	DS - Índice de partículas pequenas	**f**	Fraco
	CPUC - Concentração part. de desgaste	**M**	Médio
	ISUC - Índice Severidade de Desgaste	**F**	Forte

255

Os resultados apresentados referem-se exclusivamente às amostras ensaiadas.
Este documento não pode ser reproduzido, total ou parcialmente, sem a autorização por escrito do INEGI.

CLIENTE: ***INEGI***	MÁQUINA: Máquina de Ensaios FZG
MORADA: Porto	Ref. ÓLEO: E2 - 612
DATA: 22/12/10	ENSAIOS FZG - ADI Gears K1 HO

Fotografia 1

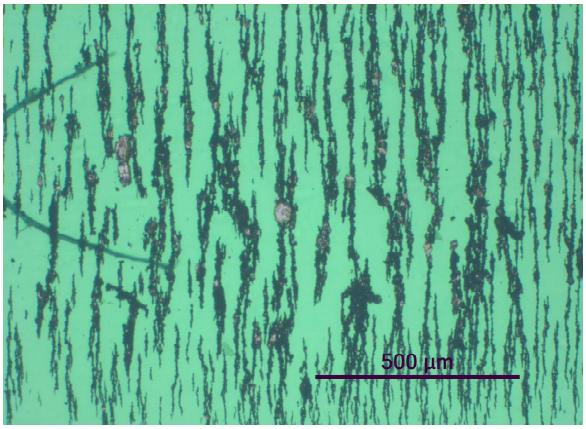

Ampliação: x 100 Diluição: 1
Localização: Núcleo Luz: Branca / Verde

Observações: Presença de partículas ferrosas de pequenas dimensões e algumas de grandes dimensões.

Fotografia 2

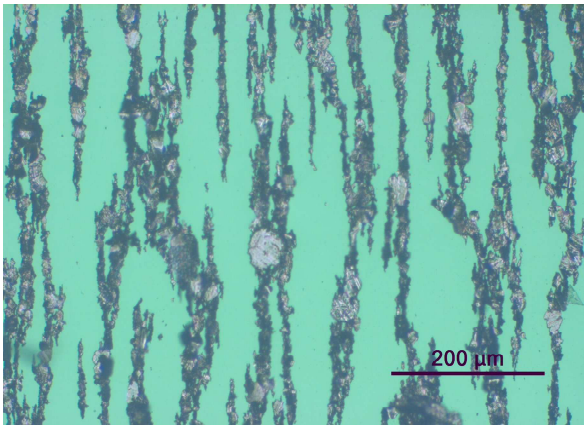

Ampliação: x 200 Diluição: 1
Localização: Núcleo Luz: Branca / Verde

Observações: Ampliação da Fotografia 1. Presença de partículas ferrosas de pequenas dimensões e algumas de grandes dimensões.

Fotografia 3

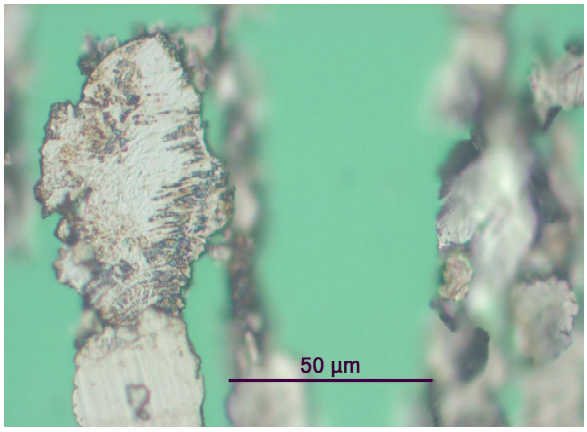

Ampliação: x 1000 Diluição: 1
Localização: Núcleo Luz: Branca / Verde

Observações: Ampliação da Fotografia 2. Partículas ferrosas laminares, algumas de grandes dimensões e ligeiramente oxidadas.

Fotografia 4

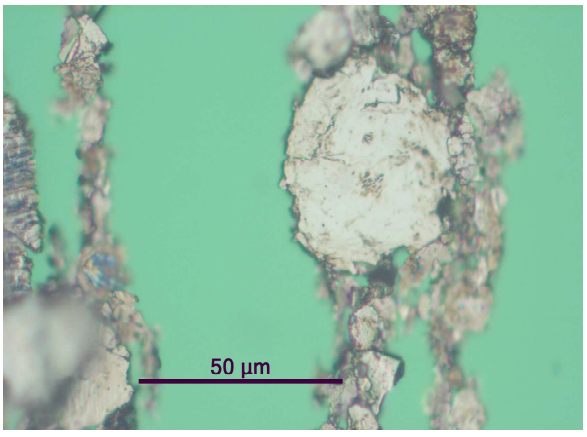

Ampliação: x 1000 Diluição: 1
Localização: Núcleo Luz: Branca / Verde

Observações: Ampliação da Fotografia 2. Partículas ferrosas laminares, algumas de grandes dimensões.

Os resultados apresentados referem-se exclusivamente às amostras ensaiadas.
Este documento não pode ser reproduzido, total ou parcialmente, sem a autorização por escrito do INEGI.

CLIENTE: ***INEGI***	MÁQUINA: Máquina de Ensaios FZG
MORADA: Porto	Ref. ÓLEO: E2 - 612
DATA: 22/12/10	ENSAIOS FZG - ADI Gears K1 LO

Fotografia 1

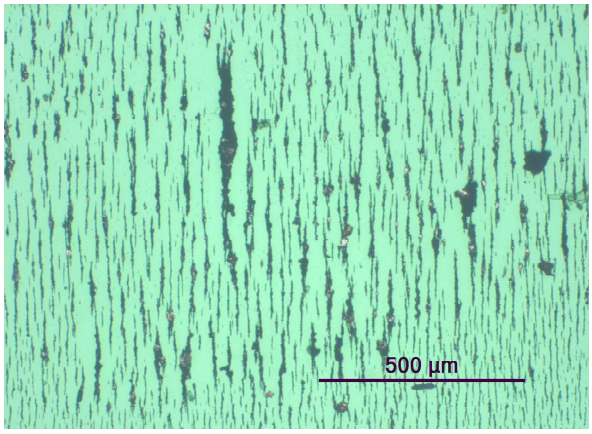

Ampliação: x 100 Diluição: 1
Localização: Núcleo Luz: Branca / Verde

Observações: Presença de partículas ferrosas de pequenas dimensões e algumas de grandes dimensões.

Fotografia 2

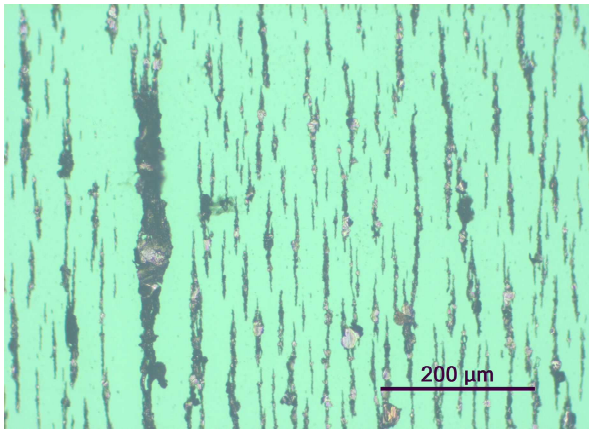

Ampliação: x 200 Diluição: 1
Localização: Núcleo Luz: Branca / Verde

Observações: Ampliação da Fotografia 1. Presença de partículas ferrosas de pequenas dimensões e algumas de grandes dimensões.

Fotografia 3

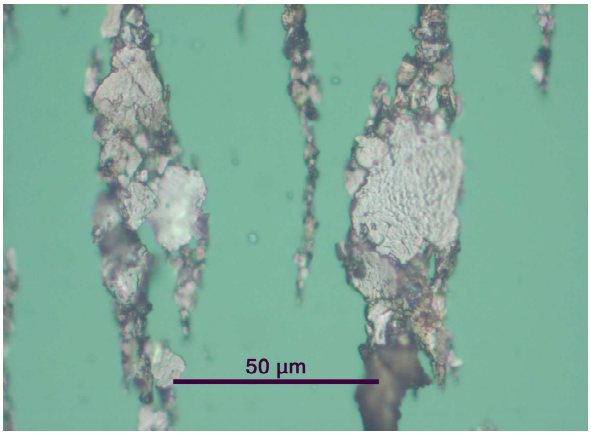

Ampliação: x 1000 Diluição: 1
Localização: Núcleo Luz: Branca / Verde

Observações: Ampliação da Fotografia 2. Partículas ferrosas laminares, algumas de grandes dimensões e ligeiramente oxidadas.

Fotografia 4

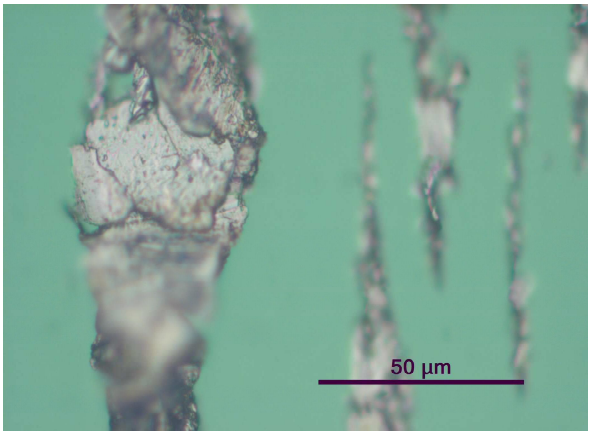

Ampliação: x 1000 Diluição: 1
Localização: Núcleo Luz: Branca / Verde

Observações: Ampliação da Fotografia 2. Partículas ferrosas laminares, algumas de grandes dimensões e ligeiramente oxidadas.

257

Os resultados apresentados referem-se exclusivamente às amostras ensaiadas.
Este documento não pode ser reproduzido, total ou parcialmente, sem a autorização por escrito do INEGI.

CLIENTE: ***INEGI***	MÁQUINA: Máquina de Ensaios FZG
MORADA: Porto	Ref. ÓLEO: E2 - 612
DATA: 22/12/10	ENSAIOS FZG - ADI Gears K5*

Fotografia 5

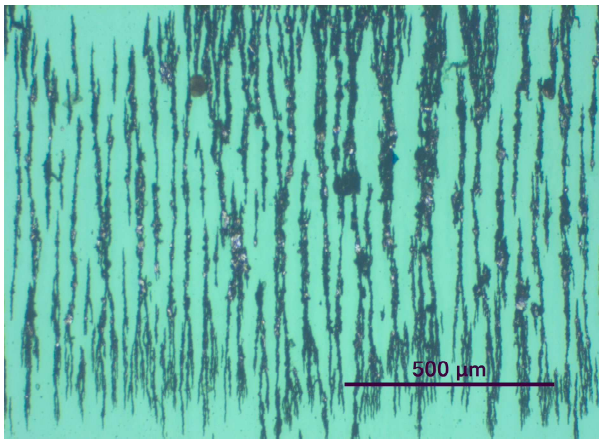

Ampliação: x 100 Diluição: 1
Localização: Núcleo Luz: Branca / Verde

Observações: Presença de partículas ferrosas de pequenas e grandes dimensões.

Fotografia 6

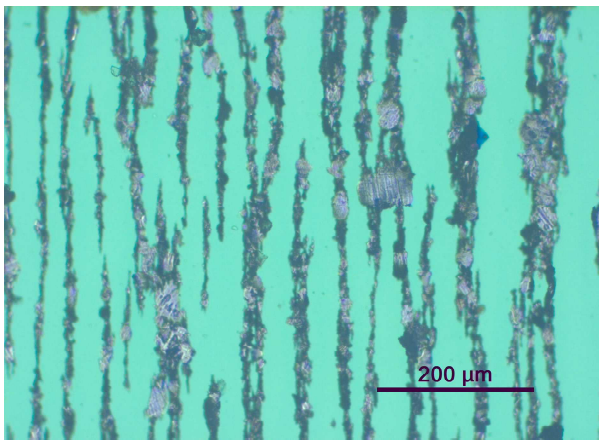

Ampliação: x 200 Diluição: 1
Localização: Núcleo Luz: Branca / Verde

Observações: Ampliação da Fotografia 5. Presença de partículas ferrosas de pequenas e grandes dimensões.

Fotografia 7

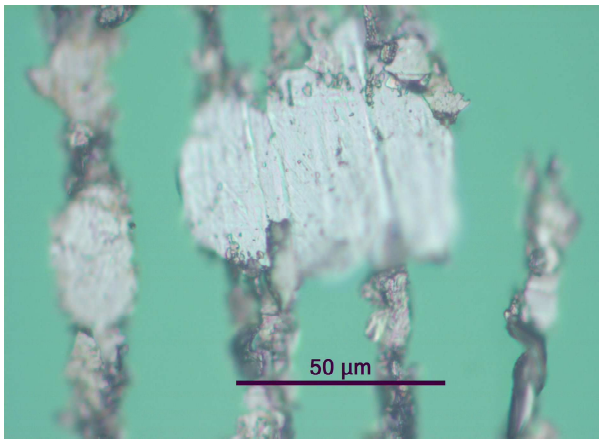

Ampliação: x 1000 Diluição: 1
Localização: Núcleo Luz: Branca / Verde

Observações: Ampliação da Fotografia 6. Partículas ferrosas laminares, algumas de grandes dimensões.

258

Fotografia 8

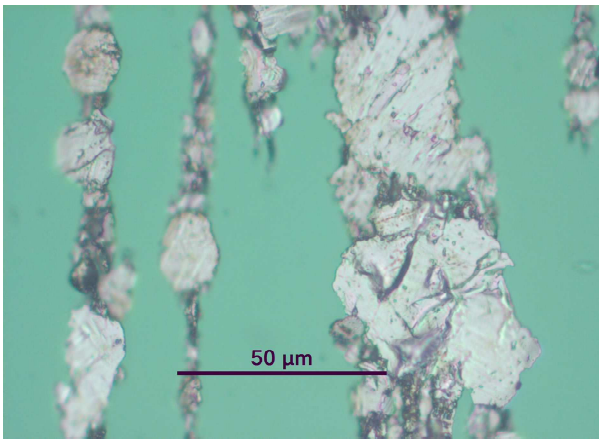

Ampliação: x 1000 Diluição: 1
Localização: Núcleo Luz: Branca / Verde

Observações: Ampliação da Fotografia 6. Partículas ferrosas laminares, algumas de grandes dimensões.

Os resultados apresentados referem-se exclusivamente às amostras ensaiadas.
Este documento não pode ser reproduzido, total ou parcialmente, sem a autorização por escrito do INEGI.

CLIENTE: ***INEGI***	MÁQUINA: Máquina de Ensaios FZG
MORADA: Porto	Ref. ÓLEO: E2 - 612
DATA: 22/12/10	ENSAIOS FZG - ADI Gears K7

Fotografia 9

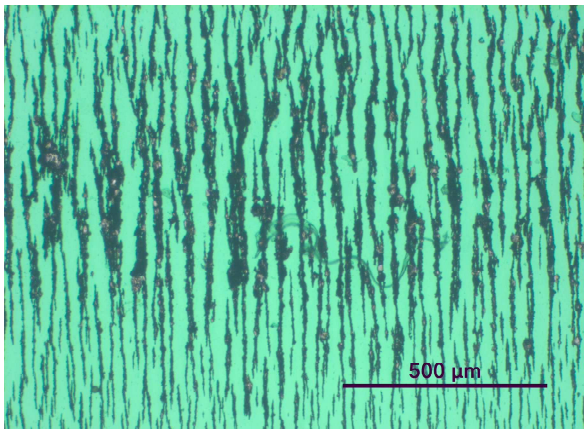

Ampliação: x 100 Diluição: 1
Localização: Núcleo Luz: Branca / Verde

Observações: Presença significativa de partículas ferrosas de pequenas e grandes dimensões.

Fotografia 10

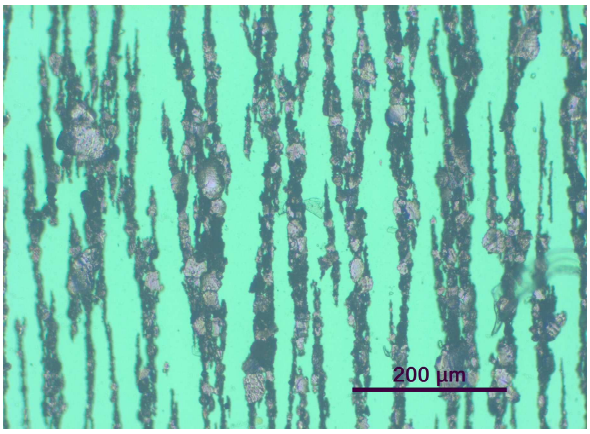

Ampliação: x 200 Diluição: 1
Localização: Núcleo Luz: Branca / Verde

Observações: Ampliação da Fotografia 9. Presença significativa de partículas ferrosas de pequenas e grandes dimensões.

Fotografia 11

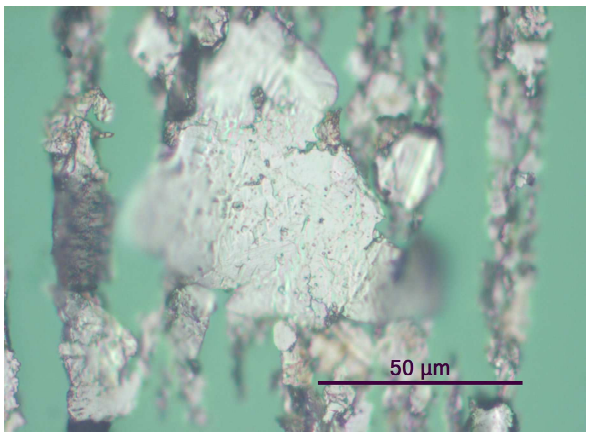

Ampliação: x 1000 Diluição: 1
Localização: Núcleo Luz: Branca / Verde

Observações: Ampliação da Fotografia 10. Partículas ferrosas de pequenas e grandes dimensões.

Fotografia 12

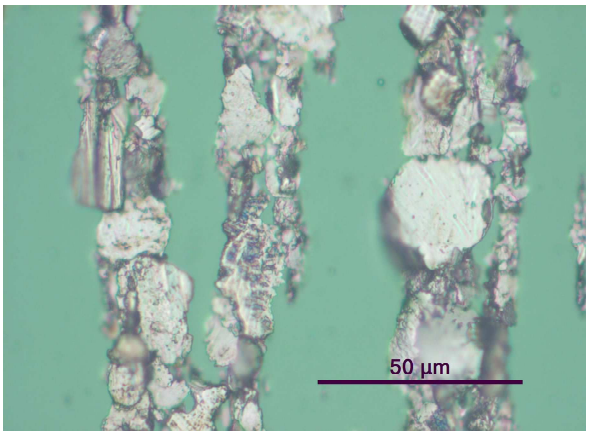

Ampliação: x 1000 Diluição: 1
Localização: Núcleo Luz: Branca / Verde

Observações: Ampliação da Fotografia 10. Partículas ferrosas de média dimensão, algumas oxidadas termicamente.

Os resultados apresentados referem-se exclusivamente às amostras ensaiadas.
Este documento não pode ser reproduzido, total ou parcialmente, sem a autorização por escrito do INEGI.

CLIENTE: ***INEGI***	MÁQUINA: Máquina de Ensaios FZG
MORADA: Porto	Ref. ÓLEO: E2 - 612
DATA: 22/12/10	ENSAIOS FZG - ADI Gears K9 (d=0,1)

Fotografia 13

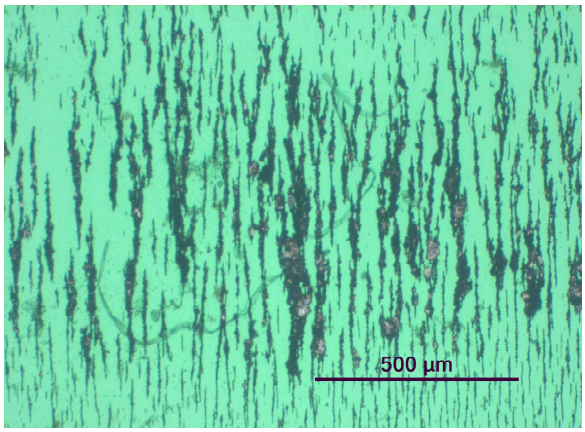

Ampliação: x 100 Diluição: 0,1
Localização: Núcleo Luz: Branca / Verde

Observações: Presença significativa de partículas ferrosas de pequenas e grandes dimensões.

Fotografia 14

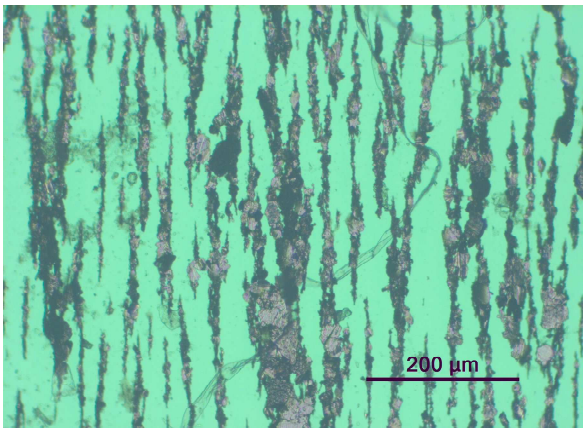

Ampliação: x 200 Diluição: 0,1
Localização: Núcleo Luz: Branca / Verde

Observações: Ampliação da Fotografia 13. Presença significativa de partículas ferrosas de pequenas e grandes dimensões.

Fotografia 15

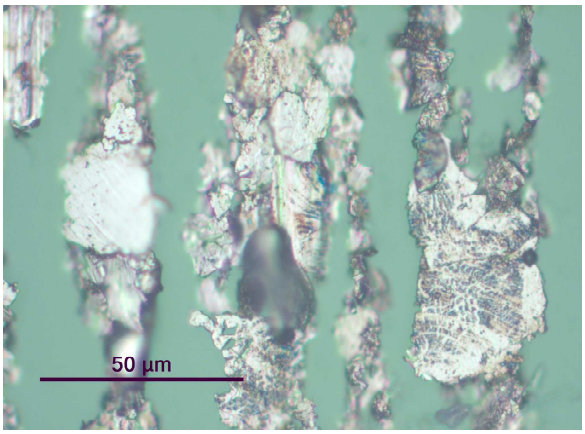

Ampliação: x 1000 Diluição: 0,1
Localização: Núcleo Luz: Branca / Verde

Observações: Ampliação da Fotografia 14. Partículas ferrosas laminares, algumas de grandes dimensões e ligeiramente oxidadas.

Fotografia 16

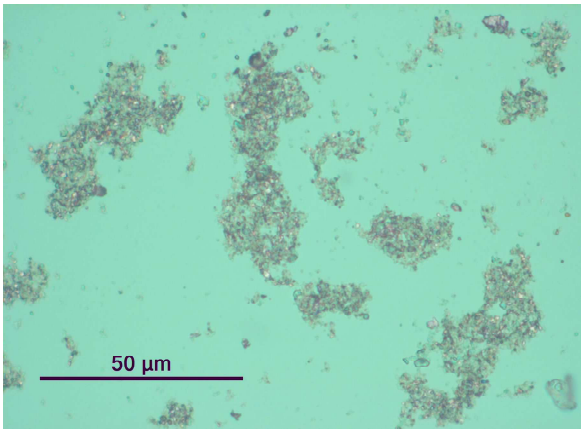

Ampliação: x 1000 Diluição: 0,1
Localização: Núcleo Luz: Branca / Verde

Observações: Presença de alguns polímeros de atrito.

260

Os resultados apresentados referem-se exclusivamente às amostras ensaiadas.
Este documento não pode ser reproduzido, total ou parcialmente, sem a autorização por escrito do INEGI.

Relatório
de
Análise de Lubrificantes

Análise nº: Tipo de análise: Confidencialidade:	89-94 / 10 Ferrometria e Ferrografia Analítica 1
Cliente: Morada: Telefone / Fax:	INEGI - Cetrib Porto
Equipamento: Lubrificante: Dossier:	FZG (ADI – 612) P1 /
Nº de páginas: Data:	8 20/12/10
Responsável: Rúbrica:	Beatriz Graça – Jorge Seabra

261

Os resultados apresentados referem-se exclusivamente às amostras ensaiadas.
Este documento não pode ser reproduzido, total ou parcialmente, sem a autorização por escrito do INEGI.

OBJECTIVO

Análise de quatro amostras de óleo lubrificante P1 resultantes de ensaios na Máquina FZG com engrenagens de ADI, para avaliação do desgaste presente.

As amostras analisadas foram as seguintes:

Amostra Nº	Ciclos	Análises efectuadas	
		Ferrometria	Ferrografia Analítica
K1	-	X	X
K5*	-	X	X
K7	-	X	X
K9*	-	X	X
K9	-	X	X

** - Amostras recolhidas no final do 1º ciclo de ensaio (1000 rpm) do correspondente estágio de carga.*

RESULTADOS DAS ANÁLISES

Nas páginas seguintes são apresentados os resultados referentes às análises de Ferrometria (DR III) e Ferrografia Analítica (FM III).

Os resultados apresentados referem-se exclusivamente às amostras ensaiadas.
Este documento não pode ser reproduzido, total ou parcialmente, sem a autorização por escrito do INEGI.

	CLIENTE: ***INEGI***			MÁQUINA: Máquina de Ensaios FZG			
	MORADA: Porto			Ref. ÓLEO: P1 - 612			
	DATA: 20/12/10			ENSAIOS FZG - ADI Gears			
IDENTIFICAÇÃO							
Amostra nº:	K1	K5*	K7	K9*	K9 Fim		
Data amostra:	Dez-10	Dez-10	Dez-10	Dez-10	Dez-10		
Análise nº:	89/10	91/10	92/10	93/10	94/10		
Ciclos/Máquina:	-	-	-	-	-		
Ciclos/Óleo:	-	-	-	-	-		
FERROMETRIA							
d:	1	0,1	0,1	0,1	0,1		
DL:	54,3	28,2	21,9	39,9	47,9		
DS:	25,2	9,2	8,1	12,5	14,4		
CPUC:	79,5	374,0	300,0	524,0	623,0		
ISUC:	2,3E+03	7,1E+04	4,1E+04	1,4E+05	2,1E+05		
FERROGRAFIA:							
Desgaste normal							
Desgaste severo							
Desgaste abrasão							
Desgaste combinado							
Desgaste fadiga							
Esferas Metálicas							
Ligas não ferrosas							
Óxidos de ferro							
Minerais/Orgânicos							
OILVIEW:							
Índice OilLife:							
Índice Oxidação:							
Índice Contaminação:							
Índice Ferromagnético:							
Grandes Contaminantes:							
Constante Dieléctrica:							
FILTRAGEM							
(Nº Partículas/10 ml)							
5 - 15 µm							
15 - 25 µm							
25 - 50 µm							
50 - 100 µm							
> 100 µm							
VISCOSIDADE							
(cSt a 40° C):							
ACIDEZ (TAN)							
(mg KOH)							
P. INFLAMAÇÃO							
(° C)							
DIAGNÓSTICO:							

LEGENDA	**DL** - Índice de partículas grandes		Não existe
	DS - Índice de partículas pequenas	**f**	Fraco
	CPUC - Concentração part. de desgaste	**M**	Médio
	ISUC - Índice Severidade de Desgaste	**F**	Forte

263

Os resultados apresentados referem-se exclusivamente às amostras ensaiadas.
Este documento não pode ser reproduzido, total ou parcialmente, sem a autorização por escrito do INEGI.

CLIENTE: ***INEGI***	MÁQUINA: Máquina de Ensaios FZG
MORADA: Porto	Ref. ÓLEO: P1 - 612
DATA: 20/12/10	ENSAIOS FZG - ADI Gears K1

Fotografia 1

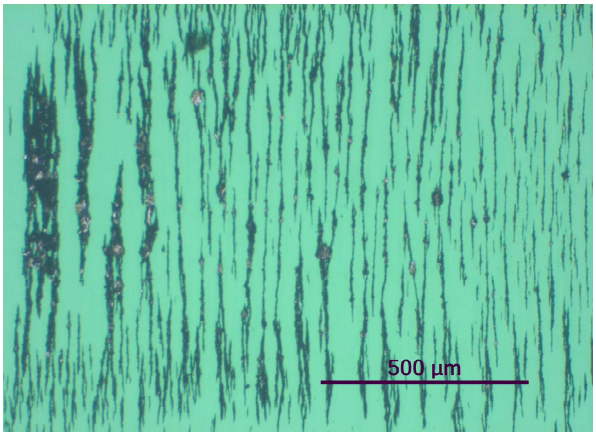

Ampliação: x 100 Diluição: 1
Localização: Núcleo Luz: Branca / Verde

Observações: Presença de partículas ferrosas, algumas de grandes dimensões.

Fotografia 2

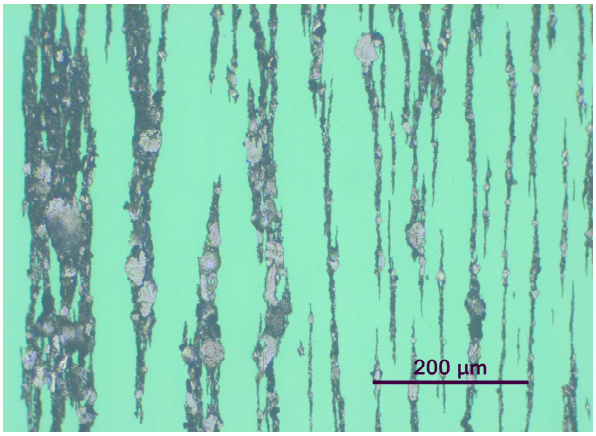

Ampliação: x 200 Diluição: 1
Localização: Núcleo Luz: Branca / Verde

Observações: Ampliação da Fotografia 1. Presença de partículas ferrosas, algumas de grandes dimensões.

Fotografia 3

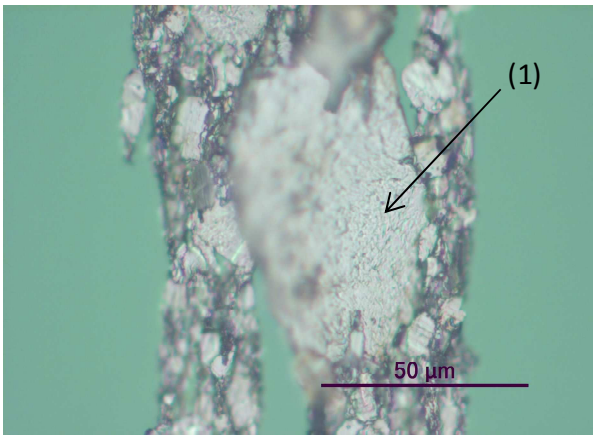

Ampliação: x 1000 Diluição: 1
Localização: Núcleo Luz: Branca / Verde

Observações: Ampliação da Fotografia 2. Partícula ferrosa laminar, típica de fadiga e de grandes dimensões (1).

Fotografia 4

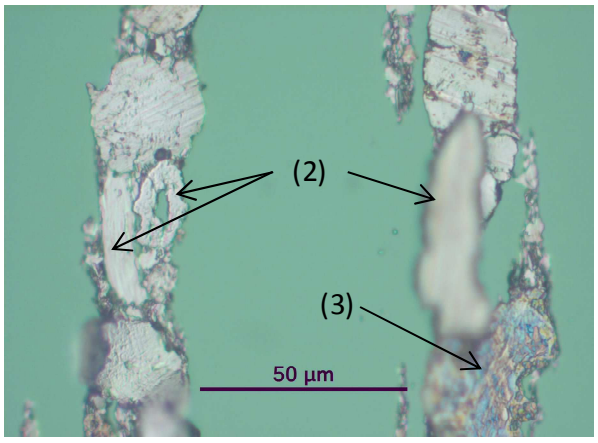

Ampliação: x 1000 Diluição: 1
Localização: Núcleo Luz: Branca / Verde

Observações: Ampliação da Fotografia 2. Partículas ferrosas laminares de média dimensão, algumas resultantes de desgaste de abrasão (2) e outras oxidadas termicamente (3).

Os resultados apresentados referem-se exclusivamente às amostras ensaiadas.
Este documento não pode ser reproduzido, total ou parcialmente, sem a autorização por escrito do INEGI.

CLIENTE: ***INEGI***	MÁQUINA: Máquina de Ensaios FZG
MORADA: Porto	Ref. ÓLEO: P1 - 612
DATA: 20/12/10	ENSAIOS FZG - ADI Gears K5* (d=0,1)

Fotografia 5

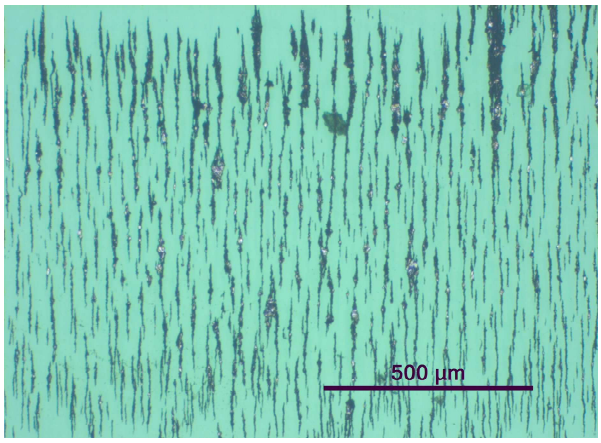

Ampliação: x 100 Diluição: 0,1
Localização: Núcleo Luz: Branca / Verde

Observações: Presença significativa de partículas ferrosas de pequenas dimensões.

Fotografia 6

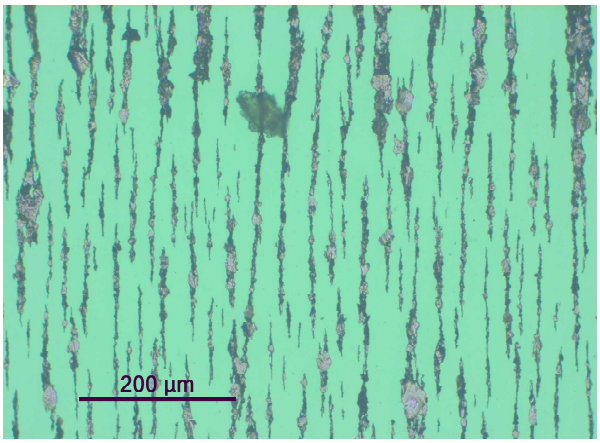

Ampliação: x 200 Diluição: 0,1
Localização: Núcleo Luz: Branca / Verde

Observações: Ampliação da Fotografia 5. Presença significativa de partículas ferrosas, algumas de grandes dimensões.

Fotografia 7

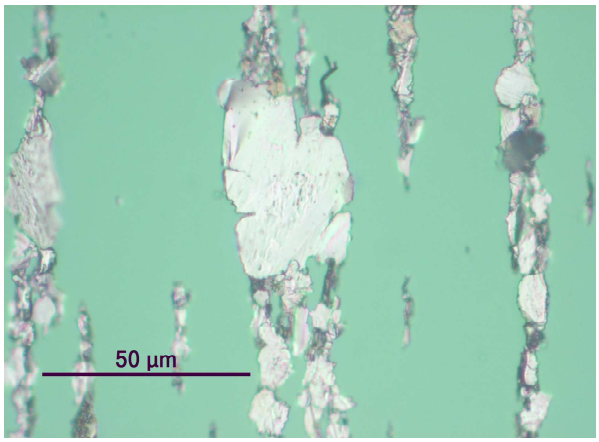

Ampliação: x 1000 Diluição: 0,1
Localização: Núcleo Luz: Branca / Verde

Observações: Ampliação da Fotografia 6. Partícula ferrosa laminar, de desgaste de fadiga e de grandes dimensões.

Fotografia 8

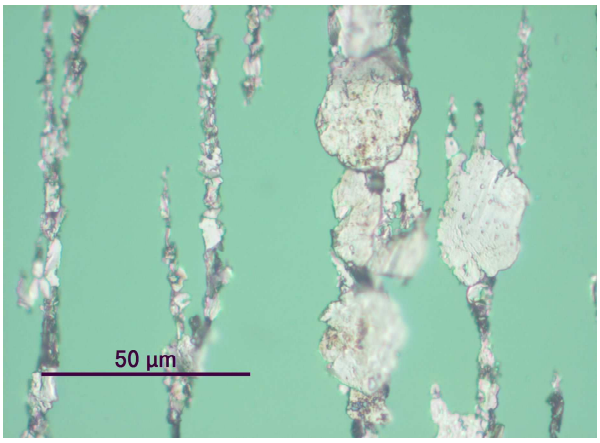

Ampliação: x 1000 Diluição: 0,1
Localização: Núcleo Luz: Branca / Verde

Observações: Ampliação da Fotografia 6. Partículas ferrosas de desgaste de fadiga de médias dimensão.

Os resultados apresentados referem-se exclusivamente às amostras ensaiadas.
Este documento não pode ser reproduzido, total ou parcialmente, sem a autorização por escrito do INEGI.

CLIENTE: ***INEGI***	MÁQUINA: Máquina de Ensaios FZG
MORADA: Porto	Ref. ÓLEO: P1 - 612
DATA: 20/12/10	ENSAIOS FZG - ADI Gears K7

Fotografia 9

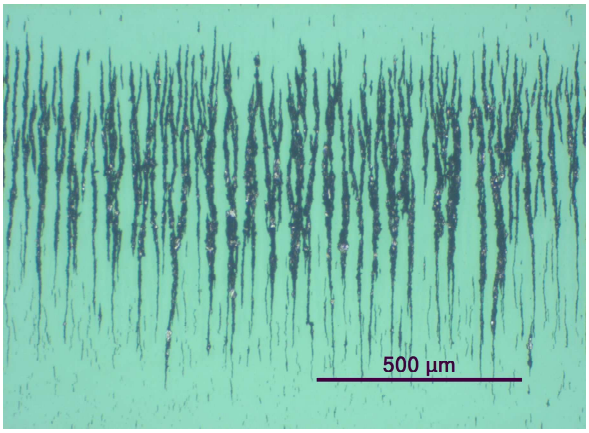

Ampliação: x 100 Diluição: 0,1
Localização: Núcleo Luz: Branca / Verde

Observações: Presença significativa de partículas ferrosas de pequenas e grandes dimensões.

Fotografia 10

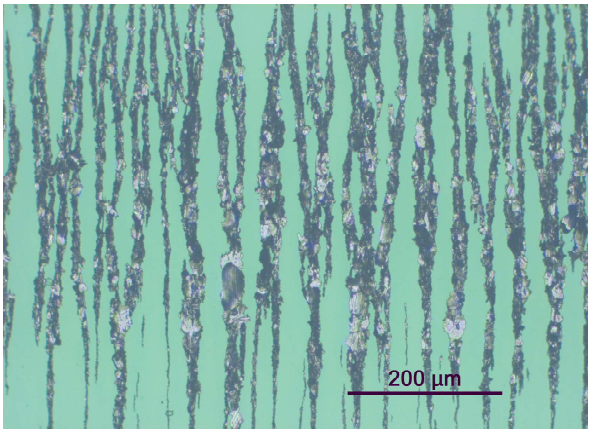

Ampliação: x 200 Diluição: 0,1
Localização: Núcleo Luz: Branca / Verde

Observações: Ampliação da Fotografia 9. Presença de algumas partículas ferrosas de grandes dimensões.

Fotografia 11

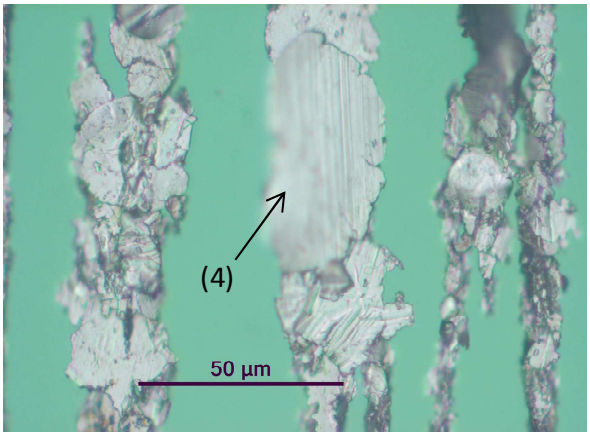

Ampliação: x 1000 Diluição: 0,1
Localização: Núcleo Luz: Branca / Verde

Observações: Ampliação da Fotografia 10. Partícula ferrosa, laminar, de desgaste combinado e de grandes dimensões (4).

Fotografia 12

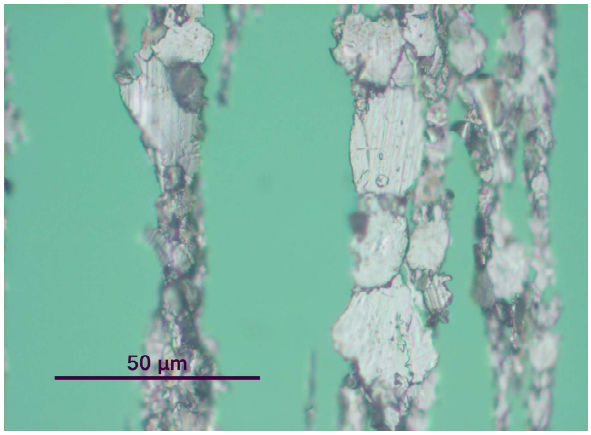

Ampliação: x 1000 Diluição: 0,1
Localização: Núcleo Luz: Branca / Verde

Observações: Ampliação da Fotografia 10. Partículas ferrosas de desgaste de média e grande dimensão.

Os resultados apresentados referem-se exclusivamente às amostras ensaiadas.
Este documento não pode ser reproduzido, total ou parcialmente, sem a autorização por escrito do INEGI.

CLIENTE: ***INEGI***	MÁQUINA: Máquina de Ensaios FZG
MORADA: Porto	Ref. ÓLEO: P1 - 612
DATA: 20/12/10	ENSAIOS FZG - ADI Gears K9* (d=0,1)

Fotografia 13

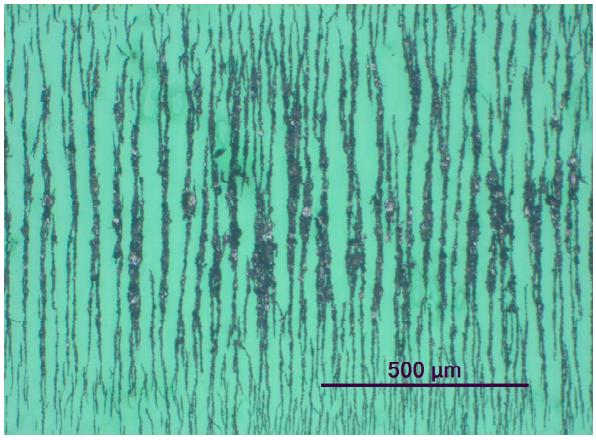

Ampliação: x 100 Diluição: 0,1
Localização: Núcleo Luz: Branca / Verde

Observações: Presença significativa de partículas ferrosas de pequenas dimensões e grandes dimensões.

Fotografia 14

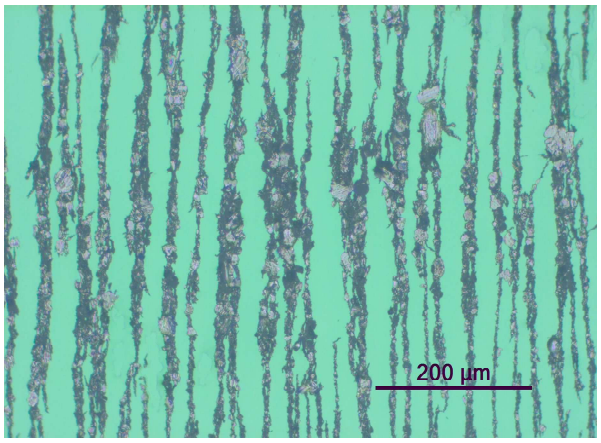

Ampliação: x 200 Diluição: 0,1
Localização: Núcleo Luz: Branca / Verde

Observações: Ampliação da Fotografia 13. Presença significativa de partículas ferrosas de pequenas dimensões e algumas de grandes dimensões.

Fotografia 15

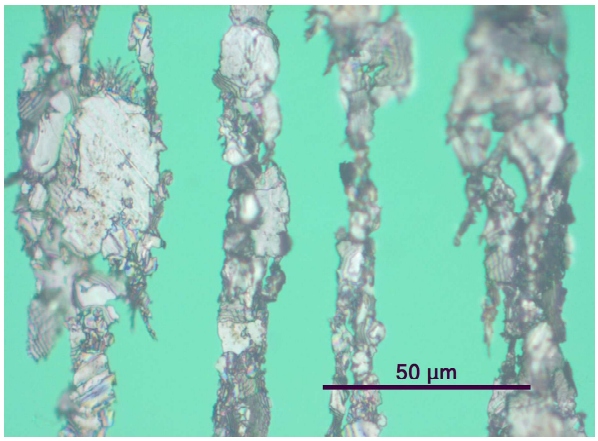

Ampliação: x 1000 Diluição: 0,1
Localização: Núcleo Luz: Branca / Verde

Observações: Ampliação da Fotografia 14. Partículas ferrosas de desgaste de fadiga de média e grande dimensão.

Fotografia 16

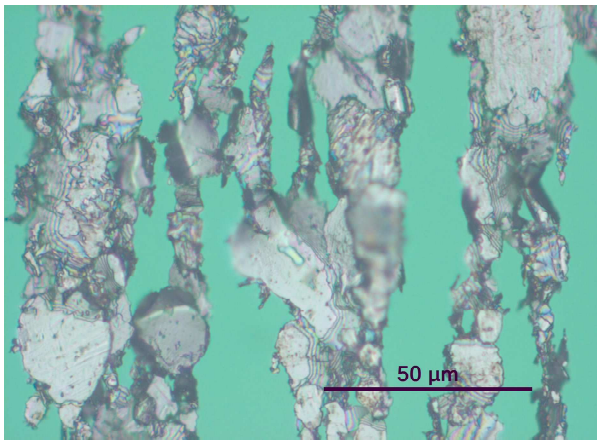

Ampliação: x 1000 Diluição: 0,1
Localização: Núcleo Luz: Branca / Verde

Observações: Ampliação da Fotografia 14. Partículas ferrosas de desgaste de fadiga de média dimensão.

Os resultados apresentados referem-se exclusivamente às amostras ensaiadas.
Este documento não pode ser reproduzido, total ou parcialmente, sem a autorização por escrito do INEGI.

CLIENTE: ***INEGI***	MÁQUINA: Máquina de Ensaios FZG
MORADA: Porto	Ref. ÓLEO: P1 - 612
DATA: 20/12/10	ENSAIOS FZG - ADI Gears K9 Fim (d=0,1)

Fotografia 17

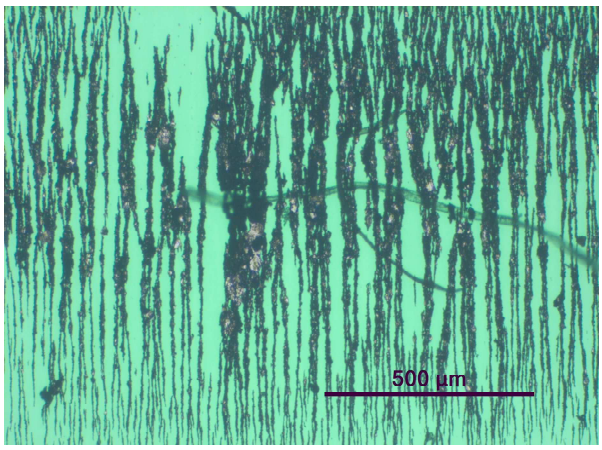

Ampliação: x 100 Diluição: 0,1
Localização: Núcleo Luz: Branca / Verde

Observações: Presença significativa de partículas ferrosas de pequenas dimensões e grandes dimensões.

Fotografia 19

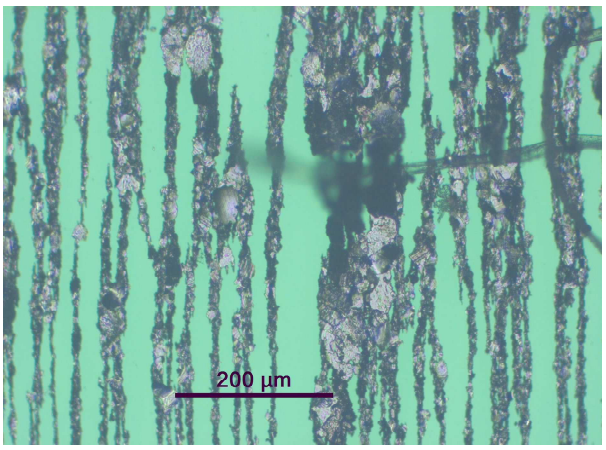

Ampliação: x 200 Diluição: 0,1
Localização: Núcleo Luz: Branca / Verde

Observações: Ampliação da Fotografia 13. Presença significativa de partículas ferrosas de pequenas dimensões e algumas de grandes dimensões.

Fotografia 18

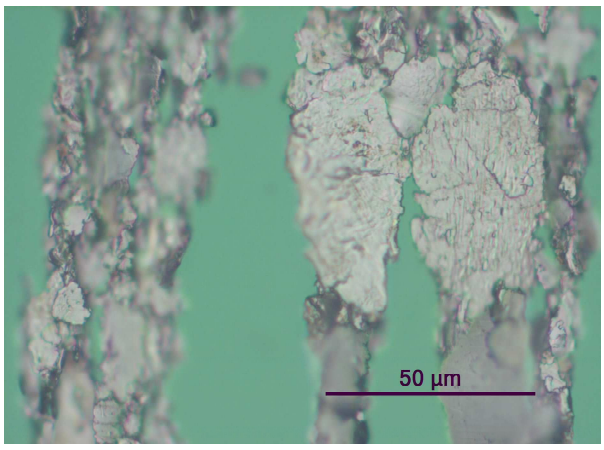

Ampliação: x 1000 Diluição: 0,1
Localização: Núcleo Luz: Branca / Verde

Observações: Ampliação da Fotografia 14. Partículas ferrosas de grandes dimensões típicas de desgaste fadiga.

Fotografia 20

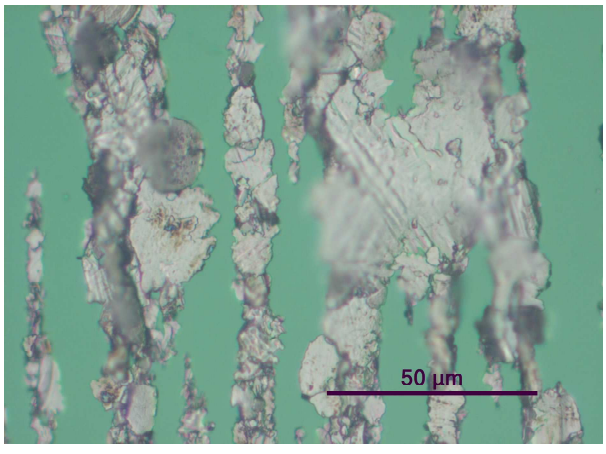

Ampliação: x 1000 Diluição: 0,1
Localização: Núcleo Luz: Branca / Verde

Observações: Ampliação da Fotografia 14. Partículas ferrosas de grandes dimensões típicas de desgaste fadiga.

Os resultados apresentados referem-se exclusivamente às amostras ensaiadas.
Este documento não pode ser reproduzido, total ou parcialmente, sem a autorização por escrito do INEGI.